Håvard Fjær Grip

# Topics in State and Parameter Estimation for Nonlinear and Uncertain Systems

Thesis for the degree of Philosophiae Doctor

Trondheim, May 2010

Norwegian University of Science and Technology
Faculty of Information Technology, Mathematics and Electrical Engineering
Department of Engineering Cybernetics

**NTNU**

Norwegian University of Science and Technology

Thesis for the degree of Philosophiae Doctor

Faculty of Information Technology, Mathematics and Electrical Engineering
Department of Engineering Cybernetics



ISBN 978-82-471-2137-5 (printed ver.)
ISBN 978-82-471-2138-2 (electronic ver.)
ISSN 1503-8181

ITK report 2010-9-W

Doctoral theses at NTNU, 2010:88

Printed by NTNU-trykk

# Summary

This thesis is submitted in partial fulfillment of the requirements for the degree of Philosphiae Doctor (PhD) at the Norwegian University of Science and Technology (NTNU). The thesis is divided into three parts, each of which addresses a specific topic within state and parameter estimation for nonlinear and uncertain systems.

Part I of the thesis is concerned with state and parameter estimation for automotive vehicles. The main focus is on estimation of the angle between the orientation of the vehicle and its direction of travel, known as the *vehicle sideslip angle*. The lateral dynamics of a car is accurately described by a linear model during normal operation, but the dynamics becomes highly nonlinear if one or more of the tires begin to lose road grip. Existing observers for estimating the vehicle sideslip angle are typically constructed as extended Kalman filters, without nonlinear stability analysis and with the drawback of being computationally expensive. The goal of Part I is to construct a vehicle sideslip observer that is less computationally expensive than the extended Kalman filter and that is based on explicit nonlinear stability analysis. The observer produces estimates of the longitudinal and lateral velocities of the vehicle, which are used to calculate the vehicle sideslip angle. In addition, estimates of the road inclination and bank angle, as well as a road-tire friction parameter, are introduced to improve accuracy. The observer is tested using measurements from production passenger cars.

Part II of the thesis is concerned with state and parameter estimation for systems perturbed by a nonlinear function of the system state, external time-varying signals, and a set of unknown, constant parameters. The majority of techniques for estimating unknown parameters in dynamic equations are based on the assumption that the parameters enter the equations linearly, which is not always accurate. Part II starts by considering the problem of parameter estimation in the case of full-state measurement, by using a modular design consisting of a *perturbation estimator* and a *parameter estimator*. The perturbation estimator estimates the full perturbation that depends on the unknown parameters, whereas the parameter estimator inverts the perturbation estimate dynamically with respect to the unknown parameters. The parameter estimates are in turn fed back to the perturbation estimator,

leading to an exponentially stable interconnection when the gains are chosen appropriately. The case of partial-state measurement is then considered for a class of systems where the perturbation is separated from the output by a left-invertible, minimum-phase linear system. To handle this case, the perturbation estimator is replaced by a *modified high-gain observer*, similar to extended high-gain observers found in the literature, which estimates both the state of the system and the perturbation. Part of the high-gain design procedure consists of transforming the linear part of the system to a special coordinate basis that explicitly reveals the system's zero structure and invertibility properties. Numerical software tools for carrying out such transformations already exist. To facilitate the transformation of systems with symbolic representations as well, Part II presents a software tool written in the mathematics software suite Maple.

Part III is concerned with output-feedback stabilization of two classes of systems containing saturations. First, global stabilization of multivariable linear time-invariant systems with saturated outputs is considered. An output-feedback design for single-input single-output systems of this type, which ensures global asymptotic stability if the linear system is controllable and observable, can already be found in the literature. This design is based on deactivating the saturation by using the sign of the output, and identifying the state of the system in a deadbeat manner once the saturation becomes inactive. The most logical extension of this design to systems with multiple outputs would be to deactivate all the saturations simultaneously; however, this is a difficult, if not impossible, task. The design presented in Part III is instead based on deactivating all of the saturations at least once, but not necessarily at the same time. The state of the system can then be identified in a deadbeat manner and controlled to the origin. Next, semiglobal stabilization of *sandwich systems*, consisting of two linear subsystems in a saturated cascade connection, is considered under the assumption that a partial-state measurement is available only from the second subsystem in the cascade. This problem is challenging because the first subsystem is separated from the output by the saturation, and the second subsystem is separated from the input by the saturation. The design presented in Part III therefore combines techniques for stabilizing systems with saturated inputs with techniques for stabilizing systems with saturated outputs. A key element of the design is a detection algorithm that determines whether the saturation is active or inactive. This detection algorithm operates on time intervals that must be chosen sufficiently small depending on the size of a compact set of admissible initial conditions.

# Contents

# Preface

This thesis presents the results of my PhD research, primarily carried out during the periods between September 2006 and April 2007, and between March 2008 and October 2009. The research was conducted at the Department of Engineering Cybernetics, Norwegian University of Science and Technology (NTNU), in Trondheim, Norway, under the guidance of Professor Tor A. Johansen, and at the School of Electrical Engineering and Computer Science, Washington State University (WSU), in Pullman, Washington, under the guidance of Professor Ali Saberi during a one-year research visit. Funding for the research was primarily provided by the Research Council of Norway, and partly by the European Union STREP project Complex Embedded Automotive Control Systems (CEmACS).

I began my PhD studies at NTNU in September 2006 after completing my MSc degree in Engineering Cybernetics in June of that year. During the final year of my MSc studies I was partially employed by SINTEF ICT, Applied Cybernetics, to work on the CEmACS project. The topic of SINTEF's involvement in this project was state estimation for automotive vehicles, with Daimler AG (formerly Daimler-Chrysler) as the industrial partner. Some of the research presented in this thesis, in particular in Chapter 3, is a continuation of the work started during that year.

Starting in May 2007 I took a leave of absence from my PhD to work on a ten-month project at Daimler Group Research and Advanced Engineering in Stuttgart, Germany. During this period I was contracted through SINTEF ICT, where I was employed as a scientific researcher. In March 2008 I returned to my PhD work in Trondheim, and in August 2008 I went to WSU as a visiting scholar. I returned again to Trondheim in September 2009 and submitted the first draft of this thesis in October 2009. The second draft was submitted in February 2010, and the final version was submitted in May 2010.

The technical content of this thesis is composed as a collection of eight selected articles, each of which makes up one of Chapters 2–9. These articles have not been modified for inclusion in the thesis, and the chapters can therefore be read independently. On the other hand, there is a degree of overlap in content between some of the chapters, and some notational conventions differ between the chapters.

While I do not think these issues will cause confusion, I apologize to the reader for any inconvenience they may cause.

I have had the benefit of working with many wonderful people during my PhD studies. First of all I would like to thank my academic supervisor, Professor Tor A. Johansen, for his inspiring guidance on both my MSc and PhD research. I am particularly grateful for his practical approach to complex problems, and for his ability to open doors to many different opportunities. I would also like to thank my co-supervisors, Dr. Glenn-Ole Kaasa at Statoil, who has given me lots of encouragement and good ideas, and Professor Lars Imsland at NTNU, whose guidance and advice—in particular during the early stages of my research—has put me far ahead of where I would otherwise have been.

My work with Daimler has provided me with tremendously valuable experience in practical engineering. For this I am indebted to Dr. Jens C. Kalkkuhl and Mr. Avshalom Suissa, whose engineering expertise and intuition have been of great inspiration. During my ten-month engagement in Stuttgart, Jens and Avshalom welcomed me as part of their team and involved me in some incredibly interesting work (the highlight being the exhilarating test drives).

Since August 2008 I have worked closely with Professor Ali Saberi at WSU. Thanks to Ali's active involvement and interest, as well as his vast knowledge and professional expertise, this work has been very interesting and productive. I would like to thank him for giving me such a warm welcome during my year at WSU and for being a good friend with whom I have enjoyed working Saturdays at Bucer's coffee shop. In my work on output-feedback control of systems with saturations, I have also benefited from working with Professor Anton A. Stoorvogel at the University of Twente in Enschede, the Netherlands.

I would like to thank my parents for introducing me to science and engineering at an early age, for helping me along the way, and always encouraging me to do my best while staking out my own course. Finally, to my dear Dana: thank you for all your patience and loving support, especially when progress was slow and the work seemed uninspiring. I wish you all the best in completing your own PhD research.

Trondheim
May 2010

Håvard Fjær Grip

# Chapter 1

# Introduction

The field of control engineering is centered around the task of manipulating physical systems to achieve a certain desired behavior. Many physical system can be modeled by a set of continuous-time differential equations of the form

$$\dot{x} = f(t, x, u), \tag{1.1}$$

where $t \in \mathbb{R}_{\geq 0}$ represents time, $x \in \mathbb{R}^n$ represents the state of the system, and $u \in \mathbb{R}^m$ represents an actuator input that can be specified by the designer. To make the system behave in a desired manner, the control engineer must design a control law that specifies the value of the actuator input $u$ at any point in time. Typically, $u$ is designed to depend on the state $x$ of the system, a strategy known as *feedback control*.

## 1.1 State Estimation

A major obstacle in the actual implementation of feedback control laws is a lack of information about the current state of the system. Typically, a measurement $y = h(t, x)$ is available from the system, but the map $h$ is in general not injective with respect to $x$. Thus, one cannot invert $h(t, x)$ to identify $x$ uniquely from $y$ at any fixed point in time. To alleviate this problem, a common strategy is to implement the control law using a state estimate $\hat{x}$ instead of the actual state.

If a control law is to be implemented based on a state estimate $\hat{x}$, then the obvious question is how such an estimate may be constructed. Since $h$ is presumed not to be injective, $\hat{x}$ cannot be a static function of $y$. Instead, $\hat{x}$ is often designed

as the output of a dynamical system

$$\dot{w} = \alpha_1(t, w, u, y),$$
$$\hat{x} = \alpha_2(t, w, u, y).$$

A dynamical system of this type that gives the estimation error $\tilde{x} := x - \hat{x}$ certain desirable properties—for example, the property that $\tilde{x}$ converges to the origin—is called an *observer*. The precise definition of an observer varies throughout the literature (see, e.g., Marino and Tomei, 1995; Trentelman, Stoorvogel, and Hautus, 2001).

### 1.1.1 Linear Time-Invariant Systems

A finite-dimensional linear time-invariant (LTI) system is described by the following equations:

$$\dot{x} = Ax + Bu, \tag{1.2a}$$
$$y = Cx + Du. \tag{1.2b}$$

A full-order observer for this system can be constructed by replicating the dynamics of the system and adding an output injection term:

$$\dot{\hat{x}} = A\hat{x} + Bu + L(y - C\hat{x} - Du). \tag{1.3}$$

The matrix $L$ is called the *observer gain* or *output injection gain*. To analyze this design, we investigate the dynamics of the error variable $\tilde{x}$:

$$\dot{\tilde{x}} = (A - LC)\tilde{x}. \tag{1.4}$$

The error dynamics (1.4) represents an LTI system that it is exponentially stable if the matrix $A - LC$ has all its eigenvalues in the open left-half complex plane. This property can be ensured by a proper selection of $L$ if, and only if, the pair of matrices $(C, A)$ is *detectable*.

A pair $(C, A)$ is detectable if all the unobservable eigenvalues of $A$ are located in the open left-half complex plane. An eigenvalue $\lambda$ of $A$ is called unobservable if

$$\operatorname{rank}\begin{bmatrix} A - \lambda I \\ C \end{bmatrix} < n.$$

A system with no unobservable eigenvalues is called *observable*. See, for example, Chen (1999); Trentelman et al. (2001) for further details.

An appealing property of linear systems is that, if an exponentially stabilizing state-feedback control law $u = Fx$ is implemented as $u = F\hat{x}$, where $\hat{x}$ is

generated by the observer (1.3) with exponentially stable error dynamics, then the resulting closed-loop system is also exponentially stable. This property is known as the *separation principle*, because it implies that the control law and the observer may be designed separately without compromising stability.

### Unknown Disturbances

The above formulation for linear systems assumes that the model (1.2) is exact. In reality, however, a physical system is often influenced by additive exogenous disturbances, both in the dynamic equation (1.2a) and in the measurement equation (1.2b). In the presence of such disturbances, the goal of having $\tilde{x}$ converge to the origin is often unrealistic. Instead, one may have to settle for $\tilde{x}$ converging to some (hopefully small) neighborhood of the origin.

Two optimization-based frameworks have been developed for designing observers to minimize or reduce the root mean square (RMS) of the estimation error $\tilde{x}$ in the presence of unknown disturbances. In the *$H_2$ framework*, the disturbances are assumed to be white noise signals of unit intensity, and the goal is to minimize or reduce the $H_2$ norm of the transfer matrix from the disturbances to the estimation error, which is equivalent to the RMS of the estimation error. In the *$H_\infty$ framework*, no statistical assumptions are made regarding the disturbances, and the goal is to minimize or reduce the $H_\infty$ norm of the transfer matrix from the disturbances to the estimation error. The $H_\infty$ norm is an upper bound on the RMS gain from the disturbance to the estimation error (see, e.g., Saberi, Stoorvogel, and Sannuti, 2006).

Some particular design methods of relevance to this thesis are discussed in the following sections.

### Kalman Filters

Perhaps the most celebrated result in the area of state estimation, the Kalman filter works on discrete-time models—often derived by discretization of a continuous-time model—of the form

$$x_k = Ax_{k-1} + Bu_k + Ww_k, \tag{1.5a}$$
$$y_k = Cx_k + Du_k + Vv_k, \tag{1.5b}$$

where $w_k$ and $v_k$ are unknown exogenous disturbances. These unknown disturbances are assumed to be Gaussian white noise signals of unit intensity, which are mutually uncorrelated. The Kalman filter produces a state estimate $\hat{x}_k$ according to the expression

$$\hat{x}_k = A\hat{x}_{k-1} + Bu_k + L_k(y_k - C\hat{x}_k - Du_k), \tag{1.6}$$

where $L_k$ is a time-varying observer gain that is computed to minimize the RMS of the estimation error. The Kalman filter algorithm is recursive and must be initialized with an estimate of the covariance of the estimation error.

The Kalman-Bucy filter is a version of the Kalman filter for continuous-time systems, which updates the state estimate as

$$\dot{\hat{x}} = A\hat{x} + Bu + L(t)(y - C\hat{x} - Du). \tag{1.7}$$

The expression (1.7) is the same as (1.3), except that the gain $L$ is replaced by a time-varying gain $L(t)$. As $t \to \infty$, $L(t)$ converges to a stationary gain matrix. This stationary gain matrix can be computed offline and used to implement an observer of the form (1.3) with constant gain, resulting in the *stationary Kalman filter*. The stationary Kalman filter minimizes the $H_2$ norm of the transfer matrix from the disturbance to the estimation error, and it is therefore optimal in the $H_2$ framework.

For an introduction to various aspects of Kalman filtering, see, for example, Brown and Hwang (1997); Grewal and Andrews (2001).

### Unknown-Input Observers

Given a system of the form (1.2) with unknown disturbances occurring in the dynamic equation (1.2a), it is sometimes possible to construct an unknown-input observer, which generates estimates that are completely unaffected by the disturbances, without making any statistical assumptions (see, e.g., Darouach, Zasadzinski, and Xu, 1994; Chen, Patton, and Zhang, 1996). These properties of unknown-input observers are obviously appealing; however, such observers can only be constructed under restrictive conditions—for example, there can only be one inherent integration between a disturbance and an output.

### High-Gain Observers

The restrictive conditions for constructing unknown-input observers motivate the search for observers that can reduce the effect of the disturbances to any desired level. High-gain observers, which can be explicitly constructed outside of any optimization framework, achieve this by increasing the gain in certain directions, to force the transfer matrix from the disturbances to the estimation error to approach zero (see, e.g., Esfandiari and Khalil, 1987; Saberi and Sannuti, 1990; Saberi, Chen, and Sannuti, 1993). Naturally, an increase in gain results in increased sensitivity to measurement noise, and thus a tradeoff must be made between rejecting a disturbance in the dynamic equations and keeping the sensitivity to measurement noise at an acceptable level.

The requirements for arbitrary suppression of a disturbance using high-gain observers are significantly less restrictive than the requirements for unknown-input observers; it is sufficient if the system is left-invertible and minimum-phase with the unknown disturbances considered as inputs.

#### Disturbance Modeling

In some cases, *a priori* information about the nature of a disturbance can be exploited to improve state estimation. For example, the disturbance signals $w_k$ and $v_k$ may not fit the white-noise assumption used in the Kalman filter. Instead, the signals may have a non-white correlation profile that can be better described as filtered white noise by the disturbance model

$$w_k = A_w w_{k-1} + B_w \omega_k, \tag{1.8a}$$

$$v_k = A_v v_{k-1} + B_v \nu_k, \tag{1.8b}$$

where $\omega_k$ and $\nu_k$ are Gaussian white noise signals of unit intensity. In this case, the system model (1.5) may be augmented with the disturbance model (1.8), and a Kalman filter may be designed for the augmented system (see, e.g., Brown and Hwang, 1997; Grewal and Andrews, 2001).

If a disturbance is known to consist of a finite number of sinusoids with known frequencies, then it can be modeled precisely by a linear system with complex pairs of eigenvalues corresponding to those frequencies. The system model (1.2) can be augmented with this marginally stable disturbance model and an observer may be designed for the augmented system, assuming it is observable (see, e.g., Saberi et al., 2006, Ch. 12, 13).

General periodic signals consisting of an infinite number of sinusoids can be modeled precisely by a system incorporating a time delay. *Repetitive control* is a design framework that makes use of such time-delay systems to handle periodic disturbances (see, e.g., Hara, Yamamoto, Omata, and Nakano, 1988). The conditions for achieving perfect rejection by repetitive control are restrictive, however. Furthermore, repetitive control generates retarded or neutral time-lag systems that are difficult to analyze (see, e.g., Hale, 1977).

### 1.1.2 Nonlinear and Time-Varying Systems

Section 1.1.1 discusses various state-estimation techniques for LTI systems. When the system in question is nonlinear or time-varying, state estimation is considerably more complicated. To begin with, the simple notions of observability and detectability for linear systems cannot be directly carried over to nonlinear systems.

For an observable LTI system, different initial conditions can be distinguished by looking at the system output on any nonempty open time interval, regardless of the input applied to the system. For an observable nonlinear system, however, different initial conditions may create identical outputs for certain inputs, or the outputs may remain identical for a long time before becoming distinct. Many different types of observability have been defined to describe the observability properties of nonlinear systems in a more fine-grained manner, for example, *uniform* observability to signify that the observability is not input-dependent, and *local* observability to signify that two initial conditions can be distinguished by observing trajectories locally (see Nijmeijer and van der Schaft, 1990; Gauthier and Bornard, 1981, for details).

Another complication of nonlinear systems is that the separation principle mentioned in Section 1.1.1 does not hold in general. Hence, separate design of the control law and the observer is in general not justified from a theoretical point of view. In practice, however, the two tasks are often successfully separated.

A large number of observer design techniques have been developed for different types of nonlinear systems. In the following sections, a few of these are discussed.

### Extended Kalman Filters

The Kalman filter discussed in Section 1.1.1 retains its optimality properties when applied to linear time-varying systems; that is, systems where the matrices $A$, $B$, $C$, and $D$ depend on time in some known fashion.

For general nonlinear systems, the extended Kalman filter (EKF) provides an approximate solution that is based on linearization around the estimated state of the system (see, e.g., Brown and Hwang, 1997; Grewal and Andrews, 2001). The EKF is easy to construct and often produces good results, and it is therefore widely used. Nevertheless, its behavior is not optimal, and proving stability of the state estimates is difficult (see, e.g., Reif, Günther, Yaz, and Unbehauen, 1999).

### Observers with Linear Error Dynamics

Sometimes systems with nonlinear dynamics can be transformed to a more desirable form by introducing nonlinear state transformations. In particular, it may be possible to obtain a system where the nonlinearities depend only on known signals. Marino and Tomei (1995, Ch. 5) gives necessary and sufficient conditions for transforming a single-input single-output (SISO) system $\dot{x} = f(x) + g(x, u)$,

$y = h(x)$ by a local or global diffeomorphism $z = T(x)$ into the form

$$\begin{aligned}
\dot{z}_1 &= z_2 + \gamma_1(y,u), && \text{(1.9a)}\\
\dot{z}_2 &= z_3 + \gamma_2(y,u), && \text{(1.9b)}\\
&\vdots\\
\dot{z}_n &= \gamma_n(y,u), && \text{(1.9c)}\\
y &= z_1. && \text{(1.9d)}
\end{aligned}$$

The system (1.9) represents an observable LTI system perturbed by the nonlinear functions $\gamma_1(y,u),\ldots,\gamma_n(y,u)$. These nonlinear functions can be evaluated, since they depend only on the input and the output, and hence an observer can be constructed as

$$\begin{aligned}
\dot{\hat{z}}_1 &= \hat{z}_2 + \gamma_1(y,u) + l_1(y-\hat{z}_1),\\
\dot{\hat{z}}_2 &= \hat{z}_3 + \gamma_2(y,u) + l_2(y-\hat{z}_1),\\
&\vdots\\
\dot{\hat{z}}_n &= \gamma_n(y,u) + l_n(y-\hat{z}_1),
\end{aligned}$$

The resulting error dynamics is linear time-invariant and can be stabilized by a proper selection of the gains $l_1,\ldots,l_n$.

### High-Gain Observers

As discussed in Section 1.1.1, high-gain observers for LTI systems can in many cases be used to suppress the effect of exogenous disturbances. The high-gain framework can also be used to construct observers for nonlinear systems, by treating the difference between a nonlinearity and some linear function as a disturbance to be suppressed. Provided the nonlinearities satisfy Lipschitz-continuity conditions, at least locally in some region of interest, asymptotically perfect estimation can often be achieved.

This strategy has been used many places in the literature, for example, in Saberi and Sannuti (1990); Khalil and Esfandiari (1993); Teel and Praly (1994); Khalil (2002, Ch. 14), where the nonlinearities are separated from the outputs by a left-invertible, minimum-phase LTI system. A somewhat different construction is used

in Gauthier and Kupka (2001), where the systems are of the following form:

$$\begin{aligned}
\dot{x}_1 &= f_1(u, x_1, x_2), \\
\dot{x}_2 &= f_2(u, x_1, x_2, x_3), \\
&\vdots \\
\dot{x}_n &= f_n(u, x_1, x_2, \ldots, x_n), \\
y &= h(u, x_1),
\end{aligned}$$

with the nonlinearities satisfying inequalities of the type

$$\left| \frac{\partial f_i}{\partial x_{i+1}}(u, x_1, \ldots, x_{i+1}) \right| \geq \alpha > 0, \quad \left| \frac{\partial h}{\partial x_1}(u, x_1) \right| \geq \alpha > 0$$

in addition to Lipschitz-continuity conditions.

### Monotonic Nonlinearities

Some types of nonlinearities are easier to handle than others. The multivariable circle criterion (see Khalil, 2002, Th. 7.1) specifies conditions for stability of the system

$$\begin{aligned}
\dot{x} &= Ax - B\psi(t, y), \\
y &= Cx - D\psi(t, y),
\end{aligned}$$

when the nonlinear function $\psi$ is a *sector function* (see Khalil, 2002, Def. 6.2). The circle criterion can be used to construct observers for systems with monotonic nonlinearities. In particular, Fan and Arcak (2003) extends the results from Arcak and Kokotović (2001) to give linear matrix inequality conditions for observer design for systems of the form

$$\begin{aligned}
\dot{x} &= Ax + G\gamma(Hx) + \rho(y, u), \\
y &= Cx,
\end{aligned}$$

where $\gamma$ satisfies a multivariable monotonicity condition

$$\frac{\partial \gamma}{\partial v}(v) + \frac{\partial \gamma}{\partial v}^{\mathsf{T}}(v) \geq 0.$$

## 1.2 Parameter Uncertainty

Sometimes a model of the form (1.1) is available to accurately describe the behavior of a physical system. Quite frequently, however, there are uncertainties in the model. Such uncertainties are problematic because control and observer design based on an uncertain model may fail to yield the desired results.

Model uncertainties can often be described in terms of a set of unknown parameters that are constant or slowly-varying. For example, the model may include an uncertain friction coefficient, a sensor bias, or a constant disturbance. In these cases, a natural strategy is to introduce estimates of the unknown parameters to be updated online. The parameter estimates may be used directly in a control or state-estimation algorithm—such algorithms are often referred to as *adaptive* algorithms. The parameter estimates may also be useful in a more indirect sense, by providing information about the physical system that can be used in a higher-level decision-making process. Some approaches for handling parameter uncertainty are discussed below. For simplicity, the discussion focuses only on SISO systems.

### Gradient Approach

One type of parameter-estimation technique begins by describing the physical system as

$$(a(s) + \bar{a}^{\mathsf{T}}(s)\theta)y = (b(s) + \bar{b}^{\mathsf{T}}(s)\theta)u, \tag{1.10}$$

where $a(s) + \bar{a}^{\mathsf{T}}(s)\theta$ and $b(s) + \bar{b}^{\mathsf{T}}(s)\theta$ represent the denominator and numerator polynomials of the system's transfer function, and $\theta$ is a vector of unknown parameters. The expression (1.10) can be rewritten as $z = \phi^{\mathsf{T}}\theta$, where $z = a(s)y - b(s)u$ and $\phi^{\mathsf{T}} = \bar{b}^{\mathsf{T}}(s)u - \bar{a}^{\mathsf{T}}(s)y$. The quantities $z$ and $\phi$ can in general not be evaluated, because they are defined in terms of non-proper transfer functions. However, if we define $z_{\mathrm{f}} = H(s)z$ and $\phi_{\mathrm{f}} = H(s)\phi$, where $H(s)$ is a low-pass filter of sufficiently high relative degree, then we obtain the *linear regression model* $z_{\mathrm{f}} = \phi_{\mathrm{f}}^{\mathsf{T}}\theta$, where $z_{\mathrm{f}}$ and $\phi_{\mathrm{f}}$ can be evaluated by using proper transfer functions.

If we produce an estimate $\hat{z}_{\mathrm{f}}$ of $z_{\mathrm{f}}$ by the expression $\hat{z}_{\mathrm{f}} := \phi_{\mathrm{f}}^{\mathsf{T}}\hat{\theta}$, where $\hat{\theta}$ is an estimate of $\theta$, then the error $e := z_{\mathrm{f}} - \hat{z}_{\mathrm{f}}$ is given by the linear relationship $e = \phi_{\mathrm{f}}^{\mathsf{T}}\tilde{\theta}$, where $\tilde{\theta} := \theta - \hat{\theta}$. The strategy is now to define a convex function $J(e)$ to be minimized, a popular choice being $J(e) = \frac{1}{2}e^2$. Then the parameter estimate $\hat{\theta}$ can be adjusted by the gradient algorithm

$$\dot{\hat{\theta}} = -\Gamma\left(\frac{\partial J}{\partial e}(e)\frac{\partial e}{\partial \hat{\theta}}\right)^{\mathsf{T}} = \Gamma e\phi_{\mathrm{f}},$$

where $\Gamma$ is a symmetric, positive-definite gain matrix (see, e.g., Ioannou and Sun, 1996). It is common to include a normalization factor in the gradient algorithm, in particular, if boundedness of $\phi_f$ is not guaranteed. For example, the parameter estimate may be implemented as

$$\dot{\hat{\theta}} = \Gamma e \frac{\phi_f}{1 + \phi_f^T \phi_f}.$$

In some cases, the gradient approach may also be used for system with a nonlinear state-space representation (see, e.g., Krstić, Kanellakopoulos, and Kokotović, 1995), as long as the unknown parameter vector $\theta$ appears linearly. The estimated parameters can be used to implement a control law or an observer.

### Least-Squares Estimation

Another way to use linear regression models is for least-squares parameter estimation. Least-squares algorithms are typically applied to discrete-time linear regression models of the form $z_k = \phi_k^T \theta$. Such models can be be generated from discrete-time systems without the need to introduce low-pass filters (see Åström and Wittenmark, 1995, Ch. 2). A least-squares estimate based on data from time 0 to time $k$ produces an estimate $\hat{\theta}$ that minimizes the error

$$\sum_{i=0}^{k} (z_i - \phi_i^T \hat{\theta})^2.$$

As $k$ increases, the size of the computation required to solve this minimization problem also increases, which poses a problem in real-time applications. To get around this problem, the least-squares estimate can be computed recursively, with only the parameter estimate and a symmetric, positive-definite $p \times p$ matrix (where $p$ is the number of parameters) having to be carried over from one time step to the next. A recursive least-squares algorithm can also be implemented for continuous-time linear regression models.

The least-squares algorithm weighs the collected data equally, no matter when the data was collected. Thus, data collected far back in time has the same influence on the parameter estimate as newly collected data. This may be undesirable if there is variation in the parameters. It is therefore common to include a forgetting factor in the algorithm, which ensures that older data is gradually forgotten.

### Lyapunov-Based Adaptation

Depending on the system, stability problems may arise when the methods mentioned above are applied to particular control or estimation problems. One way

to tackle stability issues is to carry out a Lyapunov-based design, where the time derivative of the parameter estimate $\hat{\theta}$ is explicitly chosen to make the time derivative of a Lyapunov-function candidate negative semidefinite. This approach is best illustrated by an example.

**Example 1.1.** Consider the scalar system

$$\dot{x} = \omega^{\mathsf{T}}(t)\theta + u, \tag{1.11}$$

where $\omega(t)$ is a vector of smooth, bounded signals with bounded derivatives, and $\theta$ is a vector of constant, unknown parameters. To control the state $x$ to the origin, a natural choice of control law is $u = -x - \omega^{\mathsf{T}}(t)\hat{\theta}$, where $\hat{\theta}$ is a vector of parameter estimates. This choice yields the closed-loop system

$$\dot{x} = -x + \omega^{\mathsf{T}}(t)\tilde{\theta}, \tag{1.12}$$

where $\tilde{\theta} = \theta - \hat{\theta}$. The logic behind this choice of control law is that, if the estimation error $\tilde{\theta}$ were zero, then the origin would be globally exponentially stable, as proven by using the Lyapunov function $V = \frac{1}{2}x^2$.

In the presence of a nonzero parameter-estimation error, the time derivative of $V$ is given by

$$\dot{V} = -x^2 + x\omega^{\mathsf{T}}(t)\tilde{\theta}.$$

Clearly $\dot{V}$ is not sign-definite, due to the term involving $\tilde{\theta}$. To address this problem, we create a new Lyapunov-function candidate $W = V + \frac{1}{2}\tilde{\theta}^{\mathsf{T}}\Gamma^{-1}\tilde{\theta}$, where $\Gamma$ is a symmetric, positive-definite gain matrix. Then

$$\dot{W} = -x^2 + (x\omega^{\mathsf{T}}(t) + \dot{\tilde{\theta}}^{\mathsf{T}}\Gamma^{-1})\tilde{\theta} = -x^2 + (x\omega^{\mathsf{T}}(t) - \dot{\hat{\theta}}^{\mathsf{T}}\Gamma^{-1})\tilde{\theta}.$$

By choosing $\dot{\hat{\theta}} = \Gamma\omega(t)x$, we obtain $\dot{W} = -x^2$, which proves global stability of the origin. By using the smoothness and boundedness properties of $\omega(t)$ we can show that $x$ is uniformly continuous, and we can therefore use Barbălat's lemma (Barbălat, 1959; Khalil, 2002, Lemma 8.2) to prove that $x \to 0$ as $t \to \infty$.

Example 1.1 illustrates the main idea of Lyapunov-based adaptation, namely, to obtain a system $\dot{x} = f(t, x, u) + \omega(t, x, u)\tilde{\theta}$; to find a Lyapunov-function candidate that is positive definite with respect to both $x$ and $\tilde{\theta}$; and to select $\dot{\hat{\theta}}$ to compensate for the presence of $\omega(t, x, u)\tilde{\theta}$ by canceling sign-indefinite terms in the derivative of the Lyapunov-function candidate. Sometimes this process is straightforward, as in Example 1.1. Other times it can be complicated, in particular, because there is no systematic method for finding Lyapunov functions for general nonlinear systems. Krstić et al. (1995) deals with a wide range of Lyapunov-based adaptive techniques, centered around the *backstepping* approach to nonlinear control.

### Persistency of Excitation

In the above discussion, $\hat{\theta}$ has been introduced as an estimate of the unknown parameter vector $\theta$, and $\tilde{\theta} = \theta - \hat{\theta}$ has been introduced as a parameter-estimation error. The most desirable behavior would be for $\tilde{\theta}$ to converge to the origin as $t \to \infty$. However, this does not necessarily happen with either of the approaches outlined above. To illustrate the problem, we again consider Example 1.1.

**Example 1.1 (Continued).** We have already confirmed that $x \to 0$ as $t \to \infty$, and from this we can easily show that $\omega^{\mathsf{T}}(t)\tilde{\theta}$ must also converge to zero. Suppose first that $\omega(t) = \omega$ is a constant $2 \times 1$ vector. Then $\omega^{\mathsf{T}}\tilde{\theta} = 0$ is satisfied not only for $\tilde{\theta} = 0$, but for any $\tilde{\theta}$ in the one-dimensional null space of $\omega^{\mathsf{T}}$. We may therefore expect $\tilde{\theta}$ to converge to this null space, but not to the origin.

Suppose instead that $\omega^{\mathsf{T}}(t) = [\sin(t), \cos(t)]$. For each fixed $t$, $\omega^{\mathsf{T}}(t)$ still has a one-dimensional null space. This null space keeps changing with time, however, and the only value of $\tilde{\theta}$ that always ensures $\omega^{\mathsf{T}}(t)\tilde{\theta} = 0$ is $\tilde{\theta} = 0$. Intuitively, it is therefore natural to expect $\tilde{\theta}$ to converge to the origin.

This intuition may be formalized by imposing a *persistency-of-excitation* condition on $\omega(t)$. Specifically, convergence of $\tilde{\theta}$ to the origin is guaranteed if there exist constants $T > 0$ and $\varepsilon > 0$ such that for all $t$,

$$\int_t^{t+T} \omega(\tau)\omega^{\mathsf{T}}(\tau)\,\mathrm{d}\tau \geq \varepsilon I.$$

Persistency-of-excitation conditions are crucial for ensuring parameter convergence for all the methods outlined above. Guaranteeing persistency of excitation can often be difficult, because the condition may depend on external signals that cannot be influenced by the designer.

### Nonlinear Parameterizations

Common to the approaches described above is that they all apply to systems that can be described as linear in the unknown parameters; that is, the parameter vector $\theta$ appears linearly on the right-hand side of (1.1). Techniques for handling nonlinear parameterizations are much less well-developed. State and parameter estimation for nonlinearly parameterized systems is one of the topics of this thesis, and this issue is further discussed in Section 1.3.2.

## 1.3 Topics of This Thesis

The thesis is divided into three parts, each of which deals with a particular topic within state and parameter estimation for nonlinear and uncertain systems. These three parts are discussed in the following sections.

### 1.3.1 Part I: State and Parameter Estimation for Automotive Vehicles

A longstanding trend in the automotive industry is the inclusion of increasingly advanced safety systems in passenger cars. For example, modern cars are typically equipped with an anti-lock braking system (ABS), which prevents the wheels from locking during hard braking, and many cars come with an electronic stability control system (ESC), which stabilizes the lateral motion of the car to prevent skidding. Other examples of automotive safety applications are collision warning and avoidance, rollover prevention, and crosswind compensation.

These safety systems all rely on information about the current state of the vehicle and its surroundings, and to retrieve this information a vehicle must be equipped with a set of sensors. A car with an ESC system is typically equipped with sensors for measuring the longitudinal and lateral accelerations, the steering wheel angle, the wheel speeds, and the rate of rotation around the car's vertical axis, known as the *yaw rate*.

#### Vehicle Sideslip Angle

For a car driving on a horizontal surface, the essential quantities describing its lateral motion are the yaw rate $\dot{\psi}$ and the *vehicle sideslip angle* $\beta$, which is the angle between the orientation of the vehicle and the direction of travel. The yaw rate and the vehicle sideslip angle are illustrated in Figure 1.1. Unlike the yaw rate, the vehicle sideslip angle is not measured in a standard ESC-type sensor configuration, because this would require expensive equipment that is difficult to maintain, such as optical correlation sensors. The vehicle sideslip angle must therefore be estimated based on the measurements that are available.

During normal operation of a passenger car, the vehicle sideslip angle rarely exceeds $\pm 2^\circ$ (van Zanten, 2000), and the vehicle's lateral dynamics can be described with a high degree of accuracy by a linear single-track model that is exponentially stable (see, e.g., Kiencke and Nielsen (2000) and Chapter 7 of this thesis). The linear behavior is a result of the linearity of the friction forces between each tire and the road surface with respect to the *tire-slip angle*, that is, the angle between the orientation of the tire and the direction of travel at the center of the tire. As long as the vehicle behaves according to the linear single-track model, estimation of the vehicle sideslip angle is relatively straightforward. The difficulty arises when the vehicle is pushed to the point where, by purpose or by accident, the tires begin to lose their grip on the road surface. In this case, the road-tire friction forces saturate as a function of the tire-slip angles, leading to highly nonlinear behavior. The vehicle sideslip angle may become very high, in some cases well exceeding $90^\circ$. Such situations are typically dangerous to the occupants of the vehicle.

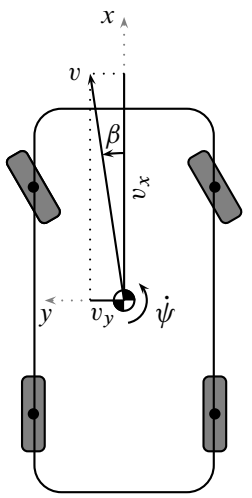


**Figure 1.1:** Illustration of the vehicle velocity, yaw rate, and vehicle sideslip angle. The vehicle velocity vector $v$ at the center of gravity is decomposed into the longitudinal velocity $v_x$ and the lateral velocity $v_y$. The angle $\beta$ between the longitudinal $x$-axis and the velocity vector $v$ is the vehicle sideslip angle. The rate of rotation around the vertical axis, known as the yaw rate, is denoted by $\dot{\psi}$.

### Goal of Part I

Many algorithms have been developed for estimating the vehicle sideslip angle. A majority of these, including those presented by van Zanten (2000); Farrelly and Wellstead (1996); Fukada (1999); Venhovens and Naab (1999); Ungoren, Peng, and Tseng (2004); Kiencke and Daiß (1997); Kiencke and Nielsen (2000); Hiemer, von Vietinghoff, Kiencke, and Matsunaga (2005); von Vietinghoff, Hiemer, and Kiencke (2005); von Vietinghoff, Olbrich, and Kiencke (2007); Suissa, Zomotor, and Böttiger (1994); Ray (1997); Best, Gordon, and Dixon (2000); Lee (2006); Hac and Simpson (2000), are based on a vehicle model—as opposed to a purely kinematic model—usually including a road-tire friction model. To yield satisfactory results, designs based on a road-tire friction model must contend with the nonlinear characteristics of the road-tire friction forces when the tires lose road grip. What is generally missing from the literature, however, is explicit stability analysis in light of this nonlinearity. Furthermore, most designs are based on the EKF, which has the drawback of being computationally complex. The issue

of computational complexity is relevant because the ultimate goal of designing a vehicle sideslip observer is implementation in production vehicles—typically on fixed-point processors with limited computational capacity.

The goal of Part I is to develop a vehicle sideslip observer based on a standard ESC-type sensor configuration with particular focus on the two issues mentioned above, namely, explicit nonlinear analysis and a reduction of computational complexity compared to the EKF. Toward this end, an observer is designed to estimate the longitudinal velocity $v_x$ and lateral velocity $v_y$, so that the vehicle sideslip angle $\beta$ can be calculated using the expression $\beta = \arctan(v_y/v_x)$. To aid the estimation of the longitudinal and lateral velocities, estimates of the *inclination* and *bank angles*, as well as a *friction parameter*, are also introduced. The term inclination angle refers to the road sloping upward or downward along the orientation of the vehicle; bank angle refers to the road sloping toward the left or the right. The friction parameter is introduced to account for variations in the road surface conditions and the tire properties.

The observer is tested on using measurements from production passenger cars, and the results are compared to an EKF similar to that of Suissa et al. (1994).

### Organization

Part I is composed of three chapters that are organized as follows:

- Chapter 2 consists of the article Grip, Imsland, Johansen, Kalkkuhl, and Suissa (2009b) from *IEEE Control Systems Magazine*. This chapter gives an overview of the full estimation algorithm.

- Chapter 3 consists of the article Grip, Imsland, Johansen, Fossen, Kalkkuhl, and Suissa (2008a) from *Automatica*. This chapter gives an in-depth presentation and analysis of the algorithm for estimating the road-tire friction parameter.

- Chapter 4 consists of the article Grip, Imsland, Johansen, Kalkkuhl, and Suissa (2009a) from the *Proceedings of the American Control Conference*. This chapter presents additional details about the algorithm for estimating the inclination and bank angles.

There is a significant degree of overlap between the three chapters in Part I, in particular, between Chapter 2 and each of the other two chapters. The emphasis in each of the three chapters is nevertheless different.

Because the chapters consist of reprinted articles, there are some differences in notation. For example, the symbol $\dot{\psi}$ is used to denote the yaw rate in Chapters

2 and 4, whereas the symbol $r$ is used in Chapter 3 to denote the same quantity. Also, the vehicle sideslip angle is defined as $\arctan(v_y/v_x)$ in Chapters 2 and 4, and as $-\arctan(v_y/v_x)$ in Chapter 3.

The results in Part I are based upon on the results reported in Imsland, Johansen, Fossen, Grip, Kalkkuhl, and Suissa (2006), where vehicle sideslip estimation was considered under the assumption of a horizontal road surface and known road-tire friction conditions. Other articles with related results, which have not been included in this thesis, are Grip, Imsland, Johansen, Fossen, Kalkkuhl, and Suissa (2006); Imsland, Grip, Johansen, Fossen, Kalkkuhl, and Suissa (2007a, 2008); Imsland, Johansen, Grip, and Fossen (2007b).

### 1.3.2 Part II: State and Parameter Estimation for Nonlinearly Parameterized Systems

As discussed in Section 1.2, there are well-developed techniques for estimating unknown, constant parameters that appear linearly in the equations of a dynamical system. When such parameters appear nonlinearly, however, fewer options are available. Part II of this thesis considers the case when the system equations are perturbed by some nonlinear function of the state, external time-varying signals, and a set of unknown, constant parameters.

To handle nonlinear parameterizations, one option is to carry out a Lyapunov-based design using a linearization of the perturbation around the current parameter estimate. Such an approach may result in poor results or unstable behavior, as discussed in Annaswamy, Skantze, and Loh (1998) (where this approach is referred to as a gradient-type approach). Another option is to estimate the parameters using an EKF, by considering the unknown parameters as part of the system state. This approach often yields good results; however, stability analysis is difficult. Introducing extra parameters to obtain a linear expression is yet another option, but doing so may increase complexity and affect performance by reducing the convergence rate of the parameter estimates or introducing stricter persistency-of-excitation conditions.

One can find several methods in the literature that are not based on linearizing the problem. In Fomin, Fradkov, and Yakubovich (1981); Ortega (1996), a Lyapunov-based approach is applied to nonlinear parameterizations with a convexity property. Annaswamy et al. (1998) presents a method based on convexity or concavity, which is extended to general nonlinear parameterizations in Loh, Annaswamy, and Skantze (1999). Other results, such as Bošković (1995, 1998); Zhang, Ge, Hang, and Chai (2000), focus on first-order systems with certain fractional parameterizations. Qu (2003) presents an approach for a class of higher-order systems with matrix fractional parameterizations, where an auxiliary esti-

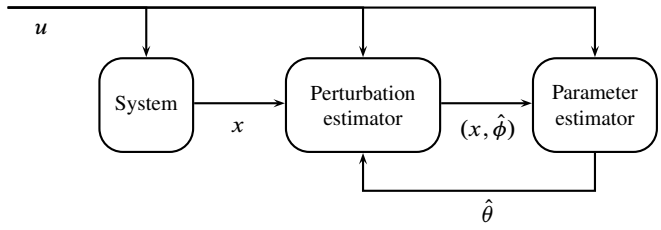


**Figure 1.2:** Illustration of the system structure in the full-state measurement case. The perturbation estimator provides an estimate of the perturbation $\phi = g(t, x, \theta)$ to the parameter estimator, and the parameter estimator inverts the perturbation estimate dynamically with respect to $\theta$. The parameter estimate is in turn fed back to the perturbation estimator, leading to an exponentially stable interconnection.

mate of the full perturbation to the system equations is used in the estimation of the unknown parameters. In Qu, Hull, and Wang (2006), an approach for more general nonlinear parameterizations is presented, where the parameter estimate used in the control law is biased by an appropriately chosen vector function. Tyukin (2003) introduces the idea of *virtual algorithms* that are designed as though the time derivative of measured variables is available, before being transformed into realizable form without explicit differentiation of the measurements. In Tyukin, Prokhorov, and van Leeuwen (2007), this idea is used to design a family of adaptation laws for monotonically parameterized perturbations in the first derivatives.

Whereas the nonlinear methods mentioned above are primarily concerned with controlling the state of a system, Part II of this thesis is primarily concerned with estimation. In particular, the focus is on providing asymptotically exact estimates of the unknown parameters, which can in turn be used for the purpose of control. The focus on exact parameter estimation restricts the class of perturbations that can be handled, by imposing strong persistency-of-excitation conditions. On the other hand, exponential stability of the estimation error is proven through explicit Lyapunov-type analysis in a conceptually simple framework. Whereas the methods mentioned above assume that a full-state measurement is available or that the nonlinearly parameterized perturbation appears in the first-order derivative of the output, the method presented in Part II specifically addresses the case of partial-state measurement, where the nonlinearly parameterized perturbation appears in higher-order derivatives of the output.

### Full-State Measurement

Part II starts by considering the system

$$\dot{x} = f(t,x) + B(t,x)(v(t,x) + \phi), \tag{1.13}$$

where $\phi = g(t,x,\theta)$ is the nonlinearly parameterized perturbation. Everything about this system is presumed known, except the parameter vector $\theta$. Furthermore, the state $x$ is measured. The design is based on the observation that, if the perturbation $\phi = g(t,x,\theta)$ were directly available, then identifying the parameter vector $\theta$ would be a matter of inverting a nonlinear equation. This line of thought leads to a modular design consisting of a *perturbation estimator* and a *parameter estimator*, as illustrated in Figure 1.2. The parameter estimator is designed to dynamically invert the expression $g(t,x,\theta)$ with exponential convergence rate, so that, in the hypothetical case that $\phi = g(t,x,\theta)$ is precisely known, an asymptotically exact parameter estimate is produced. The perturbation estimator is designed to produce an estimate of $\phi$. The two modules are then connected, so that the parameter estimator uses the estimate of $\phi$ provided by the perturbation estimator instead of the actual perturbation. The parameter estimate is in turn fed back to the perturbation estimator. By adjusting the gain of the perturbation estimator, the origin of the error dynamics of the interconnected system is rendered exponentially stable.

The outlined approach is philosophically similar to that of Tyukin (2003); Tyukin et al. (2007), where the idea of virtual algorithms is employed. However, rather than specifying algorithms of a particular form that can be realized without explicit differentiation, the modular approach presented here isolates the task of inverting a nonlinear equation as the main design challenge and gives the designer considerable freedom in how to best accomplish this task. The approach is also similar to Qu (2003), where an auxiliary estimate of the full perturbation is used to estimate unknown parameters that appear in a matrix fractional form. Besides being applicable to a more general class of perturbations, however, the approach presented here makes use of the estimated parameters in the perturbation estimator in a way that renders the overall error dynamics exponentially stable. In Qu (2003), the perturbation is instead approximated in a way that ensures convergence to some arbitrarily small ball around the origin, the size of which depends on the gain.

### Partial-State Measurement

The advantage of the modular design becomes apparent when considering the problem of dealing with a partial-state measurement. In this case, we consider

systems with linear dynamics that are perturbed by a nonlinearly parameterized perturbation, that is,

$$\dot{x} = Ax + Bu + E\phi, \tag{1.14a}$$
$$y = Cx, \tag{1.14b}$$

where $\phi = g(u, y, x, \theta)$, and $u$ is some known, time-varying input signal. The goal in this case is to estimate both the state $x$ and the unknown parameter vector $\theta$. The approach is the same as before, except that the perturbation estimator must be extended to estimate both the perturbation and the state of the system. The perturbation estimator is therefore replaced by a *modified high-gain observer*, which works by extending the state space to include $\phi$ as a state.

The modified high-gain observer is essentially a disturbance observer designed to estimate an unknown input to a linear system, with a modification to make use of the parameter estimate fed back from the parameter estimator. A linear system has a stable inverse with respect to an unknown input if it is left-invertible and minimum-phase (see Moylan, 1977), and these are precisely the conditions that we impose on the linear part of the system. The strategy of estimating unknown perturbations for the purpose of control has recently been employed in the context of performance recovery, for example, in Chakrabortty and Arcak (2009), where the perturbation appears in the first-order derivatives, and in Freidovich and Khalil (2008), where it appears at the end of an integrator chain in a SISO system and is estimated by an *extended high-gain observer*. The modified high-gain observer used in this thesis is closely related to the extended high-gain observer.

### Structural Decomposition

High-gain observer theory typically deals with minimum-phase SISO systems, or square-invertible, minimum-phase systems of uniform relative degree. The theory used to construct the modified high-gain observer in this thesis is based on Saberi and Sannuti (1990), and it encompasses a larger class of left-invertible, minimum-phase systems that are not necessarily of uniform relative degree. As part of the design procedure, the error dynamics is transformed to a *special coordinate basis* (SCB), originally introduced by Sannuti and Saberi (1987). After a linear system has been transformed to the SCB, several fundamental properties are revealed directly by its state-space representation, in particular, its finite and infinite zero structure and its invertibility properties.

Transforming an arbitrary linear system to the SCB is a complicated operation. Numerical software tools have been developed for this purpose (see Chu, Liu, and Tan, 2002; Chen, Lin, and Shamash, 2004) and implemented as part of the

*Linear Systems Toolkit* for *Matlab* (Liu, Chen, and Lin, 2005). However, it is sometimes more practical to deal with systems that have a symbolic representation, at least in the preliminary stages of design. To facilitate the transformation of systems with a symbolic representation to the SCB, Part II introduces a software tool written in the mathematics software suite *Maple*, which transforms general LTI systems represented by symbols or exact fractions to the SCB. This Maple procedure is based on a modified Silverman algorithm (Silverman, 1969) from Sannuti and Saberi (1987).

**Organization**

Part II is composed of three chapters that are organized as follows:

- Chapter 5 consists of the article Grip, Johansen, Imsland, and Kaasa (2010a) from *Automatica*. This chapter deals with parameter estimation for the system (1.13) with full-state measurement, as well as the use of a control input to compensate for the presence of the nonlinearly parameterized perturbation.

- Chapter 6 consists of the article Grip, Saberi, and Johansen (2009c), which is under review in *Systems & Control Letters*. This chapter deals with observer design and parameter estimation for the system (1.14) with partial-state measurement.

- Chapter 7 consists of the article Grip and Saberi (2010), which is due to appear in the *International Journal of Control*. This chapter deals with the use of Maple to transform general multivariable LTI systems to the SCB.

As in Part I, there are some notational inconsistencies between the chapters in Part II. For example, the SCB representation in Chapter 6 is split into three subsystems with state variables $\chi_a$, $\chi_b$, and $\chi_q$, whereas in Chapter 7, the corresponding subsystems are represented by the state variables $x_a$, $x_b$, and $x_d$.

Articles with related results, which have not been included in this thesis, are Grip, Johansen, and Imsland (2008b); Grip and Saberi (2009); Grip, Saberi, and Johansen (2009d).

### 1.3.3 Part III: Estimation and Control for Systems with Saturations

Of the nonlinearities that occur in physical systems, saturations are among the most ubiquitous. Saturations may occur due to the limited capacity of an actuator, limited range of a sensor, or physical limitations within a system. Whereas Parts I and II are primarily concerned with estimation problems, Part III is concerned

with output-feedback control of two types of systems containing saturations. State estimation plays a crucial role in controlling these systems, but control and observer design can in no way be considered separately. The reason for this is that the observability properties of the systems are highly input-dependent; that is, the systems lack the property of being uniformly observable. The results presented in Part III should primarily be viewed as proofs of existence of stabilizing controllers for the respective systems, and not as practical control designs to be implemented it their current form.

### Stabilization of Multiple-Input Multiple-Output Linear Systems with Saturated Outputs

The first problem considered in Part III is global stabilization of multivariable LTI systems with saturated outputs. This problem has previously been considered for SISO systems by Kreisselmeier (1996), and the theory presented here is an extension of those results. The strategy employed by Kreisselmeier (1996) is to drive the output out of saturation using only information about the sign of the output. Once the saturation becomes inactive—if only for a brief interval—the state of the system can be identified in a deadbeat manner. After the state has been identified, a deadbeat controller is used to control the state to the origin.

The obvious extension of this strategy to systems with multiple outputs would be to drive all the outputs simultaneously out of saturation in order to identify the state. However, it is exceedingly difficult, if not impossible, to coordinate multiple outputs so that they become unsaturated at the same time. A different strategy is therefore employed, namely, to deactivate the saturations sequentially. Each output is brought out of saturation at least once, but not necessarily at the same time. Once every output has been out of saturation at least once, the state of the system is identified and controlled to the origin.

### Semiglobal Stabilization of Sandwich Systems by Output Feedback

The second problem considered in Part III is semiglobal stabilization of *sandwich systems* by output-feedback. In this context, a sandwich system refers to the system illustrated in Figure 1.3, consisting of two linear subsystems with a saturation sandwiched between them. A partial-state measurement is available from the second subsystem. The problem of stabilizing this system is related to the problem of stabilizing systems with saturated outputs, because the first subsystem is separated from the output by the saturation. At the same time, it is related to the problem of stabilizing systems with saturated inputs, because the second subsystem is separated from the input by the saturation.

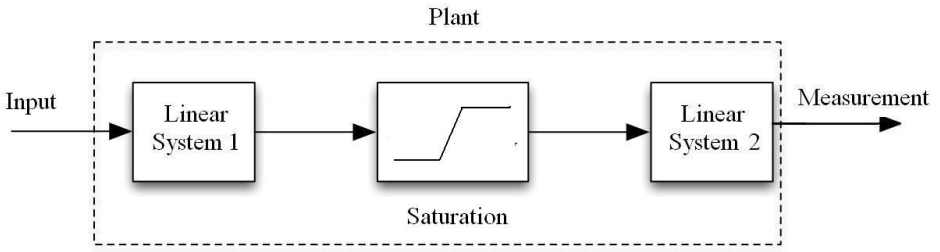


**Figure 1.3:** Sandwich system consisting of two linear subsystems with a saturation sandwiched between them. A partial state measurement is available from the second subsystem.

To handle input saturations, low-gain design methodologies have been developed in Lin and Saberi (1993, 1995); Lin (1999), and these methodologies have been generalized to handle stabilization of sandwich systems by state feedback in Wang, Stoorvogel, Saberi, Grip, Roy, and Sannuti (2009a, 2010b). The results presented here combine the ideas from Kreisselmeier (1996) for stabilization of systems with saturated outputs with those from Wang et al. (2009a, 2010b) for stabilization of sandwich systems by state feedback. Such a combination is not straightforward, however.

The main challenge is that the saturation is separated from the output by a dynamical system; thus, no direct information is available to indicate whether the sandwiched saturation is active or inactive at any given point in time. A crucial part of the control algorithm is therefore a detection scheme to determine whether the saturation is active or inactive. This detection scheme works on time intervals of a freely chosen length, and determines at the end of each interval whether the saturation was active in the positive direction on the entire interval, active in the negative direction on the entire interval, inactive on the entire interval, or both active and inactive on the interval. The interval length must be made sufficiently small depending on the size of an admissible set of initial conditions.

### Organization

Part III is composed of two chapters that are organized as follows:

- Chapter 8 consists of the article Grip, Saberi, and Wang (2010b), which has been accepted for publication in *IEEE Transactions on Automatic Control*. This chapter addresses the problem of stabilizing multivariable linear systems with saturated outputs.

- Chapter 9 consists of the article Grip, Saberi, Stoorvogel, Wang, and Roy (2009e), which will be presented at the *2010 American Control Conference*. This chapter addresses the problem of semiglobal stabilization of sandwich systems by output feedback.

As mentioned above, the results in Chapter 9 are built on the results of Wang et al. (2009a, 2010b) on stabilization of sandwich systems by state feedback. Stabilization of discrete-time sandwich systems by state feedback is treated in Wang, Stoorvogel, Saberi, Grip, and Sannuti (2009b); Wang, Saberi, Stoorvogel, and Grip (2010a).

## 1.4 Publications

For completeness, this section lists my contributions in terms of published and to-be published articles. My main contributions are covered by the following articles.

H. F. Grip, L. Imsland, T. A. Johansen, T. I. Fossen, J. C. Kalkkuhl, and A. Suissa. Nonlinear vehicle velocity observer with road-tire friction adaptation. In *Proc. IEEE Conf. Dec. Contr.*, pages 3603–3608, San Diego, CA, 2006.

H. F. Grip, L. Imsland, T. A. Johansen, T. I. Fossen, J. C. Kalkkuhl, and A. Suissa. Nonlinear vehicle side-slip estimation with friction adaptation. *Automatica*, 44(3):611–622, 2008.

H. F. Grip, T. A. Johansen, and L. Imsland. Estimation and control for systems with nonlinearly parameterized perturbations. In *Proc. IFAC World Congr.*, pages 11178–11183, Seoul, South Korea, 2008.

H. F. Grip, L. Imsland, T. A. Johansen, J. C. Kalkkuhl, and A. Suissa. Estimation of road inclination and bank angle in automotive vehicles. In *Proc. American Contr. Conf.*, pages 426–432, St. Louis, MO, 2009.

H. F. Grip and A. Saberi. Structural decomposition of linear multivariable systems using symbolic computations. In *Proc. Asian Contr. Conf.*, pages 1205–1210, Hong Kong, China, 2009.

H. F. Grip, L. Imsland, T. A. Johansen, J. C. Kalkkuhl, and A. Suissa. Vehicle sideslip estimation: Design, implementation, and experimental validation. *IEEE Contr. Syst. Mag.*, 29(5):36–52, 2009.

H. F. Grip, A. Saberi, and T. A. Johansen. State and parameter estimation for linear systems with nonlinearly parameterized perturbations. In *Proc. IEEE Conf. Dec. Contr.*, pages 8218–8225, Shanghai, China, 2009.

H. F. Grip and A. Saberi. Observer design in the presence of periodic output disturbances by mixing of past and present output data. In *Proc. IEEE Conf. Dec. Contr.*, pages 6101–6106, Shanghai, China, 2009.

H. F. Grip, T. A. Johansen, L. Imsland, and G.-O. Kaasa. Parameter estimation and compensation in systems with nonlinearly parameterized perturbations. *Automatica*, 46(1):19–28, 2010.

H. F. Grip, A. Saberi, and X. Wang. Stabilization of multiple-input multiple-output linear systems with saturated outputs. *IEEE Trans. Automat. Contr.*, 2010. Accepted.

H. F. Grip and A. Saberi. Structural decomposition of linear multivariable systems using symbolic computations. *Int. J. Contr.*, 2010. Accepted.

H. F. Grip, A. Saberi, and T. A. Johansen. Observer design and parameter estimation for linear systems with nonlinearly parameterized perturbations. Submitted to *Syst. Contr. Lett.*, 2009.

H. F. Grip, A. Saberi, A. A. Stoorvogel, X. Wang, and S. Roy. Semiglobal stabilization of sandwich systems by dynamic output feedback. In *Proc. American Contr. Conf.*, Baltimore, MD, 2010.

H. F. Grip and A. Saberi. High-gain domination of nonlinear perturbations: Transformation to a canonical form by dynamic output shaping. Submitted to *IEEE Conf. Dec. Contr.*, Atlanta, GA, 2010.

I have also contributed to the results covered by the following articles. My specific contributions are outlined below the articles.

L. Imsland, T. A. Johansen, T. I. Fossen, H. F. Grip, J. C. Kalkkuhl, and A. Suissa. Vehicle velocity estimation using nonlinear observers. *Automatica*, 42(12):2091–2103, 2006.

*My contributions to this article include the development of a gain-selection scheme for longitudinal velocity estimation; tuning, simulation, and experimental testing; smaller contributions to the theoretical analysis; and general discussion.*

L. Imsland, H. F. Grip, T. A. Johansen, T. I. Fossen, J. C. Kalkkuhl, and A. Suissa. Nonlinear observer for vehicle velocity with friction and road bank angle adaptation—Validation and comparison with an extended Kalman filter. In *Proc. SAE World Congr.*, Detroit, MI, 2007. Paper no. 2007-01-0808.

L. Imsland, H. F. Grip, T. A. Johansen, T. I. Fossen, J. C. Kalkkuhl, and A. Suissa. Nonlinear observer for vehicle velocity with friction and road bank angle adaptation—Validation and comparison with an extended Kalman filter. In A. C. Alkidas and D. C. Siegla, editors, *SAE 2007 Transactions Journal of Passenger Cars: Mechanical Systems*, pages 722–734. SAE, Warrendale, PA, 2008.

*The two foregoing articles are based on a friction-estimation algorithm that was developed as part of my MSc degree. Beyond this, my contributions to these articles include participation in developing the bank-angle estimation algorithm; tuning, simulation, and experimental testing; visiting Daimler in Germany to test the computational complexity of the estimation algorithm; and active involvement in all aspects of the underlying sideslip estimation project.*

L. Imsland, T. A. Johansen, H. F. Grip, and T. I. Fossen. On nonlinear unknown input observers—Applied to lateral vehicle velocity estimation on banked roads. *Int. J. Contr.*, 80(11):1741–1750, 2007.

*My contributions to this article include participation in developing the bank-angle estimation algorithm; tuning, testing, and simulation; and discussion regarding the theoretical content.*

X. Wang, A. A. Stoorvogel, A. Saberi, H. F. Grip, S. Roy, and P. Sannuti. Stabilization of a class of sandwich nonlinear systems via state feedback. In *Proc. IEEE Conf. Dec. Contr.*, pages 1417–1421, Shanghai, China, 2009.

X. Wang, A. A. Stoorvogel, A. Saberi, H. F. Grip, S. Roy, and P. Sannuti. Stabilization of a class of sandwich systems via state feedback. *IEEE Trans. Automat. Contr.*, 2010. Accepted.

X. Wang, A. A. Stoorvogel, A. Saberi, H. F. Grip, and P. Sannuti. Stabilization of nonlinear sandwich systems via state feedback—Discrete-time systems. Submitted to *Int. J. Robust Nonlin. Contr.*, 2009.

X. Wang, A. Saberi, A. A. Stoorvogel, and H. F. Grip. Stabilization of discrete-time sandwich systems with low-and-high gain feedback design. Submitted to *IEEE Conf. Dec. Contr.*, Atlanta, GA, 2010.

*My contributions to the four foregoing articles include discussion and collaboration in developing the details of the theoretical content; the development of simulation examples; and work on the written presentation of the material.*

## Bibliography

A. M. Annaswamy, F. P. Skantze, and A.-P. Loh. Adaptive control of continuous time systems with convex/concave parametrization. *Automatica*, 34(1):33–49, 1998.

M. Arcak and P. Kokotović. Nonlinear observers: a circle criterion design and robustness analysis. *Automatica*, 37(12):1923–1930, 2001.

K. J. Åström and B. Wittenmark. *Adaptive Control*. Addison-Wesley, Reading, MA, 2nd edition, 1995.

I. Barbălat. Systèmes d'équations différentielles d'oscillations non linéaires. *Rev. Math. Pures Appl.*, 4(2):267–270, 1959.

M. C. Best, T. J. Gordon, and P. J. Dixon. An extended adaptive Kalman filter for real-time state estimation of vehicle handling dynamics. *Vehicle Syst. Dyn.*, 34 (1):57–75, 2000.

J. D. Bošković. Stable adaptive control of a class of first-order nonlinearly parameterized plants. *IEEE Trans. Automat. Contr.*, 40(2):347–350, 1995.

J. D. Bošković. Adaptive control of a class of nonlinearly parameterized plants. *IEEE Trans. Automat. Contr.*, 43(7):930–934, 1998.

R. G. Brown and P. Y. C. Hwang. *Introduction to Random Signals and Applied Kalman Filtering*. Wiley, New York, 3rd edition, 1997.

A. Chakrabortty and M. Arcak. Time-scale separation redesigns for stabilization and performance recovery of uncertain nonlinear systems. *Automatica*, 45(1): 34–44, 2009.

B. M. Chen, Z. Lin, and Y. Shamash. *Linear Systems Theory: A Structural Decomposition Approach*. Birkhäuser, Boston, 2004.

C.-T. Chen. *Linear System Theory and Design*. Oxford University Press, New York, 3rd edition, 1999.

J. Chen, R. J. Patton, and H.-Y. Zhang. Design of unknown input observers and robust fault detection filters. *Int. J. Contr.*, 63(1):85–105, 1996.

D. Chu, X. Liu, and R. C. E. Tan. On the numerical computation of a structural decomposition in systems and control. *IEEE Trans. Automat. Contr.*, 47(11): 1786–1799, 2002.

M. Darouach, M. Zasadzinski, and S. Xu. Full-order observers for linear systems with unknown inputs. *IEEE Trans. Automat. Contr.*, 39(3):606–609, 1994.

F. Esfandiari and H. K. Khalil. Observer-based design of uncertain systems: Recovering state feedback robustness under matching conditions. In *Proc. Allerton Conf.*, pages 97–106, Monticello, IL, 1987.

X. Fan and M. Arcak. Observer design for systems with multivariable monotone nonlinearities. *Syst. Contr. Lett.*, 50(4):319–330, 2003.

J. Farrelly and P. Wellstead. Estimation of vehicle lateral velocity. In *Proc. IEEE Int. Conf. Contr. Appl.*, pages 552–557, Dearborn, MI, 1996.

V. Fomin, A. Fradkov, and V. Yakubovich, editors. *Adaptive Control of Dynamical Systems*. Nauka, Moskow, 1981.

L. B. Freidovich and H. K. Khalil. Performance recovery of feedback-linearization-based designs. *IEEE Trans. Automat. Contr.*, 53(10):2324–2334, 2008.

Y. Fukada. Slip-angle estimation for vehicle stability control. *Vehicle Syst. Dyn.*, 32(4):375–388, 1999.

J. P. Gauthier and G. Bornard. Observability for any $u(t)$ of a class of nonlinear systems. *IEEE Trans. Automat. Contr.*, 26(4):922–926, 1981.

J.-P. Gauthier and I. Kupka. *Deterministic Observation Theory and Applications*. Cambridge University Press, Cambridge, United Kingdom, 2001.

M. S. Grewal and A. P. Andrews. *Kalman Filtering: Theory and Practice*. Wiley, New York, 2nd edition, 2001.

H. F. Grip and A. Saberi. Structural decomposition of linear multivariable systems using symbolic computations. In *Proc. Asian Contr. Conf.*, pages 1205–1210, Hong Kong, China, 2009.

H. F. Grip and A. Saberi. Structural decomposition of linear multivariable systems using symbolic computations. *Int. J. Contr.*, 2010. Accepted.

H. F. Grip, L. Imsland, T. A. Johansen, T. I. Fossen, J. C. Kalkkuhl, and A. Suissa. Nonlinear vehicle velocity observer with road-tire friction adaptation. In *Proc. IEEE Conf. Dec. Contr.*, pages 3603–3608, San Diego, CA, 2006.

H. F. Grip, L. Imsland, T. A. Johansen, T. I. Fossen, J. C. Kalkkuhl, and A. Suissa. Nonlinear vehicle side-slip estimation with friction adaptation. *Automatica*, 44 (3):611–622, 2008a.

H. F. Grip, T. A. Johansen, and L. Imsland. Estimation and control for systems with nonlinearly parameterized perturbations. In *Proc. IFAC World Congr.*, pages 11178–11183, Seoul, South Korea, 2008b.

H. F. Grip, L. Imsland, T. A. Johansen, J. C. Kalkkuhl, and A. Suissa. Estimation of road inclination and bank angle in automotive vehicles. In *Proc. American Contr. Conf.*, pages 426–432, St. Louis, MO, 2009a.

H. F. Grip, L. Imsland, T. A. Johansen, J. C. Kalkkuhl, and A. Suissa. Vehicle sideslip estimation: Design, implementation, and experimental validation. *IEEE Contr. Syst. Mag.*, 29(5):36–52, 2009b.

H. F. Grip, A. Saberi, and T. A. Johansen. Observer design and parameter estimation for linear systems with nonlinearly parameterized perturbations. Submitted to *Syst. Contr. Lett.*, 2009c.

H. F. Grip, A. Saberi, and T. A. Johansen. State and parameter estimation for linear systems with nonlinearly parameterized perturbations. In *Proc. IEEE Conf. Dec. Contr.*, pages 8218–8225, Shanghai, China, 2009d.

H. F. Grip, A. Saberi, A. A. Stoorvogel, X. Wang, and S. Roy. Semiglobal stabilization of sandwich systems by dynamic output feedback. In *Proc. American Contr. Conf.*, Baltimore, MD, 2009e.

H. F. Grip, T. A. Johansen, L. Imsland, and G.-O. Kaasa. Parameter estimation and compensation in systems with nonlinearly parameterized perturbations. *Automatica*, 46(1):19–28, 2010a.

H. F. Grip, A. Saberi, and X. Wang. Stabilization of multiple-input multiple-output linear systems with saturated outputs. *IEEE Trans. Automat. Contr.*, 2010b. Accepted.

A. Hac and M. D. Simpson. Estimation of vehicle side slip angle and yaw rate. In *Proc. SAE World Congr.*, Detroit, MI, 2000. Paper no. 2000-01-0696.

J. K. Hale. *Theory of Functional Differential Equations*. Springer-Verlag, New York, 1977.

S. Hara, Y. Yamamoto, T. Omata, and M. Nakano. Repetitive control system: A new type servo system for periodic exogenous signals. *IEEE Trans. Automat. Contr.*, 33(7):659–668, 1988.

M. Hiemer, A. von Vietinghoff, U. Kiencke, and T. Matsunaga. Determination of the vehicle body slip angle with non-linear observer strategies. In *Proc. SAE World Congr.*, Detroit, MI, 2005. Paper no. 2005-01-0400.

L. Imsland, T. A. Johansen, T. I. Fossen, H. F. Grip, J. C. Kalkkuhl, and A. Suissa. Vehicle velocity estimation using nonlinear observers. *Automatica*, 42(12): 2091–2103, 2006.

L. Imsland, H. F. Grip, T. A. Johansen, T. I. Fossen, J. C. Kalkkuhl, and A. Suissa. Nonlinear observer for vehicle velocity with friction and road bank angle adaptation—Validation and comparison with an extended Kalman filter. In *Proc. SAE World Congr.*, Detroit, MI, 2007a. Paper no. 2007-01-0808.

L. Imsland, T. A. Johansen, H. F. Grip, and T. I. Fossen. On nonlinear unknown input observers—Applied to lateral vehicle velocity estimation on banked roads. *Int. J. Contr.*, 80(11):1741–1750, 2007b.

L. Imsland, H. F. Grip, T. A. Johansen, T. I. Fossen, J. C. Kalkkuhl, and A. Suissa. Nonlinear observer for vehicle velocity with friction and road bank angle adaptation—Validation and comparison with an extended Kalman filter. In A. C. Alkidas and D. C. Siegla, editors, *SAE 2007 Transactions Journal of Passenger Cars: Mechanical Systems*, pages 722–734. SAE, Warrendale, PA, 2008.

P. A. Ioannou and J. Sun. *Robust Adaptive Control*. Prentice-Hall, Upper Saddle River, NJ, 1996.

H. Khalil and F. Esfandiari. Semiglobal stabilization of a class of nonlinear systems using output feedback. *IEEE Trans. Automat. Contr.*, 38(9):1412–1415, 1993.

H. K. Khalil. *Nonlinear Systems*. Prentice-Hall, Upper Saddle River, NJ, 3rd edition, 2002.

U. Kiencke and A. Daiß. Observation of lateral vehicle dynamics. *Contr. Eng. Pract.*, 5(8):1145–1150, 1997.

U. Kiencke and L. Nielsen. *Automotive Control Systems: For Engine, Driveline, and Vehicle*. Springer, Berlin, 2000.

G. Kreisselmeier. Stabilization of linear systems in the presence of output measurement saturation. *Syst. Contr. Lett.*, 29(1):27–30, 1996.

M. Krstić, I. Kanellakopoulos, and P. V. Kokotović. *Nonlinear and Adaptive Control Design*. Wiley, New York, 1995.

H. Lee. Reliability indexed sensor fusion and its application to vehicle velocity estimation. *J. Dyn. Syst. Meas. Contr.*, 128(2):236–243, 2006.

Z. Lin. *Low gain feedback*, volume 240 of *Lecture Notes in Contr. Inform. Sci.* Springer, Berlin, 1999.

Z. Lin and A. Saberi. Semi-global exponential stabilization of linear systems subject to "input saturation" via linear feedbacks. *Syst. Contr. Lett.*, 21(3):225–239, 1993.

Z. Lin and A. Saberi. Semi-global exponential stabilization of linear discrete-time systems subject to input saturation via linear feedbacks. *Syst. Contr. Lett.*, 24 (2):125–132, 1995.

X. Liu, B. M. Chen, and Z. Lin. Linear systems toolkit in Matlab: Structural decompositions and their applications. *J. Contr. Theor. Appl.*, 3(3):287–294, 2005.

A.-P. Loh, A. M. Annaswamy, and F. P. Skantze. Adaptation in the presence of a general nonlinear parameterization: An error model approach. *IEEE Trans. Automat. Contr.*, 44(9):1634–1652, 1999.

R. Marino and P. Tomei. *Nonlinear Control Design: Geometric, Adaptive and Robust*. Prentice-Hall, Upper Saddle River, NJ, 1995.

P. J. Moylan. Stable inversion of linear systems. *IEEE Trans. Automat. Contr.*, 22 (1):74–78, 1977.

H. Nijmeijer and A. van der Schaft. *Nonlinear Dynamical Control Systems*. Springer-Verlag, New York, 1990.

R. Ortega. Some remarks on adaptive neuro-fuzzy systems. *Int. J. Adapt. Contr. Signal Process.*, 10(1):79–83, 1996.

Z. Qu. Adaptive and robust controls of uncertain systems with nonlinear parameterization. *IEEE Trans. Automat. Contr.*, 48(10):1817–1823, 2003.

Z. Qu, R. A. Hull, and J. Wang. Globally stabilizing adaptive control design for nonlinearly-parametrized systems. *IEEE Trans. Automat. Contr.*, 51(6):1073–1079, 2006.

L. R. Ray. Nonlinear tire force estimation and road friction identification: Simulation and experiments. *Automatica*, 33(10):1819–1833, 1997.

K. Reif, S. Günther, E. Yaz, and R. Unbehauen. Stochastic stability of the discrete-time extended Kalman filter. *IEEE Trans. Automat. Contr.*, 44(4):714–728, 1999.

A. Saberi and P. Sannuti. Observer design for loop transfer recovery and for uncertain dynamical systems. *IEEE Trans. Automat. Contr.*, 35(8):878–897, 1990.

A. Saberi, B. M. Chen, and P. Sannuti. *Loop Transfer Recovery: Analysis and Design*. Springer, London, 1993.

A. Saberi, A. A. Stoorvogel, and P. Sannuti. *Filtering Theory*. Birkhäuser, Boston, 2006.

P. Sannuti and A. Saberi. Special coordinate basis for multivariable linear systems—Finite and infinite zero structure, squaring down and decoupling. *Int. J. Contr.*, 45(5):1655–1704, 1987.

L. M. Silverman. Inversion of multivariable linear systems. *IEEE Trans. Automat. Contr.*, 14(3):270–276, 1969.

A. Suissa, Z. Zomotor, and F. Böttiger. Method for determining variables characterizing vehicle handling. US Patent 5,557,520, 1994. Filed Jul. 29, 1994; issued Sep. 17, 1996.

A. Teel and L. Praly. Global stabilizability and observability imply semi-global stabilizability by output feedback. *Syst. Contr. Lett.*, 22(5):313–325, 1994.

H. L. Trentelman, A. A. Stoorvogel, and M. L. J. Hautus. *Control Theory for Linear Systems*. Springer, London, 2001.

I. Y. Tyukin. Adaptation algorithms in finite form for nonlinear dynamic objects. *Autom. Rem. Contr.*, 64(6):951–974, 2003.

I. Y. Tyukin, D. V. Prokhorov, and C. van Leeuwen. Adaptation and parameter estimation in systems with unstable target dynamics and nonlinear parametrization. *IEEE Trans. Automat. Contr.*, 52(9):1543–1559, 2007.

A. Y. Ungoren, H. Peng, and H. E. Tseng. A study on lateral speed estimation methods. *Int. J. Vehicle Auton. Syst.*, 2(1–2):126–144, 2004.

A. T. van Zanten. Bosch ESP systems: 5 years of experience. In *Proc. Automot. Dyn. Stab. Conf.*, Troy, MI, 2000. Paper no. 2000-01-1633.

P. J. T. Venhovens and K. Naab. Vehicle dynamics estimation using Kalman filters. *Vehicle Syst. Dyn.*, 32(2):171–184, 1999.

A. von Vietinghoff, M. Hiemer, and U. Kiencke. Nonlinear observer design for lateral vehicle dynamics. In *Proc. IFAC World Congr.*, pages 988–993, Prague, Czech Republic, 2005.

A. von Vietinghoff, S. Olbrich, and U. Kiencke. Extended Kalman filter for vehicle dynamics determination based on a nonlinear model combining longitudinal and lateral dynamics. In *Proc. SAE World Congr.*, Detroit, MI, 2007. Paper no. 2007-01-0834.

X. Wang, A. A. Stoorvogel, A. Saberi, H. F. Grip, S. Roy, and P. Sannuti. Stabilization of a class of sandwich nonlinear systems via state feedback. In *Proc. IEEE Conf. Dec. Contr.*, pages 1417–1421, Shanghai, China, 2009a.

X. Wang, A. A. Stoorvogel, A. Saberi, H. F. Grip, and P. Sannuti. Stabilization of nonlinear sandwich systems via state feedback—Discrete-time systems. Submitted to *Int. J. Robust Nonlin. Contr.*, 2009b.

X. Wang, A. Saberi, A. A. Stoorvogel, and H. F. Grip. Stabilization of discrete-time sandwich systems with low-and-high gain feedback design. Submitted to *IEEE Conf. Dec. Contr.*, Atlanta, GA, 2010a.

X. Wang, A. A. Stoorvogel, A. Saberi, H. F. Grip, S. Roy, and P. Sannuti. Stabilization of a class of sandwich systems via state feedback. *IEEE Trans. Automat. Contr.*, 2010b. Accepted.

T. Zhang, S. S. Ge, C. C. Hang, and T. Y. Chai. Adaptive control of first-order systems with nonlinear parameterization. *IEEE Trans. Automat. Contr.*, 45(8): 1512–1516, 2000.

# Part I

# State and Parameter Estimation for Automotive Vehicles

# Chapter 2

# Vehicle Sideslip Estimation: Design, Implementation, and Experimental Validation

## 2.1 Introduction

Control systems that help the driver avoid accidents, or limit the damage in case of an accident, have become ubiquitous in modern passenger cars. For example, new cars typically have an anti-lock braking system (ABS), which prevents the wheels from locking during hard braking, and they often have an electronic stability control system (ESC), which stabilizes the lateral motion of the vehicle to prevent skidding. Collision warning and avoidance, rollover prevention, crosswind stabilization, and preparation for an impending accident by adjusting seat positions and seat belts are additional examples of control systems for automotive safety.

These systems rely on information about the state of the vehicle and its surroundings. To obtain this information, modern cars are equipped with various sensors. For a typical car with an ESC system, necessary measurements include the steering wheel angle, wheel angular velocities, lateral acceleration, and the rate of rotation around the vertical body-fixed axis, known as the *yaw rate*. These measurements alone contain a great deal of information about the state of the vehicle. The speed of the car can be estimated using the wheel angular velocities, and a linear reference model taking the speed, steering wheel angle, and additional measurements as inputs can be used to predict the behavior of the car under normal driving conditions. The predicted behavior can be compared to the actual behavior of the car; ESC systems, for example, use the brakes to correct the deviation from a yaw reference model when the vehicle starts to skid (van Zanten, 2000).

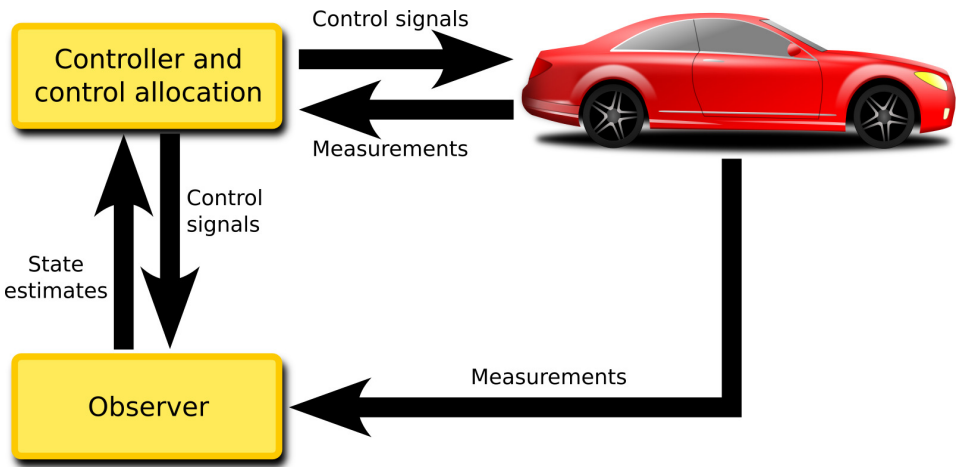


**Figure 2.1:** The relationship between the car, an observer, and a controller with control allocation. The observer combines measurements from the car with a dynamic model, to provide estimates of unmeasured states to the controller.

Although some quantities are easily measured, others are difficult to measure because of high cost or impracticality. When some quantity cannot be measured directly, it is often necessary to estimate it using the measurements that are available. Observers combine the available measurements with dynamic models to estimate unknown dynamic states. Often, dynamic models of sufficient accuracy are not available, and must be carefully constructed as part of the observer design. The observer estimates can be used to implement control algorithms, as Figure 2.1 illustrates.

### 2.1.1 Vehicle Sideslip Angle

When a car is driven straight on a flat surface, the direction of travel at the center of gravity (CG) remains the same as the orientation of the vehicle (that is, the direction of the longitudinal axis). When the car turns, however, it exhibits a yaw rate, causing the orientation to change, and a lateral acceleration directed toward the center of the turn. The car also exhibits a velocity component perpendicular to the orientation, known as the lateral velocity. Nonzero lateral velocity means that the orientation of the vehicle and the direction of travel are no longer the same. The lateral velocity differs from one point on the vehicle body to another; as a point of reference, we use the vehicle's CG.

The angle between the orientation of the vehicle and the direction of travel at the CG is called the *vehicle sideslip angle*. In production cars, the vehicle sideslip angle is not measured, because this measurement requires expensive equipment such as optical correlation sensors. Under normal circumstances, when the car is driven safely without danger of losing road grip, the vehicle sideslip angle is small, not exceeding $\pm 2°$ for the average driver (van Zanten, 2000). Moreover, for a given speed in normal driving situations, the steering characteristics specify a tight connection between the steering wheel angle, yaw rate, lateral acceleration, and vehicle sideslip angle. The vehicle sideslip angle can therefore be estimated using a static model or a simple linear, dynamic model. In extreme situations, however, when the vehicle is pushed to the physical limits of adhesion between the tires and the road surface, the behavior of the car is highly nonlinear, and the tight coupling of the vehicle sideslip angle to various measured quantities is lost. This behavior is due to the nonlinearity of the friction forces between the tires and the road surface. In these situations, the vehicle sideslip angle can become large, and knowledge about it is essential for a proper description of vehicle behavior. Accurate online estimation of the vehicle sideslip angle has the potential to enable development of new automotive safety systems, and to improve existing algorithms that use information about the vehicle sideslip angle, such as ESC.

### 2.1.2 Previous Research

Many designs for estimating velocity and sideslip angle are found in the literature. These designs are typically based on linear or quasi-linear techniques (Farrelly and Wellstead, 1996; Fukada, 1999; Venhovens and Naab, 1999; Ungoren, Peng, and Tseng, 2004). A nonlinear observer linearizing the observer error dynamics is presented in Kiencke and Daiß (1997); Kiencke and Nielsen (2000). An observer based on forcing the dynamics of the nonlinear estimation error to follow the dynamics of a linear reference system is investigated in Hiemer, von Vietinghoff, Kiencke, and Matsunaga (2005); von Vietinghoff, Hiemer, and Kiencke (2005). In Hiemer et al. (2005); von Vietinghoff et al. (2005) availability of the longitudinal road-tire friction forces is assumed, whereas in von Vietinghoff, Olbrich, and Kiencke (2007) the longitudinal forces used in the estimation algorithm are calculated from the brake pressure, clutch position, and throttle angle. An extended Kalman filter (EKF) based on a road-tire friction model, which includes estimation of a road-tire friction coefficient, the inclination angle, and the bank angle, is developed in Suissa, Zomotor, and Böttiger (1994). The term inclination angle refers to the road sloping upward or downward along the orientation of the vehicle; bank angle refers to the road sloping toward the left or the right. Alternative EKFs are used in Ray (1997), which estimates velocity and tire forces without the explicit

use of a road-tire friction model; and in Best, Gordon, and Dixon (2000), which is based on a linear model of the road-tire friction forces with online estimation of road-tire friction parameters. In Lee (2006) a linear observer for the vehicle velocity is used as an input to a Kalman filter based on the kinematic equations of motion. In Hac and Simpson (2000) the sideslip angle is estimated along with both the yaw rate and a road-tire friction coefficient without the use of a yaw rate measurement.

A majority of designs, including van Zanten (2000); Farrelly and Wellstead (1996); Fukada (1999); Venhovens and Naab (1999); von Vietinghoff et al. (2005, 2007); Ungoren et al. (2004); Kiencke and Daiß (1997); Kiencke and Nielsen (2000); Hiemer et al. (2005); Suissa et al. (1994); Ray (1997); Best et al. (2000); Lee (2006); Hac and Simpson (2000), are based on a vehicle model, usually including a model of the road-tire friction forces. The main argument against using such a model is its inherent uncertainty. Changes in the loading of the vehicle and the tire characteristics, for example, introduce unknown variations in the model. A different direction is taken in Klier, Reim, and Stapel (2008), where a six-degree-of-freedom inertial sensor cluster is used in an EKF that relies mainly on open-loop integration of the kinematic equations, without a vehicle or friction model. The main measurement equation comes from the longitudinal velocity, which is calculated separately based primarily on the wheel speeds. This idea is similar to the kinematic observer approach in Farrelly and Wellstead (1996). Designs of this type are sensitive to unknown *sensor bias* and *drift*, as well as misalignment of the sensor cluster. Sensor bias refers to a constant error in the measurement signal; drift refers to a slowly varying error. Drift in inertial sensors is primarily caused by variations in temperature.

To estimate the vehicle sideslip angle in real-world situations, some information about the surroundings of the vehicle is usually needed. In particular, the road bank angle has a significant effect on the lateral velocity. Furthermore, when a design includes modeling of the road-tire friction forces, as in van Zanten (2000); Farrelly and Wellstead (1996); Fukada (1999); Venhovens and Naab (1999); Ungoren et al. (2004); Kiencke and Daiß (1997); Kiencke and Nielsen (2000); Hiemer et al. (2005); von Vietinghoff et al. (2005, 2007); Suissa et al. (1994); Best et al. (2000); Hac and Simpson (2000), information about the road surface conditions is needed. When estimating the longitudinal velocity, knowledge of the inclination angle is useful when the wheel speeds fail to provide high-quality information. Some model-based designs, such as Fukada (1999); Ungoren et al. (2004); Suissa et al. (1994); Ray (1997); Best et al. (2000); Hac and Simpson (2000), take unknown road surface conditions into account, but it is more commonly assumed that the road surface conditions are known, or that the vehicle is driven in a way that minimizes the impact of the road surface conditions. Similarly, although a hor-

izontal road surface is typically assumed, Fukada (1999); Ungoren et al. (2004); Suissa et al. (1994); Klier et al. (2008) consider inclination and bank angles. Estimation of the road bank angle is considered in Tseng (2001), which is based on transfer functions from the steering angle and road bank angle to the yaw rate and lateral acceleration, and in Sentouh, Sebsadji, Mammar, and Glaser (2007), which uses an EKF to estimate the sideslip angle, which is in turn used in a linear unknown-input observer to estimate the road bank angle.

Inertial measurements are combined with GPS measurements in Ryu and Gerdes (2004); Bevly, Gerdes, and Wilson (2002); Bevly (2004); Bevly, Ryu, and Gerdes (2006); Farrell (2008) to provide estimates of the sideslip angle. Designs of this type often include estimates of the bank angle and inclination angle.

### 2.1.3 Goal of This Article

The goal of this article is to develop a vehicle sideslip observer that takes the nonlinearities of the system into account, both in the design and theoretical analysis. Design goals include a reduction of computational complexity compared to the EKF in order to make the observer suitable for implementation in embedded hardware, and a reduction in the number of tuning parameters compared to the EKF. The design is based on a standard sensor configuration, and is subjected to extensive testing in realistic conditions.

Parts of the theoretical foundation for the observer design, as well as some preliminary experimental results, are found in Imsland, Johansen, Fossen, Grip, Kalkkuhl, and Suissa (2006), which assumes known road-tire friction properties and a horizontal road surface, and in Grip, Imsland, Johansen, Fossen, Kalkkuhl, and Suissa (2008), where the approach from Imsland et al. (2006) is extended to take unknown road surface conditions into account. In Imsland, Grip, Johansen, Fossen, Kalkkuhl, and Suissa (2007a) a comparison is made between an EKF and an observer modified from Imsland et al. (2006); Grip et al. (2008), with an added algorithm for bank-angle estimation developed in Imsland, Johansen, Grip, and Fossen (2007b). In the present article, we extend the approach of Imsland et al. (2006); Grip et al. (2008) by estimating the inclination and bank angles. We refer to the resulting observer as the *nonlinear vehicle sideslip observer* (NVSO). The NVSO has undergone extensive and systematic testing in a variety of situations. Tests have been performed on both test tracks and normal roads, on high- and low-friction surfaces, and with significant inclination and bank angles. Based on the results of this testing, we discuss strengths and weaknesses of the NVSO design, as well as practical implementation and tuning. We compare the experimental results with those of an EKF. Since much of the discussion concerns modeling accuracy, observability, and constraints imposed by the sensor configuration, the results and

observations are applicable in a wider sense to alternative model-based designs with similar sensor configurations.

### 2.1.4 Sensor Configuration

A crucial design consideration in estimation problems of this type is the choice of sensor configuration. Typical automotive-grade sensor configurations are characterized by the need to minimize costs, which often translates into sensors with low resolution, narrow range, and significant noise, bias, and drift. The availability and quality of sensors place fundamental constraints on the accuracy that can be expected from any estimation scheme. Bias and drift in inertial sensors is particularly limiting, because it prohibits accurate integration of kinematic equations, except over short time spans.

We focus on a standard sensor configuration found in modern cars with an ESC system, consisting of measurements of the longitudinal and lateral accelerations, the yaw rate, the steering wheel angle, and the wheel speeds. Although GPS measurements would be a valuable addition to the measurements mentioned above, GPS navigation systems are not yet standard equipment, even in high-end passenger cars. Moreover, GPS signals are sometimes unavailable or degraded, for example, when driving through tunnels, under bridges, or near large structures such as steep mountains or tall buildings. We therefore do not consider GPS measurements to be available.

The ESC-type sensor configuration lacks measurements of the vertical acceleration and the angular rates around the vehicle's longitudinal and lateral axes, known as the *roll* and *pitch rates*, respectively. In addition, ESC-type sensors may have significant bias and drift, which prohibits a design based exclusively on kinematic equations, such as Klier et al. (2008). We therefore supplement the kinematic equations with a vehicle model that includes a model of the road-tire friction forces.

## 2.2 Vehicle Model

For a car driving on a horizontal surface, the longitudinal and lateral velocities at the CG are governed by the equations of motion (Kiencke and Nielsen, 2000)

$$\dot{v}_x = a_x + \dot{\psi} v_y, \tag{2.1}$$

$$\dot{v}_y = a_y - \dot{\psi} v_x, \tag{2.2}$$

where $v_x$ and $v_y$ are the longitudinal and lateral velocities, $a_x$ and $a_y$ are the longitudinal and lateral accelerations, and $\dot{\psi}$ is the yaw rate. Each of the equations

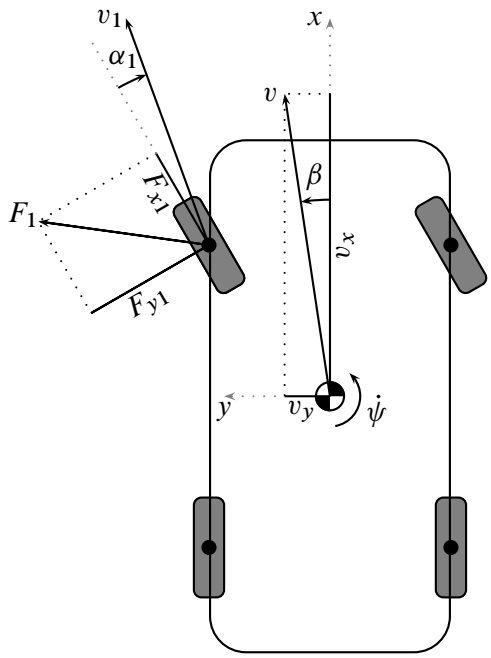


**Figure 2.2:** Illustration of the vehicle velocity, yaw rate, vehicle sideslip angle, tire-slip angle, and road-tire friction forces. The vehicle velocity vector $v$ at the CG is decomposed into the longitudinal velocity $v_x$, which is positive in the forward direction, and the lateral velocity $v_y$, which is positive in the leftward direction. The angle $\beta$ between the longitudinal $x$-axis and the velocity vector $v$ is the vehicle sideslip angle, which is defined as positive in the counterclockwise direction. For the front left wheel, the velocity vector $v_1$ at the wheel center is shown. The angle $\alpha_1$ between $v_1$ and the longitudinal axis of the tire is the tire-slip angle, which is defined as positive in the clockwise direction. The positive tire-slip angle shown in the figure generates a positive lateral tire force $F_{y1}$. The longitudinal tire force $F_{x1}$ is generated by a nonzero longitudinal tire slip. Together, $F_{x1}$ and $F_{y1}$ make up the tire force vector $F_1$. Similar road-tire friction forces are also generated for the other three tires.

(2.1), (2.2) includes an acceleration term and a term involving the yaw rate $\dot{\psi}$. The accelerations are directly related to the forces acting on the vehicle, attributable mainly to road-tire friction. The terms involving the yaw rate appear because the coordinate system in which we resolve the velocities and accelerations is fixed to the car, which rotates with respect to an inertial coordinate system. The vehicle is illustrated in Figure 2.2, where the velocities and yaw rate are shown together with the vehicle sideslip angle $\beta$, which is given as $\beta = \arctan(v_y/v_x)$.

### 2.2.1 Road-Tire Friction

When the driver turns the steering wheel to make a regular turn, the tires on the front axle of the car become misaligned with the direction of travel, and we obtain a *tire-slip angle*. The tire-slip angle is conceptually similar to the vehicle sideslip angle, except that the relevant frame of reference is associated with a single tire rather than the vehicle body. In particular, the tire-slip angle is defined as the angle between the velocity vector at the center of the wheel and the orientation of the tire. This definition is illustrated for the front left wheel in Figure 2.2, where $\alpha_1$ denotes the tire-slip angle. A nonzero tire-slip angle implies a nonzero velocity in the lateral direction of the tire, relative to the road surface. Because the tire is elastic, however, it does not simply slide laterally over the road surface. As a point on the tire tread rolls into contact with the surface, its path is deflected and it briefly grips the surface as it passes through the contact patch. This process results in a deformation of the tire, and the tire's resistance to this deformation generates lateral forces that lead the car to start turning (Haney, 2003, Ch. 6). As the car starts to turn, tire-slip angles are also built up for the rear tires. After an initial transient, a steady state is reached where the road-tire friction forces balance to give zero net moment on the vehicle body, as well as constant lateral acceleration and lateral velocity.

We also define the longitudinal tire slip, as the normalized difference between the circumferential speed of the tire and the speed of the wheel center along the orientation of the tire. Longitudinal tire slip gives rise to longitudinal friction forces, as illustrated in Figure 2.2 by $F_{x1}$. Collectively, we refer to the longitudinal tire slip and lateral tire-slip angle as the tire slips.

During normal driving the road-tire friction forces are approximately linear with respect to the tire slips. The lateral friction forces are then modeled as $F_{y1} = C_y\alpha_1$, where the constant $C_y$ is the *cornering stiffness*. In extreme situations, however, the tire slips may become so large that this linearity is lost. Beyond a certain point, the tire loses road grip and the road-tire friction forces begin to saturate, meaning that an increase in the tire slips does not result in a corresponding increase in the friction forces. This effect can be seen in Figure 2.3, where the lateral road-tire friction force is plotted against the tire-slip angle after being normalized by dividing it by the vertical contact force. The curves in Figure 2.3 correspond to varying degrees of road grip due to various road surface conditions, ranging roughly from ice for the lower curve to dry asphalt for the upper one. The road surface conditions are represented by a friction coefficient $\mu_H$, which is lower for more slippery surfaces. The region where the friction forces are linear with respect to the tire-slip angle is called the *linear region*. Beyond the linear region, where the tire-slip angles are larger, is the *nonlinear region*.

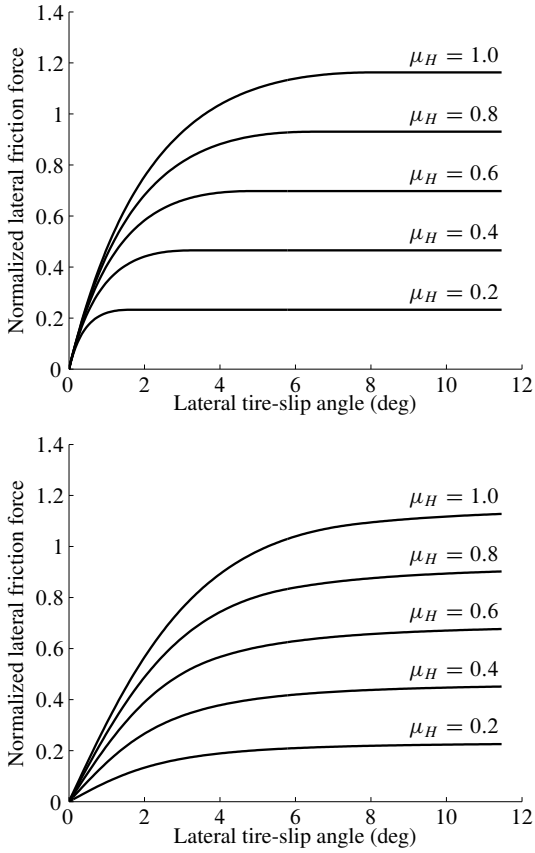


**Figure 2.3:** Nonlinear road-tire friction curves. The lateral tire force, which is normalized by dividing it by the vertical contact force, is plotted against the lateral tire-slip angle for various road surface conditions. Where the tire-slip angles are small, the forces increase linearly, and we call this the linear region. For larger tire-slip angles, in the nonlinear region, the forces saturate. The curves to the left are created with the longitudinal tire slip kept at zero. The curves to the right are created with a large longitudinal tire slip.

When the friction forces saturate for the front tires before they do so at the rear, the car stops responding properly to steering inputs, a situation known as understeer or plowing. Conversely, when the friction forces saturate for the rear tires first, the car becomes severely oversteered and may become unstable, a situation known as fishtailing. The point at which severe under- or oversteer occurs depends on the driving maneuver, the tires, the design of the vehicle, and the properties of the road surface. As Figure 2.3 makes clear, road-tire friction forces saturate

sooner on low-friction surfaces, such as ice, than on high-friction surfaces, such as asphalt. For a more comprehensive description of road-tire friction, and more detailed definitions, see Kiencke and Nielsen (2000); Pacejka (2006).

#### Modeling the Road-Tire Friction Forces

As with many alternative designs for vehicle sideslip estimation (van Zanten, 2000; Farrelly and Wellstead, 1996; Fukada, 1999; Venhovens and Naab, 1999; Ungoren et al., 2004; Kiencke and Daiß, 1997; Kiencke and Nielsen, 2000; Hiemer et al., 2005; von Vietinghoff et al., 2005, 2007; Suissa et al., 1994; Best et al., 2000; Hac and Simpson, 2000), a key component of the NVSO is a road-tire friction model. The road-tire friction model takes measurements and observer estimates as inputs, and returns estimates of the road-tire friction forces. The expression $F_{y1} = C_y\alpha_1$ is an example of a linear friction model, but to account for the nonlinearity of road-tire friction forces for large tire slips, a nonlinear model is needed. A widely used nonlinear road-tire friction model is the *magic formula* (Pacejka, 2006). Like linear road-tire friction models, nonlinear models such as the magic formula are based on tire slips. But instead of increasing linearly with the tire slips, the friction forces in nonlinear models are made to follow curves similar to those seen in Figure 2.3.

The NVSO is not designed with a particular road-tire friction model in mind. Instead, we use a nonlinear friction model satisfying specific physical properties, and we base the design and analysis on these properties. The curves in Figure 2.3 are created with a friction model for which the physical road-tire friction curves are approximated by fractional polynomial expressions, similar to Kiencke and Nielsen (2000, Ch. 7.2).

### 2.2.2 The Lateral Acceleration

According to Newton's second law, the vehicle acceleration along each direction is equal to the total force acting on the vehicle in that direction, divided by the mass. When the road surface is slanted, rather than horizontal, gravity acts on the vehicle in the tangent plane of the road surface, which affects the vehicle velocity. Assume for now that the road surface is horizontal. The dominant forces acting in the plane are the road-tire friction forces; we ignore smaller influences such as wind and air resistance. The road-tire friction forces are algebraic functions of the tire slips, which in turn are algebraic functions of the vehicle velocity. Consequently, measurements of the vehicle accelerations depend algebraically on the vehicle velocities, and the accelerations can therefore be used as indirect measurements of the velocities. In particular, the lateral acceleration $a_y$ contains valuable information about the lateral velocity.

To see how the relationship between the lateral acceleration $a_y$ and the lateral velocity $v_y$ can be used, we consider what happens to the lateral road-tire friction forces when we perturb $v_y$ while keeping everything else constant. From Figure 2.2, we see that if $v_y$ is increased, the lateral component of the velocity vector $v_1$ at the center of the front left wheel is also increased, and the tire-slip angle $\alpha_1$ for the front left tire is therefore decreased (note that the sign convention for the tire-slip angle is opposite from the sign convention for the vehicle sideslip angle). This decrease in the tire-slip angle leads to a decrease in the lateral road-tire friction force $F_{y1}$, as indicated by the shape of the friction curves in Figure 2.3. Put differently, $F_{y1}$ is perturbed in a negative direction in response to a positive perturbation in $v_y$. The lateral road-tire friction forces for the remaining three tires are affected in the same way by a perturbation in $v_y$.

The above discussion suggests that the total lateral force on the vehicle, and therefore the lateral acceleration $a_y$, is perturbed in a negative direction in response to a positive perturbation in $v_y$. Indeed, it is demonstrated in Imsland et al. (2006) that, except in some particular cases that we discuss below, the partial derivative $\partial a_y/\partial v_y$ is less than some negative number when $a_y$ is considered as a function of $v_y$. We therefore consider $a_y$ to be strictly decreasing with respect to $v_y$. This monotonicity is a key property in the NVSO design.

#### Roll Correction

During a turn, the vehicle body is typically at a slight roll angle $\phi$ around the $x$-axis, relative to the road surface. The roll angle is roughly proportional to the lateral acceleration and thus can be approximated as $\phi \approx p_\phi a_y$, where the constant $p_\phi$ is the roll-angle gradient and $a_y$ is the lateral acceleration in the tangent plane of the road surface, as above. The roll angle $\phi$ causes the lateral acceleration measurement to be influenced by an additive gravity component $\sin(\phi)g \approx \phi g$, where $g$ is the acceleration of gravity. The measured lateral acceleration is therefore approximately $(1 + p_\phi g)a_y$. The gravity influence due to roll angle is undesirable, and to remove it we divide the acceleration measurement by the constant factor $1 + p_\phi g$. Throughout the article, we therefore assume that $a_y$ is a measurement that is not influenced by the roll angle.

## 2.3 Observer Design

To estimate the vehicle sideslip angle, we estimate the longitudinal and lateral velocities $v_x$ and $v_y$ at the CG, and then calculate the vehicle sideslip angle from the velocities using the expression $\beta = \arctan(v_y/v_x)$. We assume for now that

there is no uncertainty in the friction model regarding the road surface conditions. We discuss the estimation of longitudinal and lateral velocity separately, ignoring at first the coupling between the two estimates. Throughout the rest of this article, a hat indicates an estimated quantity, and a tilde indicates an estimation error; thus $\hat{v}_x$ is an estimate of $v_x$, and $\tilde{v}_x := v_x - \hat{v}_x$. The goal is to stabilize the estimation error and make it vanish asymptotically, for example, by making the origin of the observer error dynamics asymptotically or exponentially stable.

### 2.3.1 Longitudinal-Velocity Estimation

A conventional speedometer approximates the longitudinal vehicle velocity by using the wheel speeds. The wheel speeds usually provide good measurements of the longitudinal velocity, but the accuracy is sometimes severely reduced, for example, during strong acceleration or braking, and in situations where one or more of the wheels are spinning or locked.

To estimate the longitudinal velocity we use the observer

$$\dot{\hat{v}}_x = a_x + \dot{\psi}\hat{v}_y + K_{v_x}(t)(v_{x,\text{ref}} - \hat{v}_x), \tag{2.3}$$

where $\hat{v}_y$ is an estimate of the lateral velocity as specified below, $K_{v_x}(t)$ is a time-varying gain, and $v_{x,\text{ref}}$ is a reference velocity calculated from the wheel speeds, which plays the role of measurement. The observer (2.3) is a copy of the system equation (2.1) with an added injection term $K_{v_x}(t)(v_{x,\text{ref}} - \hat{v}_x)$. When $v_{x,\text{ref}}$ represents the true longitudinal velocity, the error dynamics obtained by subtracting (2.3) from (2.1) are

$$\dot{\tilde{v}}_x = \dot{\psi}\tilde{v}_y - K_{v_x}(t)\tilde{v}_x. \tag{2.4}$$

Ignoring for the moment the error $\tilde{v}_y$, global exponential stability of the origin of (2.4) can be verified if $K_{v_x}(t)$ is larger than some positive number, that is, $K_{v_x}(t) \geq K_{v_x,\min} > 0$. The primary challenge therefore lies in producing a reference velocity $v_{x,\text{ref}}$ and selecting a sensible gain $K_{v_x}(t)$.

#### Reference Velocity and Gain

The four wheel speeds, together with the steering wheel angle and the yaw rate, can be used to create four separate measurements of $v_x$. It is possible to create a reference velocity by taking a weighted average of these four measurements, with weightings determined by various factors, such as the spread in the four measurements and whether the car is braking or accelerating (Imsland et al., 2006; Grip et al., 2008). To make speed estimation as reliable as possible in every situation, however, car manufacturers have developed sophisticated reference velocity algorithms that use information from a variety of sources, such as the accelerations,

brake pressures, engine torque, and status information from ABS, ESC, and drive-slip control systems. The goal is to determine which wheel speeds provide accurate information about the longitudinal velocity at any given time, for example, during heavy braking or acceleration. We therefore assume that a reference velocity is available to the observer.

No matter how much effort is put into the reference velocity algorithm, the accuracy of $v_{x,\text{ref}}$ varies. We take this variation into account through the time-varying gain $K_{v_x}(t)$, which is intended to reflect the accuracy of the reference velocity. When the accuracy is deemed to be low, the gain $K_{v_x}(t)$ is reduced to make the observer less reliant on the reference velocity and more reliant on integration of the system equations. In creating $K_{v_x}(t)$, all of the sources of information that are used to create $v_{x,\text{ref}}$ can be used. A measure of the accuracy of $v_{x,\text{ref}}$ may indeed be naturally available from the inner workings of the reference velocity algorithm. For the experimental results presented in this article, we use a simple algorithm that is based on reducing the nominal gain depending on the variance of the four measurements, on the theory that agreement between the measurements indicates high accuracy. Design of $K_{v_x}(t)$ is heuristic and must therefore be empirically based.

### 2.3.2 Lateral-Velocity Estimation

The wheel speeds can be used to create measurements of the longitudinal velocity. For the lateral velocity, however, we do not have a similar source of information, and estimating lateral velocity is therefore more difficult. We start by introducing $\hat{a}_y(t,\hat{x})$, which denotes an estimate of the lateral acceleration $a_y$. We use $\hat{x}$ to denote the vector of estimated velocities $\hat{v}_x$ and $\hat{v}_y$, and $x$ to denote the vector of actual velocities $v_x$ and $v_y$. The estimate $\hat{a}_y(t,\hat{x})$ is formed by using the nonlinear friction model for each wheel, where measurements of the steering wheel angle, yaw rate, and wheel speeds, as well as the estimated velocities $\hat{v}_x$ and $\hat{v}_y$, are used as inputs. The friction forces modeled for each wheel are added up in the lateral direction of the vehicle and divided by the mass, resulting in the lateral acceleration estimate $\hat{a}_y(t,\hat{x})$. The time argument in $\hat{a}_y(t,\hat{x})$ denotes the dependence of $\hat{a}_y$ on time-varying signals such as the steering wheel angle and yaw rate. We also define $\tilde{a}_y(t,\tilde{x}) := a_y - \hat{a}_y(t,\hat{x})$, where $\tilde{x} := x - \hat{x}$. To write $\tilde{a}_y(t,\tilde{x})$ as a function of $t$ and $\tilde{x}$, we replace $\hat{x}$ with $x - \tilde{x}$ and absorb $x$ in the time argument.

To estimate the lateral velocity we use the observer

$$\dot{\hat{v}}_y = a_y - \dot{\psi}\hat{v}_x - K_{v_y}(a_y - \hat{a}_y(t,\hat{x})), \tag{2.5}$$

where $K_{v_y}$ is a positive gain. The observer consists of a copy of the original system (2.2) and an injection term $-K_{v_y}(a_y - \hat{a}_y(t,\hat{x}))$. The error dynamics obtained by

subtracting (2.5) from (2.2) are

$$\dot{\tilde{v}}_y = -\dot{\psi}\tilde{v}_x + K_{v_y}\tilde{a}_y(t,\tilde{x}). \tag{2.6}$$

To see why the injection term asymptotically stabilizes the observer error, assume for the moment that the longitudinal-velocity estimate $\hat{v}_x$ is exact, meaning that the lateral-velocity estimate $\hat{v}_y$ is the only uncertain input to $\hat{a}_y(t,\hat{x})$. Assuming furthermore that the friction model is continuously differentiable, the assumption that $a_y$ is strictly decreasing with respect to $v_y$ means that we can use the mean value theorem to write

$$\tilde{a}_y(t,\tilde{x}) = -\eta(t,\tilde{x})\tilde{v}_y, \tag{2.7}$$

where $\eta(t,\tilde{x}) \geq \eta_{\min} > 0$ for some constant $\eta_{\min}$. The error dynamics can therefore be written as $\dot{\tilde{v}}_y = -K_{v_y}\eta(t,\tilde{x})\tilde{v}_y$. It is then easy to verify that the origin of the error dynamics is globally exponentially stable.

We have so far ignored the coupling between the longitudinal and lateral observer components. For each observer component, a quadratic Lyapunov function can be used to verify the global exponential stability property. Taking the coupling between the observer components into account, we use the sum of the two Lyapunov functions as a Lyapunov-function candidate for the full error dynamics (2.4), (2.6). With an additional assumption that the partial derivative of the friction model with respect to $v_x$ is bounded, we can verify that the origin of (2.4), (2.6) is globally exponentially stable, provided $K_{v_x}(t)$ is chosen large enough to dominate the cross terms that occur because of the coupling. The observer is also input-to-state stable with respect to errors in the reference velocity $v_{x,\text{ref}}$ (Imsland et al., 2006).

## 2.4 Unknown Road Surface Conditions

The observer presented in the previous section depends on the construction of a lateral acceleration estimate $\hat{a}_y(t,\hat{x})$ as a function of measured signals and velocity estimates. The approach works well when the road-tire friction model from which $\hat{a}_y(t,\hat{x})$ is computed is accurately parameterized. However, the friction model is sensitive to changes in the road surface conditions, as seen in Figure 2.3. Since information about the road surface conditions is not available, we modify the observer to take this uncertainty into account by introducing a friction parameter to be estimated together with the velocities.

### 2.4.1 Parameterization

The friction parameter can be defined in several ways. In Imsland et al. (2007a); Grip, Imsland, Johansen, Fossen, Kalkkuhl, and Suissa (2006) the road-tire friction coefficient $\mu_H$ is chosen as the parameter to be estimated. We instead scale the friction forces by redefining $\hat{a}_y$ as $\hat{a}_y(t, \hat{x}, \theta) = \theta \hat{a}_y^*(t, \hat{x})$, where $\theta$ is the friction parameter. The value $\hat{a}_y^*(t, \hat{x})$ is given by

$$\hat{a}_y^*(t, \hat{x}) = \frac{\hat{a}_y(t, \hat{x}; \mu_H^*)}{\mu_H^*},$$

where $\hat{a}_y(t, \hat{x}; \mu_H^*)$ represents the lateral acceleration estimate calculated using a nominal value $\mu_H^*$ of the friction coefficient. In words, $\hat{a}_y^*(t, \hat{x})$ is a normalized lateral acceleration estimate based on a fixed road-tire friction coefficient, and $\theta$ is a scaling factor that changes depending on the road surface. As is evident from Figure 2.3, variation in $\mu_H$ does not correspond precisely to a scaling of the friction forces. The friction parameter is nevertheless closely related to $\mu_H$, and, for large tire-slip angles, where the curves in Figure 2.3 flatten out, $\theta \approx \mu_H$. Because the friction parameter appears linearly, the design and analysis is simplified compared to estimating $\mu_H$ directly.

The friction parameter is defined with respect to the lateral acceleration of the vehicle, rather than the friction forces at each wheel. This definition means that, on a nonuniform road surface, the parameter represents an average of the road-tire friction properties over all the wheels. In the stability analysis we assume that the friction parameter is positive and constant.

### 2.4.2 Modified Observer Design

Since the longitudinal-velocity estimation does not depend on the friction model, we consider only the lateral-velocity estimation. We modify the lateral-velocity estimate to obtain

$$\dot{\hat{v}}_y = a_y - \dot{\psi}\hat{v}_x + K_{v_y}\Lambda(t, \hat{x})\xi(t, \hat{x})(a_y - \hat{a}_y(t, \hat{x}, \hat{\theta})), \tag{2.8}$$

and introduce an estimate of $\theta$, given by

$$\dot{\hat{\theta}} = K_\theta \Lambda(t, \hat{x})\hat{a}_y^*(t, \hat{x})(a_y - \hat{a}_y(t, \hat{x}, \hat{\theta})). \tag{2.9}$$

The value $\xi(t, \hat{x})$ in (2.8) is an approximate slope of the line between

$$(\hat{v}_y, \hat{a}_y^*(t, \chi_1)) \text{ and } (v_y, \hat{a}_y^*(t, \chi_2)),$$

with $\chi_1 = [\hat{v}_x, \hat{v}_y]^\mathsf{T}$ and $\chi_2 = [\hat{v}_x, v_y]^\mathsf{T}$. The slope is negative, according to (2.7), and the approximation can be made in several ways (Grip et al., 2008). We choose $\xi(t, \hat{x}) = [\partial \hat{a}_y^* / \partial \hat{v}_y](t, \hat{x})$, which is sufficiently accurate to give good performance in practical experiments. In the analysis below, we assume that $\xi(t, \hat{x})$ represents the true slope. The value $\Lambda(t, \hat{x})$ is a strictly positive scaling that can be chosen freely. We choose $\Lambda(t, \hat{x}) = (\xi^2(t, \hat{x}) + \hat{a_y^*}^2(t, \hat{x}))^{-1/2}$ as a normalization factor to prevent large variations in the magnitude of the gain on the right-hand side of (2.8), (2.9), because such variations can cause numerical problems when implementing the observer. In the following discussion of the lateral-velocity and friction estimation, we ignore the longitudinal-velocity error $\tilde{v}_x$.

Analysis of the observer (2.8), (2.9) starts with the Lyapunov-function candidate

$$V = \theta \tilde{v}_y^2 + \frac{K_{v_y}}{K_\theta} \tilde{\theta}^2.$$

The time derivative of $V$ is negative semidefinite, satisfying

$$\dot{V} \leq -k \tilde{a}_y^2(t, \tilde{x}, \tilde{\theta}),$$

for some positive $k$, where $\tilde{a}_y(t, \tilde{x}, \tilde{\theta}) = a_y - \hat{a}_y(t, \hat{x}, \hat{\theta})$. From the negative semidefiniteness of $\dot{V}$ we conclude that the origin of the error dynamics is uniformly globally stable. Stability is not enough, however; we also need to show that the error vanishes with time. The bound on $\dot{V}$ suggests that this behavior occurs if the observer error is observable from $\tilde{a}_y(t, \tilde{x}, \tilde{\theta})$. We therefore use the results from Loría, Panteley, Popović, and Teel (2005) to prove that if $\tilde{a}_y(t, \tilde{x}, \tilde{\theta})$ satisfies a property known as *uniform δ-persistency of excitation* with respect to $\tilde{v}_y$ and $\tilde{\theta}$, then the origin is uniformly globally asymptotically stable.

The excitation condition takes the form of an inequality. Specifically, for each $(\tilde{x}, \tilde{\theta})$ we assume that there exist positive constants $T$ and $\varepsilon$ such that

$$\int_t^{t+T} \tilde{a}_y^2(\tau, \tilde{x}, \tilde{\theta}) \, \mathrm{d}\tau \geq \varepsilon(\tilde{v}_y^2 + \tilde{\theta}^2) \tag{2.10}$$

holds for all $t \geq 0$. The inequality (2.10) requires the error $\tilde{a}_y(t, \tilde{x}, \tilde{\theta})$ to contain information about both the lateral-velocity error and the friction-parameter error, when taken over sufficiently long time windows. An implication of (2.10) is that $\tilde{a}_y(t, \tilde{x}, \tilde{\theta})$ cannot remain zero for an extended period of time unless both the lateral-velocity error and the friction-parameter error are also zero. This implication hints at the invariance-like origins of the stability proof; the results applied from Loría et al. (2005) are based on Matrosov's theorem, a counterpart to the Krasovskii-LaSalle invariance principle that is applicable to nonautonomous systems. Note that, unlike some nonlinear persistency of excitation conditions, the

condition in (2.10) does not depend on knowledge about the trajectories of the observer error. This property allows the condition to be evaluated based on the physical behavior of the car in different situations.

Under conditions given in Grip et al. (2008), the excitation condition can also be used directly in the Lyapunov function, by letting

$$V = \theta \tilde{v}_y^2 + \frac{K_{v_y}}{K_\theta} \tilde{\theta}^2 - \mu \int_t^\infty \mathrm{e}^{t-\tau} \tilde{a}_y^2(\tau, \tilde{x}, \tilde{\theta})\, \mathrm{d}\tau,$$

where $\mu$ is a small positive number. In this case, $\dot{V}$ is negative definite in a region around the origin, yielding local exponential stability.

### 2.4.3 Physical Interpretation

The excitation condition (2.10) has a clear physical interpretation. This condition is satisfied when there is sufficient variation in the lateral movement so that the road surface conditions influence the behavior of the car; it is not satisfied when there is no variation in the lateral movement. We can therefore estimate the lateral velocity and the friction parameter simultaneously during dynamic maneuvers, but we cannot expect to do so during steady-state maneuvers. This conclusion has intuitive appeal. It is clear, for example, that we cannot determine the road surface conditions from the lateral acceleration when the car is driven straight for an indefinitely long time. An analogy to this situation is a person trying to determine how slippery the pavement is without moving around, and without the aid of visual information. A secondary result regarding the observer is that when the car is driven straight for an indefinitely long time, the velocity errors $\tilde{v}_x$ and $\tilde{v}_y$ still converge to zero, even though the friction-parameter error $\tilde{\theta}$ does not (Grip et al., 2008).

### 2.4.4 When to Estimate Friction

In normal driving situations, the tire slips are well within the linear region, and the road surface conditions have little impact on the behavior of the car (Hac and Simpson, 2000). Moreover, the excitation condition shows that variation in the lateral movement of the car is needed to estimate the friction parameter. These observations suggest that it is often undesirable to estimate the friction parameter, and we therefore estimate it only when necessary and possible.

When the friction parameter is not estimated, we choose to let it be exponentially attracted to a default value $\theta^*$ corresponding to a high-friction surface. There are two reasons for choosing $\theta^*$ high, rather than low. The first reason is that driving on high-friction surfaces such as asphalt and concrete is more common than driving on low-friction surfaces such as ice and snow. The second reason is that

using a friction parameter that is too low results in vehicle sideslip estimates that are too high, often by a large amount.

To determine when to estimate friction, we use a linear reference model for the yaw rate to determine when the car becomes over- or understeered. We also estimate $\dot{v}_y$, according to (2.2), by $a_y - \dot{\psi}\hat{v}_x$, highpass-filtered with a 10-s time constant. A high estimate of $\dot{v}_y$ indicates a fast-changing sideslip angle, which in turn indicates a high level of excitation and that some of the tires might be in the nonlinear region. When the $\dot{v}_y$ estimate is high, and the reference yaw rate is above a threshold value, we turn the friction estimation on. We also turn the friction estimation on when the car is oversteered; and when the vehicle's ESC system is active, but not due to steady-state understeer. A small delay in turning the friction estimation off reduces chattering in the friction-estimation condition.

It is worth examining whether friction estimation is sometimes necessary, but not possible due to a lack of excitation. This situation can occur during long, steady-state maneuvers with one or more of the tires in the nonlinear region. On high-friction surfaces, maneuvers of this type are easily carried out. A standard identification maneuver consists of driving along a circle while slowly increasing the speed until the circle can no longer be maintained. Toward the end of this circle maneuver, it is common for the front tires to be well within the nonlinear region, leading to severe steady-state understeer. Recall, however, that the friction parameter is attracted to a high default value when friction estimation is turned off. For steady-state maneuvers on high-friction surfaces, the default friction parameter is therefore approximately correct. On slippery surfaces such as snow and ice, maintaining a steady-state maneuver for a long time with some of the tires in the nonlinear region is more difficult. If such a situation occurs, however, it can lead to estimation errors, typically in the direction of underestimated vehicle sideslip angle.

The difficulty in handling low-excitation situations is not specific to the NVSO. Because the problem is fundamentally a lack of information, all estimation strategies suffer in low-excitation situations. It is always possible to perform open-loop integration of the kinematic equations, but the accuracy is then entirely dependent on the sensor specifications.

Experimental results indicate that the friction-estimation condition has a large impact on the performance of the observer, in particular on low-friction surfaces. If friction estimation is turned on too late, the observer might fail to capture sudden changes in the vehicle sideslip angle. If friction estimation is turned on without sufficient excitation, modeling errors and sensor bias might cause the friction parameter to be estimated as too low, leading to large errors in the estimated vehicle sideslip angle. The friction-estimation condition therefore requires careful tuning, involving some tradeoffs in performance for different situations.

## 2.5 Inclination and Bank Angles

The above discussion assumes that the road surface is horizontal. This assumption is usually not accurate, however, and we now consider nonzero inclination and bank angles. To define these angles, we say that the orientation of the road surface is obtained from the horizontal position by an inclination-angle rotation $\Theta$ around the vehicle's $y$-axis and a subsequent bank-angle rotation $\Phi$ around the $x$-axis. The inclination and bank angles cause gravity components to appear in (2.1), (2.2), which become (Klier et al., 2008)

$$\dot{v}_x = a_x + \dot{\psi} v_y + g \sin(\Theta), \tag{2.11}$$

$$\dot{v}_y = a_y - \dot{\psi} v_x - g \cos(\Theta) \sin(\Phi). \tag{2.12}$$

In (2.11), (2.12), $a_x$ and $a_y$ denote the accelerations measured by the accelerometers, which equal the total road-tire friction forces acting on the vehicle divided by the mass, as before. We assume that the inclination and bank angles vary slowly enough compared to the dynamics of the system to be modeled as constants.

We return to the observer without friction estimation as the basis for adding inclination- and bank-angle estimation. The approximate effect of a nonzero inclination or bank angle is to create an estimation bias, which is more pronounced for the lateral-velocity estimate. Inspired by the theory of nonlinear unknown-input observers, one method for estimating the bank angle is developed in Imsland et al. (2007b); however, the nature of the disturbance suggests that something similar to standard integral action is appropriate. We present such a solution here, at first dealing with the inclination and bank angles separately.

### 2.5.1 Inclination Angle

We define $\theta_{\mathrm{i}} = \sin(\Theta)$, and introduce an estimate $\hat{\theta}_{\mathrm{i}}$ of $\theta_{\mathrm{i}}$. Typical inclination angles are small enough that $\Theta \approx \theta_{\mathrm{i}}$, and the estimate $\hat{\theta}_{\mathrm{i}}$ is therefore considered an estimate of the inclination angle. We use $\hat{\theta}_{\mathrm{i}}$ to compensate for the disturbance, by letting

$$\dot{\hat{v}}_x = a_x + \dot{\psi} \hat{v}_y + g\hat{\theta}_{\mathrm{i}} + K_{v_x}(t)(v_{x,\mathrm{ref}} - \hat{v}_x), \tag{2.13}$$

where $\hat{\theta}_{\mathrm{i}}$ is given by

$$\dot{\hat{\theta}}_{\mathrm{i}} = K_{\theta_{\mathrm{i}}} K_{v_x}(t)(v_{x,\mathrm{ref}} - \hat{v}_x), \tag{2.14}$$

with $K_{\theta_{\mathrm{i}}}$ a positive gain. The total gain in (2.14) is $K_{\theta_{\mathrm{i}}} K_{v_x}(t)$. The reason for including the time-varying gain $K_{v_x}(t)$ in (2.14) is the same as in the longitudinal-velocity estimation (2.13), namely, that we wish to rely less on the reference velocity $v_{x,\mathrm{ref}}$ whenever it is of poor quality.

To justify this approach, we use the theory of absolute stability (Khalil, 2002, Ch. 7.1). We split the gain $K_{v_x}(t)$ into a constant part and a time-varying part by writing $K_{v_x}(t) = a + (K_{v_x}(t) - a)$, where $0 < a < K_{v_x,\min}$, and $K_{v_x,\min}$ is a lower bound on $K_{v_x}(t)$. Ignoring for the moment the lateral-velocity error $\tilde{v}_y$, and assuming that $v_{x,\mathrm{ref}}$ represents the true longitudinal velocity, we write the error dynamics of the longitudinal-velocity and inclination-angle estimates as the interconnection of the linear time-invariant system

$$\begin{aligned}\dot{\tilde{v}}_x &= -a\tilde{v}_x + g\tilde{\theta}_\mathrm{i} + u,\\ \dot{\tilde{\theta}}_\mathrm{i} &= -K_{\theta_\mathrm{i}} a\tilde{v}_x + K_{\theta_\mathrm{i}} u\end{aligned}$$

with the time-varying sector function $u = -(K_{v_x}(t) - a)\tilde{v}_x$. With $K_{\theta_\mathrm{i}}$ chosen sufficiently small compared to $a$, the transfer function from $u$ to $\tilde{v}_x$ is strictly positive real. Using the circle criterion (Khalil, 2002, Th. 7.1), we can conclude that the origin of the error dynamics is globally exponentially stable.

### 2.5.2 Bank Angle

We handle the bank angle in roughly the same way as the inclination angle. We define $\theta_\mathrm{b} = \cos(\Theta)\sin(\Phi)$, and introduce an estimate $\hat{\theta}_\mathrm{b}$ of $\theta_\mathrm{b}$. Typical bank and inclination angles are small enough that $\Phi \approx \theta_\mathrm{b}$, and $\hat{\theta}_\mathrm{b}$ is therefore considered an estimate of the bank angle. Using $\hat{\theta}_\mathrm{b}$ for compensation in the observer without friction estimation, we obtain

$$\dot{\hat{v}}_y = a_y - \dot{\psi}\hat{v}_x - g\hat{\theta}_\mathrm{b} - K_{v_y}(a_y - \hat{a}_y(t,\hat{x})). \tag{2.15}$$

Since no counterpart to $v_{x,\mathrm{ref}}$ is available for the lateral velocity, we again use the lateral acceleration as an indirect measurement of the lateral velocity, letting

$$\dot{\hat{\theta}}_\mathrm{b} = K_{\theta_\mathrm{b}}(a_y - \hat{a}_y(t,\hat{x})). \tag{2.16}$$

Ignoring the effect of the longitudinal-velocity error $\tilde{v}_x$, we write the error dynamics of the lateral-velocity and bank-angle estimates as the interconnection of the linear time-invariant system

$$\begin{aligned}\dot{\tilde{v}}_y &= -K_{v_y}\eta_{\min}\tilde{v}_y - g\tilde{\theta}_\mathrm{b} + K_{v_y}u,\\ \dot{\tilde{\theta}}_\mathrm{b} &= K_{\theta_\mathrm{b}}\eta_{\min}\tilde{v}_y - K_{\theta_\mathrm{b}}u\end{aligned}$$

with the time-varying sector nonlinearity $u = -(\eta(t,\tilde{x}) - \eta_{\min})\tilde{v}_y$. With $K_{\theta_\mathrm{b}}$ chosen sufficiently small compared to $K_{v_y}$ and $\eta_{\min}$, we conclude, as above, that the origin of the error dynamics is globally exponentially stable.

Absolute stability provides two separate Lyapunov functions, $V_1$ for the ($\tilde{v}_x$, $\tilde{\theta}_\mathrm{i}$) subsystem and $V_2$ for the ($\tilde{v}_y$, $\tilde{\theta}_\mathrm{b}$) subsystem. Following the proof of the circle criterion (Khalil, 2002, Th. 7.1), an excess term $-(K_{v_x,\min} - a)\tilde{v}_x^2$ appears in the time derivative $\dot{V}_1$. This term can be made arbitrarily negative by increasing the difference between $K_{v_x,\min}$ and $a$. We thus form a new Lyapunov-function candidate as the weighted sum $V_1 + cV_2$, where $c$ is a positive constant. By choosing $c$ sufficiently large and using the excess term to dominate the cross terms, global exponential stability of the overall error dynamics, including the subsystem coupling that we have so far ignored, is proven.

Exponential stability is a useful property because it implies a certain level of robustness to perturbations (Khalil, 2002, Ch. 9). For example, an accelerometer bias added to (2.15), (2.16) can perturb the solutions, typically producing a bias in the bank-angle estimate, but it does not cause the estimates to drift off or become unstable.

## 2.6 Combined Approach

The above discussion extends the initial observer design in two separate directions, namely, by adding estimation of a friction parameter and by adding estimation of the inclination and bank angles. Including these extensions simultaneously causes no problem in the longitudinal direction, because the estimation of the longitudinal velocity and inclination angle does not depend on the friction model. In the lateral direction, however, more careful consideration is needed.

The lateral-velocity estimate changes depending on whether friction estimation is turned on or off, as can be seen from (2.5) and (2.8). Because of this change, we also modify the bank-angle estimate when friction estimation is turned on, by replacing (2.16) with

$$\dot{\hat{\theta}}_\mathrm{b} = -K_{\theta_\mathrm{b}} \Lambda(t, \hat{x}) \xi(t, \hat{x}) (a_y - \hat{a}_y(t, \hat{x}, \hat{\theta})). \tag{2.17}$$

With this modification the error dynamics for the lateral-velocity and bank-angle estimates can still be written in the form required by the absolute-stability analysis.

In previous sections tunable gains are used to dominate cross terms that appear in the Lyapunov analysis. When estimating friction, however, the stability margin depends on the excitation condition placed on the error $\tilde{a}_y(t, \tilde{x}, \tilde{\theta})$, specifically, $T$ and $\varepsilon$ in (2.10), which cannot be modified using tunable gains. We therefore cannot find a particular set of gains to guarantee stability in combination with bank-angle estimation. From a practical point of view, it can be difficult to distinguish the effect of low friction and a bank angle, as noted in van Zanten (2000). This observation suggests that, with the chosen sensor configuration, the estimation

problem is poorly conditioned in some situations, and the difficulty in analyzing the combined approach reflects this problem.

The simplest strategy for avoiding interference between the friction estimation and the bank-angle estimation would be to disable the bank-angle estimation whenever friction estimation is turned on. This strategy, however, may cause problems when driving on slippery surfaces in hilly terrains, where combinations of large vehicle sideslip angles and large bank angles may occur. For this reason, we need to perform bank-angle estimation when estimating friction, but we set the gain lower when one of three conditions holds. The first condition is $|a_y - \hat{a}_y(t, \hat{x}, \hat{\theta})| > c_1$ for some $c_1 > 0$. The second condition is $|\ddot{\psi} - \hat{\ddot{\psi}}(t, \hat{x}, \hat{\theta})| > c_2$ for some $c_2 > 0$, where $\ddot{\psi}$ is the yaw acceleration found by numerical differentiation of the yaw rate, and $\hat{\ddot{\psi}}(t, \hat{x}, \hat{\theta})$ is calculated using the friction model in the same way as $\hat{a}_y(t, \hat{x}, \hat{\theta})$ with the forces scaled by $\hat{\theta}$. The third condition is $\text{sign}(\dot{\psi}_{\text{ref}}) = \text{sign}(\dot{\psi})$ and $(|\dot{\psi}_{\text{ref}}| - |\dot{\psi}|)\hat{v}_x > c_3$ for some $c_3 > 0$, where $\dot{\psi}_{\text{ref}}$ is the reference yaw rate used in the friction-estimation condition. From experimental data, these conditions are found to reduce the negative interference of the bank-angle estimation on low-friction surfaces. We emphasize, however, that the conditions are heuristic and that alternative conditions may be equally good or better, in particular, when different types of vehicles are used.

The full observer that merges the friction-parameter estimation and the inclination- and bank-angle estimation has two modes. In the first mode, with friction estimation turned off, the observer equations are

$$\dot{\hat{v}}_x = a_x + \dot{\psi}\hat{v}_y + g\hat{\theta}_{\text{i}} + K_{v_x}(t)(v_{x,\text{ref}} - \hat{v}_x), \tag{2.18}$$

$$\dot{\hat{v}}_y = a_y - \dot{\psi}\hat{v}_x - g\hat{\theta}_{\text{b}} - K_{v_y}(a_y - \hat{a}_y(t, \hat{x}, \hat{\theta})), \tag{2.19}$$

$$\dot{\hat{\theta}} = K_{\text{e}}(\theta^* - \hat{\theta}), \tag{2.20}$$

$$\dot{\hat{\theta}}_{\text{i}} = K_{\theta_{\text{i}}} K_{v_x}(t)(v_{x,\text{ref}} - \hat{v}_x), \tag{2.21}$$

$$\dot{\hat{\theta}}_{\text{b}} = K_{\theta_{\text{b}}}(t)(a_y - \hat{a}_y(t, \hat{x}, \hat{\theta})). \tag{2.22}$$

We see from (2.20) that the friction-parameter estimate is exponentially attracted to the default value $\theta^*$. In the second mode, with friction estimation turned on, the observer equations are

$$\dot{\hat{v}}_x = a_x + \dot{\psi}\hat{v}_y + g\hat{\theta}_{\text{i}} + K_{v_x}(t)(v_{x,\text{ref}} - \hat{v}_x), \tag{2.23}$$

$$\dot{\hat{v}}_y = a_y - \dot{\psi}\hat{v}_x - g\hat{\theta}_{\text{b}} + K_{v_y}\Lambda(t, \hat{x})\xi(t, \hat{x})(a_y - \hat{a}_y(t, \hat{x}, \hat{\theta})), \tag{2.24}$$

$$\dot{\hat{\theta}} = K_\theta \Lambda(t, \hat{x})\hat{a}_y^*(t, \hat{x})(a_y - \hat{a}_y(t, \hat{x}, \hat{\theta})), \tag{2.25}$$

$$\dot{\hat{\theta}}_{\mathrm{i}} = K_{\theta_{\mathrm{i}}} K_{v_x}(t)(v_{x,\mathrm{ref}} - \hat{v}_x), \tag{2.26}$$

$$\dot{\hat{\theta}}_{\mathrm{b}} = -K_{\theta_{\mathrm{b}}}(t)\Lambda(t,\hat{x})\xi(t,\hat{x})(a_y - \hat{a}_y(t,\hat{x},\hat{\theta})). \tag{2.27}$$

In both modes, $K_{\theta_{\mathrm{b}}}(t)$ is reduced according to the practical conditions described above. Based on experimental results, we set the gain $K_{\theta_{\mathrm{i}}}$, which is used for inclination-angle estimation, to be lower for the second mode than for the first. The best choice of observer gains and other tunable parameters, such as threshold values for logical conditions, are likely to vary depending on the vehicle type and model.

## 2.7 Remarks about Road-Tire Friction

The above development assumes a strictly decreasing relationship between the lateral acceleration and the lateral velocity. The curves in Figure 2.3 nevertheless flatten out for large tire-slip angles, suggesting that, when the friction forces are simultaneously saturated for all four tires, the strictly decreasing relationship might not hold for limited periods of time. Reflecting this possibility, the stability results in Imsland et al. (2006) are stated as regional. We can prove stability of the observer with friction estimation (2.8), (2.9) using the weaker condition of a nonstrictly decreasing relationship, because $\eta(t,\tilde{x}) = 0$ is acceptable in (2.7) for limited periods of time (Grip et al., 2008). However, the observer tends to act as an open-loop integrator when the friction forces become saturated for all of the tires. If the situation persists for a long time, the achievable performance is therefore dictated by the sensor specifications, and the estimates may start to drift off due to sensor bias. It is difficult to overcome this deficiency because the vehicle model provides no useful information for stabilizing the estimates when all of the friction forces are saturated. In some applications it is desirable to detect large vehicle sideslip angles, in excess of 90°, which means that the tire forces may remain saturated for a considerable amount of time.

It is also common for the actual friction curves to decrease slightly, rather than to flatten out, for large tire-slip angles. Even the weakened condition of a nonstrictly decreasing relationship may therefore fail to hold in some extreme situations. Nonlinear friction models, like the magic formula, typically model this decrease. Not modeling this decrease may lead to limited modeling errors in some situations, but has a stabilizing effect on the observer dynamics itself. More to the point, experimental results indicate that this discrepancy does not cause a deterioration in the quality of the estimates.

## 2.8 Implementation and Practical Modifications

For implementation in real-time hardware, the observer (2.18)–(2.27) is discretized using the forward Euler method with a sample time of 10 ms. At each time step the reference velocity $v_{x,\text{ref}}$ and the gain $K_{v_x}(t)$ are updated. The friction model used in Figure 2.3 is also used in the implementation, with nominal friction coefficient $\mu_H^* = 1$. The default friction parameter is set to $\theta^* = 1$.

The friction model needs information about the vertical contact forces between the tires and the road, known as the wheel loads. These loads change during driving, depending mainly on the acceleration of the vehicle. We therefore use the measured longitudinal and lateral accelerations to calculate the wheel loads, similar to Kiencke and Nielsen (2000, Ch. 7.4).

The friction model specifies an algebraic relationship between the tire slips and the road-tire friction forces. In reality, however, dynamic effects known as tire relaxation dynamics cause a small phase lag in the buildup of forces. Although the tire relaxation dynamics are negligible at high speeds, taking them into account can yield improvements at low speeds. We approximate the effect of the tire relaxation dynamics using an approach similar to that in Pacejka (2006, Ch. 1) by filtering the output of the friction model using the first-order transfer function $1/(Ts + 1)$, where $T = T_e + l_e/\hat{v}_x$ is a speed-dependent time constant, which is small for large velocities.

To calculate the steering angles for the front wheels, we use a lookup table based on a steering transmission curve, with the measured steering wheel angle as the input. We do not use the output of the lookup table directly, however, because the steering angles are also affected by elasto-kinematic effects in the wheel suspension system (Matschinsky, 2007). A simplified way to account for these effects is the introduction of *caster*, which is the distance between the wheel contact point and the point where the steering axis intersects the road (Bosch, 2005). The caster acts as a moment arm causing the lateral road-tire friction forces to exert a torque on the steering axis. Positive caster causes the steering wheel to naturally return to the neutral position when it is released, thereby contributing to the stability of the steering system. To account for the effect of caster, the output from the lookup table must be reduced in proportion to the lateral road-tire friction forces. Following Pacejka (2006, Ch. 1), we calculate the steering angle for each of the front wheels using the expression $\delta_y = \delta_u - F_{y_f} e/c_l$, where $\delta_y$ is the steering angle, $\delta_u$ is the output of the lookup table, $F_{y_f}$ is the sum of the lateral road-tire friction forces for the front wheels, $e$ is the caster length, and $c_l$ is a steering stiffness constant. We calculate $F_{y_f}$ directly from the output of the friction model, which in turn depends on the steering angles, meaning that the expression for $\delta_y$ specifies a nonlinear algebraic equation. For practical purposes, this problem is solved by using a delay of

one time step for the value $F_{y_f}$ used in the calculation of $\delta_y$, to avoid an algebraic loop in the solution.

We restrict the estimated friction parameter $\hat{\theta}$ to the interval [0.05, 1.1], which spans the range of road surfaces that one can expect to encounter. We thereby obtain a discrete-time equivalent of a continuous-time parameter projection, which is theoretically justified in the continuous-time analysis (Grip et al., 2006). We also ensure that $1.2g\hat{\theta} \geq (a_x^2 + a_y^2)^{1/2}$, since $1.2\hat{\theta}g$ is the approximate maximum acceleration achievable from the friction model when multiplied by the friction parameter. This maximum must never be smaller than the actual acceleration of the vehicle.

## 2.9 Experimental Testing

Using data from a rear-wheel-drive passenger car, we test the observer in various situations, including dynamic and steady-state maneuvers on high- and low-friction surfaces, with different tires and at different speeds. The measurements are taken from automotive-grade sensors with no additional bias correction, and are filtered with a 15-Hz discrete lowpass filter before entering the observer. The inertial sensors are different for the high-friction and low-friction tests. For the high-friction tests, the yaw-rate sensor specifications indicate that bias and drift together may add up to a maximum of $3.5°/\mathrm{s}$, and the acceleration sensor specifications indicate that bias and drift may add up to a maximum of $1.0\ \mathrm{m/s^2}$. For the low-friction tests, the corresponding numbers are $3.5°/\mathrm{s}$ for the yaw-rate sensor and $0.6\ \mathrm{m/s^2}$ for the acceleration sensors.

As a reference, we use an optical correlation sensor to obtain independent vehicle velocities. The tuning of the observer and the parameterization of the friction model are the same for all tests, even though the tires are different.

The required accuracy of the vehicle sideslip estimate depends on the application. Typically, the error must be less than about 1° if the estimate is to be used for feedback control. When the main goal is to detect severe skidding, for example, to tighten seat belts before an impending accident, the requirements are less stringent. It is then sufficient to estimate large vehicle sideslip angles, approximately in the range 10–130°. An error of 2–3° degrees, or approximately 10% for vehicle sideslip angles larger than 30°, is then acceptable.

### 2.9.1 Comparison with EKF

We compare the observer estimates to those of an EKF similar to the one presented in Suissa et al. (1994). The states in the EKF are the longitudinal and lateral veloci-

ties, the inclination and bank angles, and the friction coefficient $\mu_H$. The dynamic model used in the EKF is based on (2.11), (2.12), where the yaw rate is considered a known, time-varying quantity. The derivatives of the friction coefficient, inclination angle, and bank angle are modeled as filtered white noise. The resulting dynamic model is linear time varying, which improves the accuracy of the EKF prediction compared to using a nonlinear dynamic model. The measurement equations are given by the force and moment balances through the nonlinear friction model for the longitudinal acceleration $a_x$, the lateral acceleration $a_y$, and the yaw acceleration $\ddot{\psi}$, which is calculated by numerically differentiating $\dot{\psi}$. In addition, an externally calculated reference velocity is used as a measurement. The EKF switches between slow and fast estimation of the friction coefficient, depending on the situation. The switching rule is the same as for the nonlinear observer, and the same friction model is used in both designs. As with the NVSO, the continuous-time model is discretized using the forward Euler method with a sample time of 10 ms. For efficient and stable numerical implementation, the Bierman algorithm (Bierman, 2006) is used in the measurement update process. The execution time of the NVSO is approximately one-third of that of the EKF. In the NVSO, the friction model dominates other computations.

### 2.9.2 Dynamic Maneuvers on High-Friction Surfaces

We begin with two examples of dynamic, high-excitation maneuvers on dry asphalt. The first maneuver consists of a series of steps in the steering wheel angle, carried out at a constant, high speed of 200 km/h. The lateral acceleration alternates between approximately $\pm 0.4g$. Figure 2.4 shows the results for the vehicle sideslip angle, friction parameter, and bank angle. The bank angle is estimated at approximately 2.2°, whereas the actual bank angle is approximately 1.5°, the difference being attributable to sensor bias. The resulting estimate of the vehicle sideslip angle is accurate to within approximately 0.3°. The friction estimation is activated briefly at each step, but is otherwise inactive.

The second example is an ISO-standard double lane-change maneuver, carried out at approximately 120 km/h, on a surface with a slight bank angle of approximately 0.5°. The car reaches a lateral acceleration of $-0.90g$ during the maneuver. Figure 2.5 shows the vehicle sideslip angle and the friction parameter. During this maneuver, the tires are brought well into the nonlinear region. Even though the lane change is carried out on a high-friction surface, the friction parameter is estimated far below its default value $\theta^* = 1$, suggesting that there are significant inaccuracies in the friction model during this maneuver. A sideslip estimation error of approximately 1.4° is briefly reached.

In general, for dynamic maneuvers on high-friction surfaces, the high degree of excitation means that inaccuracies in the friction model can to some extent be compensated by the friction parameter, as happens in the lane-change example.

### 2.9.3 Steady-State Maneuvers on High-Friction Surfaces

We now consider two examples of a steady-state circle maneuver on dry asphalt. In the first example, 18-inch summer tires are used; in the second example, 17-inch winter tires are used. The tests are otherwise the same. The car is driven counterclockwise along a circle with a 40-m radius, while the longitudinal velocity is slowly increased until the circle can no longer be maintained because of severe understeer. The maximum lateral accelerations reached toward the end of the maneuvers are $0.93g$ and $0.84g$, respectively. Figure 2.6 shows the vehicle sideslip angle for both maneuvers. The estimated vehicle sideslip angle is more accurate in the upper plot than in the lower one, where the sideslip estimation error reaches approximately 1.4° toward the end. This result indicates that the friction model more accurately matches the tires used for the first example than for the second. Because of the low level of excitation, the friction parameter cannot be used to compensate for errors in the friction model.

The EKF performs poorly for the circle maneuvers, mainly because it brings the estimated friction coefficient slightly below the initial value early in the maneuver, whereas the NVSO estimates friction only at the very end. The difference in results therefore has more to do with implementation details and tuning than with the fundamental properties of each method. Nevertheless, the examples illustrate the sensitivity of friction-based estimation designs to errors in the friction model for low-excitation maneuvers of this kind.

### 2.9.4 Low-Friction Surfaces

We now look at two examples from low-friction surfaces. In the first example, the car is driven around a circle on a lake covered with ice and snow. Figure 2.7 shows the longitudinal velocity, vehicle sideslip angle, and friction parameter. The car exhibits very large vehicle sideslip angles at several points, and the sideslip estimation error remains smaller than 3° for most of the test. A notable exception is the period between 140 s and 160 s, when a large vehicle sideslip angle is sustained for a long time. Reduced excitation results in inaccurate estimation of the vehicle sideslip angle in this situation.

The final example is carried out on snow-covered mountain roads. Figure 2.8 shows the vehicle sideslip angle, inclination angle, and bank angle. In contrast to

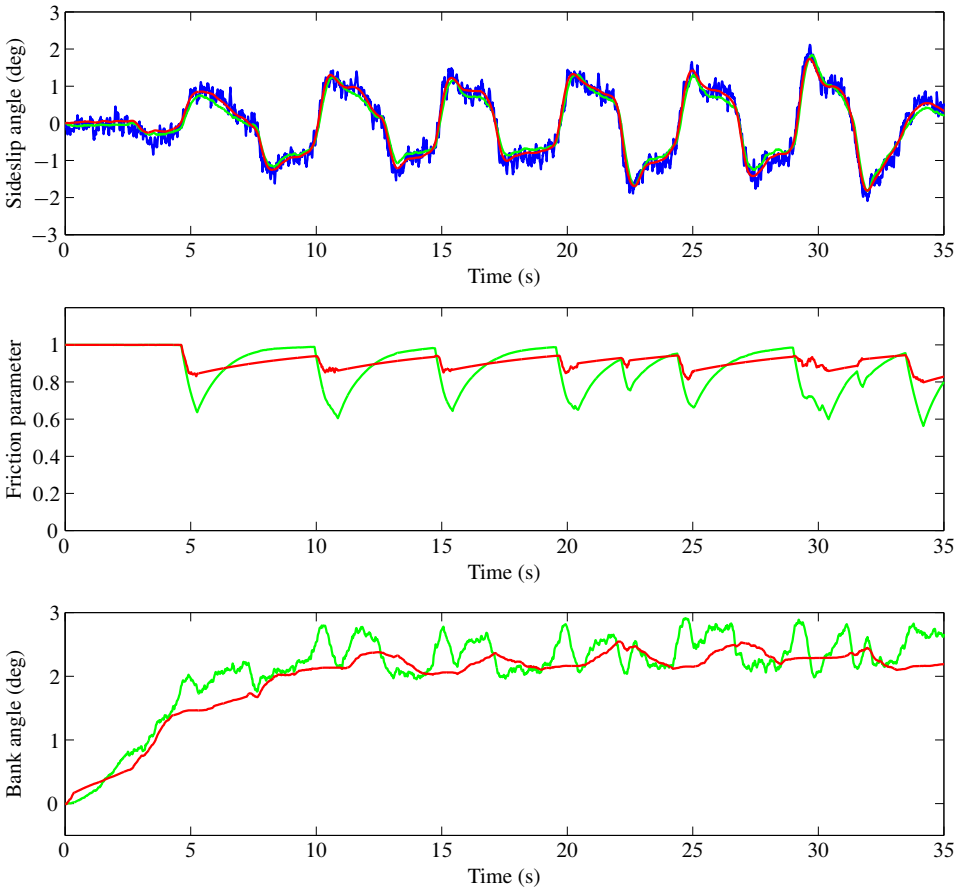


**Figure 2.4:** Experimental results for periodic steps in the steering angle at 200 km/h. The uppermost plot shows the actual vehicle sideslip angle (blue) and the vehicle sideslip angles estimated by the EKF (green) and the NVSO (red). The middle plot shows the friction coefficient estimated by the EKF (green) and the friction parameter estimated by the NVSO (red). The lowest plot shows the bank angles estimated by the EKF (green) and the NVSO (red).

the lake example, large inclination and bank angles occur in this example. We do not know the true values of the inclination and bank angles, but the magnitudes of the estimates are plausible. The vehicle sideslip angle reaches approximately $-14°$, and the estimation error remains smaller than $1.5°$. In this example, estimating the bank angle at the same time as the friction parameter is necessary to avoid deterioration of the sideslip estimate.

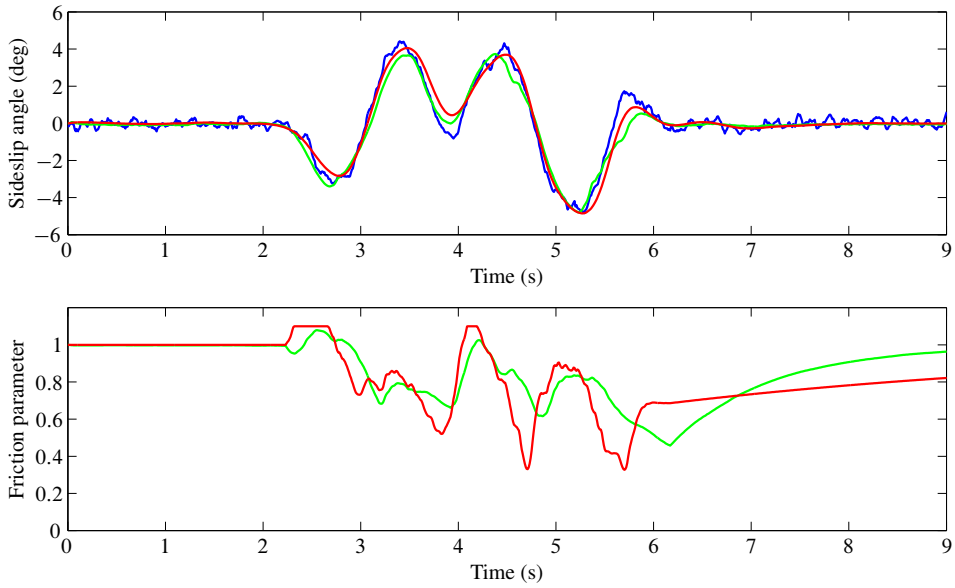


**Figure 2.5:** Experimental results for an ISO-standard double lane-change maneuver at 120 km/h. The upper plot shows the actual vehicle sideslip angle (blue) and the vehicle sideslip angles estimated by the EKF (green) and the NVSO (red). The lower plot shows the friction coefficient estimated by the EKF (green) and the friction parameter estimated by the NVSO (red).

## 2.10 Concluding Remarks

Based on extensive experimental tests we conclude that, overall, the NVSO performs as well as the EKF, while achieving a significant reduction in execution time. The reduction is likely to be even more significant on production hardware with a fixed-point microprocessor, since the computations largely consist of floating-point operations. The NVSO is based on nonlinear analysis, which contributes toward understanding the strengths and limitations of the observer, the EKF, and alternative designs with similar sensor configurations. The number of observer gains in the NVSO is smaller than the number of tunable elements in the EKF. Nevertheless, because of the switching between different operating regimes and the various thresholds involved in the switching logic, tuning the NVSO is nontrivial.

The observer estimates are typically of high quality. As illustrated by the examples, however, the design is sensitive to errors in the friction model, in particular during steady-state maneuvers, and the accuracy of the friction model depends to some extent on the tires. A full, systematic analysis of the response of the observer

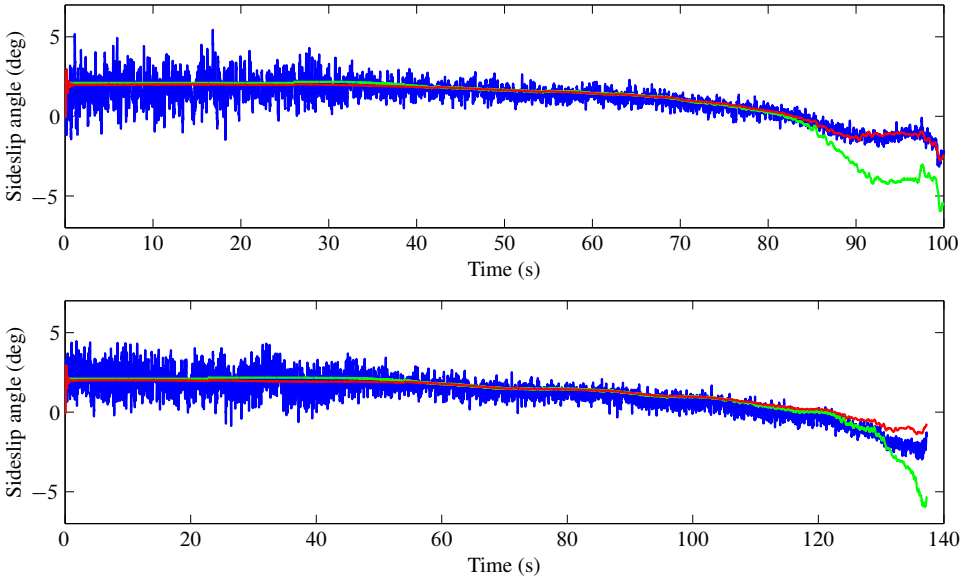


**Figure 2.6:** Experimental results for circle maneuvers with a 40-m radius and different tires. Each plot shows the actual vehicle sideslip angle (blue) and the vehicle sideslip angles estimated by the EKF (green) and the NVSO (red). In the upper plot, 18-inch summer tires are used. In the lower plot, 17-inch winter tires are used.

to various model uncertainties and sensor inaccuracies is a formidable task that is yet to be carried out.

Furthermore, problems remain in some situations involving low-friction surfaces. These problems can largely be attributed to the difficulty of distinguishing a nonzero bank angle from low friction. The NVSO's method of combining friction estimation and bank-angle estimation is a weakness in the present design, and the ad hoc approach of selectively reducing the bank-angle gain based on various criteria is likely to need revision and improvement before the NVSO can reach production quality. The EKF is in general better at automatically distinguishing the influences of low friction and a nonzero bank angle, giving it an advantage in some situations, and suggesting that there is still room for improving the NVSO.

A central strategy in the NVSO design is to estimate the total force acting in the lateral direction of the car by using a friction model, and to subtract this estimate from the total force measured through the lateral acceleration. The resulting difference produces the quantity $\tilde{a}_y(t, \tilde{x}, \tilde{\theta})$ when divided by the mass. By using the yaw acceleration $\ddot{\psi}$ it is possible to separate between the lateral friction forces on the front and rear axles. We can then produce two quantities similar to $\tilde{a}_y(t, \tilde{x}, \tilde{\theta})$,

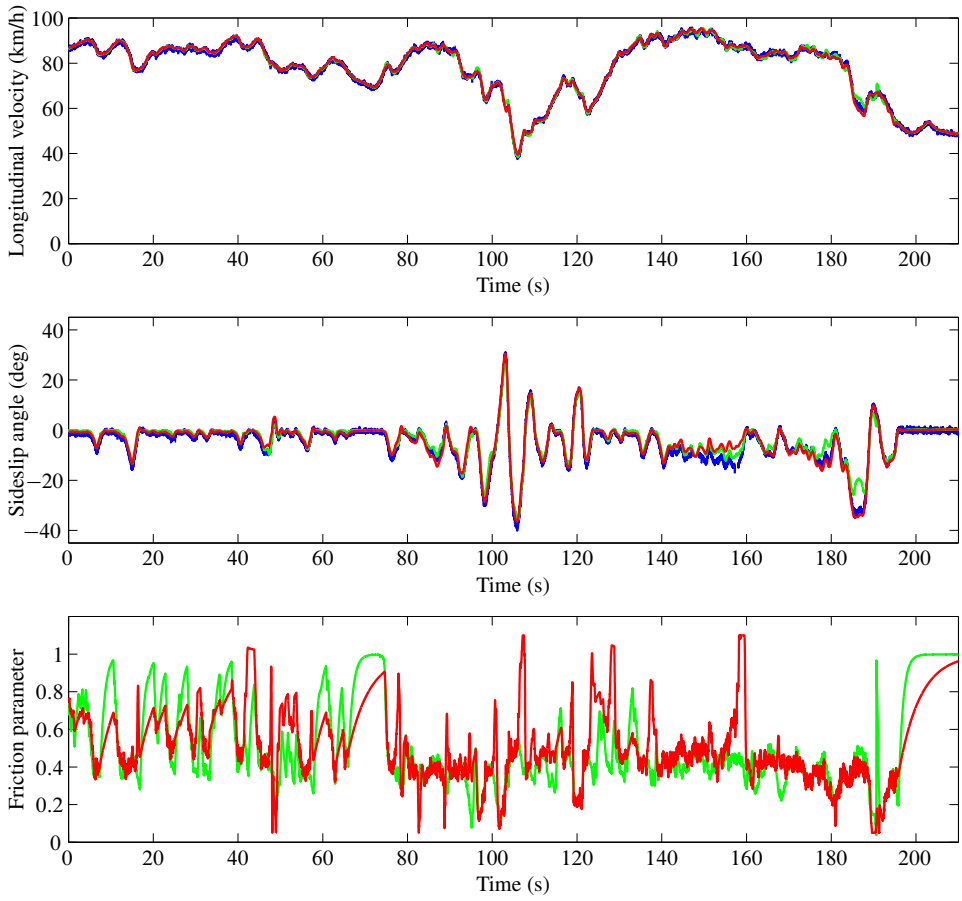


**Figure 2.7:** Experimental results for driving on an ice- and snow-covered lake. The uppermost plot shows the actual longitudinal velocity (blue) and the longitudinal velocities estimated by the EKF (green) and the NVSO (red). The middle plot shows the actual vehicle sideslip angle (blue) and the vehicle sideslip angles estimated by the EKF (green) and the NVSO (red). The lowest plot shows the friction coefficient estimated by the EKF (green) and the friction parameter estimated by the NVSO (red).

one for the front axle and one for the rear axle. The NVSO design can be carried out in the same way using these two quantities, resulting in two injection terms in the derivatives of the lateral-velocity and bank-angle estimates. We can furthermore use separate friction parameters for the front and rear axles. This strategy shows some promise with respect to improving the separation between nonzero bank angles and low-friction surfaces. Since we have not obtained a consistent

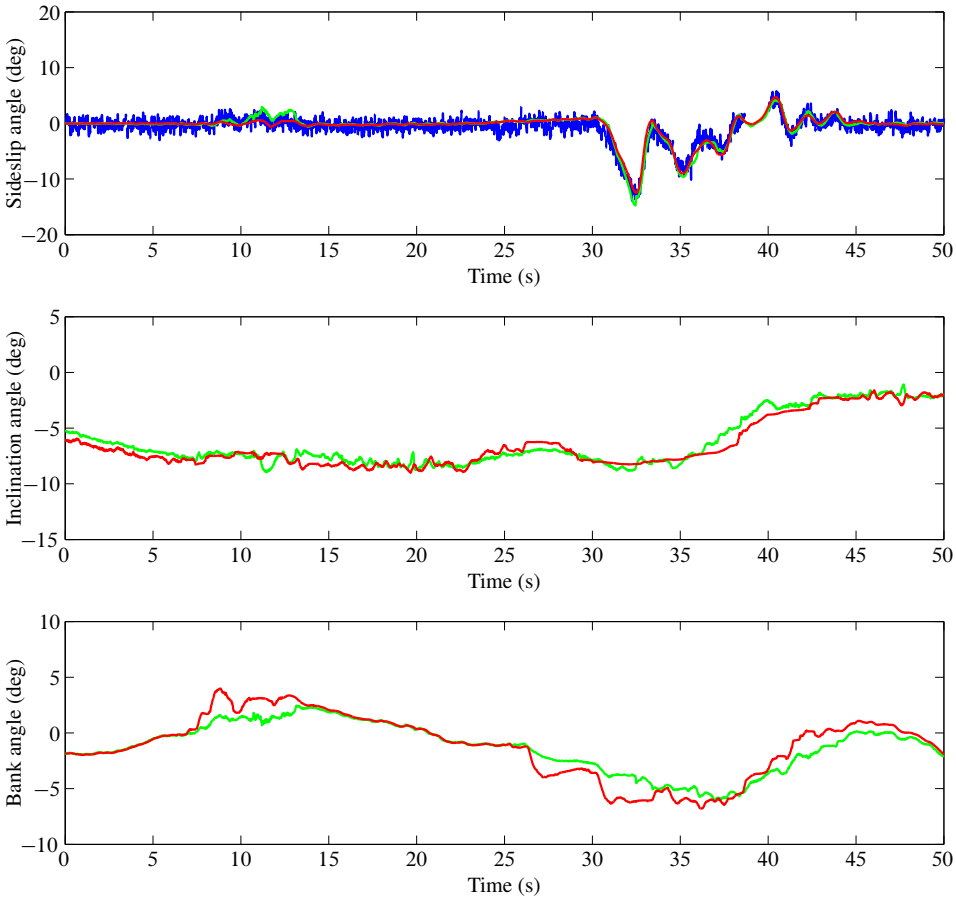


**Figure 2.8:** Experimental results for driving on snow-covered mountain roads. The uppermost plot shows the actual vehicle sideslip angle (blue) and the vehicle sideslip angles estimated by the EKF (green) and the NVSO (red). The middle plot shows the inclination angles estimated by the EKF (green) and the NVSO (red). The lowest plot shows the bank angles estimated by the EKF (green) and the NVSO (red).

improvement in quality, however, we have not used this type of design for the experimental results presented in this article.

A limitation imposed by the sensor configuration is that derivative information about the inclination and bank angles is not available in the form of roll- and pitch-rate measurements. The estimates of the inclination and bank angles are therefore produced by a form of integral action, which, in the case of the bank-angle estimation, depends on the friction model. With this solution, the inclination- and bank-

angle estimates tend to capture low-frequency disturbances, which also includes sensor bias. The estimates have a limited ability to respond to rapid changes, which is is underscored by upper limits on the allowable gains $K_{\theta_i}$ and $K_{\theta_b}$. Preliminary results indicate that significant improvement can be obtained in this respect if derivative information is made available by using a six-degree-of-freedom sensor cluster.

Fundamentally, the level of accuracy that can consistently be achieved with any estimation strategy depends on the sensor configuration. As discussed at several points, the achievable performance is dictated by the sensor specifications in situations where the vehicle model provides no useful information. It is our opinion that, to achieve a consistent vehicle sideslip error of less than 1°, it is necessary to improve on the standard ESC-type sensor configuration considered in this article.

## Acknowledgments

The research presented in this article is supported by the European Commission STREP project *Complex Embedded Automotive Control Systems*, contract 004175, and the Research Council of Norway, and was partly conducted while Håvard Fjær Grip, Lars Imsland, and Tor A. Johansen were associated with SINTEF ICT, Applied Cybernetics, NO-7465 Trondheim, Norway.

## Bibliography

M. C. Best, T. J. Gordon, and P. J. Dixon. An extended adaptive Kalman filter for real-time state estimation of vehicle handling dynamics. *Vehicle Syst. Dyn.*, 34 (1):57–75, 2000.

D. M. Bevly. Global Positioning System (GPS): A low-cost velocity sensor for correcting inertial sensor errors on ground vehicles. *J. Dyn. Syst. Meas. Contr.*, 126(2):255–264, 2004.

D. M. Bevly, J. C. Gerdes, and C. Wilson. The use of GPS based velocity measurements for measurement of sideslip and wheel slip. *Vehicle Syst. Dyn.*, 38 (2):127–147, 2002.

D. M. Bevly, J. Ryu, and J. C. Gerdes. Integrating INS sensors with GPS measurements for continuous estimation of vehicle sideslip, roll, and tire cornering stiffness. *IEEE Trans. Intell. Transport. Syst.*, 7(4):483–493, 2006.

G. J. Bierman. *Factorization Methods for Discrete Sequential Estimation*. Dover, New York, 2006.

Bosch. *Automotive Handbook*. SAE, Warrendale, PA, 6th edition, 2005.

J. A. Farrell. *Aided Navigation: GPS with High Rate Sensors*. McGraw-Hill, New York, 2008.

J. Farrelly and P. Wellstead. Estimation of vehicle lateral velocity. In *Proc. IEEE Int. Conf. Contr. Appl.*, pages 552–557, Dearborn, MI, 1996.

Y. Fukada. Slip-angle estimation for vehicle stability control. *Vehicle Syst. Dyn.*, 32(4):375–388, 1999.

H. F. Grip, L. Imsland, T. A. Johansen, T. I. Fossen, J. C. Kalkkuhl, and A. Suissa. Nonlinear vehicle velocity observer with road-tire friction adaptation. In *Proc. IEEE Conf. Dec. Contr.*, pages 3603–3608, San Diego, CA, 2006.

H. F. Grip, L. Imsland, T. A. Johansen, T. I. Fossen, J. C. Kalkkuhl, and A. Suissa. Nonlinear vehicle side-slip estimation with friction adaptation. *Automatica*, 44 (3):611–622, 2008.

A. Hac and M. D. Simpson. Estimation of vehicle side slip angle and yaw rate. In *Proc. SAE World Congr.*, Detroit, MI, 2000. Paper no. 2000-01-0696.

P. Haney. *The Racing & High-Performance Tire: Using Tires to Tune for Grip & Balance*. SAE, Warrendale, PA, 2003.

M. Hiemer, A. von Vietinghoff, U. Kiencke, and T. Matsunaga. Determination of the vehicle body slip angle with non-linear observer strategies. In *Proc. SAE World Congr.*, Detroit, MI, 2005. Paper no. 2005-01-0400.

L. Imsland, T. A. Johansen, T. I. Fossen, H. F. Grip, J. C. Kalkkuhl, and A. Suissa. Vehicle velocity estimation using nonlinear observers. *Automatica*, 42(12): 2091–2103, 2006.

L. Imsland, H. F. Grip, T. A. Johansen, T. I. Fossen, J. C. Kalkkuhl, and A. Suissa. Nonlinear observer for vehicle velocity with friction and road bank angle adaptation—Validation and comparison with an extended Kalman filter. In *Proc. SAE World Congr.*, Detroit, MI, 2007a. Paper no. 2007-01-0808.

L. Imsland, T. A. Johansen, H. F. Grip, and T. I. Fossen. On nonlinear unknown input observers—Applied to lateral vehicle velocity estimation on banked roads. *Int. J. Contr.*, 80(11):1741–1750, 2007b.

H. K. Khalil. *Nonlinear Systems*. Prentice-Hall, Upper Saddle River, NJ, 3rd edition, 2002.

U. Kiencke and A. Daiß. Observation of lateral vehicle dynamics. *Contr. Eng. Pract.*, 5(8):1145–1150, 1997.

U. Kiencke and L. Nielsen. *Automotive Control Systems: For Engine, Driveline, and Vehicle*. Springer, Berlin, 2000.

W. Klier, A. Reim, and D. Stapel. Robust estimation of vehicle sideslip angle—An approach w/o vehicle and tire models. In *Proc. SAE World Congr.*, Detroit, MI, 2008. Paper no. 2008-01-0582.

H. Lee. Reliability indexed sensor fusion and its application to vehicle velocity estimation. *J. Dyn. Syst. Meas. Contr.*, 128(2):236–243, 2006.

A. Loría, E. Panteley, D. Popović, and A. R. Teel. A nested Matrosov theorem and persistency of excitation for uniform convergence in stable nonautonomous systems. *IEEE Trans. Automat. Contr.*, 50(2):183–198, 2005.

W. Matschinsky. *Radführungen der Straßenfahrzeuge: Kinematik, Elasto-Kinematik und Konstruktion*. Springer-Verlag, New York, 3rd edition, 2007.

H. B. Pacejka. *Tire and Vehicle Dynamics*. SAE, Warrendale, PA, 2nd edition, 2006.

L. R. Ray. Nonlinear tire force estimation and road friction identification: Simulation and experiments. *Automatica*, 33(10):1819–1833, 1997.

J. Ryu and J. C. Gerdes. Integrating inertial sensors with Global Positioning System (GPS) for vehicle dynamics control. *J. Dyn. Syst. Meas. Contr.*, 126(2): 243–254, 2004.

C. Sentouh, Y. Sebsadji, S. Mammar, and S. Glaser. Road bank angle and faults estimation using unknown input proportional-integral observer. In *Proc. European Contr. Conf.*, pages 5131–5138, Kos, Greece, 2007.

A. Suissa, Z. Zomotor, and F. Böttiger. Method for determining variables characterizing vehicle handling. US Patent 5,557,520, 1994. Filed Jul. 29, 1994; issued Sep. 17, 1996.

H. E. Tseng. Dynamic estimation of road bank angle. *Vehicle Syst. Dyn.*, 36(4): 307–328, 2001.

A. Y. Ungoren, H. Peng, and H. E. Tseng. A study on lateral speed estimation methods. *Int. J. Vehicle Auton. Syst.*, 2(1–2):126–144, 2004.

A. T. van Zanten. Bosch ESP systems: 5 years of experience. In *Proc. Automot. Dyn. Stab. Conf.*, Troy, MI, 2000. Paper no. 2000-01-1633.

P. J. T. Venhovens and K. Naab. Vehicle dynamics estimation using Kalman filters. *Vehicle Syst. Dyn.*, 32(2):171–184, 1999.

A. von Vietinghoff, M. Hiemer, and U. Kiencke. Nonlinear observer design for lateral vehicle dynamics. In *Proc. IFAC World Congr.*, pages 988–993, Prague, Czech Republic, 2005.

A. von Vietinghoff, S. Olbrich, and U. Kiencke. Extended Kalman filter for vehicle dynamics determination based on a nonlinear model combining longitudinal and lateral dynamics. In *Proc. SAE World Congr.*, Detroit, MI, 2007. Paper no. 2007-01-0834.

# Chapter 3

# Nonlinear Vehicle Side-Slip Estimation with Friction Adaptation

***Abstract:*** *A nonlinear observer for estimation of the longitudinal velocity, lateral velocity, and yaw rate of a vehicle, designed for the purpose of vehicle side-slip estimation, is modified and extended in order to work for different road surface conditions. The observer relies on a road-tire friction model and is therefore sensitive to changes in the adhesion characteristics of the road surface. The friction model is parametrized with a single friction parameter, and an update law is designed. The adaptive observer is proven to be uniformly globally asymptotically stable and uniformly locally exponentially stable under a persistency-of-excitation condition and a set of technical assumptions, using results related to Matrosov's theorem. The observer is tested on recorded data from two test vehicles and shows good results on a range of road surfaces.*

## 3.1 Introduction

A current focus of the automotive industry is the development of active safety systems, which assist the driver in order to avoid dangerous situations. As such systems become more advanced, they depend to an increasing extent on accurate information about the state of the vehicle and its surroundings. Much of this information can be obtained by direct measurement, but the appropriate sensors may be unreliable, inaccurate, or prohibitively expensive. Observers are therefore used to provide accurate and reliable estimates of important states.

Observers that estimate vehicle velocity usually rely on road-tire friction models, which model the friction forces between the tires of the vehicle and the road surface. As the adhesion characteristics between the tires and the road depend on the road surface, knowledge about the current road surface conditions is important for this type of observer to work properly.

Several different methods for obtaining information about road surface conditions have previously been studied. In Ono et al. (2003), a least-squares method is used on measurements of wheel angular velocity to estimate the slope of the friction force versus the tire slip. An observer for lateral velocity in Fukada (1999) includes a filtering scheme for estimating the maximum road-tire friction coefficient, based primarily on using the lateral acceleration measurement during times when this provides a good measurement of the coefficient. A similar approach is taken in Hac and Simpson (2000). In Gustafsson (1997), a Kalman filter is used to classify road surface conditions, by inspecting the ratio between slip values of the driven wheels and the normalized friction force, obtained using wheel angular velocities and engine torque. In Ray (1997), an extended Kalman filter (EKF) is combined with statistical methods in order to estimate the maximum road-tire friction coefficient, using measurements of the yaw and roll rates, wheel angular velocities, and longitudinal and lateral accelerations, as well as knowledge of the steering angle and total brake line pressure. Other examples of EKFs are presented in Suissa, Zomotor, and Böttiger (1994) and Best, Gordon, and Dixon (2000). In Nishira, Kawabe, and Shin (1999), wheel angular velocity, longitudinal tire slip, and wheel torque is used to generate an estimate of the wheel angular velocity and for adaptation of a friction parameter. Wheel angular velocity and torque is used in Canudas-de-Wit, Petersen, and Shiriaev (2003) for estimation of the longitudinal velocity and wheel angular velocity, and adaptation of a friction parameter. In both Nishira et al. (1999) and Canudas-de-Wit et al. (2003), convergence of the adapted friction parameters under conditions of nonzero longitudinal tire slip is studied.

In addition to accuracy and reliability, production cost is an important matter in vehicle serial production. To reduce cost, observer designs should be computationally efficient and be based on cheap sensor configurations. In Imsland, Johansen, Fossen, Grip, Kalkkuhl, and Suissa (2006a), a nonlinear observer for vehicle velocity is presented with stability guarantees. The observer is computationally efficient and is based on measurements commonly available in modern cars. A significant weakness of the observer is that it relies on a friction model that must be tuned to the current road surface conditions. In Grip, Imsland, Johansen, Fossen, Kalkkuhl, and Suissa (2006), the authors addressed this issue for a reduced-order observer for lateral velocity by presenting a method for adaptation of the friction model to different road surface conditions. In the current paper, an

improved version of this adaptive observer is presented, and in Section 3.5, it is extended to include longitudinal velocity and yaw rate. The observer retains the advantage of being less computationally expensive than an EKF. The ultimate goal of the observer design is accurate estimation of the vehicle side-slip angle.

The stability analysis presented in this paper relies crucially on the concept of persistency of excitation (PE), introduced by Åström and Bohlin (1965). This concept has been developed in various directions to deal with situations where regressors are dependent not only on external, time-varying signals, but on the states of the system, which is the case for the system considered in this paper. One approach to dealing with state-dependent regressors is to consider a PE condition along the trajectories of the states. The drawback of this approach is that, in general, the trajectories of the states must be known in advance. Another approach is to consider the states a parameter, and to evaluate a PE condition over all values of this parameter. This idea is combined with a generalization of Matrosov's theorem in Loría, Panteley, Popović, and Teel (2005), the results of which are used in this paper. Although the specific trajectories of the states need not be known, the PE conditions resulting from this approach are in general difficult to verify. In the present case, we nevertheless offer a natural and intuitively reasonable interpretation of the PE condition, which is directly related to driving patterns and supported by experimental results.

Systems similar to the one considered in this paper have previously been investigated under PE conditions (Ortega and Fradkov, 1993; Zhang, Ioannou, and Chien, 1996; Panteley, Loría, and Teel, 2001). Another example of observer design with analysis similar to what is presented here can be found in Loría and de León Morales (2003).

### 3.1.1 Notation

Conventional notation is used for denoting estimated variables and error variables, meaning that for some variable $z$, $\hat{z}$ denotes its estimate and $\tilde{z} = z - \hat{z}$. When considering error dynamics, a function depending on an estimated variable $\hat{z}$ may be written as a function of the error variable $\tilde{z}$ and $t$, by noting that $\hat{z} = z - \tilde{z}$ and considering $z$ a time-varying signal. For a vector $z$, $z_{\{i,j\}}$ denotes the vector obtained by stacking elements $i$ and $j$ of $z$. The norm operator $\|\cdot\|$ denotes the Euclidean norm. The closed ball with center 0 and radius $r$ is denoted $\overline{B}(r) = \{z \mid \|z\| \leq r\}$. The minimum eigenvalue of a matrix $A$ is denoted $\lambda_{\min}(A)$. The positive real numbers are denoted $\mathbb{R}_{>0}$.

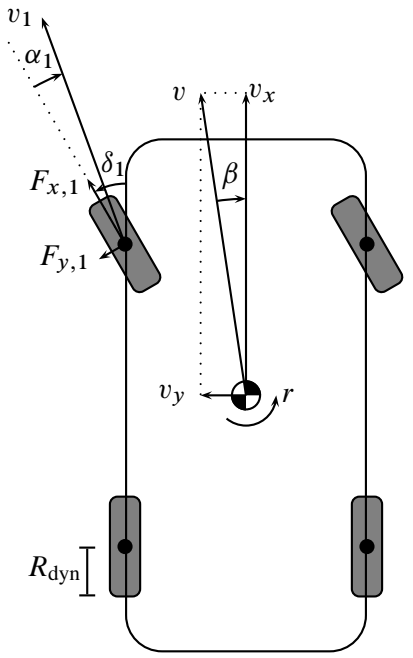


**Figure 3.1:** Schematic overview of vehicle

## 3.2 Vehicle Model and Preliminaries

The vehicle is illustrated in Figure 3.1. Of primary interest is the side-slip angle $\beta$, which is the angle between the longitudinal direction of the vehicle and the direction of travel at the center of gravity (CG). To obtain the side-slip angle, we shall estimate the longitudinal velocity $v_x$ and the lateral velocity $v_y$ at the CG, from which $\beta = -\arctan(v_y/v_x)$ can be calculated.

The vehicle is assumed to be moving on a flat, horizontal surface. In general, there are environmental forces, such as wind forces and air resistance, acting on the vehicle. In our model, these are disregarded; we assume that only road-tire friction forces act on the vehicle.

### 3.2.1 Friction Modeling

Several semi-empirical models for road-tire friction exist, the most well-known of which is the Magic Formula (Pacejka, 2006). This paper is not based on a particular friction model; instead, it is assumed that the friction model adheres

to certain assumptions, which will be formally stated later. Thus, the design is not bound to a particular friction model, but instead allows for a range of friction models to be used.

Road-tire friction forces are usually calculated based on the normal force between a tire and the road, and tire slip values. The tire slip values are measures of the relative difference between the vehicle velocity and the circumferential velocity of the tire in its longitudinal and lateral directions. Exact definitions of tire slips vary, but one possible definition, used for the experimental results in this paper, is

$$\lambda_{x,i} = \frac{\omega_i R_{\text{dyn}} - \|v_i\| \cos\alpha_i}{\|v_i\|}, \quad \lambda_{y,i} = \sin\alpha_i,$$

where $\lambda_{x,i}$ and $\lambda_{y,i}$ are the longitudinal and lateral slips of wheel number $i$; $R_{\text{dyn}}$ is the dynamic radius of the tire; $\omega_i$ is the angular velocity of the wheel; $v_i$ is the velocity vector of the vehicle above the wheel center; and $\alpha_i$ is the angle between the longitudinal direction of the wheel and the vector $v_i$ (see illustration of front-left wheel in Figure 3.1).

It is common to define the friction coefficient $\mu = F/F_z$, where $F$ is the magnitude of the road-tire friction force and $F_z$ is the magnitude of the vertical normal force. Everything else being the same, $\mu$ is in general lower on more slippery surfaces. The value $\mu$ is, however, not constant for a particular surface. The road surface conditions are therefore more suitably described by the maximum value of $\mu$ for a particular surface. Throughout this paper, $\mu_H$ is used to denote some parameter used in the friction model to characterize the road-tire friction properties, usually the maximum road-tire friction coefficient.

In the following, we denote by $d$ a vector containing all time-varying signals used in the friction model, except the lateral velocity $v_y$ and the coefficient $\mu_H$. The contents of $d$ may be different depending on the friction model used, but we assume availability of certain measurements to be included in $d$:

- the longitudinal acceleration ($a_x$)
- the lateral acceleration ($a_y$)
- the yaw rate ($r$)
- the wheel angular velocities ($\omega_i, i = 1, \ldots, 4$)
- the wheel angles ($\delta_i, i = 1, \ldots, 4$)

The wheel angles $\delta_i$ are in practice calculated from the measured steering wheel angle $\delta$. Because estimation of the longitudinal velocity $v_x$ is not considered until Section 3.5, it is at this point assumed available as a measurement and included in $d$. We denote the friction forces by vector-valued functions $F_i(d, v_y, \mu_H)$.

### 3.2.2 Vehicle Model

The vehicle is modeled as a rigid body and is studied in a body-fixed coordinate system with the origin located at the CG. The friction forces $F_i(d, v_y, \mu_H)$ are calculated in wheel-fixed coordinate systems, rotated by angles $\delta_i$ with respect to the body-fixed one. The resultant force acting on the vehicle in the lateral direction is denoted

$$f_y(d, v_y, \mu_H) = \sum_{i=1}^{4} [0\ 1] R(\delta_i) F_i(d, v_y, \mu_H),$$

where $R(\delta_i)$ are rotational matrices between the wheel-fixed coordinate systems and the body-fixed one. Using Newton's second law, we may write $ma_y = f_y(d, v_y, \mu_H)$, where $m$ is the mass of the vehicle. The equation of motion in the lateral direction is (see, e.g., Kiencke and Nielsen, 2000)

$$\dot{v}_y = a_y - r v_x. \tag{3.1}$$

## 3.3 Adaptive Observer

In Imsland et al. (2006a), the lateral velocity part of the observer includes a stabilizing injection term that relies on the friction model. The friction model is assumed to be tuned to the current road surface conditions. This assumption is now removed, and a method is developed for adaptation of the friction model to different road surface conditions.

### 3.3.1 Friction Model Parametrization

It is necessary to identify one or more parameters that characterize different road surface conditions and tire properties, and which are suitable for adaptation. One possibility is to use $\mu_H$ for adaptation, as is done in Grip et al. (2006). In this paper, a closely related parameter, which is easier to deal with and results in slightly better performance, is chosen. We may write

$$f_y(d, v_y, \mu_H) = \theta f_y^*(d, v_y), \tag{3.2}$$

where $\theta$ is the parameter to be adapted. The function $f_y^*$ is defined as

$$f_y^*(d, v_y) = \frac{1}{\mu_H^*} \sum_{i=1}^{4} [0\ 1] R(\delta_i) F_i(d, v_y, \mu_H^*),$$

where $\mu_H^*$ is some fixed nominal value of $\mu_H$.

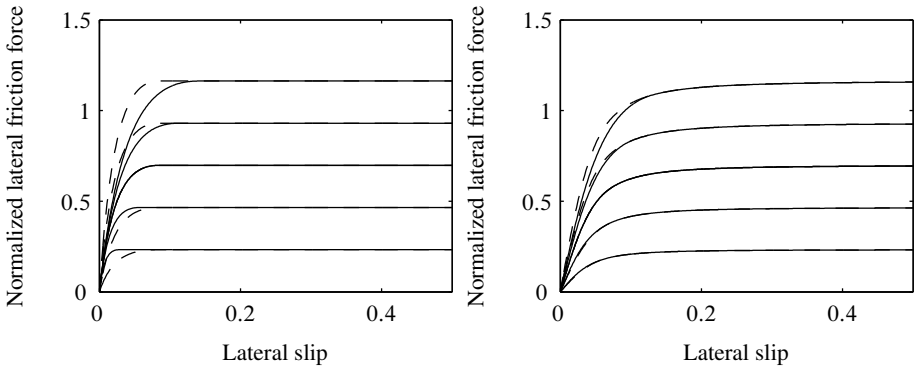


(a) Zero longitudinal tire slip (b) Longitudinal slip set to 0.05

**Figure 3.2:** Friction curves for different friction parameters (dashed) and $\mu_H$ (solid)

**Assumption 3.1.** *The friction parameter $\theta$ is constant and strictly positive, with known upper and lower bounds, such that $\dot{\theta} = 0$ and $0 < \theta_{\min} \leq \theta \leq \theta_{\max}$.*

Compared to using $\mu_H$ for adaptation, choosing $\theta$ as described above offers certain benefits, because the parameter enters linearly into (3.2). The drawback of the chosen parametrization is that Assumption 3.1 is less realistic, since $\theta$ cannot be expected to be completely time-invariant even if the road surface conditions remain unchanged. In order to compare the two parameters $\mu_H$ and $\theta$, Figure 3.2 shows the magnitude of the calculated friction force in the lateral direction of a single wheel, normalized by division with the normal force $F_z$. The solid curves are generated using different values of $\mu_H$ in the friction model, while the dashed curves are generated by using a nominal coefficient $\mu_H^* = 0.6$ and varying $\theta$.[1]

The difference seen in Figure 3.2 may result in rapid variations in the friction parameter when the driving pattern is highly varied. This is illustrated in Figure 3.3, where $\theta$ is plotted for simulated maneuvers with increasingly rapid variations on a high-friction ($\mu_H = 1.0$) and a low-friction ($\mu_H = 0.3$) surface. Assumption 3.1 must be seen as a necessary design assumption, which is known to be an imprecise description of the true physical system. While a varied driving pattern causes variation in $\theta$, it also results in greater robustness of the observer to be presented, as will be shown in Section 3.4. Moreover, experimental results indicate that the observer is indeed robust with respect to the error made in making this assumption.

[1]The comparison in Figure 3.2 is for a single wheel. In most practical situations, the friction forces for each wheel are different, and some of the difference in parametrization will average out in the resultant force.

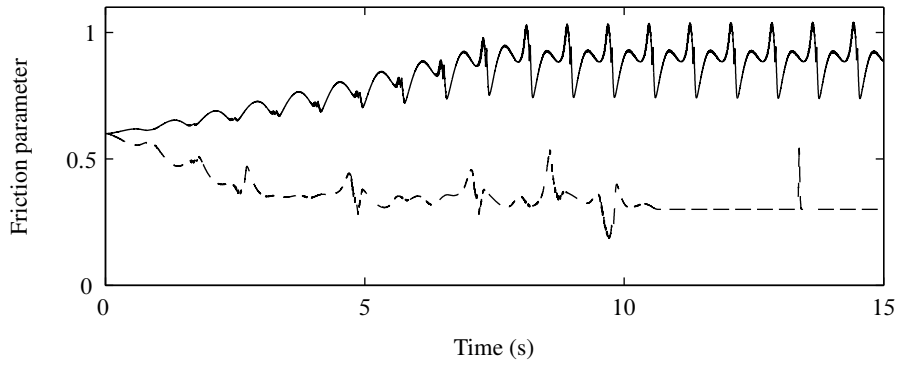


**Figure 3.3:** Friction parameter for maneuver on high-friction (solid) and low-friction (dashed) surface

Using a single parameter to describe different road surfaces is a simplification of the true physical system. Such a parametrization cannot, for example, describe situations where the surface is different below each wheel. For the lateral velocity estimation in this paper it is, however, enough to identify the effect of surface changes on the resultant lateral force, without regard to how this manifests itself physically (this is no longer true when yaw rate estimation is added, but given that feedback from the yaw rate measurement is available, this does not present significant problems). While a design could be based on a richer parametrization, for example by using one parameter per wheel, separate ones for the lateral resultant force and yaw moment, or by expressing the friction model in terms of several basis functions, the added complexity does not seem warranted in light of the good results obtained using the simple one-parameter scheme.

### 3.3.2 Observer and Stability Results

Before proposing an observer and presenting stability results, some extra assumptions are needed. We define the vector $x = [v_y, \theta]^\mathsf{T}$ of states to be estimated.

**Assumption 3.2.** *There exist compact sets $D_d \subset \mathbb{R}^m$ and $D_{v_y} \subset \mathbb{R}$ such that*

- $(d, v_y) \in D_d \times D_{v_y}$;
- *$d$ and $v_y$ are uniformly continuous in $t$ on $\mathbb{R}$; and*
- *$F_i(d, v_y, \mu_H^*)$ and $[\partial F_i / \partial v_y](d, v_y, \mu_H^*)$ are continuous on $D_d \times \mathbb{R} \times \{\mu_H^*\}$.*

**Assumption 3.3.** *There exists a known function* $\xi\colon D_d \times \mathbb{R}^2 \to \mathbb{R}$ *such that* $\xi(d, \hat{x})$ *and* $[\partial\xi/\partial\hat{x}](d, \hat{x})$ *are continuous on* $D_d \times \mathbb{R}^2$ *and*

$$f_y^*(d, v_y) - f_y^*(d, \hat{v}_y) = \xi(d, \hat{x})(v_y - \hat{v}_y). \tag{3.3}$$

*Remark* 3.1. According to the mean value theorem, there always exists a value such that (3.3) holds if $\xi(d, \hat{x})$ is given that value. In general it is, however, not possible to obtain this exact value without knowing $v_y$. Fortunately, it is not difficult to obtain a sufficiently good approximation of the value, as will be discussed in Section 3.6.

For presentation of the error dynamics, we define the function

$$\tilde{a}_y(t, \tilde{x}) = a_y - \frac{1}{m}\hat{\theta} f_y^*(d, \hat{v}_y).$$

This represents the difference between the actual lateral acceleration and an estimate obtained using the friction model. The notation $\hat{f}_y^* = f_y^*(d, \hat{v}_y)$, $\xi = \xi(d, \hat{x})$, and $\tilde{a}_y = \tilde{a}_y(t, \tilde{x})$ is used for the sake of brevity.

The following observer is proposed:

$$\dot{\hat{v}}_y = a_y - r v_x + K_{v_y} \Lambda \xi \left( m a_y - \hat{\theta} \hat{f}_y^* \right), \tag{3.4a}$$

$$\dot{\hat{\theta}} = \Gamma K_{v_y} \Lambda \hat{f}_y^* \left( m a_y - \hat{\theta} \hat{f}_y^* \right), \tag{3.4b}$$

where $K_{v_y}$ and $\Gamma$ are positive gains and $\Lambda = \Lambda(d, \hat{x})$ refers to some choice function $\Lambda\colon D_d \times \mathbb{R}^2 \to [\Lambda_{\min}, \Lambda_{\max}] \subset \mathbb{R}_{>0}$, defined such that $\Lambda(d, \hat{x})$ and $[\partial\Lambda/\partial\hat{x}](d, \hat{x})$ are continuous on $D_d \times \mathbb{R}^2$. This function is used to scale the observer equations for numerical reasons, and its exact shape is not important for the stability analysis. Subtracting (3.4a) from (3.1) we obtain the following error dynamics:

$$\dot{\tilde{v}}_y = -K_{v_y} m \Lambda \xi \tilde{a}_y, \tag{3.5a}$$

$$\dot{\tilde{\theta}} = -\Gamma K_{v_y} m \Lambda \hat{f}_y^* \tilde{a}_y. \tag{3.5b}$$

Assumptions 3.1–3.3 imply that the right-hand side of (3.5) is continuous in $t$ and locally Lipschitz continuous in $\tilde{x}$, uniformly in $t$.

**Lemma 3.1.** *If Assumptions* 3.1–3.3 *hold, then the origin of the error dynamics* (3.5) *is uniformly globally stable* (UGS).

*Proof.* We define a Lyapunov function candidate (LFC)

$$V(\tilde{x}) = \frac{1}{2m^2}\left( \theta\Gamma \tilde{v}_y^2 + \tilde{\theta}^2 \right),$$

which is positive definite and radially unbounded. Its time derivative along the trajectories of (3.5) is

$$\dot{V}(t,\tilde{x}) = -\frac{1}{m}\Gamma K_{v_y}\Lambda\tilde{a}_y\left(\theta\xi\tilde{v}_y + \hat{f}_y^*\tilde{\theta}\right).$$

We may write

$$m\tilde{a}_y = \theta\left(f_y^*(d,v_y) - \hat{f}_y^*\right) + \hat{f}_y^*\tilde{\theta} = \theta\xi\tilde{v}_y + \hat{f}_y^*\tilde{\theta}.$$

Using this for substitution yields

$$\dot{V}(t,\tilde{x}) = -\Gamma K_{v_y}\Lambda\tilde{a}_y^2 \leq -\Gamma K_{v_y}\Lambda_{\min}\tilde{a}_y^2.$$

It follows that the origin of (3.5) is UGS (see, e.g., Loría et al., 2005, Def. 1). □

Building on Lemma 3.1, uniform global asymptotic stability (UGAS) of the origin of the error dynamics (3.5) is proven in the following theorem, subject to an excitation condition that will be extensively discussed. We define the functions

$$\eta_{v_y}(t,\tilde{v}_y) = \begin{cases} \frac{1}{m}\theta\frac{f_y^*(d,v_y)-f_y^*(d,\hat{v}_y)}{\tilde{v}_y}, & \tilde{v}_y \neq 0; \\ \frac{1}{m}\theta\frac{\partial f_y^*}{\partial v_y}(d,v_y), & \tilde{v}_y = 0, \end{cases} \tag{3.6}$$

$$\eta_\theta(t,\tilde{v}_y) = \frac{1}{m}f_y^*(d,\hat{v}_y). \tag{3.7}$$

Using these functions, we may write

$$\tilde{a}_y = \eta_{v_y}(t,\tilde{v}_y)\tilde{v}_y + \eta_\theta(t,\tilde{v}_y)\tilde{\theta}. \tag{3.8}$$

Hence, $\eta_{v_y}(t,\tilde{v}_y)$ and $\eta_\theta(t,\tilde{v}_y)$ are measures of the influence of $\tilde{v}_y$ and $\tilde{\theta}$ on $\tilde{a}_y$.

**Theorem 3.1** (UGAS of lateral velocity observer)**.** *Suppose that for each* $\tilde{v}_y \in \mathbb{R}$*, there exist* $T > 0$ *and* $\varepsilon > 0$ *such that for all* $t \in \mathbb{R}$*,*

$$\int_t^{t+T}\eta_{v_y}^2(\tau,\tilde{v}_y)\,\mathrm{d}\tau\int_t^{t+T}\eta_\theta^2(\tau,\tilde{v}_y)\,\mathrm{d}\tau - \left(\int_t^{t+T}\eta_{v_y}(\tau,\tilde{v}_y)\eta_\theta(\tau,\tilde{v}_y)\,\mathrm{d}\tau\right)^2 > \varepsilon. \tag{3.9}$$

*If Assumptions* 3.1–3.3 *hold, then the origin of the error dynamics* (3.5) *is* UGAS.

*Remark* 3.2. The condition expressed by (3.9) concerns the relationship between the two signals $\eta_{v_y}(\cdot, \tilde{v}_y)$ and $\eta_\theta(\cdot, \tilde{v}_y)$. To see this, it is useful to note that according to the Cauchy-Schwartz inequality, the left-hand side is always non-negative, and it is positive if and only if the continuous signals $\eta_{v_y}(\cdot, \tilde{v}_y)$ and $\eta_\theta(\cdot, \tilde{v}_y)$ are linearly independent on $[t, t+T]$ (see, e.g., Young, 1988, Theorem 1.9). Loosely speaking, the condition can be fulfilled by guaranteeing that the signals vary in a sufficiently independent manner within such time windows. In practical terms, this amounts to requiring that the driving pattern is somewhat varied, not consisting of indefinitely long periods of driving along a straight path or in a circle at constant speed.[2] This is discussed in detail in Section 3.7.

*Proof (Theorem* 3.1*).* From Lemma 3.1, we know that the origin of the error dynamics is UGS. We may therefore use Loría et al. (2005, Theorem 4). The function $\tilde{a}_y$ is locally Lipschitz continuous in $\tilde{x}$, uniformly in $t$. Hence, for each $\Delta > 0$, there exists a $\mu > 0$ such that for all $(t, \tilde{x}) \in \mathbb{R} \times \overline{B}(\Delta)$, $\max\left\{|V(\tilde{x})|, |\tilde{a}_y|\right\} \leq \mu$, where $V$ is the Lyapunov function from the proof of Lemma 3.1. We define $Y : \mathbb{R}^2 \times \mathbb{R} \to \mathbb{R}$ as

$$Y(z, \psi) = -\Gamma K_{v_y} \Lambda_{\min} \psi^2.$$

We have that $\dot{V}(t, \tilde{x}) \leq Y(\tilde{x}, \tilde{a}_y)$, $Y(z, \psi) \leq 0$, and $Y(z, \psi) = 0 \implies \psi = 0$.

We may write

$$\int_t^{t+T} \tilde{a}_y^2(\tau, \tilde{x})\, \mathrm{d}\tau = \tilde{x}^\mathsf{T} W(t, \tilde{v}_y) \tilde{x},$$

where

$$W(t, \tilde{v}_y) = \int_t^{t+T} \begin{bmatrix} \eta_{v_y}^2(\tau, \tilde{v}_y) & \eta_{v_y}(\tau, \tilde{v}_y)\eta_\theta(\tau, \tilde{v}_y) \\ \eta_{v_y}(\tau, \tilde{v}_y)\eta_\theta(\tau, \tilde{v}_y) & \eta_\theta^2(\tau, \tilde{v}_y) \end{bmatrix} \mathrm{d}\tau.$$

Note that for each $\tilde{v}_y$, $\eta_{v_y}(\tau, \tilde{v}_y)$ and $\eta_\theta(\tau, \tilde{v}_y)$ are uniformly bounded. The second-order leading principal minor (or determinant) of $W(t, \tilde{v}_y)$ is

$$\int_t^{t+T} \eta_{v_y}^2(\tau, \tilde{v}_y)\, \mathrm{d}\tau \int_t^{t+T} \eta_\theta^2(\tau, \tilde{v}_y)\, \mathrm{d}\tau - \left( \int_t^{t+T} \eta_{v_y}(\tau, \tilde{v}_y)\eta_\theta(\tau, \tilde{v}_y)\, \mathrm{d}\tau \right)^2.$$

From (3.9), this expression evaluates to some value greater than $\varepsilon$. The first-order leading principal minor of $W(t, \tilde{v}_y)$ is $\int_t^{t+T} \eta_{v_y}^2(\tau, \tilde{v}_y)\, \mathrm{d}\tau$, which is obviously non-negative. It is also nonzero because the determinant would otherwise be zero. Hence, for each $\tilde{v}_y$, $W(t, \tilde{v}_y)$ is positive definite with a uniformly lower bounded

[2] It is important to note (i) that $\tilde{v}_y = 0$ does not imply that either signal is zero, and (ii) that the condition may hold even if one or both of the signals are zero for limited periods of time.

determinant and upper bounded eigenvalues, which means that $\lambda_{\min}(W(t, \tilde{v}_y)) > \varepsilon' > 0$ for some $\varepsilon'$. Therefore, for all $t \in \mathbb{R}$, $\int_t^{t+T} \tilde{a}_y^2(\tau, \tilde{x})\,\mathrm{d}\tau \geq \varepsilon' \|\tilde{x}\|^2$. Boundedness of the integrand for each $\tilde{x}$ in turn implies that for each $\tilde{x} \neq 0$, there exist $\varepsilon^* > 0$ and $T > 0$ such that for all $t \in \mathbb{R}$, $\int_t^{t+T} |\tilde{a}_y(\tau, \tilde{x})|\,\mathrm{d}\tau \geq \varepsilon^*$. This means that $\tilde{a}_y$ is uniformly $\delta$-persistently exciting (U$\delta$-PE) with respect to $\tilde{x}$ by Loría et al. (2005, Lemma 1), and it is also zero for $\tilde{x} = 0$.

The right-hand sides of (3.5a) and (3.5b) consist of $\tilde{a}_y$ multiplied by factors that are bounded for all $(t, \tilde{x}) \in \mathbb{R} \times \overline{B}(\Delta)$. Hence, there exists a constant $K_1(\Delta)$ such that for all $(t, \tilde{x}) \in \mathbb{R} \times \overline{B}(\Delta)$, $\|g(t, \tilde{x})\| \leq K_1(\Delta)|\tilde{a}_y|$, where $g(t, \tilde{x})$ denotes the right-hand side of (3.5). □

The observer (3.4) allows the estimated friction parameter $\hat{\theta}$ to take on any value, but from physical considerations, we know that $\theta$ is confined to a small region, as reflected by Assumption 3.1. We may use this extra knowledge by implementing a parameter projection (see, e.g., Ioannou and Sun, 1996), while preserving the stability properties of the error dynamics. Doing so, we may ensure that for all $t \geq t_0$, $\theta_{\min} - \theta_\varepsilon \leq \hat{\theta} \leq \theta_{\max} + \theta_\varepsilon$ (where $\theta_\varepsilon > 0$ is some arbitrarily small constant), as long as $\hat{\theta}$ is within those bounds at $t = t_0$ (see Grip et al., 2006).

## 3.4 Robustness

Equilibrium points with the UGAS property are locally input-to-state stable and therefore robust to small perturbations, as mentioned in Loría et al. (2005). By using a different LFC, which includes a term similar to one of the auxiliary functions used in the proof of Loría et al. (2005, Theorem 4), we obtain a stronger local stability result. The approach is similar to the proof of Loría, Panteley, Popović, and Teel (2006, Propositions 3 and 4), where uniform local exponential stability (ULES) is proven for a particular class of systems.

**Theorem 3.2** (ULES of lateral velocity observer)**.** *Suppose that Assumptions* 3.1–3.3 *and the condition expressed by* (3.9) *hold. Then the origin of the error dynamics* (3.5) *is* ULES.

*Proof.* We define the LFC

$$V_{\mathrm{PE}}(t, \tilde{x}) = V(\tilde{x}) - \gamma \int_t^\infty \mathrm{e}^{t-\tau} \tilde{a}_y^2(\tau, \tilde{x})\,\mathrm{d}\tau,$$

where $\gamma > 0$ is a constant and $V$ is the Lyapunov function from the proof of Lemma 3.1. In the remainder of the proof, it is assumed that $\tilde{x} \in \overline{B}(\Delta)$ for some

arbitrary $\Delta > 0$. Because $\tilde{a}_y$ is locally Lipschitz continuous in $\tilde{x}$, uniformly in $t$, and zero for $\tilde{x} = 0$, there exists a $K_2(\Delta)$ such that $|\tilde{a}_y| \leq K_2(\Delta)\|\tilde{x}\|$. We therefore have

$$\begin{aligned} V_{\mathrm{PE}}(t,\tilde{x}) &\geq \frac{1}{2m^2}\left(\theta\Gamma\tilde{v}_y^2 + \tilde{\theta}^2\right) - \gamma K_2^2(\Delta)\|\tilde{x}\|^2 \int_t^\infty \mathrm{e}^{t-\tau}\,\mathrm{d}\tau \\ &\geq \left(\frac{1}{2m^2}\min\{1,\theta\Gamma\} - \gamma K_2^2(\Delta)\right)\|\tilde{x}\|^2. \end{aligned}$$

Choosing $\gamma < \min\{1,\theta\Gamma\}/(2m^2K_2^2(\Delta))$ ensures that $V_{\mathrm{PE}}$ is positive definite and bounded:

$$\begin{aligned} \left(\frac{1}{2m^2}\min\{1,\theta\Gamma\} - \gamma K_2^2(\Delta)\right)\|\tilde{x}\|^2 \leq V_{\mathrm{PE}}(t,\tilde{x}) \\ \leq \frac{1}{2m^2}\max\{1,\theta\Gamma\}\|\tilde{x}\|^2. \end{aligned} \tag{3.10}$$

For the time derivative along the trajectories of (3.5), we have

$$\begin{aligned} \dot{V}_{\mathrm{PE}}(t,\tilde{x}) \leq &-\left(\Gamma K_{v_y}\Lambda_{\min} - \gamma\right)\tilde{a}_y^2 - \gamma\int_t^\infty \mathrm{e}^{t-\tau}\tilde{a}_y^2(\tau,\tilde{x})\,\mathrm{d}\tau \\ &- 2\gamma\int_t^\infty \mathrm{e}^{t-\tau}\tilde{a}_y(\tau,\tilde{x})\frac{\partial\tilde{a}_y}{\partial\tilde{x}}(\tau,\tilde{x})\,\mathrm{d}\tau\; g(t,\tilde{x}), \end{aligned}$$

where $g(t,\tilde{x})$ denotes the right-hand side of (3.5). The continuity properties of the friction model imply that $\|[\partial\tilde{a}_y/\partial\tilde{x}](t,\tilde{x})\| \leq K_3(\Delta)$. It can be shown that the left-hand side of (3.9) is continuous in $\tilde{v}_y$, uniformly in $t$, which means that $[-\Delta,\Delta]$ is covered by open neighborhoods around each $\tilde{v}_y$ for which (3.9) holds with the same $T$ and $\varepsilon$. Since $[-\Delta,\Delta]$ is compact, this cover has finite subcover, and hence we may choose $T_\Delta > 0$ and $\varepsilon_\Delta > 0$ such that (3.9) holds uniformly for all $(t,\tilde{x}) \in \mathbb{R}\times\overline{B}(\Delta)$ with $T = T_\Delta$ and $\varepsilon = \varepsilon_\Delta$. Defining $W$ as in the proof of Theorem 3.1 with $T = T_\Delta$ and using the boundedness property of the elements of $W(t,\tilde{v}_y)$ on $\mathbb{R}\times\overline{B}(\Delta)$, we may define $\varepsilon'_\Delta$ accordingly, such that

$$\int_t^{t+T_\Delta}\tilde{a}_y^2(\tau,\tilde{x})\,\mathrm{d}\tau = \tilde{x}^\mathsf{T}W(t,\tilde{v}_y)\tilde{x} \geq \varepsilon'_\Delta\|\tilde{x}\|^2.$$

From this, we may write

$$\begin{aligned} \dot{V}_{\mathrm{PE}}(t,\tilde{x}) \leq &-(\Gamma K_{v_y}\Lambda_{\min} - \gamma)\tilde{a}_y^2 - \gamma\varepsilon'_\Delta\mathrm{e}^{-T_\Delta}\|\tilde{x}\|^2 \\ &+ 2\gamma K_1(\Delta)K_2(\Delta)K_3(\Delta)\|\tilde{x}\||\tilde{a}_y|, \end{aligned} \tag{3.11}$$

where $K_1(\Delta)$ is defined in the proof of Theorem 3.1. Selecting

$$\gamma < \frac{\Gamma K_{v_y} \Lambda_{\min}}{1 + K_1^2(\Delta) K_2^2(\Delta) K_3^2(\Delta) \varepsilon_\Delta'^{-1} \mathrm{e}^{T_\Delta}}$$

ensures that $\dot{V}_{\mathrm{PE}}(t, \tilde{x})$ is negative definite and bounded by

$$\dot{V}_{\mathrm{PE}}(t, \tilde{x}) \leq -c \left( \|\tilde{x}\|^2 + |\tilde{a}_y|^2 \right),$$

for some $c > 0$. This can be seen by writing (3.11) in quadratic, symmetric matrix form and investigating the leading principal minors. According to Khalil (2002, Theorem 4.10), the origin of (3.5) is therefore ULES. □

The combination of UGAS and ULES implies that the system is uniformly exponentially stable within any compact neighborhood of the origin, and hence it is unnecessary to investigate the region of attraction in Theorem 3.2. The proof indicates that the stability margin depends on the amount of excitation in the system.

## 3.5 Extension to Longitudinal Velocity and Yaw Rate

The adaptive observer design is now extended to include estimation of longitudinal velocity and yaw rate. The vector $d$ is redefined to exclude the values $v_x$ and $r$, and these values are instead used as explicit arguments to $F_i$. The vehicle model for the longitudinal velocity and yaw rate can be written as

$$\begin{aligned} \dot{v}_x &= a_x + r v_y, \\ \dot{r} &= \frac{1}{J} f_r(d, v_x, v_y, r, \mu_H), \end{aligned}$$

where $J$ is the vehicle moment of inertia around the vertical axis through the CG. The function $f_r$ represents the yaw moment, and we assume that it can be expressed as $f_r(d, v_x, v_y, r, \mu_H) = \theta f_r^*(d, v_x, v_y, r)$, where

$$f_r^*(d, v_x, v_y, r) = \frac{1}{\mu_H^*} \sum_{i=1}^{4} g_i^{\mathsf{T}} R(\delta_i) F_i(d, v_x, v_y, r, \mu_H^*).$$

The vectors $g_i$ are geometry vectors defined for convenience (see Imsland et al., 2006a).

*Remark* 3.3. Using the same type of parametrization, and the same parameter, for calculation of the yaw moment as for the lateral acceleration is a significant simplification, because different tire slip values for the front and rear wheels will give

the difference seen in Figure 3.2 much more impact. In normal driving situations without large tire slip values, one may therefore expect large inaccuracies. Essentially the same design as the one given in this paper can, however, be implemented with adaptation of $\mu_H$ instead, albeit at the cost of making other assumptions (see Imsland, Grip, Johansen, Fossen, Kalkkuhl, and Suissa, 2007). The choice of the best parametrization for a final implementation is a topic of current research.

We now write

$$f_y^*(d, v_x, v_y, r) = \frac{1}{\mu_H^*} \sum_{i=1}^{4} [0\ 1] R(\delta_i) F_i(d, v_x, v_y, r, \mu_H^*).$$

The vector $x$ is defined as $x = [v_x, v_y, r, \theta]^\mathsf{T}$ and Assumptions 3.2 and 3.3 now take the following form:

**Assumption 3.2′.** *There exist compact sets $D_d \subset \mathbb{R}^m$, $D_{v_x} \subset \mathbb{R}$, $D_{v_y} \subset \mathbb{R}$ and $D_r \subset \mathbb{R}$ such that*

- $(d, v_x, v_y, r) \in D_d \times D_{v_x} \times D_{v_y} \times D_r$;
- *$d$, $v_x$, $v_y$, and $r$ are uniformly continuous in $t$ on $\mathbb{R}$;*
- *$F_i(d, v_x, v_y, r, \mu_H^*)$ and their partial derivatives with respect to $v_x$, $v_y$, and $r$ are continuous on $D_d \times \mathbb{R} \times \mathbb{R} \times \mathbb{R} \times \{\mu_H^*\}$; and*
- *$[\partial F_i/\partial v_x](d, v_x, v_y, r, \mu_H^*)$ and $[\partial F_i/\partial r](d, v_x, v_y, r, \mu_H^*)$ are uniformly bounded on $D_d \times \mathbb{R} \times D_{v_y} \times \mathbb{R} \times \{\mu_H^*\}$.*

**Assumption 3.3′.** *There exist known functions $\xi\colon D_d \times \mathbb{R}^4 \to \mathbb{R}$ and $\zeta\colon D_d \times \mathbb{R}^4 \to \mathbb{R}$ such that $\xi(d, \hat{x})$, $\zeta(d, \hat{x})$, $[\partial\xi/\partial\hat{x}](d, \hat{x})$, and $[\partial\zeta/\partial\hat{x}](d, \hat{x})$ are continuous on $D_d \times \mathbb{R}^4$ and*

$$f_y^*(d, \hat{v}_x, v_y, \hat{r}) - f_y^*(d, \hat{v}_x, \hat{v}_y, \hat{r}) = \xi(d, \hat{x})(v_y - \hat{v}_y), \tag{3.12}$$

$$f_r^*(d, \hat{v}_x, v_y, \hat{r}) - f_r^*(d, \hat{v}_x, \hat{v}_y, \hat{r}) = \zeta(d, \hat{x})(v_y - \hat{v}_y). \tag{3.13}$$

We redefine $\tilde{a}_y(t, \tilde{x}) = a_y - (1/m)\hat{\theta} f_y^*(d, \hat{v}_x, \hat{v}_y, \hat{r})$. The functions $\eta_{v_y}$ and $\eta_\theta$ remain the same as before; that is, they are functions of $v_x$ and $r$, and not of the estimates $\hat{v}_x$ and $\hat{r}$.[3] The notation $\Lambda = \Lambda(d, \hat{x})$, $\hat{f}_y^* = f_y^*(d, \hat{v}_x, \hat{v}_y, \hat{r})$, $\hat{f}_r^* = f_r^*(d, \hat{v}_x, \hat{v}_y, \hat{r})$, $\xi = \xi(d, \hat{x})$, $\zeta = \zeta(d, \hat{x})$, and $\tilde{a}_y = \tilde{a}_y(t, \tilde{x})$ is used for the sake of brevity.

[3] Note that (3.8) does not hold with the new definition of $\tilde{a}_y$.

The following observer is proposed:

$$\dot{\hat{v}}_x = a_x + r\hat{v}_y + \sum_{i=1}^{4} K_i(t)\left(v_{x,i} - \hat{v}_x\right), \tag{3.14a}$$

$$\dot{\hat{v}}_y = a_y - r\hat{v}_x + K_{v_y}\Lambda\xi\left(ma_y - \hat{\theta}\hat{f}_y^*\right) + \frac{\Gamma_2}{\Gamma_1}\zeta\left(r - \hat{r}\right), \tag{3.14b}$$

$$\dot{\hat{r}} = \frac{1}{J}\hat{\theta}\hat{f}_r^* + K_r\left(r - \hat{r}\right), \tag{3.14c}$$

$$\dot{\hat{\theta}} = \Gamma_1 K_{v_y}\Lambda\hat{f}_y^*\left(ma_y - \hat{\theta}\hat{f}_y^*\right) + \Gamma_2\hat{f}_r^*\left(r - \hat{r}\right), \tag{3.14d}$$

where $K_r$, $\Gamma_1$, and $\Gamma_2$ are positive gains. The values $K_i(t)$ are continuously chosen, time-varying gains, and $v_{x,i}$ are longitudinal velocities calculated from the individual wheel angular velocities and the yaw rate. For the stability proofs, the weighted average $\sum_{i=1}^{4} K_i(t)v_{x,i} / \sum_{i=1}^{4} K_i(t)$ is assumed to be an exact measurement of $v_x$ (see Imsland et al. (2006a) for a detailed discussion of the longitudinal velocity estimation).

**Theorem 3.3** (UGAS of full observer)**.** *Suppose that Assumptions* 3.1*,* 3.2′*, and* 3.3′ *and the condition expressed by* (3.9) *hold. Then there exist constants* $C_1 > 0$ *and* $C_2 > 0$ *such that if the gains are chosen according to* $\sum_{i=1}^{4} K_i(t) > C_1$ *and* $K_r > C_2$*, then the origin of the error dynamics corresponding to the observer* (3.14) *is* UGAS.

*Proof (Outline).* We define the LFC

$$V(\tilde{x}) = \frac{1}{2}(\Gamma_1\theta\tilde{v}_x^2 + \Gamma_1\theta\tilde{v}_y^2 + \Gamma_2 J\tilde{r}^2 + \tilde{\theta}^2).$$

Using the assumptions, it can be shown that with the proper selection of gains,

$$\dot{V}(t,\tilde{x}) \leq -c\left(\tilde{v}_x^2 + \tilde{r}^2 + \tilde{a}_y^2\right),$$

where $c$ is some positive constant. We define

$$\phi(t,\tilde{x}) = a_y - (1/m)\hat{\theta}f_y^*(d, v_x, \hat{v}_y, r).$$

It can be shown that for $(t,\tilde{x}) \in \mathbb{R} \times \overline{B}(\Delta)$, there exists a $K(\Delta)$ such that defining $Y : \mathbb{R}^4 \times \mathbb{R} \to \mathbb{R}$ as

$$Y(z,\psi) = -c(\|z_{\{1,3\}}\|^2 + \max\{\psi^2 - K(\Delta)|\psi|\|z_{\{1,3\}}\|, 0\})$$

yields $\dot{V}(t,\tilde{x}) \leq Y(\tilde{x}, \phi(t,\tilde{x}))$, $Y(z,\psi) \leq 0$, and $Y(z,\psi) = 0 \implies z_{\{1,3\}} = 0$, $\psi = 0$. The rest of the proof follows along the same lines as the proof of Theorem 3.1 with the U$\delta$-PE condition imposed on the function $\phi$ instead of $\tilde{a}_y$. □

**Theorem 3.4** (ULES of full observer)**.** *Suppose that Assumptions* 3.1*,* 3.2′*, and* 3.3′ *and the condition expressed by* (3.9) *hold. Then there exist constants* $C_1 > 0$ *and* $C_2 > 0$ *such that if the gains are chosen according to* $\sum_{i=1}^{4} K_i(t) > C_1$ *and* $K_r > C_2$*, then the origin of the error dynamics corresponding to the observer* (3.14) *is* ULES.

*Proof (Outline).* The proof follows along the same lines as the proof of Theorem 3.2, using the LFC

$$V_{\mathrm{PE}}(t, \tilde{x}) = V(\tilde{x}) - \gamma \int_t^\infty \mathrm{e}^{t-\tau} \phi^2(\tau, \tilde{x}) \, \mathrm{d}\tau,$$

where $V$ and $\phi$ are defined in the proof of Theorem 3.3. □

*Remark* 3.4. The constants $C_1$ and $C_2$ in Theorems 3.3 and 3.4 depend on $K_{v_y}$, $\Gamma_1$, and $\Gamma_2$, which must be chosen first.

## 3.6 Approximation of $\xi$ and $\zeta$

In Assumption 3.3′, it is assumed that we can obtain values $\xi(d, \hat{x})$ such that (3.12) holds exactly. The challenge is to find the gradient of the line connecting the values $f_y^*(d, \hat{v}_x, v_y, \hat{r})$ and $f_y^*(d, \hat{v}_x, \hat{v}_y, \hat{r})$. In general, the exact values cannot be found, because $v_y$ is unavailable, but the shape of this function makes the task of approximating the value appealing. In Imsland et al. (2006a, Assumption 2), it is assumed that the friction model fulfills the condition $[\partial f_y^* / \partial v_y](d, v_x, v_y, r) \leq c < 0$ within a region. For the purpose of estimating $\xi$, we instead make the assumption that for all $(d, v_x, v_y, r) \in D_d \times \mathbb{R} \times \mathbb{R} \times \mathbb{R}$, $[\partial f_y^* / \partial v_y](d, v_y, v_x, r) \leq 0$. According to this, $\xi$ is always non-positive, and hence one possible approximation is a negative constant. Although extremely crude, this approximation is surprisingly effective. It is also a safe choice in the sense that it limits errors by ensuring that the feedback from $\tilde{a}_y$ in the lateral velocity estimation never disappears. A somewhat better solution is to use a truncated Taylor series expansion around some nominal value $v_y^*$ or around the estimate $\hat{v}_y$. In the latter case, the ULES property of the origin of the error dynamics is guaranteed to be preserved (even without the above assumption). One may also use considerations of convexity and concavity to identify situations in which any error from the Taylor series expansion actually improves stability (see Annaswamy, Skantze, and Loh, 1998), and use this information to create an estimation scheme based on a combination of the above approaches. Experimental results indicate that errors in the approximation have little effect on performance as long as it is ensured that $\xi$ is not close to zero for long periods of time. This is largely because any error in the approximation

becomes a potential problem only if there is variation in the lateral velocity, which also when the robustness of the observer is greatest.

For approximating $\zeta$, a Taylor series expansion around $\hat{v}_y$ is a good enough approximation, because the gain $K_r$ can be used to suppress the error. Moreover, the actual values of $\zeta$ are small, so the term where this value enters in (3.14b), although necessary for the technical proofs, has a negligible impact on the estimates when the observer is properly tuned.

## 3.7 Excitation Condition

The excitation condition given by (3.9) is essential for the stability results presented in this paper, and despite its technical nature, it has an intuitively appealing interpretation. As explained in Remark 3.2, it concerns the relationship between two signals, $\eta_{v_y}(\cdot, \tilde{v}_y)$ and $\eta_\theta(\cdot, \tilde{v}_y)$. If $\tilde{v}_y$ is fixed at a specific value, then, essentially, the remaining time-varying signals affecting $\eta_{v_y}$ and $\eta_\theta$ should cause $\eta_{v_y}(t, \tilde{v}_y)$ and $\eta_\theta(t, \tilde{v}_y)$ to vary independently within any time period of a certain length.

The functions $\eta_{v_y}$ and $\eta_\theta$ depend nonlinearly on many different time-varying signals, which cause them to behave differently. In particular, the inequality

$$[\partial f_y^* / \partial v_y](d, v_x, v_y, r) \leq 0$$

implies that $\eta_{v_y}(t, \tilde{v}_y)$ is non-positive at all times. By contrast, $\eta_\theta(t, \tilde{v}_y)$ varies much in the same way as the lateral acceleration, and is likely to frequently switch signs, at least for moderate values of $\tilde{v}_y$. Furthermore, we note that $\eta_{v_y}$ and $\eta_\theta$ are essentially measures of the influence of $\tilde{v}_y$ and $\tilde{\theta}$ on $\tilde{a}_y$. The plots in Section 3.3.1 clearly indicate that the relation between these varies along the slip curves.

This translates into a requirement that the driving pattern should be somewhat varied; in particular, the condition will be satisfied if there is variation in the lateral velocity and acceleration. A certain amount of steering, acceleration, or braking in order to cause variation in the lateral tire slips is required. It is not necessary that this happen all the time, but by choosing a large enough $T$, it must be possible to guarantee some variation within any time interval of that length.

The intuitive appeal of this condition is clear: it is impossible to tell anything about the road surface conditions based on the lateral movement of the vehicle, unless there is actually some variation in that movement. With this condition is mind, it is natural to distinguish between three general driving patterns.

### 3.7.1 Varied Lateral Velocity

If there is variation in the lateral velocity, the excitation condition will be fulfilled, and hence Theorems 3.3 and 3.4 apply. We may therefore expect convergence of all estimates.

### 3.7.2 Straight-Path Driving

If the vehicle is driven along a straight path for an indefinitely long time, the excitation condition will not be fulfilled. We state a separate result for this case.

**Theorem 3.5** (Convergence during straight-path driving)**.** *Suppose that Assumptions* 3.1*,* 3.2′*, and* 3.3′ *hold and that for each* $\varepsilon_1 > 0$*, there exists an* $\varepsilon_2 > 0$ *such that* $|\hat{v}_y| > \varepsilon_1$*,* $r = 0$*,* $\delta = 0 \implies |f_y^*(d, v_x, \hat{v}_y, 0)| > \varepsilon_2$*. If for all* $t \geq t_0$*,* $a_y = 0$*,* $v_y = 0$*,* $r = 0$*,* $\delta = 0$*, and* $\hat{\theta} \geq \theta_{\min} - \theta_\varepsilon > 0$*, then* $\lim_{t\to\infty}(\tilde{v}_x, \tilde{v}_y, \tilde{r}) = 0$*.*

*Proof (Outline).* Using the Lyapunov function $V$ from Theorem 3.3, Barbălat's lemma (Barbălat, 1959) can be used to conclude that $\lim_{t\to\infty}(\tilde{v}_x, \tilde{r}, \tilde{a}_y) = 0$. Using the extra condition in Theorem 3.5 and the continuity properties of $f_y^*$, it can be shown that this implies $\lim_{t\to\infty} \hat{v}_y = 0$. □

*Remark* 3.5. In practical terms, the extra condition in Theorem 3.5 means that if the steering wheel angle is zero and the vehicle is not rotating, any nonzero lateral velocity will generate a nonzero lateral acceleration. This is reasonable from a physical point of view and is likely to hold for most friction models. The condition that $\hat{\theta} \geq \theta_{\min} - \theta_\varepsilon$ is ensured by parameter projection, as discussed in Section 3.3.2.

### 3.7.3 Sustained Circle Maneuver

In a practical implementation, the estimates may begin to drift during particularly long-lasting circle maneuvers with little excitation. This type of situation can be detected, and a proper response can be built in. When the goal is estimation of vehicle side-slip, using an estimated friction parameter that is too high is far safer than using one that is too low, as explained by Fukada (1999). The response is therefore to let $\hat{\theta}$ be drawn toward a high value.

## 3.8 Experimental Validation

In this section, some results from practical testing of the observer in one passenger car with rear-wheel drive (Vehicle A) and one larger vehicle with four wheel drive

(Vehicle B), are presented. For a detailed comparison between an EKF and an observer implementation similar to the one presented in this paper, see Imsland et al. (2007).

### 3.8.1 Practical Implementation

A discrete version of the observer is implemented using the forward Euler integration method with step size 0.01 s. The gains $K_i(t)$ for estimation of the longitudinal velocity are updated at each time step.[4] The measurements of longitudinal and lateral acceleration, yaw rate, steering wheel angle, and wheel angular velocities are provided by production-type sensors; and, for the purpose of observer validation, the longitudinal and lateral velocities are measured using optical correlation sensors. The nominal value of $\mu_H$ is set to $\mu_H^* = 1.0$, and the friction parameter bounds are chosen as $\theta_{\min} = 0.1$ and $\theta_{\max} = 1.0$.

#### Friction Model

The friction model used is a proprietary one of similar complexity to the Magic Formula, and it has not been modified for use in the observer. It has the desirable property that the slip curves, plotted in Figure 3.2, flatten out rather than descend for large slip values. This helps to ensure that the inequality

$$[\partial f_y^*/\partial v_y](d, v_x, v_y, r) \leq 0$$

from Section 3.6 always holds for the model. This is desirable even if this inequality can be broken in the real system for brief periods of time, resulting in a limited model error. With the exception of wheel radius, the friction model is tuned with identical tire parameters for both vehicles, even though the actual tires used are different. The accelerations $a_x$ and $a_y$ are used in order to estimate the load distribution, and thereby the vertical normal force $F_z$ for each wheel.

A relatively simple method based loosely on the discussion in Section 3.6 is chosen for approximation of $\xi$. Most of the time, $\xi = [\partial \hat{f}_y^*/\partial \hat{v}_y]$ and the scaling $\Lambda$ is set to $1/\|[\xi, \hat{f}_y^*]\|$. But in certain cases, if $|ma_y| < |\hat{\theta}\hat{f}_y^*|$ and $[\partial \hat{f}_y^*/\partial \hat{v}_y] > -|\hat{f}_y^*|$, then $\xi = -|\hat{f}_y^*|$ and $\Lambda = 1/(2|\hat{f}_y^*|)$. The reason for not using the partial derivative at all times is a practical one, to ensure that enough weight is given to the feedback in the lateral velocity part of the observer (compared to the friction adaptation part), in situations where this has proven to be important through experimental results. The scaling $\Lambda$ is saturated at $\Lambda_{\min} = 10^{-6}$ and $\Lambda_{\max} = 10^6$.

[4] For a description of how these are chosen, see Imsland, Johansen, Fossen, Kalkkuhl, and Suissa (2006b).

#### Monitoring of Excitation Condition

As discussed in Section 3.7.3, it is sensible to let the friction parameter be drawn toward a high value whenever there is insufficient excitation for estimation of the friction parameter. To approximately monitor the excitation condition, we look at variation in the value $\hat{f}_y^*/\|[\xi, \hat{f}_y^*]\|$. The value is high-pass filtered, squared, and then low-pass filtered. If the output is below a threshold value, the friction coefficient is drawn exponentially toward the value 1.

#### Signal Processing in Update Law

Slow drift and bias in the lateral acceleration measurement influence the value $\tilde{a}_y$ in the observer error dynamics and has an adverse effect on performance. Because it is the dynamic behavior of $\tilde{a}_y$ that is useful for adaptation of the friction parameter, $\tilde{a}_y$ is high-pass filtered in the parameter update law, using the transfer function $s/(s + 0.25)$.

### 3.8.2 Experimental Results, Vehicle A

The observer for Vehicle A is implemented using the gains $K_{v_y} = 1/m$, $K_r = 40$, $\Gamma_1 = 4$, and $\Gamma_2 = 0.1/J$. Results from the first test with Vehicle A are shown in Figure 3.4. The vehicle is driven on ice, mostly along a straight path with a few sharp turns. The adapted friction parameter varies largely in stages, changing quickly during turns and little between turns.

The second test represents a circle maneuver on asphalt, and the results can be seen in Figure 3.5. Throughout the first half of the test, the modification for handling low excitation is active, and hence the friction parameter remains constant. It then starts varying, but remains high.

### 3.8.3 Experimental Results, Vehicle B

The four-wheel drive complicates estimation of the longitudinal velocity for Vehicle B. For simplicity, the longitudinal velocity measurement provided by the optical correlation sensor is therefore used in the tests presented here. The observer for Vehicle B is implemented with the gains $K_{v_y} = 1/m$, $K_r = 40$, $\Gamma_1 = 5$, and $\Gamma_2 = 1/J$. The first test is a slalom-like maneuver on a snow surface, with the results shown in Figure 3.6. For about 20 s, the vehicle is accelerated from about 1 m/s to approximately 21 m/s. Throughout the rest of the test, it mostly decelerates, to about 12 m/s at the end of the test. For the first part of the test, the low-excitation modification is active, but when the vehicle starts turning, the friction parameter starts quickly changing.

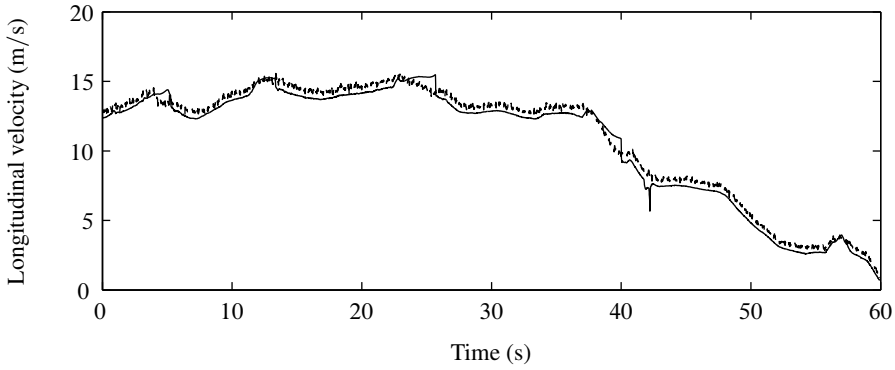


(a) Real (dashed) and estimated (solid) longitudinal velocity

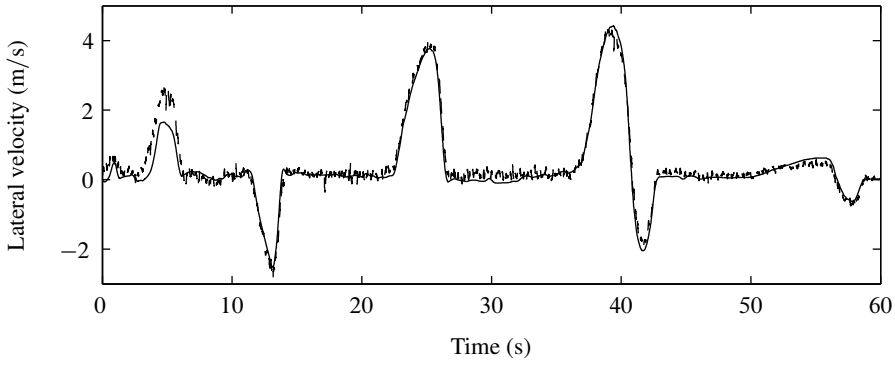


(b) Real (dashed) and estimated (solid) lateral velocity

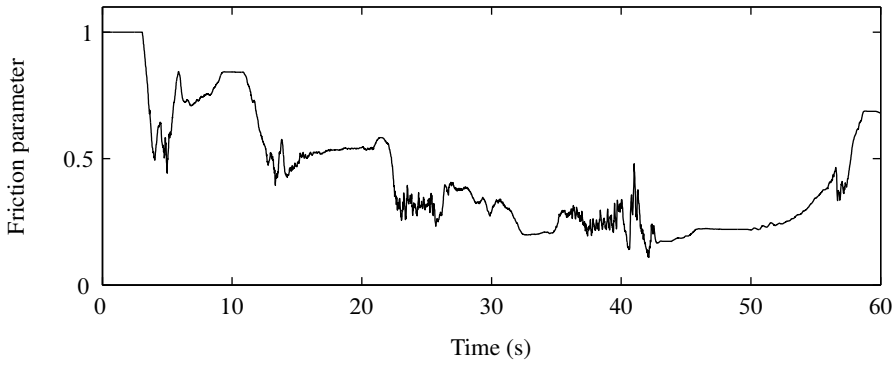


(c) Estimated friction parameter

**Figure 3.4:** Results for Vehicle A on ice

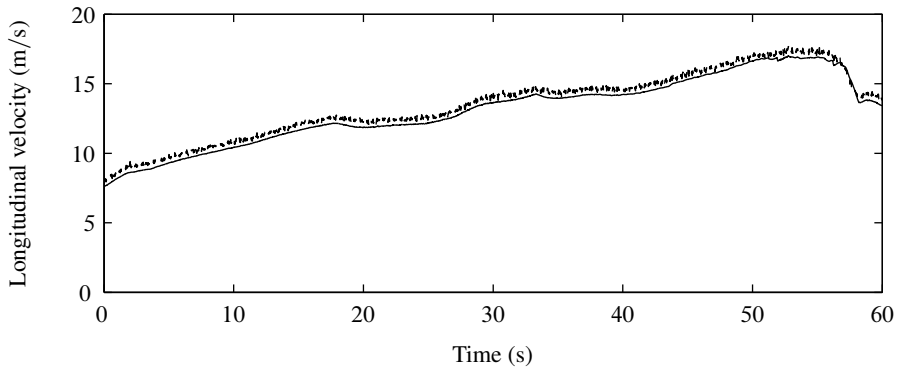


(a) Real (dashed) and estimated (solid) longitudinal velocity

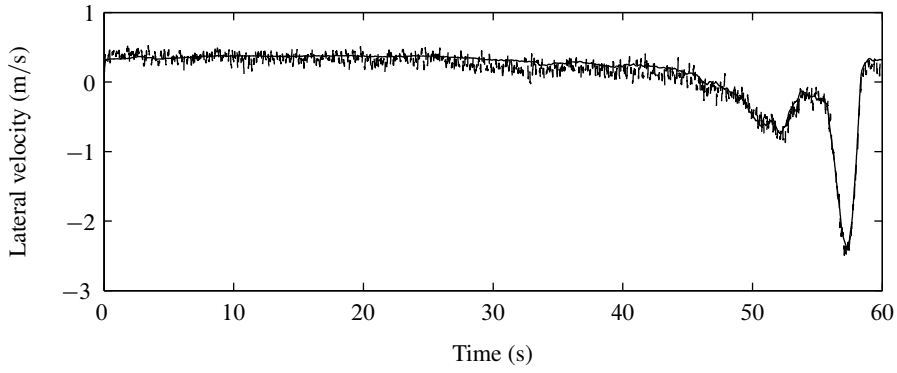


(b) Real (dashed) and estimated (solid) lateral velocity

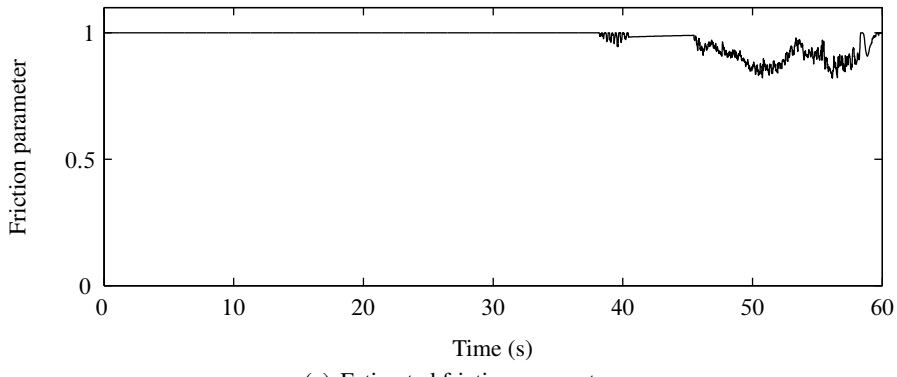


(c) Estimated friction parameter

**Figure 3.5:** Results for Vehicle A on asphalt

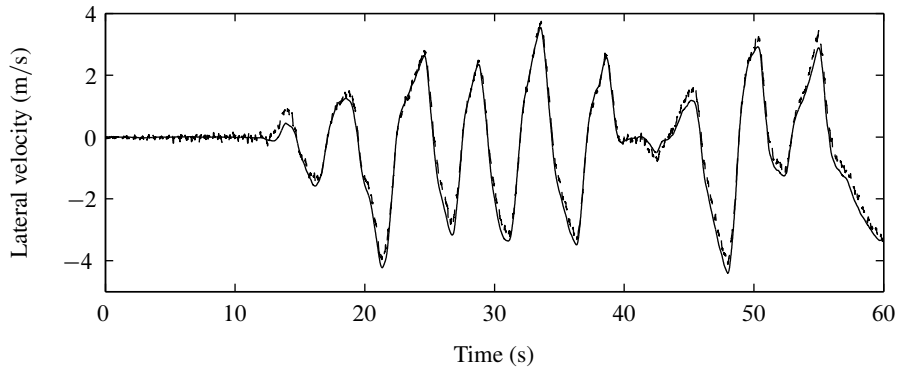


(a) Real (dashed) and estimated lateral velocity

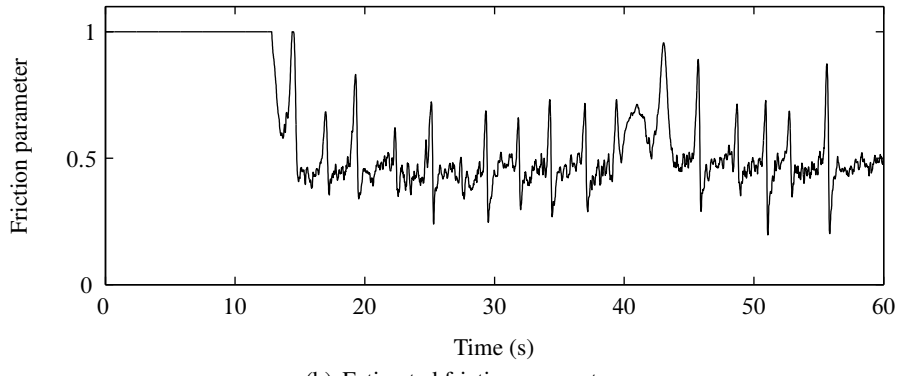


(b) Estimated friction parameter

**Figure 3.6:** Results for Vehicle B on snow

The final test is a slalom-like maneuver on asphalt, with the results shown in Figure 3.7. The longitudinal velocity varies relatively slowly in the range 21–30 m/s during the test. For this test, the initial value of the friction parameter is set much too low, at 0.1, which causes an initial inaccuracy.

The estimated friction parameter varies much more for Vehicle B than for Vehicle A. This indicates that the parameters used in the friction model are a better match for the tires on Vehicle A. The results for Vehicle B also indicate robustness with respect to errors in the friction model.

## 3.9 Concluding Remarks

In this paper, the results from Imsland et al. (2006a) are extended to create a nonlinear vehicle velocity observer with adaptation to different road surface conditions,

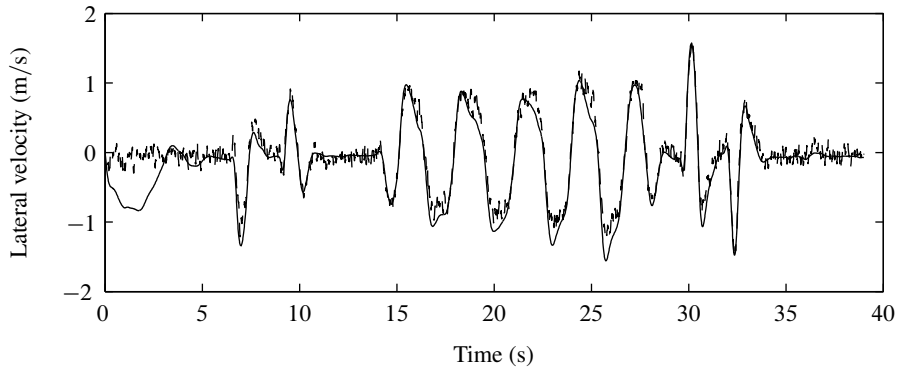


(a) Real (dashed) and estimated lateral velocity

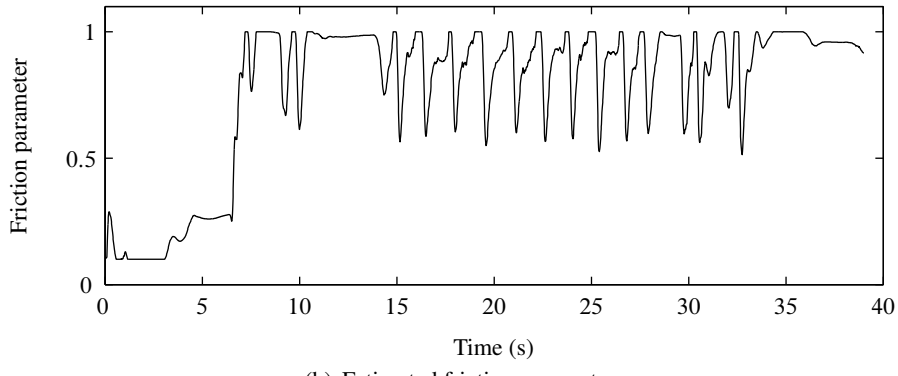


(b) Estimated friction parameter

**Figure 3.7:** Results for Vehicle B on asphalt

and the stability properties of this observer are analyzed. Experimental results confirm that the method has merit and can function in real, non-ideal circumstances. The results also support the excitation condition found in the theoretical analysis and the practical interpretation of it.

The model used in this paper does not include the effect of any nonzero road bank angle, which will induce additional lateral forces on the vehicle and therefore have an adverse effect on estimation. In a final implementation, this should preferably be addressed through additional estimation of the road bank angle. Some discussion on this topic and on how it may be handled can be found in Imsland et al. (2007).

## Acknowledgement

The authors wish to thank Dr. Antonio Loría for helpful discussion.

## Bibliography

A. M. Annaswamy, F. P. Skantze, and A.-P. Loh. Adaptive control of continuous time systems with convex/concave parametrization. *Automatica*, 34(1):33–49, 1998.

K.-J. Åström and T. Bohlin. Numerical identification of linear dynamic systems from normal operating records. In P. Hammond, editor, *Proc. IFAC Symp. Theor. Self-Adapt. Contr. Syst.*, Teddington, United Kingdom, 1965.

I. Barbălat. Systèmes d'équations différentielles d'oscillations non linéaires. *Rev. Math. Pures Appl.*, 4(2):267–270, 1959.

M. C. Best, T. J. Gordon, and P. J. Dixon. An extended adaptive Kalman filter for real-time state estimation of vehicle handling dynamics. *Vehicle Syst. Dyn.*, 34 (1):57–75, 2000.

C. Canudas-de-Wit, M. L. Petersen, and A. Shiriaev. A new nonlinear observer for tire/road distributed contact friction. In *Proc. IEEE Conf. Dec. Contr.*, pages 2246–2251, Maui, HI, 2003.

Y. Fukada. Slip-angle estimation for vehicle stability control. *Vehicle Syst. Dyn.*, 32(4):375–388, 1999.

H. F. Grip, L. Imsland, T. A. Johansen, T. I. Fossen, J. C. Kalkkuhl, and A. Suissa. Nonlinear vehicle velocity observer with road-tire friction adaptation. In *Proc. IEEE Conf. Dec. Contr.*, pages 3603–3608, San Diego, CA, 2006.

F. Gustafsson. Slip-based tire-road friction estimation. *Automatica*, 33(6):1087–1099, 1997.

A. Hac and M. D. Simpson. Estimation of vehicle side slip angle and yaw rate. In *Proc. SAE World Congr.*, Detroit, MI, 2000. Paper no. 2000-01-0696.

L. Imsland, T. A. Johansen, T. I. Fossen, H. F. Grip, J. C. Kalkkuhl, and A. Suissa. Vehicle velocity estimation using nonlinear observers. *Automatica*, 42(12): 2091–2103, 2006a.

L. Imsland, T. A. Johansen, T. I. Fossen, J. C. Kalkkuhl, and A. Suissa. Nonlinear observer for vehicle velocity estimation. In *Proc. SAE World Congr.*, Detroit, MI, 2006b. Paper no. 2006-01-1282.

L. Imsland, H. F. Grip, T. A. Johansen, T. I. Fossen, J. C. Kalkkuhl, and A. Suissa. Nonlinear observer for vehicle velocity with friction and road bank angle adaptation—Validation and comparison with an extended Kalman filter. In *Proc. SAE World Congr.*, Detroit, MI, 2007. Paper no. 2007-01-0808.

P. A. Ioannou and J. Sun. *Robust Adaptive Control*. Prentice-Hall, Upper Saddle River, NJ, 1996.

H. K. Khalil. *Nonlinear Systems*. Prentice-Hall, Upper Saddle River, NJ, 3rd edition, 2002.

U. Kiencke and L. Nielsen. *Automotive Control Systems: For Engine, Driveline, and Vehicle*. Springer, Berlin, 2000.

A. Loría and J. de León Morales. On persistently exciting observers and a nonlinear separation principle: Application to the stabilization of a generator. *Int. J. Contr.*, 76(6):607–617, 2003.

A. Loría, E. Panteley, D. Popović, and A. R. Teel. A nested Matrosov theorem and persistency of excitation for uniform convergence in stable nonautonomous systems. *IEEE Trans. Automat. Contr.*, 50(2):183–198, 2005.

A. Loría, E. Panteley, D. Popović, and A. R. Teel. Persistency of excitation for uniform convergence in nonlinear control systems. Univ. California, Davis, CA [Online], 2006. Available: http://front.math.ucdavis.edu/math.OC/0301335.

H. Nishira, T. Kawabe, and S. Shin. Road friction estimation using adaptive observer with periodical $\sigma$-modification. In *Proc. IEEE Int. Conf. Contr. Appl.*, pages 662–667, Kohala Coast, HI, 1999.

E. Ono, K. Asano, M. Sugai, S. Ito, M. Yamamoto, M. Sawada, and Y. Yasui. Estimation of automotive tire force characteristics using wheel velocity. *Contr. Eng. Pract.*, 11(12):1361–1370, 2003.

R. Ortega and A. Fradkov. Asymptotic stability of a class of adaptive systems. *Int. J. Adapt. Contr. Signal Process.*, 7(4):255–260, 1993.

H. B. Pacejka. *Tire and Vehicle Dynamics*. SAE, Warrendale, PA, 2nd edition, 2006.

E. Panteley, A. Loría, and A. R. Teel. Relaxed persistency of excitation for uniform asymptotic stability. *IEEE Trans. Automat. Contr.*, 46(12):1874–1886, 2001.

L. R. Ray. Nonlinear tire force estimation and road friction identification: Simulation and experiments. *Automatica*, 33(10):1819–1833, 1997.

A. Suissa, Z. Zomotor, and F. Böttiger. Method for determining variables characterizing vehicle handling. US Patent 5,557,520, 1994. Filed Jul. 29, 1994; issued Sep. 17, 1996.

N. Young. *An introduction to Hilbert space*. Cambridge University Press, Cambridge, United Kingdom, 1988.

Y. Zhang, P. A. Ioannou, and C.-C. Chien. Parameter convergence of a new class of adaptive controllers. *IEEE Trans. Automat. Contr.*, 41(10):1489–1493, 1996.

# Chapter 4

# Estimation of Road Inclination and Bank Angle in Automotive Vehicles

***Abstract:*** *We extend an observer design for estimation of the vehicle sideslip angle on horizontal surfaces to include estimation of the road inclination angle and the road bank angle. The design makes use of a nonlinear road-tire friction model, and the nonlinearity of the road-tire friction forces are taken into account in the theoretical analysis of the design. Using an absolute-stability argument we show that, under a set of technical assumptions, the origin of the observer error dynamics is globally exponentially stable. Taking unknown road-surface conditions into account, we discuss simultaneous estimation of the road bank angle and a road-tire friction parameter, which is complicated by the dependence of the friction-parameter estimation on lateral excitation of the vehicle. To improve performance on low-friction surfaces, we modulate the observer gains based on a set of practical conditions. Using experimental data from a passenger car, we investigate the performance of the approach.*

## 4.1 Introduction

For implementation of automotive control algorithms, accurate information about the state of the vehicle and its surroundings is important. Whereas some quantities can be obtained by direct measurement, others are difficult to measure because of high cost or impracticality. Among the quantities that are not measured in production vehicles is the angle between the heading of the vehicle and the direction of travel, known as the vehicle sideslip angle. To estimate the vehicle sideslip an-

gle, it is common to estimate the longitudinal and lateral velocities of the vehicle, denoted $v_x$ and $v_y$, and to calculate the sideslip angle as $\arctan(v_y/v_x)$.

The longitudinal and lateral velocities are influenced by gravity components due to slanting of the road surface. For velocity observers that rely on the vehicle's dynamic equations of motion, knowledge about the slanting of the road surface is therefore important. Nevertheless, sideslip estimation designs often assume that the road surface is flat and horizontal. Designs that take the slanting of the road surface into account include Suissa, Zomotor, and Böttiger (1994); Fukada (1999); Klier, Reim, and Stapel (2008).

Knowledge about the slanting of the road surface is of interest for purposes other than sideslip estimation, and several designs focus specifically on estimation of the road bank angle. These include Tseng (2001), which is based on transfer functions from the steering angle and road bank angle to the yaw rate and lateral acceleration, and Sentouh, Sebsadji, Mammar, and Glaser (2007); Sebsadji, Glaser, Mammar, and Netto (2008), which use an extended Kalman filter (EKF) to estimate the sideslip angle, which is in turn used in a linear unknown-input observer to estimate the road bank angle. Several GPS-based designs, such as Bevly (2004); Ryu and Gerdes (2004), estimate the road inclination or bank angle. In this paper, we do not assume availability of GPS measurements.

### 4.1.1 Contributions of This Paper

Sideslip estimation designs found in literature are usually based on linear or quasi-linear techniques. Most commonly, an EKF is employed. Although often effective, the EKF is difficult to analyze because the algorithm is derived through linearization of the prediction error (Brown and Hwang, 1997). Other potential disadvantages associated with the EKF are high computational complexity—due to the need to solve the Riccati equation at each time step—and a large number of tuning parameters.

In Imsland, Johansen, Fossen, Grip, Kalkkuhl, and Suissa (2006); Grip, Imsland, Johansen, Fossen, Kalkkuhl, and Suissa (2008), the authors presented a nonlinear vehicle sideslip observer for a vehicle traveling on a flat, horizontal surface. The main features of this observer are a reduction in computational complexity and in the number of tuning parameters compared to an EKF. In addition, analysis of stability and robustness in Imsland et al. (2006); Grip et al. (2008) is carried out in a nonlinear setting. Inspired by the theory of nonlinear unknown-input observers, an extension of Imsland et al. (2006) for estimating the bank angle is developed in Imsland, Johansen, Grip, and Fossen (2007); however, the nature of the disturbance introduced by road surface slanting suggests that something similar to regular integral action is appropriate. In this paper, we present such a solution,

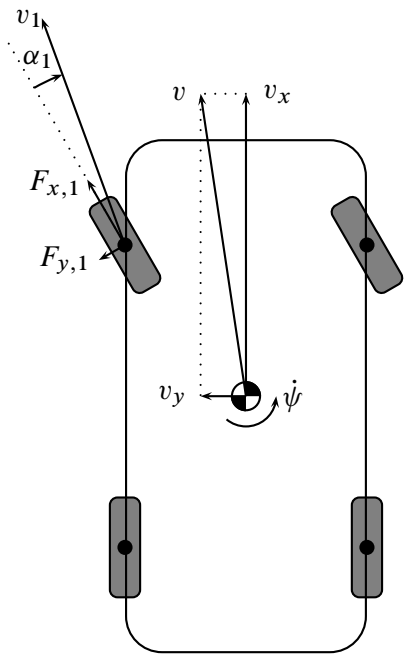


**Figure 4.1:** Illustration of the car

extending the design from Imsland et al. (2006); Grip et al. (2008) to include estimation of the road inclination and bank angles. We analyze the stability of the design, taking the nonlinearity of the road-tire friction forces into account.

### 4.1.2 Sensor Configuration

In our design, we assume that measurements of the longitudinal and lateral accelerations, wheel speeds, steering wheel angle, and yaw rate are available. These measurements can be considered standard in modern passenger cars with an electronic stability control system (ESC).

## 4.2 Road-Tire Friction

When a car turns, the tires become misaligned with the direction of travel. The angle between the direction the tire is pointing in and the velocity vector of the

vehicle above the center of the tire is called the tire slip angle. Figure 4.1 illustrates the tire slip angle $\alpha_1$ for the front-left wheel. A nonzero tire slip angle gives rise to friction forces in the lateral direction of the tire, illustrated by $F_{y,1}$ in Figure 4.1. The longitudinal tire slip, defined as a normalized difference between the circumferential velocity of the tire and the velocity of the tire center, gives rise to longitudinal friction forces, illustrated by $F_{x,1}$ in Figure 4.1. Collectively, we refer to the longitudinal tire slip and lateral tire slip angle as the tire slips.

During normal driving the road-tire friction forces are approximately linear with respect to the tire slips. When the tire slips become large, however, the road-tire friction forces saturate, meaning that an increase in the tire slips does not result in a corresponding increase in friction forces.

A key component of the design presented in this paper is a road-tire friction model. The road-tire friction model takes measurements and observer estimates as inputs, and returns estimates of the road-tire friction forces. To account for the nonlinearity of the road-tire friction forces for large tire slips, a fully nonlinear model is needed. A widely used example of a nonlinear tire model is the *magic formula* (Pacejka, 2006).

The observer presented in this paper is not designed with a particular road-tire friction model in mind. Instead, we assume that a nonlinear friction model satisfying some physically reasonable properties is used, and we base the design and analysis on these properties. The experiments are carried out using a proprietary road-tire friction model of a complexity comparable to the magic formula.

### 4.2.1 Monotonicity

According to Newton's second law, the vehicle's acceleration in a particular direction is equal to the sum of the forces acting in that direction, divided by the mass. For a vehicle traveling on a horizontal surface, the most significant forces acting in the road-surface plane are the road-tire friction forces, and we ignore smaller influences such as wind forces and air resistance. The road-tire friction forces are functions of the tire slips, which in turn are functions of the vehicle velocities. Consequently, the measurements of the vehicle accelerations are indirect measurements of the vehicle velocities.

To see how the connection between the accelerations and the velocities can be exploited, we consider what happens if we change the lateral velocity $v_y$ while keeping everything else constant. When the lateral velocity increases, it causes the tire slip angles to decrease. At each wheel, the decrease in the tire slip angle generally leads to a decrease in the lateral road-tire friction force. As a net result, the acceleration $a_y$ decreases when the lateral velocity $v_y$ increases, meaning that the

relationship between $a_y$ and $v_y$ can be modeled as monotonic.[1] It is demonstrated in Imsland et al. (2006) that, except in some particular cases, the partial derivative $\partial a_y / \partial v_y$ is smaller than some negative number. In Imsland et al. (2006), the monotonicity property is exploited to make $a_y$ an indirect measurement of $v_y$.

When the vehicle is moving on a slanted surface, gravity components influence the velocity of the vehicle, in addition to the road-tire friction forces. Nevertheless, because the accelerometers are influenced by the same gravity forces as the vehicle itself, the measured accelerations still correspond to the sum of the road-tire friction forces divided by the mass. This means that, even on a slanted surface, we can still exploit the monotonicity property of the measured lateral acceleration as an indirect measurement of $v_y$.

## 4.3 Velocity Estimation on Horizontal Surface

Before introducing the design for estimation of the inclination and bank angles, we briefly review the design from Imsland et al. (2006). For a vehicle traveling on a horizontal surface, the vehicle velocities are governed by the equations of motion (Kiencke and Nielsen, 2000)

$$\dot{v}_x = a_x + \dot{\psi} v_y, \tag{4.1a}$$

$$\dot{v}_y = a_y - \dot{\psi} v_x, \tag{4.1b}$$

where $v_x$ and $v_y$ are the longitudinal and lateral velocities, $a_x$ and $a_y$ are the longitudinal and lateral accelerations, and $\dot{\psi}$ is the yaw rate. Throughout the rest of this paper, a hat indicates an estimated quantity, and a tilde indicates an estimation error, meaning that $\hat{v}_x$ is an estimate of $v_x$, and $\tilde{v}_x := v_x - \hat{v}_x$. We discuss the longitudinal-velocity estimate $\hat{v}_x$ and the lateral-velocity estimate $\hat{v}_y$ separately, ignoring at first the interconnections between the two estimates.

### 4.3.1 Longitudinal-Velocity Estimation

The longitudinal-velocity estimate is given by

$$\dot{\hat{v}}_x = a_x + \dot{\psi} \hat{v}_y + K_{v_x}(t)(v_{x,\mathrm{ref}} - \hat{v}_x), \tag{4.2}$$

where $K_{v_x}(t) \geq K_{v_x,\min} > 0$ is a time-varying gain, and $v_{x,\mathrm{ref}}$ is a reference velocity calculated from the wheel speeds.

To calculate the reference velocity, we use the four wheel speeds, the steering wheel angle, and the yaw rate to obtain four separate estimates of the longitudinal velocity. The reference velocity is calculated as a weighted average of these

[1] See Section 4.6 for further remarks on this topic.

four velocity estimates, and the gain $K_{v_x}(t)$ is made to reflect the quality of the reference velocity. When the quality of the reference velocity is deemed to be low, the gain is reduced, making the observer less reliant on the reference velocity, and more reliant on integration of the system equations. The primary factor in determining the quality of the reference velocity is the spread in the four velocity estimates from the wheel speeds.

Ignoring the lateral-velocity error $\tilde{v}_y$, global exponential stability of the longitudinal-velocity error is easily proven when we assume that $v_{x,\text{ref}}$ represents the true longitudinal velocity.

### 4.3.2 Lateral-Velocity Estimation

For the lateral velocity, we start by introducing $\hat{a}_y(t, \hat{v}_x, \hat{v}_y)$, which denotes an estimate of the lateral acceleration $a_y$. The estimate $\hat{a}_y(t, \hat{v}_x, \hat{v}_y)$ is formed by using the nonlinear friction model for each wheel, where the measurements of the steering wheel angle, yaw rate, and wheel speeds, as well as the estimated velocities $\hat{v}_x$ and $\hat{v}_y$, are used as inputs. The friction forces modeled for each wheel are added up in the lateral direction of the vehicle and divided by the mass, resulting in the lateral-acceleration estimate $\hat{a}_y(t, \hat{v}_x, \hat{v}_y)$. The $t$ in $\hat{a}_y(t, \hat{v}_x, \hat{v}_y)$ denotes the dependence of $\hat{a}_y$ on time-varying signals such as the steering wheel angle. We also write $\tilde{a}_y(t, \tilde{v}_x, \tilde{v}_y) := a_y - \hat{a}_y(t, \hat{v}_x, \hat{v}_y)$.

The lateral-velocity estimate is given by

$$\dot{\hat{v}}_y = a_y - \dot{\psi}\hat{v}_x - K_{v_y}(a_y - \hat{a}_y(t, \hat{v}_x, \hat{v}_y)), \tag{4.3}$$

where $K_{v_y}$ is a positive gain. Analysis of (4.3) is based on the following assumption:

**Assumption 4.1.** *There exists a continuous function $\delta(t, \tilde{v}_y) \geq \delta_{\min} > 0$ such that, if $\tilde{v}_x = 0$, then*

$$\tilde{a}_y(t, 0, \tilde{v}_y) = -\delta(t, \tilde{v}_y)\tilde{v}_y. \tag{4.4}$$

Assumption 4.1 is justified by the previous discussion of the monotonic relationship between $a_y$ and $v_y$, by using the mean value theorem. Using Assumption 4.1, global exponential stability of the lateral-velocity error is easily verified when the longitudinal-velocity error $\tilde{v}_x$ is ignored.

### 4.3.3 Combined Longitudinal- and Lateral-Velocity Estimation

When we take the interconnections between the two observer equations (4.2), (4.3) into account, we require an additional assumption:

**Assumption 4.2.** *There exists a continuous, uniformly bounded function*

$$\kappa(t, \tilde{v}_x, \tilde{v}_y)$$

*such that*

$$\hat{a}_y(t, v_x, \hat{v}_y) - \hat{a}_y(t, \hat{v}_x, \hat{v}_y) = \kappa(t, \tilde{v}_x, \tilde{v}_y)\tilde{v}_x.$$

Using Assumption 4.2, we can verify that the origin of the error dynamics for the observer (4.2), (4.3) is globally exponentially stable, provided $K_{v_x,\min}$ is chosen large enough to dominate the cross-terms that occur because of the interconnections. The observer is also input-to-state stable with respect to errors in the reference velocity $v_{x,\text{ref}}$. For more details, we refer to Imsland et al. (2006).

## 4.4 Inclination and Bank Angle

We now consider the presence of nonzero inclination and bank angles. To define these angles precisely, we say that the orientation of the road surface is obtained from the horizontal position by a rotation around the vehicle's $y$-axis equal to the inclination angle $\Theta$, and a subsequent rotation around the $x$-axis equal to the bank angle $\Phi$. The inclination and bank angles cause gravity components to appear in the equations of motion, and we rewrite (4.1) as (Klier et al., 2008)

$$\dot{v}_x = a_x + \dot{\psi} v_y + g \sin(\Theta), \tag{4.5a}$$

$$\dot{v}_y = a_y - \dot{\psi} v_x - g \cos(\Theta) \sin(\Phi), \tag{4.5b}$$

where $g$ is the acceleration of gravity. It is important to note that in (4.5), $a_x$ and $a_y$ denote the accelerations measured by the accelerometers. We assume that the inclination and bank angles vary slowly enough compared to the dynamics of the system to be modeled as constants.

### 4.4.1 Inclination Angle

We define $\theta_\text{i} = \sin(\Theta)$, and introduce an estimate $\hat{\theta}_\text{i}$ of $\theta_\text{i}$. Although we can solve for the inclination angle by writing $\Theta = \arcsin(\theta_\text{i})$, typical inclination angles are small enough that $\Theta \approx \theta_\text{i}$. The estimate $\hat{\theta}_\text{i}$ is therefore considered an estimate of the inclination angle. We use $\hat{\theta}_\text{i}$ to compensate for the disturbance, by letting

$$\dot{\hat{v}}_x = a_x + \dot{\psi} \hat{v}_y + g\hat{\theta}_\text{i} + K_{v_x}(t)(v_{x,\text{ref}} - \hat{v}_x), \tag{4.6}$$

where $\hat{\theta}_\text{i}$ is given by

$$\dot{\hat{\theta}}_\text{i} = K_{\theta_\text{i}} K_{v_x}(t)(v_{x,\text{ref}} - \hat{v}_x), \tag{4.7}$$

with $K_{\theta_i}$ a positive gain. If the gain in (4.7) were constant, the inclination-angle estimation would be recognized as regular integral action. Instead, we let the gain in (4.7) vary in direct proportion to $K_{v_x}(t)$. The reason for using a time-varying gain is the same as in the longitudinal-velocity estimation itself, namely that we wish to rely less on the reference velocity $v_{x,\text{ref}}$ whenever it is of poor quality.

To justify this approach, we use the theory of *absolute stability* (Khalil, 2002, Ch. 7.1). We split the gain $K_{v_x}(t)$ into a constant and a time-varying part by writing $K_{v_x}(t) = a + (K_{v_x}(t) - a)$, where $0 < a < K_{v_x,\min}$. Ignoring for the moment the lateral-velocity error $\tilde{v}_y$, and assuming that $v_{x,\text{ref}}$ represents the true longitudinal velocity, we write the error dynamics of the longitudinal-velocity and inclination-angle estimates as the interconnection of the linear time-invariant (LTI) system

$$\dot{\tilde{v}}_x = -a\tilde{v}_x + g\tilde{\theta}_i + u, \tag{4.8a}$$

$$\dot{\tilde{\theta}}_i = -K_{\theta_i} a\tilde{v}_x + K_{\theta_i} u \tag{4.8b}$$

with the time-varying sector function $u = -(K_{v_x}(t) - a)\tilde{v}_x$.

**Lemma 4.1.** *If the gain $K_{\theta_i}$ is chosen such that $0 < K_{\theta_i} < a/g$, then the origin of* (4.8) *is globally exponentially stable.*

*Proof.* The function $\phi_x(t, \tilde{v}_x) = (K_{v_x}(t) - a)\tilde{v}_x$ belongs to the sector $[0, \infty]$, because $\phi_x(t, \tilde{v}_x)\tilde{v}_x \geq 0$ (Khalil, 2002, Def. 6.2). The transfer function from $u$ to $\tilde{v}_x$ is given by

$$G(s) = \frac{s + gK_{\theta_i}}{s^2 + as + gK_{\theta_i} a}.$$

According to Khalil (2002, Th. 7.1), we only have to show that $G(s)$ is strictly positive real to demonstrate that the interconnection is absolutely stable and that (4.8) is globally exponentially stable. We use Khalil (2002, Lemma 6.1) to show that $G(s)$ is strictly positive real. The poles of $G(s)$ are given by $(-a \pm \sqrt{a^2 - 4gK_{\theta_i} a})/2$. For any $K_{\theta_i} > 0$, $\text{Re}(\sqrt{a^2 - 4gK_{\theta_i} a}) < a$; hence, $G(s)$ is Hurwitz. We find $\text{Re}(G(j\omega))$:

$$\text{Re}(G(j\omega)) = \frac{(a - gK_{\theta_i})\omega^2 + g^2 K_{\theta_i}^2 a}{(gK_{\theta_i} a - \omega^2)^2 + a^2\omega^2}.$$

If $K_{\theta_i} < a/g$, then $a - gK_{\theta_i} > 0$, and hence $\text{Re}(G(j\omega)) > 0$ for all $\omega \in \mathbb{R}$. We have that $G(\infty) = \lim_{s\to\infty} G(s) = 0$. Hence, we must prove that $\lim_{\omega\to\infty} \omega^2 \text{Re}(G(j\omega)) > 0$. We have

$$\omega^2 \text{Re}(G(j\omega)) = \frac{(a - gK_{\theta_i})\omega^4 + g^2 K_{\theta_i}^2 a\omega^2}{\omega^4 - 2gK_{\theta_i} a\omega^2 + g^2 K_{\theta_i}^2 a^2 + a^2\omega^2}$$

Hence $\lim_{\omega\to\infty} \omega^2 \mathrm{Re}(G(j\omega)) = a - gK_{\theta_\mathrm{i}} > 0$, which proves that $G(s)$ is strictly positive real, provided $K_{\theta_\mathrm{i}} < a/g$. □

### 4.4.2 Bank Angle

We handle the bank angle in roughly the same way as the inclination angle. We define $\theta_\mathrm{b} = \cos(\Theta)\sin(\Phi)$ and introduce an estimate $\hat{\theta}_\mathrm{b}$ of $\theta_\mathrm{b}$. Typical bank and inclination angles are small enough that $\Phi \approx \theta_\mathrm{b}$, and $\hat{\theta}_\mathrm{b}$ is therefore considered an estimate of the bank angle. Using $\hat{\theta}_\mathrm{b}$ for compensation in the observer (4.3), we obtain

$$\dot{\hat{v}}_y = a_y - \dot{\psi}\hat{v}_x - g\hat{\theta}_\mathrm{b} - K_{v_y}(a_y - \hat{a}_y(t, \hat{v}_x, \hat{v}_y)). \tag{4.9}$$

We again use the lateral acceleration as an indirect measurement of the lateral velocity, letting

$$\dot{\hat{\theta}}_\mathrm{b} = K_{\theta_\mathrm{b}}(a_y - \hat{a}_y(t, \hat{v}_x, \hat{v}_y)), \tag{4.10}$$

where $K_{\theta_\mathrm{b}}$ is a positive gain.

Ignoring the effect of the longitudinal-velocity error $\tilde{v}_x$, we write the error dynamics of the lateral-velocity and bank-angle estimates as the interconnection of the LTI system

$$\dot{\tilde{v}}_y = -K_{v_y}\delta_{\min}\tilde{v}_y - g\tilde{\theta}_\mathrm{b} + K_{v_y}u, \tag{4.11a}$$

$$\dot{\tilde{\theta}}_\mathrm{b} = K_{\theta_\mathrm{b}}\delta_{\min}\tilde{v}_y - K_{\theta_\mathrm{b}}u \tag{4.11b}$$

with the time-varying sector nonlinearity $u = -(\delta(t, \tilde{v}_y) - \delta_{\min})\tilde{v}_y$.

**Lemma 4.2.** *If the gain $K_{\theta_\mathrm{i}}$ is chosen such that $0 < K_{\theta_\mathrm{i}} < K_{v_y}^2\delta_{\min}/g$, then the origin of* (4.11) *is globally exponentially stable.*

*Proof (Outline).* The function $\phi_y(t, \tilde{v}_y) = (\delta(t, \tilde{v}_y) - \delta_{\min})\tilde{v}_y$ belongs to the sector $[0, \infty]$, because $\phi_y(t, \tilde{v}_y)\tilde{v}_y \geq 0$. The proof proceeds as the proof of Lemma 4.1, with the transfer function

$$G(s) = \frac{K_{v_y}s + gK_{\theta_\mathrm{b}}}{s^2 + K_{v_y}\delta_{\min}s + gK_{\theta_\mathrm{b}}\delta_{\min}}.$$

The resulting gain requirement is $K_{\theta_\mathrm{b}} < K_{v_y}^2\delta_{\min}/g$. □

### 4.4.3 Combined Analysis

We have so far ignored the interconnections between the $(\tilde{v}_x, \tilde{\theta}_\mathrm{i})$-subsystem and the $(\tilde{v}_y, \tilde{\theta}_\mathrm{b})$-subsystem. With the help of Lemmas 4.1 and 4.2, we can now state a theorem for the combined system, taking the interconnections into account.

**Theorem 4.1.** *There exists a constant $C > 0$ such that if the gains $K_{\theta_i}$, $K_{\theta_b}$, and $K_{v_x}(t)$ are chosen such that $0 < K_{\theta_i} < a/g$, $0 < K_{\theta_b} < K_{v_y}^2 \delta_{\min}/g$, and $K_{v_x,\min} > C$, then the origin of the error dynamics for the observer* (4.6), (4.7), (4.9), (4.10) *is globally exponentially stable.*

*Proof.* From the proof of Khalil (2002, Th. 7.1) there is a Lyapunov function $V_1 = \frac{1}{2}x_1^\top P_1 x_1$, where $x_1 := [\tilde{v}_x, \tilde{\theta}_i]^\top$, such that, along the trajectories of (4.8),

$$\dot{V}_1 \leq -\varepsilon_1 x_1^\top P_1 x_1 - \tilde{v}_x \phi_x(t, \tilde{v}_x) \leq -\varepsilon_1 x_1^\top P_1 x_1 - (K_{v_x,\min} - a)\tilde{v}_x^2,$$

for some $\varepsilon_1 > 0$. There is a also a Lyapunov function $V_2 = \frac{1}{2}x_2^\top P_2 x_2$, where $x_2 := [\tilde{v}_y, \tilde{\theta}_b]^\top$, such that, along the trajectories of (4.11), $\dot{V}_2 \leq -\varepsilon_2 x_2^\top P_2 x_2$, for some $\varepsilon_2 > 0$.

If we include the effect of $\tilde{v}_y$ on the $x_1$-subsystem, we get an extra perturbation $[\dot{\psi}\tilde{v}_y, 0]^\top$ on the right-hand side in (4.8). If we include the effect of $\tilde{v}_x$ on the $x_2$-subsystem, we get an extra perturbation

$$[-\dot{\psi}\tilde{v}_x + K_{v_y}\kappa(t, \tilde{v}_x, \tilde{v}_y)\tilde{v}_x, -K_{\theta_b}\kappa(t, \tilde{v}_x, \tilde{v}_y)\tilde{v}_x]^\top$$

on the right-hand side in (4.11), where $\kappa(t, \tilde{v}_x, \tilde{v}_y)$ comes from Assumption 4.2, by writing $\tilde{a}_y(t, \tilde{v}_x, \tilde{v}_y) = a_y - \hat{a}_y(t, v_x, \hat{v}_y) + \hat{a}_y(t, v_x, \hat{v}_y) - \hat{a}_y(t, \hat{v}_x, \hat{v}_y) = -\delta(t, \tilde{v}_y)\tilde{v}_y + \kappa(t, \tilde{v}_x, \tilde{v}_y)\tilde{v}_x$. Using the Lyapunov function $V = V_1 + cV_2$, where $c > 0$ is yet to be determined, we have

$$\begin{aligned}\dot{V} \leq\ & -\varepsilon_1 \lambda_{\min}(P_1)\|x_1\|^2 + m_{\dot{\psi}}\|P_1\|\|x_1\|\|x_2\| \\ & + cm\|P_2\|\|x_2\||\tilde{v}_x| - (K_{v_x,\min} - a)\tilde{v}_x^2 - c\varepsilon_2\lambda_{\min}(P_2)\|x_2\|^2,\end{aligned}$$

where $m_{\dot{\psi}}$ is a bound on $|\dot{\psi}|$, $m$ is a bound on

$$\|[-\dot{\psi} + K_{v_y}\kappa(t, \tilde{v}_x, \tilde{v}_y), -K_{\theta_b}\kappa(t, \tilde{v}_x, \tilde{v}_y)]\|,$$

and $\lambda_{\min}(P_i)$, $i = 1, 2$, denotes the minimum eigenvalue of $P_i$. We can split the right-hand side of the inequality by writing $\dot{V} \leq -W_1 - W_2$, where

$$W_1 = \begin{bmatrix}\|x_1\| & \|x_2\|\end{bmatrix}\begin{bmatrix}\varepsilon_1\lambda_{\min}(P_1) & -\frac{m_{\dot{\psi}}}{2}\|P_1\| \\ -\frac{m_{\dot{\psi}}}{2}\|P_1\| & \frac{c\varepsilon_2}{2}\lambda_{\min}(P_2)\end{bmatrix}\begin{bmatrix}\|x_1\| \\ \|x_2\|\end{bmatrix},$$

and

$$W_2 = \begin{bmatrix}\|x_2\| & |\tilde{v}_x|\end{bmatrix}\begin{bmatrix}\frac{c\varepsilon_2}{2}\lambda_{\min}(P_2) & -\frac{1}{2}cm\|P_2\| \\ -\frac{1}{2}cm\|P_2\| & K_{v_x,\min} - a\end{bmatrix}\begin{bmatrix}\|x_2\| \\ |\tilde{v}_x|\end{bmatrix}.$$

The first-order principal minor of the $2 \times 2$ matrix in the $W_1$ expression is

$$\varepsilon_1\lambda_{\min}(P_1) > 0.$$

The second-order principal minor is

$$\frac{1}{2}c\varepsilon_1\varepsilon_2\lambda_{\min}(P_1)\lambda_{\min}(P_2) - \frac{1}{4}m_{\dot{\psi}}^2\|P_1\|^2,$$

which is made positive by letting

$$c > m_{\dot{\psi}}^2\|P_1\|^2/(2\varepsilon_1\varepsilon_2\lambda_{\min}(P_1)\lambda_{\min}(P_2)).$$

Hence, the matrix is positive definite. The first-order principal minor of the $2 \times 2$ matrix in the $W_2$ expression is $\frac{1}{2}c\varepsilon_2\lambda_{\min}(P_2) > 0$. The second-order principal minor is $\frac{1}{2}c\varepsilon_2\lambda_{\min}(P_2)(K_{v_x,\min} - a) - \frac{1}{4}c^2m^2\|P_2\|^2$, which is made positive by letting $K_{v_x,\min} > C := a + cm^2\|P_2\|^2/(2\varepsilon_2\lambda_{\min}(P_2))$ Hence, both matrices are positive definite, meaning that $\dot{V}$ is negative definite. □

Summing up the results of the stability analysis, global exponential stability of the observer error is guaranteed if the gains $K_{\theta_i}$, $K_{\theta_b}$ are chosen sufficiently low, and the minimum value $K_{v_x,\min}$ of $K_{v_x}(t)$ is chosen sufficiently high. Even though there is no upper limit on $K_{v_x}(t)$, it is of obvious interest to limit this gain, to avoid direct propagation of $v_{x,\text{ref}}$ to the estimate $\hat{v}_x$.

## 4.5 Unknown Road-Surface Conditions

The observer (4.6), (4.7), (4.9), (4.10) depends on the construction of a lateral-acceleration estimate $\hat{a}_y(t, \hat{v}_x, \hat{v}_y)$ as a function of measured signals and velocity estimates. This approach assumes that there is no uncertainty in the friction model with respect to the road-surface conditions. In reality, however, the friction model is sensitive to changes in the road-surface conditions for large tire slips. In Grip et al. (2008), the design from Imsland et al. (2006) is altered to take unknown road-surface conditions into account, by estimating a friction parameter $\theta$ along with the velocities.

The longitudinal-velocity and inclination-angle estimates do not depend on the friction model; hence, no changes are necessary to (4.6), (4.7). We focus on the lateral-velocity and friction-parameter estimation from Grip et al. (2008), given by

$$\dot{\hat{v}}_y = a_y - \dot{\psi}\hat{v}_x + K_{v_y}\Lambda(t, \hat{v}_x, \hat{v}_y)\xi(t, \hat{v}_x, \hat{v}_y)(a_y - \hat{a}_y(t, \hat{v}_x, \hat{v}_y, \hat{\theta})), \quad (4.12a)$$

$$\dot{\hat{\theta}} = K_\theta\Lambda(t, \hat{v}_x, \hat{v}_y)\hat{a}_y^*(t, \hat{v}_x, \hat{v}_y)(a_y - \hat{a}_y(t, \hat{v}_x, \hat{v}_y, \hat{\theta})). \quad (4.12b)$$

Here $\hat{a}_y$ has been redefined as

$$\hat{a}_y(t, \hat{v}_x, \hat{v}_y, \hat{\theta}) = \hat{\theta}\hat{a}_y^*(t, \hat{v}_x, \hat{v}_y),$$

where $\hat{a}_y^*(t, \hat{v}_x, \hat{v}_y)$ is the lateral-acceleration estimate from the friction model, obtained using a nominal parameterization corresponding to a high-friction surface. The estimated friction parameter $\hat{\theta}$ scales the output of the friction model to adapt to different road-surface conditions. The value $\xi(t, \hat{v}_x, \hat{v}_y)$ is the approximated slope of the line between $(\hat{v}_y, \hat{a}_y^*(t, \hat{v}_x, \hat{v}_y))$ and $(v_y, \hat{a}_y^*(t, \hat{v}_x, v_y))$, which is negative according to Assumption 4.1. The function $\Lambda(t, \hat{v}_x, \hat{v}_y)$ is a freely chosen, strictly positive scaling function, which we define as $\Lambda(t, \hat{v}_x, \hat{v}_y) = (\xi^2(t, \hat{v}_x, \hat{v}_y) + \hat{a_y^*}^2(t, \hat{v}_x, \hat{v}_y))^{-1/2}$ to give the observer good numerical properties. Under the assumptions in Grip et al. (2008), the estimation error for (4.12) is uniformly globally asymptotically stable and locally exponentially stable. For details, we refer to Grip et al. (2008).

A central assumption in Grip et al. (2008) concerns the lateral excitation of the vehicle. In order to simultaneously estimate the lateral velocity and the friction parameter, there needs to be variation in the vehicle's lateral movement. During stationary maneuvers, such as straight driving, we cannot estimate the friction parameter along with the lateral velocity, and the friction estimation therefore has to be turned off.

### 4.5.1 When to Estimate Friction

Because lateral excitation is needed for the friction estimation, and because estimation of the friction parameter is unnecessary during normal driving with small tire slips, we leave the friction estimation off most of the time, and only turn it on in certain cases. When to turn the friction estimation on is determined in a manner similar to that of an ESC system and alternative approaches found in literature (for example, Fukada, 1999; Hac and Simpson, 2000). Using a linear reference model for the yaw rate, we determine when the car becomes over- or understeered. We also estimate $\dot{v}_y$, according to (4.1b), by $a_y - \dot{\psi}\hat{v}_x$, highpass-filtered with a 10-s time constant. When $\dot{v}_y$ is high, it indicates a fast-changing sideslip angle, which in turn indicates a high level of excitation and that some of the tires might be in the nonlinear region. When the estimate of $\dot{v}_y$ is high, and the reference yaw rate is above a threshold value, we therefore turn the friction estimation on. We also turn the friction estimation on when the car is oversteered; and when the vehicle's ESC system is active, but not due to stationary understeer. A small delay in turning friction estimation off reduces chattering in the friction estimation condition.

### 4.5.2 Combining Friction Estimation with Bank-Angle Estimation

We can modify (4.12a) to take the bank angle into account, by redefining

$$\dot{\hat{v}}_y = a_y - \dot{\psi}\hat{v}_x - g\hat{\theta}_{\mathrm{i}} + K_{v_y}\Lambda(t,\hat{v}_x,\hat{v}_y)\xi(t,\hat{v}_x,\hat{v}_y)(a_y - \hat{a}_y(t,\hat{v}_x,\hat{v}_y,\hat{\theta})). \tag{4.13}$$

Because the lateral-velocity estimation in (4.13) is different from (4.9), we also alter the bank-angle estimation to make it fit within the absolute-stability framework:

$$\dot{\hat{\theta}}_{\mathrm{b}} = -K_{\theta_{\mathrm{b}}}\Lambda(t,\hat{v}_x,\hat{v}_y)\xi(t,\hat{v}_x,\hat{v}_y)(a_y - \hat{a}_y(t,\hat{v}_x,\hat{v}_y,\hat{\theta})). \tag{4.14}$$

In the previous Lyapunov analysis, we have used tunable gains to dominate cross-terms that appear in the time derivative of the Lyapunov function. A Lyapunov function is available from Grip et al. (2008) to prove exponential stability of the lateral-velocity and friction-parameter error, within an arbitrarily large region of attraction around the origin. This Lyapunov function can be combined with the Lyapunov function for the bank-angle estimation error. However, the stability margin from Grip et al. (2008) depends on the level of excitation, which cannot be changed by increasing the gains, and the conditions for asymptotic stability are therefore difficult or impossible to verify. We therefore cannot find a particular set of observer gains to guarantee asymptotic stability when friction estimation is combined with bank-angle estimation.

From a practical point of view, it is often difficult to distinguish the effect of low friction and a nonzero bank angle in experimental data, something that is also noted in van Zanten (2000). This observation suggests that the difficulties we encounter in analyzing the combined approach reflects a genuine observability problem. How to combine friction estimation and bank-angle estimation is therefore a matter of practical consideration.

The simplest strategy would be to turn the bank-angle estimation off whenever friction estimation is turned on. With this strategy, however, it is possible to provoke problems when driving on slippery surfaces in hilly terrains, where combinations of large vehicle sideslip angles and large bank angles may occur. For this reason, we leave the bank-angle estimation on when estimating friction, albeit with the gain set lower whenever one of three conditions hold. The first condition is that $|a_y - \hat{a}_y(t,\hat{v}_x,\hat{v}_y,\hat{\theta})| > c_1$ for some $c_1 > 0$. The second condition is that $|\ddot{\psi} - \hat{\ddot{\psi}}(t,\hat{v}_x,\hat{v}_y,\hat{\theta})| > c_2$ for some $c_2 > 0$, where $\ddot{\psi}$ is the yaw acceleration found by numerical differentiation of the yaw rate, and $\hat{\ddot{\psi}}(t,\hat{v}_x,\hat{v}_y,\hat{\theta})$ is calculated using the friction model in the same way as $\hat{a}_y(t,\hat{v}_x,\hat{v}_y,\hat{\theta})$, with the forces scaled by

$\hat{\theta}$. The third condition is that $\text{sign}(\dot{\psi}_{\text{ref}}) = \text{sign}(\dot{\psi})$ and $(|\dot{\psi}_{\text{ref}}| - |\dot{\psi}|)\hat{v}_x > c_3$ for some $c_3 > 0$, where $\dot{\psi}_{\text{ref}}$ is the reference yaw rate used in the friction estimation conditions described in Section 4.5.1. From experimental data, these conditions are found to reduce the negative interference of the bank-angle estimation on low-friction surfaces. We emphasize, however, that these conditions are purely practical and that alternative conditions may be equally good or better.

### 4.5.3 Final Observer

The final observer that we end up with has two modes, without friction estimation and with friction estimation. Without friction estimation we use equations (4.6), (4.7), (4.9), (4.10), where $\hat{a}_y(t, \hat{v}_x, \hat{v}_y)$ is replaced by the friction-parameter dependent $\hat{a}_y(t, \hat{v}_x, \hat{v}_y, \hat{\theta})$, and the friction parameter is attracted to a high default value: $\dot{\hat{\theta}} = K_{\text{e}}(\theta^* - \hat{\theta})$. With friction estimation we use (4.6), (4.7), (4.13), (4.12b), (4.14).

In both modes, $K_{\theta_{\text{b}}}$ is reduced according to the practical conditions described above. Based on experimental results, we also choose to set the gain $K_{\theta_{\text{i}}}$ for the inclination-angle estimation lower for the second mode than for the first.

## 4.6 Some Remarks about Road-Tire Friction

Throughout this paper, we assume a strictly monotonic relationship between the lateral acceleration and the lateral velocity. For large tire slip angles, however, the road-tire friction forces saturate completely, and may decrease slightly. In certain extreme situations with large tire slips for all tires, the monotonicity assumption may therefore fail to hold. Reflecting this possibility, the stability results in Imsland et al. (2006) are stated as regional rather than global. We have chosen to simplify the analysis by operating in the global domain. In the friction model used in the experiments, the friction forces saturate for large tire slip angles, but do not decrease. This helps ensure stability of the observer equations.

## 4.7 Implementation and Experimental Results

The observer is discretized using the forward-Euler method with a 10-ms sample time. The measurements are taken from production-type sensors, and are filtered with a 15-Hz lowpass filter, without any correction for sensor bias. Some notable implementation details are the following:

- The wheel loads are calculated using the acceleration measurements, as in Kiencke and Nielsen (2000, Ch. 7.4).

- Tire relaxation dynamics are approximated in a manner similar to Pacejka (2006, Ch. 1), by filtering the output of the friction model with a transfer function $1/(Ts + 1)$, where $T = T_e + l_e/\hat{v}_x$.

- The front-axle steering angles are calculated using the measured steering wheel angle and a lookup table based on a steering transmission curve. The effect of caster is included by making the steering angles dependent on the estimated lateral road-tire friction forces for the front axle, according to Pacejka (2006, Ch. 1).

- The effect of vehicle roll on the lateral-acceleration measurement is compensated by multiplying the measured lateral acceleration with $1/(1 + p_g g)$, where $p_g$ is the roll-angle gradient.

- As in Grip et al. (2008), the range of possible friction parameters is limited. The estimated friction parameter must belong to $[0.05, 1.1]$ and, in addition, we ensure that $1.2g\hat{\theta} \geq (a_x^2 + a_y^2)^{1/2}$. We do so because $1.2\hat{\theta}g$ is the approximate maximum acceleration achievable from the friction model when multiplied by the friction parameter, and this maximum should never be smaller than the actual acceleration of the vehicle.

The first experiment is a circle maneuver with a 40-m radius, carried out on dry asphalt. The longitudinal velocity is slowly increased from about 10 km/h to about 65 km/h, when the circle can no longer be maintained because of severe understeer. The area on which the circle maneuver takes place has a constant slope of $0.5°$; hence, both the inclination angle and the bank angle oscillate between $\pm 0.5°$ as the maneuver takes place. The results are shown in Figure 4.2. Until approximately 88 s into the test, the bank angle follows the reference well, albeit with a phase lag. The phase lag can be made smaller by increasing the gain, but this is not desirable for the sideslip angle estimate. After 88 s, the bank-angle estimate reacts slowly to changes, because the gain is then reduced according to the practical conditions in Section 4.5.2. There is also a small offset in the bank angle, attributable to offsets in the measurements of the steering wheel angle, lateral acceleration, and yaw rate. For the inclination angle there is a significant offset, caused by an offset in the longitudinal-acceleration sensor. Nevertheless, the estimated sideslip angle is accurate.

The second experiment consists of driving downhill from a mountain top on snow-covered roads. In this experiment, we have no reference for the inclination

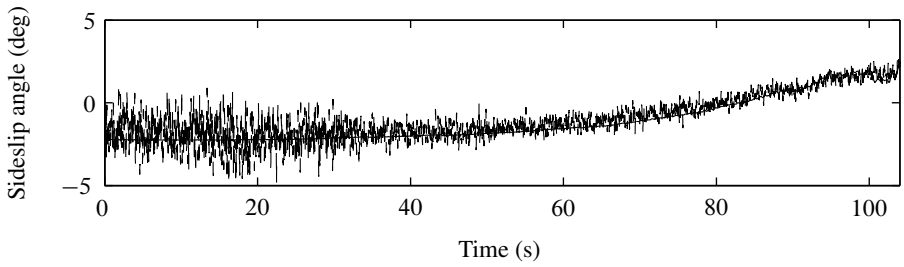


(a) Real (dashed) and estimated (solid) sideslip angle

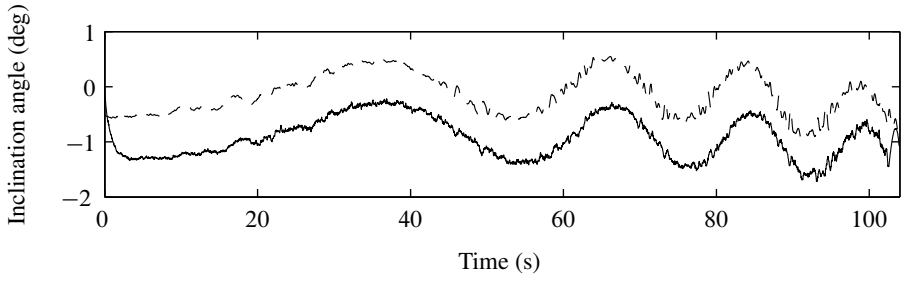


(b) Real (dashed) and estimated (solid) inclination angle

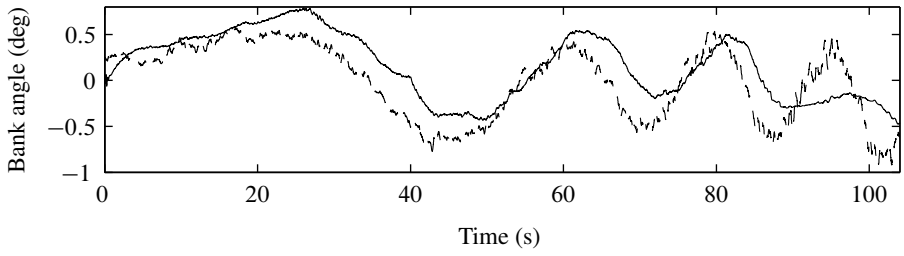


(c) Real (dashed) and estimated (solid) bank angle

**Figure 4.2:** Experimental results for circle maneuver

and bank angles; hence we have to evaluate the estimates based on plausibility and on the quality of the estimated sideslip angle. The results are shown in Figure 4.3. Qualitatively, the estimates match well with the terrain, indicating a varying but steep descent, and significant road bank angles. The resulting sideslip angle estimate is accurate.

It is evident from Figure 4.2 that offsets found in production-type sensors have a significant impact on the achievable accuracy of the inclination- and bank-angle estimation. Correction for inertial sensor offsets is a fundamental, challenging problem that lies outside the scope of this paper.

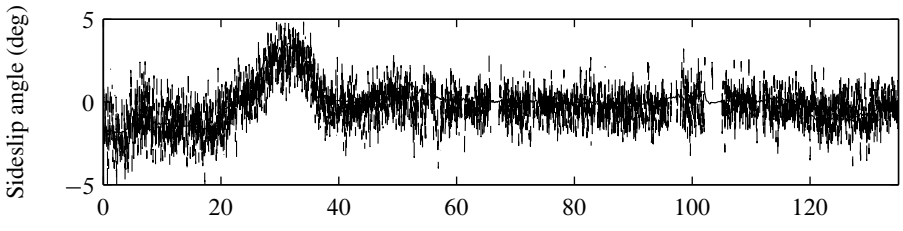


(a) Real (dashed) and estimated (solid) sideslip angle

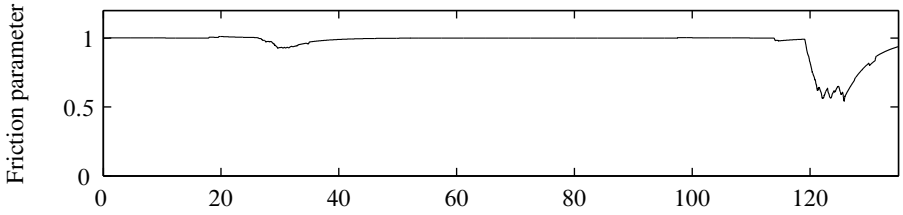


(b) Estimated friction parameter

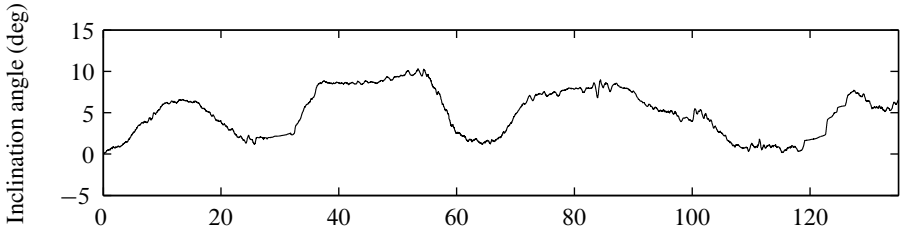


(c) Estimated inclination angle

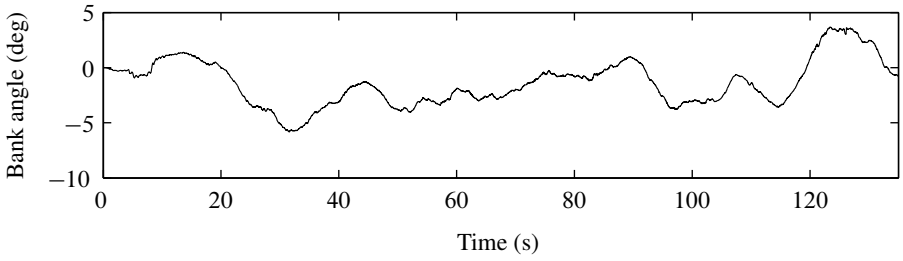


(d) Estimated bank angle

**Figure 4.3:** Experimental results for mountain driving

## 4.8 Concluding Remarks

The primary reason for estimating the road inclination and bank angle is to improve estimation of the sideslip angle on slanted road surfaces. In this respect, experimental results are mostly good; in most situations, the estimates of the sideslip angle are of high quality. Problems persist, however, in some situations on low-friction surfaces. The problems can largely be attributed to the difficulty of distinguishing a nonzero bank angle from low friction. The method of combining friction estimation and bank-angle estimation is a weakness of the present design, which limits the achievable performance. The ad-hoc approach of selectively reducing the bank angle gain based on various criteria is likely to need revision and improvement for the observer to reach production quality. Preliminary results indicate that eventual availability of six-degree-of-freedom inertial sensors in production vehicles is likely to help, by making estimation of the bank angle less dependent on the friction model.

With respect to providing accurate estimates of the inclination and bank angle, the approach gives plausible estimates in most normal driving situations, but sensor offsets and other slowly-varying errors propagate to the inclination- and bank-angle estimates. In extreme situations with large tire slip angles, the estimates often become temporarily implausible, due primarily to inaccuracies in the friction model.

## Bibliography

D. M. Bevly. Global Positioning System (GPS): A low-cost velocity sensor for correcting inertial sensor errors on ground vehicles. *J. Dyn. Syst. Meas. Contr.*, 126(2):255–264, 2004.

R. G. Brown and P. Y. C. Hwang. *Introduction to Random Signals and Applied Kalman Filtering*. Wiley, New York, 3rd edition, 1997.

Y. Fukada. Slip-angle estimation for vehicle stability control. *Vehicle Syst. Dyn.*, 32(4):375–388, 1999.

H. F. Grip, L. Imsland, T. A. Johansen, T. I. Fossen, J. C. Kalkkuhl, and A. Suissa. Nonlinear vehicle side-slip estimation with friction adaptation. *Automatica*, 44 (3):611–622, 2008.

A. Hac and M. D. Simpson. Estimation of vehicle side slip angle and yaw rate. In *Proc. SAE World Congr.*, Detroit, MI, 2000. Paper no. 2000-01-0696.

L. Imsland, T. A. Johansen, T. I. Fossen, H. F. Grip, J. C. Kalkkuhl, and A. Suissa. Vehicle velocity estimation using nonlinear observers. *Automatica*, 42(12): 2091–2103, 2006.

L. Imsland, T. A. Johansen, H. F. Grip, and T. I. Fossen. On nonlinear unknown input observers—Applied to lateral vehicle velocity estimation on banked roads. *Int. J. Contr.*, 80(11):1741–1750, 2007.

H. K. Khalil. *Nonlinear Systems*. Prentice-Hall, Upper Saddle River, NJ, 3rd edition, 2002.

U. Kiencke and L. Nielsen. *Automotive Control Systems: For Engine, Driveline, and Vehicle*. Springer, Berlin, 2000.

W. Klier, A. Reim, and D. Stapel. Robust estimation of vehicle sideslip angle—An approach w/o vehicle and tire models. In *Proc. SAE World Congr.*, Detroit, MI, 2008. Paper no. 2008-01-0582.

H. B. Pacejka. *Tire and Vehicle Dynamics*. SAE, Warrendale, PA, 2nd edition, 2006.

J. Ryu and J. C. Gerdes. Estimation of vehicle roll and road bank angle. In *Proc. American Contr. Conf.*, pages 2110–2115, Boston, MA, 2004.

Y. Sebsadji, S. Glaser, S. Mammar, and M. Netto. Vehicle roll and road bank angles estimation. In *Proc. IFAC World Congr.*, pages 7091–7097, Seoul, South Korea, 2008.

C. Sentouh, Y. Sebsadji, S. Mammar, and S. Glaser. Road bank angle and faults estimation using unknown input proportional-integral observer. In *Proc. European Contr. Conf.*, pages 5131–5138, Kos, Greece, 2007.

A. Suissa, Z. Zomotor, and F. Böttiger. Method for determining variables characterizing vehicle handling. US Patent 5,557,520, 1994. Filed Jul. 29, 1994; issued Sep. 17, 1996.

H. E. Tseng. Dynamic estimation of road bank angle. *Vehicle Syst. Dyn.*, 36(4): 307–328, 2001.

A. T. van Zanten. Bosch ESP systems: 5 years of experience. In *Proc. Automot. Dyn. Stab. Conf.*, Troy, MI, 2000. Paper no. 2000-01-1633.

# Part II

# State and Parameter Estimation for Nonlinearly Parameterized Systems

# Chapter 5

# Parameter Estimation and Compensation in Systems with Nonlinearly Parameterized Perturbations

***Abstract:*** *We consider a class of systems influenced by perturbations that are nonlinearly parameterized by unknown constant parameters, and develop a method for estimating the unknown parameters. The method applies to systems where the states are available for measurement, and perturbations with the property that an exponentially stable estimate of the unknown parameters can be obtained if the whole perturbation is known. The main contribution is to introduce a conceptually simple, modular design that gives freedom to the designer in accomplishing the main task, which is to construct an update law to asymptotically invert a nonlinear equation. Compensation for the perturbations in the system equations is considered for a class of systems with uniformly globally bounded solutions, for which the origin is uniformly globally asymptotically stable when no perturbations are present. We also consider the case when the parameters can only be estimated when the controlled state is bounded away from the origin, and show that we may still be able to achieve convergence of the controlled state. We illustrate the method through examples, and apply it to the problem of downhole pressure estimation during oil well drilling.*

## 5.1 Introduction

An important issue in model-based control is the handling of unknown perturbations to system equations. Such perturbations can be the result of external disturbances or internal plant changes, such as a configuration change, system fault, or changes in physical plant characteristics. Frequently, the perturbations can be characterized in terms of a vector of unknown, constant parameters.

Adaptive control techniques counteract such perturbations by using estimates of the unknown parameters that are updated online. When the perturbations are linear with respect to the unknown parameters, adaptive control design is often straightforward, and techniques for handling such cases are well developed (see, e.g., Krstić, Kanellakopoulos, and Kokotović, 1995; Ioannou and Sun, 1996). In the nonlinear case the range of available design techniques is more limited. One approach is to use a gradient algorithm, as in linearly parameterized systems, which may yield poor results or unstable behavior for nonlinear parameterizations (see discussion in Annaswamy, Skantze, and Loh, 1998). Another common strategy is implementing an extended Kalman filter (EKF) for estimation of the unknown parameters. Although this often yields good results, analysis of the stability properties of an EKF is difficult (see, e.g., Reif, Günther, Yaz, and Unbehauen, 1999). Introducing extra parameters to obtain a linear expression is sometimes possible, but doing so may increase the complexity and affect the performance by reducing the convergence rate of the parameter estimates or introducing stricter persistency-of-excitation conditions.

Some techniques that do not resort to approximations are found in the literature. In Fomin, Fradkov, and Yakubovich (1981); Ortega (1996), the stability and convergence of the controlled state are proven for a gradient-type approach for nonlinear parameterizations with a convexity property. Annaswamy et al. (1998) exploit the convexity or concavity of some parameterizations by introducing a tuning function and adaptation based on a min-max optimization strategy, achieving arbitrarily accurate tracking of the controlled states. This approach is extended to general nonlinear parameterizations in Loh, Annaswamy, and Skantze (1999), and parameter convergence is studied in Cao, Annaswamy, and Kojić (2003). Other results, such as Bošković (1995, 1998); Zhang, Ge, Hang, and Chai (2000), focus on first-order systems with certain fractional parameterizations, proving convergence of the controlled state. In Qu (2003), an approach is introduced for a class of higher-order systems with matrix fractional parameterizations, which achieves global boundedness and ultimate boundedness with a desired precision. Here, an auxiliary estimate of the full perturbation is used in the estimation of the unknown parameters, the same principle upon which the results in this paper are based. In Qu, Hull, and Wang (2006), an approach for more general nonlinear parameteriza-

tions is presented, where the parameter estimate used in the control law is biased by an appropriately chosen vector function.

Another way of dealing with undesired perturbations is found in Chakrabortty and Arcak (2009), where a high-gain approach is used to produce an estimate of the perturbation, which is then used for control. By increasing the gain, the estimate is made to converge arbitrarily fast, and the transient performance of the unperturbed system can therefore be recovered. The approach considered in this paper has similarities to Chakrabortty and Arcak (2009), but it also exploits available structural information by estimating an unknown parameter vector in addition to the full perturbation. The parameter estimate is produced by a parameter estimation module that is designed as if the perturbation were known. In the actual implementation, however, the estimate of the perturbation is used. This idea is similar to the ideas in Tyukin (2003), where adaptive update laws of a certain structure, called *virtual algorithms*, are designed as if time derivatives of the measurements were available, before being transformed into realizable form without explicit differentiation of the measurements. In Tyukin, Prokhorov, and van Leeuwen (2007), this principle is used to design a family of adaptation laws for monotonically parameterized perturbations in the first derivatives.

The main contribution of this paper is a nonlinear parameter estimation design with a clear modular structure. The design is split into two modules: a perturbation estimator, and a parameter estimator constructed by the designer to asymptotically invert a nonlinear equation. The modular structure is conceptually simple, and it isolates the task of inverting the nonlinear equation, giving the designer freedom in how to best accomplish this task. Through a series of propositions, we provide guidelines for how to construct the parameter estimator, and we obtain explicit Lyapunov functions that prove exponential convergence of the parameter estimates. One of the main advantages of the modular structure is extensibility. In particular, it is demonstrated in Grip, Saberi, and Johansen (2009) that the perturbation estimator can be extended to handle systems with partial state measurement, where the perturbation appears in higher-order derivatives of the output. The method can often be used to provide fast parameter estimates, which may be useful not only for direct compensation, but as part of other control schemes where fast parameter estimates are required, for example, traditional adaptive approaches combined with parameter resetting (see, e.g., Bakkeheim, Johansen, Smogeli, and Sørensen, 2008).

### 5.1.1 Preliminaries

We use conventional notation to denote estimates and error variables. For a vector $z$, $\hat{z}$ represents its estimate and $\tilde{z} = z - \hat{z}$ is an error variable. We denote by

$z_i$ the $i$'th element of $z$, when this is clear from the context. The norm operator $\|\cdot\|$ denotes the Euclidean norm for vectors and the induced Euclidean norm for matrices. For a symmetric, positive-definite matrix $P$ and a vector $z$, we write $\|z\|_P = (z^\mathsf{T} P z)^{1/2}$. The maximum and minimum eigenvalues of a symmetric matrix $P$ are denoted $\lambda_{\max}(P)$ and $\lambda_{\min}(P)$. The open and closed balls around the origin with radius $\varepsilon$ are denoted $B(\varepsilon)$ and $\overline{B}(\varepsilon)$, respectively. We denote by $\mathbb{R}_{\geq 0}$ and $\mathbb{R}_{>0}$ the non-negative and the positive real numbers. For a set $E \subset \mathbb{R}^n$, we write $(E - E) := \{z_1 - z_2 \in \mathbb{R}^n \mid z_1, z_2 \in E\}$. Throughout this paper, when considering systems of the form $\dot{z} = F(t, z)$, we implicitly assume that $F : \mathbb{R}_{\geq 0} \times \mathbb{R}^n \to \mathbb{R}^n$ is piecewise continuous in $t$ and locally Lipschitz continuous in $z$, uniformly in $t$, on $\mathbb{R}_{\geq 0} \times \mathbb{R}^n$. The solution of this system, initialized at time $t_0 \geq 0$ with initial condition $z(t_0)$, is denoted $z(t)$. The continuity assumptions on $F$ allow us to conclude that $z(t)$ is uniquely defined for all $t \geq t_0$ if it is known not to escape from some compact subset of the state space (see Khalil, 2002, Ch. 3).

## 5.2 Problem Formulation

We consider systems that, by the appropriate state transformations and choice of control law, can be expressed in the following form:

$$\dot{x} = f(t, x) + B(t, x)\left(g(t, x, \theta) + v(t, x)\right), \tag{5.1}$$

where $x \in \mathbb{R}^n$ is a measured state vector and $\theta \in \mathbb{R}^p$ is a vector of unknown, constant parameters. The functions $f : \mathbb{R}_{\geq 0} \times \mathbb{R}^n \to \mathbb{R}^n$, $B : \mathbb{R}_{\geq 0} \times \mathbb{R}^n \to \mathbb{R}^{n \times m}$ and $v : \mathbb{R}_{\geq 0} \times \mathbb{R}^n \to \mathbb{R}^m$ can be evaluated from available measurements, and $g : \mathbb{R}_{\geq 0} \times \mathbb{R}^n \times \mathbb{R}^p \to \mathbb{R}^m$ can be evaluated if $\theta$ is known.

In most practical circumstances, it is known from physical considerations that $\theta$ is restricted to some bounded set of values. This is a significant advantage when it comes to satisfying the assumptions made later in this paper. To simplify the exposition, we therefore assume that the set of possible parameters is bounded. In designing update laws for parameter estimates, we also assume that a parameter projection can be implemented as described in Krstić et al. (1995), restricting the parameter estimates to a compact, convex set $\Theta \subset \mathbb{R}^p$, defined slightly larger than the set of possible parameter values. The parameter projection is denoted $\mathrm{Proj}(\cdot)$, and is described in Appendix 5.A.

All functions on the right-hand side of (5.1) are well defined and bounded for each bounded $(t, x, \theta) \in \mathbb{R}_{\geq 0} \times \mathbb{R}^n \times \Theta$. We assume that $g(t, x, \theta)$ is continuously differentiable with respect to $\theta$ for all $\theta \in \Theta$. As we construct an estimator, additional smoothness requirements may be needed for $f$, $B$, $g$, and $v$, as well

as other functions, to guarantee that the piecewise continuity and local Lipschitz conditions in Section 5.1.1 hold for all systems involved. It is left to the designer to check these requirements.

## 5.3 Parameter Estimation

In this section, we present a method for estimating the unknown parameter vector $\theta$ when $x(t)$ is bounded. Let $\phi := B(t,x)g(t,x,\theta)$ represent the full unknown perturbation in (5.1). The idea behind the estimation scheme is as follows. We first design an update law that exponentially estimates $\theta$ based on the quantity $\phi$, as though $\phi$ were known. We then produce an estimate of $\phi$ and implement the update law based on this estimate instead of the real perturbation.

### 5.3.1 Estimation of $\theta$ from $\phi$

We denote by $\hat{\phi}$ the estimate of the perturbation $\phi$. We shall later explain how to construct this estimate; for now, we concentrate on how to find $\theta$ in the hypothetical case of a perfect perturbation estimate. For this to work, there needs to exist an update law

$$\dot{\hat{\theta}} = u_\theta(t,x,\hat{\phi},\hat{\theta}), \tag{5.2}$$

which, if $\hat{\phi} = \phi$, would provide an unbiased asymptotic estimate of $\theta$. This is the subject of the following assumption on the dynamics of the error variable $\tilde{\theta} := \theta - \hat{\theta}$.

**Assumption 5.1.** *For each compact set $K \subset \mathbb{R}^n$, there exist a differentiable function $V_u\colon \mathbb{R}_{\geq 0} \times (\Theta - \Theta) \to \mathbb{R}_{\geq 0}$; positive constants $a_1$, $a_2$ and $a_4$; and a continuous function $a_3\colon \mathbb{R}^n \to \mathbb{R}_{\geq 0}$ that is positive outside the origin, such that, for all $(t,x,\phi,\hat{\theta}) \in \mathbb{R}_{\geq 0} \times K \times \mathbb{R}^n \times \Theta$,*

$$a_1\|\tilde{\theta}\|^2 \leq V_u(t,\tilde{\theta}) \leq a_2\|\tilde{\theta}\|^2, \tag{5.3}$$

$$\frac{\partial V_u}{\partial t}(t,\tilde{\theta}) - \frac{\partial V_u}{\partial \tilde{\theta}}(t,\tilde{\theta})u_\theta(t,x,\phi,\hat{\theta}) \leq -a_3(x)\|\tilde{\theta}\|^2, \tag{5.4}$$

$$\left\| \frac{\partial V_u}{\partial \tilde{\theta}}(t,\tilde{\theta}) \right\| \leq a_4\|\tilde{\theta}\|. \tag{5.5}$$

*Furthermore, the update law* (5.2) *ensures that, if $\hat{\theta}(t_0) \in \Theta$, then, for all $t \geq t_0$, $\hat{\theta}(t) \in \Theta$.*

Satisfying Assumption 5.1 constitutes the greatest challenge in applying the method in this paper, and this is therefore discussed in detail in the next section.

### 5.3.2 Satisfying Assumption 5.1

We shall focus mostly on the case when Assumption 5.1 can be satisfied with $a_3(x) \geq a_3^* > 0$. This guarantees that the origin of the error dynamics $\dot{\tilde{\theta}} = -u_\theta(t, x, \phi, \theta - \tilde{\theta})$, which occurs if $\hat{\phi} = \phi$, is uniformly exponentially stable with $(\Theta - \Theta)$ contained in the region of attraction. Essentially this amounts to asymptotically solving the inversion problem of finding $\theta$ given $\phi = B(t, x)g(t, x, \theta)$. In the following, we shall discuss some possibilities for how to satisfy Assumption 5.1. As a useful reference, we point to Nicosia, Tornambè, and Valigi (1994), which deals with the use of state observers for inversion of nonlinear maps.

The most obvious way to satisfy Assumption 5.1 is to invert the equality $\phi = B(t, x)g(t, x, \theta)$ algebraically, and to let $\hat{\theta}$ be attracted to this solution.

**Proposition 5.1.** *Suppose that, for all $(t, x) \in \mathbb{R}_{\geq 0} \times \mathbb{R}^n$, we can find a unique solution for $\theta$ from the equation $\phi = B(t, x)g(t, x, \theta)$. Then Assumption* 5.1 *is satisfied with $a_3(x) \geq a_3^* > 0$ by using the update law $u_\theta(t, x, \hat{\phi}, \hat{\theta}) = \mathrm{Proj}(\Gamma(\theta^*(t, x, \hat{\phi}) - \hat{\theta}))$, where $\theta^*(t, x, \hat{\phi})$ denotes the solution of the inversion problem found from $\hat{\phi}$, and $\Gamma$ is a symmetric positive-definite gain matrix.*

*Proof.* The proof follows from using the function $V_u(t, \tilde{\theta}) = \frac{1}{2}\tilde{\theta}^\mathsf{T}\Gamma^{-1}\tilde{\theta}$ when $\hat{\phi} = \phi$, and the property (Krstić et al., 1995, Lemma E.1) that $-\tilde{\theta}^\mathsf{T}\Gamma^{-1}\mathrm{Proj}(\tau) \leq -\tilde{\theta}^\mathsf{T}\Gamma^{-1}\tau$. From the proof of Krstić et al. (1995, Lemma E.1), we find that, if $\hat{\theta}(t_0) \in \Theta$, then the solution $\hat{\theta}(t)$ remains in $\Theta$. □

**Example 5.1.** Consider the perturbation $B(t, x)g(t, x, \theta) = h((2 + \sin(t))\theta)$, where $h$ is some explicitly invertible, nonlinear mapping. For each $t \in \mathbb{R}_{\geq 0}$, we can solve the inversion problem and find $\theta^*(t, x, \hat{\phi}) = h^{-1}(\hat{\phi})/(2 + \sin(t))$.

Often it is only possible to invert the equation $\phi = B(t, x)g(t, x, \theta)$ part of the time. In this case, Assumption 5.1 may still be satisfied if solutions are available with a certain regularity. The following proposition deals with this case.

**Proposition 5.2.** *Suppose that there exists a known, piecewise continuous function $l: \mathbb{R}_{\geq 0} \times \mathbb{R}^n \to [0, 1]$,[1] and that, for all $(t, x) \in \mathbb{R}_{\geq 0} \times \mathbb{R}^n$, $l(t, x) > 0$ implies that we can find a unique solution for $\theta$ from the equation $\phi = B(t, x)g(t, x, \theta)$. Suppose furthermore that there exist $T > 0$ and $\varepsilon > 0$ such that, for all $t \in \mathbb{R}_{\geq 0}$, $\int_t^{t+T} l(\tau, x(\tau))\,\mathrm{d}\tau \geq \varepsilon$. Then Assumption* 5.1 *is satisfied with $a_3(x) \geq a_3^* > 0$*

[1] *Remark added after publication:* The concept of piecewise continuity is not precisely defined for functions on multivariable domains. For technical correctness, it should instead be understood that the function $t \mapsto l(t, x(t))$ is piecewise continuous. See also footnote in the proof in Appendix 5.B.

*by using the update law* $u_\theta(t,x,\hat{\phi},\hat{\theta}) = \mathrm{Proj}(l(t,x)\Gamma(\theta^*(t,x,\hat{\phi}) - \hat{\theta}))$*, where* $\theta^*(t,x,\hat{\phi})$ *denotes the solution of the inversion problem found from* $\hat{\phi}$ *whenever* $l(t,x) > 0$*, and* $\Gamma$ *is a symmetric positive-definite gain matrix.*

*Proof.* See Appendix 5.B. □

**Example 5.2.** Consider the perturbation $B(t,x)g(t,x,\theta) = h(\sin(t)\theta)$, where $h$ is some explicitly invertible, nonlinear mapping. The inversion problem is poorly conditioned when $\sin(t)$ is close to zero, and unsolvable for $\sin(t) = 0$. Proposition 5.2 nevertheless applies by letting, for example, $l(t,x) = 0$ when $|\sin(t)| < \varepsilon$ and $l(t,x) = 1$ when $|\sin(t)| \geq \varepsilon$, where $0 < \varepsilon < 1$.

When it is not possible or desirable to solve the inversion problem explicitly, it is often possible to implement the update function as a numerical search for the solutions.

**Proposition 5.3.** *Suppose that there exist a symmetric positive-definite matrix* $P$ *and a function* $M\colon \mathbb{R}_{\geq 0} \times \mathbb{R}^n \times \Theta \to \mathbb{R}^{p\times n}$ *such that, for all* $(t,x) \in \mathbb{R}_{\geq 0} \times \mathbb{R}^n$*, and for all pairs* $\theta_1, \theta_2 \in \Theta$*,*

$$M(t,x,\theta_1)B(t,x)\frac{\partial g}{\partial \theta}(t,x,\theta_2) + \frac{\partial g}{\partial \theta}^{\mathsf{T}}(t,x,\theta_2)B^{\mathsf{T}}(t,x)M^{\mathsf{T}}(t,x,\theta_1) \geq 2P. \quad (5.6)$$

*Then Assumption* 5.1 *is satisfied with* $a_3(x) \geq a_3^* > 0$ *by using the update law* $u_\theta(t,x,\hat{\phi},\hat{\theta}) = \mathrm{Proj}(\Gamma M(t,x,\hat{\theta})(\hat{\phi} - B(t,x)g(t,x,\hat{\theta})))$*, where* $\Gamma$ *is a symmetric positive-definite gain matrix.*

*Proof.* See Appendix 5.B. □

**Example 5.3.** Consider the perturbation $B(t,x)g(t,x,\theta) = g(\theta) = [\theta_1, \theta_1^2 + \theta_2]^{\mathsf{T}}$. Selecting $M(t,x,\hat{\theta}) = M = \mathrm{diag}(K_M, 1)$ yields

$$M\frac{\partial g}{\partial \theta}(\theta) + \frac{\partial g}{\partial \theta}^{\mathsf{T}}(\theta)M^{\mathsf{T}} = 2\begin{bmatrix} K_M & \theta_1 \\ \theta_1 & 1 \end{bmatrix}.$$

Using the fact that $\theta_1$ is bounded within $\Theta$, it is easily confirmed that, if $K_M$ is chosen sufficiently large, then $M[\partial g/\partial\theta](\theta) + [\partial g/\partial\theta]^{\mathsf{T}}(\theta)M^{\mathsf{T}} \geq 2P$, where $P$ is symmetric positive definite.

Proposition 5.3 applies to certain monotonic perturbations for which a solution can be found arbitrarily fast by increasing the gain $\Gamma$. In many cases, this is not possible, because the inversion problem is singular the whole time or part of the time. The following proposition applies to cases where a solution is only available by using data over longer periods of time, by incorporating a persistency-of-excitation condition.

**Proposition 5.4.** *Suppose that there exist a piecewise continuous function*

$$S: \mathbb{R}_{\geq 0} \times \mathbb{R}^n \to \mathbb{S}_{p+},$$

*where $\mathbb{S}_{p+}$ is the cone of $p \times p$ symmetric positive-semidefinite matrices,*[2] *and a function $M: \mathbb{R}_{\geq 0} \times \mathbb{R}^n \times \Theta \to \mathbb{R}^{p \times n}$, both bounded for bounded $x$, such that, for all $(t, x) \in \mathbb{R}_{\geq 0} \times \mathbb{R}^n$, and for all pairs $\theta_1, \theta_2 \in \Theta$,*

$$M(t,x,\theta_1)B(t,x)\frac{\partial g}{\partial \theta}(t,x,\theta_2) + \frac{\partial g}{\partial \theta}^{\mathsf{T}}(t,x,\theta_2)B^{\mathsf{T}}(t,x)M^{\mathsf{T}}(t,x,\theta_1) \geq 2S(t,x). \quad (5.7)$$

*Suppose furthermore that there exist numbers $T > 0$ and $\varepsilon > 0$ such that, for all $t \in \mathbb{R}_{\geq 0}$, $\int_t^{t+T} S(\tau, x(\tau))\,\mathrm{d}\tau \geq \varepsilon I$, and that, for all $(t, x, \hat{\theta}) \in \mathbb{R}_{\geq 0} \times \mathbb{R}^n \times \Theta$, $\|B(t,x)(g(t,x,\theta) - g(t,x,\hat{\theta}))\| \leq L_g(\tilde{\theta}^{\mathsf{T}} S(t,x)\tilde{\theta})^{1/2}$, for some $L_g > 0$. Then Assumption 5.1 is satisfied with $a_3(x) \geq a_3^* > 0$ by using the update law $u_\theta(t, x, \hat{\phi}, \hat{\theta}) = \mathrm{Proj}(\Gamma M(t,x,\hat{\theta})(\hat{\phi} - B(t,x)g(t,x,\hat{\theta})))$, where $\Gamma$ is a symmetric positive-definite gain matrix.*

*Proof.* See Appendix 5.B. □

**Example 5.4.** Consider the perturbation from Example 5.3 multiplied by $\sin(t)$; that is, $B(t,x)g(t,x,\theta) = g(t,\theta) = \sin(t)[\theta_1, \theta_1^2 + \theta_2]^{\mathsf{T}}$. Using the same argument as in Example 5.3, we may choose $M(t,x,\hat{\theta}) = M(t) = \sin(t)\mathrm{diag}(K_M, 1)$ to satisfy (5.7). We then have $S(t,x) = S(t) = \sin^2(t)P$, where $P$ is the positive-definite matrix from Example 5.3. For any $T > 0$ there is an $\varepsilon > 0$ such that $\int_t^{t+T} P \sin^2(\tau)\,\mathrm{d}\tau \geq \varepsilon I$ for all $t \in \mathbb{R}_{\geq 0}$, which means that the integral condition in Proposition 5.4 is satisfied. Finally, we have $\|g(t,\theta) - g(t,\hat{\theta})\| \leq L_g(\tilde{\theta}^{\mathsf{T}} S(t)\tilde{\theta})^{1/2}$, where

$$L_g = \max_{(t,\theta)\in\mathbb{R}_{\geq 0}\times\Theta} \|[\partial g/\partial\theta](t,\theta)\|/\lambda_{\min}(P)^{1/2}.$$

Hence, Proposition 5.4 applies.

*Remark* 5.1. When looking for the function $M$, a good starting point is

$$M(t,x,\hat{\theta}) = \frac{\partial g}{\partial \theta}^{\mathsf{T}}(t,x,\hat{\theta})B^{\mathsf{T}}(t,x).$$

[2] *Remark added after publication:* Similar to the footnote on page 126, it should here be understood that each scalar element of the function $t \mapsto S(t, x(t))$ is piecewise continuous.

This choice makes the parameter update law into a gradient search in the direction of steepest descent for the function $\|B(t,x)(g(t,x,\theta) - g(t,x,\hat{\theta}))\|^2$, scaled by the gain $\Gamma$. Indeed, this choice of $M$ often works even if it fails to satisfy either of Propositions 5.3 or 5.4. In the special case where the perturbation is linear in the unknown parameters, this choice of $M$ always satisfies (5.7), and the remaining conditions in Proposition 5.4 coincide with standard persistency-of-excitation conditions for parameter identification in linear adaptive theory (see, e.g., Marino and Tomei, 1995, Ch. 5). Future research will include investigation of more systematic ways of finding the function $M$ for nonlinear parameterizations.

We end this section with an example illustrating that the above approaches may be combined.

**Example 5.5.** Consider the perturbation

$$B(t,x)g(t,x,\theta) = \begin{bmatrix} \theta_1^{1/3} \\ \sin(\theta_1 a(t))\theta_2 \end{bmatrix}$$

with $\theta$ known to be bounded and $\theta_1$ known to be bounded away from zero, and where $a(t)$ is some persistently excited signal with a bounded derivative. Clearly, we can find $\theta_1$ by inversion, simply taking $\theta_1^*(\hat{\phi}) = \hat{\phi}_1^3$. Hence, $\theta_1$ is handled according to Proposition 5.1. When $\theta_1$ is known, we can find $\theta_2$ by numerical search according to Proposition 5.4. We therefore implement the second part of the update law according to Proposition 5.4, substituting $\theta_1$ with $\hat{\phi}^3$, which results in $u_\theta(t,x,\hat{\phi},\hat{\theta}) = \text{Proj}(\Gamma[\hat{\phi}_1^3 - \hat{\theta}_1, \sin(\hat{\phi}_1^3 a(t))(\hat{\phi}_2 - \sin(\hat{\phi}_1^3 a(t))\hat{\theta}_2)]^\mathsf{T})$.

### 5.3.3 Estimator

We now introduce the full estimator:

$$\dot{z} = -K_\phi\big(f(t,x) + B(t,x)v(t,x) + \hat{\phi}\big) \tag{5.8a}$$

$$\quad - B(t,x)\frac{\partial g}{\partial \theta}(t,x,\hat{\theta})u_\theta(t,x,\hat{\phi},\hat{\theta}), \tag{5.8b}$$

$$\hat{\phi} = z + K_\phi x + B(t,x)g(t,x,\hat{\theta}), \tag{5.8c}$$

$$\dot{\hat{\theta}} = u_\theta(t,x,\hat{\phi},\hat{\theta}), \tag{5.8d}$$

where $K_\phi$ is a symmetric positive-definite gain matrix. The full estimator consists of two parts: an estimator for $\phi$, described by (5.8b), (5.8c), and the update law from Section 5.3.1. To study the properties of the estimator, we consider the dynamics of the errors $\tilde{\phi}$ and $\tilde{\theta}$. Taking the time derivative of $\tilde{\phi} = \phi - \hat{\phi}$, we may

write

$$\begin{aligned}\dot{\hat{\phi}} &= K_\phi\big(f(t,x) + B(t,x)v(t,x) + \hat{\phi}\big) \\ &\quad + B(t,x)\frac{\partial g}{\partial \theta}(t,x,\hat{\theta})u_\theta(t,x,\hat{\phi},\hat{\theta}) - K_\phi \dot{x} \\ &\quad - B(t,x)\frac{\partial g}{\partial \theta}(t,x,\hat{\theta})u_\theta(t,x,\hat{\phi},\hat{\theta}) + d(t,x,\tilde{\theta}),\end{aligned} \tag{5.9}$$

where

$$\begin{aligned}d(t,x,\tilde{\theta}) := \frac{\partial}{\partial t}\big(B(t,x)(g(t,x,\theta) - g(t,x,\hat{\theta}))\big) \\ + \frac{\partial}{\partial x}\big(B(t,x)(g(t,x,\theta) - g(t,x,\hat{\theta}))\big)\dot{x}.\end{aligned} \tag{5.10}$$

The function $d(t,x,\tilde{\theta})$ can be seen as the time derivative of $B(t,x)(g(t,x,\theta) - g(t,x,\hat{\theta}))$ when $\hat{\theta}$ is kept constant. Using the expression

$$\dot{x} - f(t,x) - B(t,x)v(t,x) = \phi,$$

we may rewrite the above expression and write the error dynamics of the estimator as

$$\dot{\tilde{\phi}} = -K_\phi\tilde{\phi} + d(t,x,\tilde{\theta}), \tag{5.11a}$$

$$\dot{\tilde{\theta}} = -u_\theta(t,x,\phi,\hat{\theta}) + \big(u_\theta(t,x,\phi,\hat{\theta}) - u_\theta(t,x,\hat{\phi},\hat{\theta})\big). \tag{5.11b}$$

For convenience, we define the error variable $\xi := [\tilde{\phi}^\mathsf{T}, \tilde{\theta}^\mathsf{T}]^\mathsf{T}$ and the set $\Xi := \mathbb{R}^n \times (\Theta - \Theta)$.

**Assumption 5.2.** *For all $(t,x,\tilde{\theta}) \in \mathbb{R}_{\geq 0} \times \mathbb{R}^n \times (\Theta - \Theta)$, the function $d(t,x,\tilde{\theta})$ is well defined; for each compact set $K \subset \mathbb{R}^n$, there exist continuous functions $L_1(x) > 0$ and $L_2(x) > 0$ such that, for all $(t,x,\tilde{\theta}) \in \mathbb{R}_{\geq 0} \times K \times (\Theta - \Theta)$, $\|d(t,x,\tilde{\theta})\| \leq L_1(x)\|\tilde{\theta}\|$; and for all $(t,x,\phi,\hat{\phi},\hat{\theta}) \in \mathbb{R}_{\geq 0} \times K \times \mathbb{R}^n \times \mathbb{R}^n \times \Theta$, $\|u_\theta(t,x,\phi,\hat{\theta}) - u_\theta(t,x,\hat{\phi},\hat{\theta})\| \leq L_2(x)\|\tilde{\phi}\|$.*

*Remark* 5.2. When checking the condition $\|u_\theta(t,x,\phi,\hat{\theta}) - u_\theta(t,x,\hat{\phi},\hat{\theta})\| \leq L_2(x)\|\tilde{\phi}\|$, the projection in the update law can be disregarded, because the property is retained under projection (see Appendix 5.A.1).

The Lipschitz-type conditions in Assumption 5.2 may appear difficult to satisfy. Note, however, that $\tilde{\theta} \in (\Theta - \Theta)$, which means that we are dealing with a local Lipschitz condition for $d$. For $u_\theta$, we need to satisfy a global condition in the sense that $\phi$ and $\hat{\phi}$ are not presumed bounded. Indeed, such a condition may

often fail to hold, as demonstrated by Example 5.5, where the term $\hat{\phi}_1^3$ is used. In most cases, however, the perturbation $\phi$ depends on physical quantities with known bounds, and from these a bound on $\phi$ can often be found. It is then possible to modify $u_\theta$ to include a saturation of $\hat{\phi}$, thereby reducing the requirement to a local condition that is much more easily satisfied. With the inclusion of a saturation, Example 5.5 does satisfy Assumption 5.2. If a particular update law is modified by including a saturation, it does not affect the validity of conditions (5.3)–(5.5) in Assumption 5.1, since the saturation has no effect when $\hat{\phi} = \phi$.

**Theorem 5.1.** *Suppose that Assumptions* 5.1 *and* 5.2 *hold with* $a_3(x) \geq a_3^* > 0$ *and that, for all* $t \in \mathbb{R}_{\geq 0}$, $\|x(t)\|$ *is uniformly bounded. Then there exists* $k_\phi > 0$ *such that, if* $K_\phi$ *is chosen such that* $\lambda_{\min}(K_\phi) > k_\phi$, *then the origin of* (5.11) *is uniformly exponentially stable with* $\Xi$ *contained in the region of attraction.*

*Proof.* By assumption, $x(t) \in K$, where $K \subset \mathbb{R}^n$ is a compact set. We can therefore make use of Assumptions 5.1 and 5.2 for this particular $K$. Boundedness of $x$ ensures that $\phi$ is well defined for all times. By Assumption 5.1, $\hat{\theta}(t_0) \in \Theta$ implies that the solution $\hat{\theta}(t)$ cannot escape $\Theta$, and hence $\tilde{\theta}(t)$ cannot escape $(\Theta - \Theta)$. From (5.11a) and the expression $\|d(t, x, \tilde{\theta})\| \leq L_1^* \|\tilde{\theta}\|$, where $L_1^*$ is a bound on $L_1(x)$ on $K$, it is therefore easily seen that $\tilde{\phi}$ remains bounded. Thus, if $\xi(t_0) \in \Xi$, then, for all $t \geq t_0$, $\xi(t)$ is uniquely defined and remains in a compact subset of $\Xi$. We define the function $V_{\mathrm{p}}(t, \xi) = V_{\mathrm{u}}(t, \tilde{\theta}) + \frac{1}{2}\tilde{\phi}^{\mathsf{T}}\tilde{\phi}$ and investigate its time derivative on the set $\Xi$ along the trajectories of (5.11):

$$\begin{aligned} \dot{V}_{\mathrm{p}}(t, \xi) = {} & \frac{\partial V_{\mathrm{u}}}{\partial t}(t, \tilde{\theta}) - \frac{\partial V_{\mathrm{u}}}{\partial \tilde{\theta}}(t, \tilde{\theta}) u_\theta(t, x, \phi, \hat{\theta}) \\ & + \frac{\partial V_{\mathrm{u}}}{\partial \tilde{\theta}}(t, \tilde{\theta}) \big( u_\theta(t, x, \phi, \hat{\theta}) - u_\theta(t, x, \hat{\phi}, \hat{\theta}) \big) \\ & - \tilde{\phi}^{\mathsf{T}} K_\phi \tilde{\phi} + \tilde{\phi}^{\mathsf{T}} d(t, x, \tilde{\theta}). \end{aligned} \tag{5.12}$$

From the inequalities in Assumptions 5.1 and 5.2,

$$\begin{aligned} \dot{V}_{\mathrm{p}}(t, \xi) \leq {} & -a_3(x)\|\tilde{\theta}\|^2 - \lambda_{\min}(K_\phi)\|\tilde{\phi}\|^2 + \|\tilde{\phi}\| \|d(t, x, \tilde{\theta})\| \\ & + \left\| \frac{\partial V_{\mathrm{u}}}{\partial \tilde{\theta}}(t, \tilde{\theta}) \right\| \|u_\theta(t, x, \phi, \hat{\theta}) - u_\theta(t, x, \hat{\phi}, \hat{\theta})\|. \end{aligned} \tag{5.13}$$

This expression can be rewritten as $\dot{V}_{\mathrm{p}}(t, \xi) \leq -\zeta^{\mathsf{T}} Q(x) \zeta$, where $\zeta = [\|\tilde{\phi}\|, \|\tilde{\theta}\|]^{\mathsf{T}}$ and

$$Q(x) = \begin{bmatrix} \lambda_{\min}(K_\phi) & -\frac{1}{2}(a_4 L_2(x) + L_1(x)) \\ -\frac{1}{2}(a_4 L_2(x) + L_1(x)) & a_3(x) \end{bmatrix}. \tag{5.14}$$

To check for positive-definiteness of $Q(x)$, we note that its first-order leading principal minor is $\lambda_{\min}(K_\phi) > 0$. The second-order leading principal minor

is $a_3(x)\lambda_{\min}(K_\phi) - \frac{1}{4}(a_4 L_2(x) + L_1(x))^2$, which is positive if $\lambda_{\min}(K_\phi) > k_\phi := (a_4 L_2^* + L_1^*)^2/(4a_3^*)$, where $L_2^*$ is a bound on $L_2(x)$ on $K$. Hence, we have on $\Xi$ that $\dot{V}_{\mathrm{p}}(t,\xi(t)) \leq -\lambda_{\min}(Q(x))\|\xi(t)\|^2$. Moreover, we have that $V_{\mathrm{p}}(t,\xi) \leq \max\{a_2, \frac{1}{2}\}\|\xi\|^2$. From the preceding two expressions, we have that $\dot{V}_{\mathrm{p}}(t,\xi(t)) \leq -2\lambda V_{\mathrm{p}}(t,\xi(t))$, where $\lambda := \min_{x\in K} \lambda_{\min}(Q(x))/\max\{2a_2, 1\}$. By the comparison lemma (Khalil, 2002, Lemma 3.4), we therefore have $V_{\mathrm{p}}(t,\xi(t)) \leq V_{\mathrm{p}}(t_0,\xi(t_0))\exp(-2\lambda(t-t_0))$. This leads to $\|\xi(t)\| \leq k_{\mathrm{e}}\|\xi(t_0)\|\exp(-\lambda(t-t_0))$, where $k_{\mathrm{e}} = (\max\{a_2, \frac{1}{2}\}/\min\{a_1, \frac{1}{2}\})^{1/2}$. □

*Remark* 5.3. We assume in Theorem 5.1 that the state $x$ is uniformly bounded. In pure estimation problems, where no control is implemented based on the parameter estimates, this is usually a reasonable assumption, because the states involved are typically derived from bounded physical quantities.

## 5.4 Closed-Loop Compensation

We now consider how the parameter estimates can be used to compensate for the perturbation in (5.1). Suppose that the control inputs available in the original system can be chosen to yield a system on the following form:

$$\dot{x} = f(t,x) + B(t,x)\big(g(t,x,\theta) - g(t,x,\hat{\theta})\big). \tag{5.15}$$

Here, $v(t,x)$ in (5.1) has been substituted with the control $-g(t,x,\hat{\theta})$.

**Assumption 5.3.** *The function $f(t,x)$ is continuously differentiable on $\mathbb{R}_{\geq 0}\times\mathbb{R}^n$; the origin of the nominal system $\dot{x} = f(t,x)$ is uniformly globally asymptotically stable* (UGAS)*; for any trajectory $\hat{\theta}(t) \in \Theta$, the solutions $x(t)$ of the perturbed system* (5.15) *are uniformly globally bounded* (UGB)*; and for each compact set $K \subset \mathbb{R}^n$ there exists a class $\mathcal{K}$ function $\gamma$ such that, for all $(t,x,\hat{\theta}) \in \mathbb{R}_{\geq 0}\times K\times\Theta$, $\|B(t,x)(g(t,x,\theta) - g(t,x,\hat{\theta}))\| \leq \gamma(\|\tilde{\theta}\|)$.*

In Assumption 5.3, we assume that $f(t,x)$ is a stabilizing function that ensures UGB irrespective of the parameter estimate. In this case, the only control needed is a term $-g(t,x,\hat{\theta})$ to cancel the perturbation, as seen in (5.15). Essentially, the UGB assumption means that a parameter error confined to $(\Theta - \Theta)$ cannot make the states of the system arbitrarily large compared to their initial values. In many cases, this assumption is not automatically satisfied, and one may need to apply additional control to shape $f(t,x)$. The assumption is most easily satisfied if the asymptotic growth rate of $f(t,x)$ with respect to $x$ is greater than the asymptotic growth rate of the error term $B(t,x)(g(t,x,\theta) - g(t,x,\hat{\theta}))$. To ensure this, one may introduce control in the form of nonlinear damping with a sufficiently high

growth rate, similar to the technique used in adaptive backstepping (Krstić et al., 1995). We also refer to Panteley and Loría (2001) for an extensive discussion on how to ensure UGB. Note that controllability of the system depends on the properties of $f(t,x)$ and $B(t,x)$.

**Theorem 5.2.** *Suppose that Assumptions* 5.1–5.3 *hold such that* $a_3(x) \geq a_3^* > 0$. *Then for each compact neighborhood* $K' \subset \mathbb{R}^{2n}$ *of the origin, there exists* $k_\phi > 0$ *such that, if* $K_\phi$ *is chosen such that* $\lambda_{\min}(K_\phi) > k_\phi$, *then the origin of* (5.15), (5.11) *is uniformly asymptotically stable with* $K' \times (\Theta - \Theta)$ *contained in the region of attraction.*

*Proof.* This proof is based on the proof of Panteley and Loría (2001, Lemma 2). The UGAS property of the unperturbed system, together with the fact that $f(t,x)$ is locally Lipschitz continuous in $x$, uniformly in $t$, and continuously differentiable on $\mathbb{R}_{\geq 0} \times \mathbb{R}^n$, implies by Panteley and Loría (2001, Prop. 1) the existence of a Lyapunov function $V_x(t,x)$; class $\mathcal{K}_\infty$ functions $\alpha_1$ and $\alpha_2$; and a class $\mathcal{K}$ function $\alpha_4$ such that, for all $(t,x) \in \mathbb{R}_{\geq 0} \times \mathbb{R}^n$,

$$\alpha_1(\|x\|) \leq V_x(t,x) \leq \alpha_2(\|x\|), \tag{5.16}$$

$$\frac{\partial V_x}{\partial t}(t,x) + \frac{\partial V_x}{\partial x}(t,x) f(t,x) \leq -V_x(t,x), \tag{5.17}$$

$$\left\| \frac{\partial V_x}{\partial x}(t,x) \right\| \leq \alpha_4(\|x\|). \tag{5.18}$$

As before, we know that $\hat{\theta}(t_0) \in \Theta$ implies that $\hat{\theta}(t)$ remains in $\Theta$. Let $R > 0$ be chosen large enough that $\Omega := \{(x,\xi) \mid \|(x,\xi)\| \leq R\} \supset K' \times (\Theta - \Theta)$. For any $0 < r \leq R$, we know that if $\|(x(t_0), \xi(t_0))\| \leq r$, then $\|x(t_0)\| \leq r$, which by the UGB property from Assumption 5.3 implies that there exists a $c_x(r) > 0$ such that, for all $t \geq t_0$, $\|x(t)\| \leq c_x(r)$. It follows that, for all $(x(t_0), \xi(t_0)) \in \Omega$ such that $\xi(t_0) \in \Xi$, $x(t)$ is restricted to some compact set $K$. Let therefore $\lambda_{\min}(K_\phi)$ be chosen large enough to ensure exponential stability of the estimator according to Theorem 5.1 based on the set $K$. Then we know that $\|\xi(t)\| \leq k_e \|\xi(t_0)\| \exp(-\lambda(t - t_0))$. This implies that, if $\|(x(t_0), \xi(t_0))\| \leq r$ and $\xi(t_0) \in \Xi$, then $\|(x(t), \xi(t))\| \leq c(r)$, where $c(r) := (c_x^2(r) + (k_e r)^2)^{1/2}$.

Define $v_x(t) = V_x(t, x(t))$. We then have $\dot{v}_x(t) \leq -v_x(t) + \alpha_4(c(r))\beta(r, t - t_0)$, where $\beta(r, t - t_0) := \gamma(k_e r \exp(-\lambda(t - t_0)))$ is a class $\mathcal{KL}$ function by Khalil (2002, Lemma 4.2). Let $\tau_0 \geq t_0$. Multiplying by $\exp(t - \tau_0)$ on both sides and rearranging, we have, for all $t \geq \tau_0$, $\frac{\mathrm{d}}{\mathrm{d}t}(v_x(t)\exp(t - \tau_0)) \leq \alpha_4(c(r))\beta(r, t - t_0)\exp(t - \tau_0)$. Integrating from $\tau_0$ to $t$ on both sides and multiplying by $\exp(-(t - \tau_0))$, we have $v_x(t) \leq v_x(\tau_0)\exp(-(t - \tau_0)) + \alpha_4(c(r)) \int_{\tau_0}^{t} \exp(-(t - s))\beta(r, s - t_0)\,\mathrm{d}s$, which means that replacing $\tau_0$ with $t_0$ in the above expression yields, for

all $t \geq t_0$, $v_x(t) \leq v_x(t_0)\exp(-(t-t_0)) + \alpha_4(c(r))\beta(r,0)\int_{t_0}^{t}\exp(-(t-s))\,\mathrm{d}s \leq v_x(t_0) + \alpha_4(c(r))\beta(r,0)(1-\exp(-(t-t_0))) \leq \gamma'(r)$, where $\gamma'(r) := \alpha_2(r) + \alpha_4(c(r))\beta(r,0)$. Hence, $\|x(t)\| \leq \alpha_1^{-1}(\gamma'(r))$, and $\alpha_1^{-1} \circ \gamma'$ is a class $\mathcal{K}_\infty$ function by Khalil (2002, Lemma 4.2). Furthermore, we have, for $\|(x(t_0), \xi(t_0))\| \leq r$ and $\xi(t_0) \in \Xi$, $\|(x(t), \xi(t))\| \leq \gamma''(r)$, where $\gamma''(r) := ((\alpha_1^{-1}(\gamma'(r)))^2 + (k_e r)^2)^{1/2}$ is a class $\mathcal{K}_\infty$ function. Let $c \leq R$ be sufficiently small such that $\|\xi\| \leq c \implies \xi \in \Xi$. By the above, we have that, for all $\|(x(t_0), \xi(t_0))\| \leq r < c$ and for all $t \geq t_0$, $\|(x(t), \xi(t))\| \leq \gamma''(r)$, which means that the origin of (5.15), (5.11) is uniformly stable.

For some $\varepsilon_1 > 0$, define $T_1$ large enough that $\alpha_4(c(r))\beta(r, T_1) \leq \frac{1}{2}\varepsilon_1$. Substituting $\tau_0 = t_0 + T_1$ into the earlier bound on $v_x(t)$, we obtain that, $\forall t \geq t_0 + T_1$,

$$\begin{aligned} v_x(t) &\leq v_x(t_0 + T_1)\mathrm{e}^{-(t-t_0-T_1)} \\ &\quad + \alpha_4(c(r))\int_{t_0+T_1}^{t}\beta(r, s-t_0)\mathrm{e}^{-(t-s)}\,\mathrm{d}s \\ &\leq \gamma'(r)\mathrm{e}^{-(t-t_0-T_1)} + \frac{\varepsilon_1}{2}. \end{aligned} \tag{5.19}$$

Now let $T_2 \geq T_1$ be chosen large enough that $\gamma'(r)\exp(-(T_2 - T_1)) \leq \frac{1}{2}\varepsilon_1$. Then we have, for all $t \geq t_0 + T_2$, $v_x(t) \leq \gamma'(r)\exp(-(T_2 - T_1)) + \frac{1}{2}\varepsilon_1 \leq \varepsilon_1$. Hence, for all $t \geq t_0 + T_2$, $\|x(t)\| \leq \alpha_1^{-1}(\varepsilon_1)$. Define $\varepsilon$ such that $\varepsilon_1 = \alpha_1(\varepsilon/\sqrt{2})$ and let $T \geq T_2$ be large enough that $k_e r\exp(-\lambda T) \leq \varepsilon/\sqrt{2}$. Then $\forall t \geq t_0 + T$, $\|(x(t), \xi(t))\| \leq (\frac{1}{2}\varepsilon^2 + \frac{1}{2}\varepsilon^2)^{1/2} = \varepsilon$. Since $\varepsilon$ can be chosen arbitrarily small, and the above holds for all initial conditions such that $(x(t_0), \xi(t_0)) \in \Omega$ and $\xi(t_0) \in \Xi$, it follows that the whole system (5.15), (5.11) is uniformly asymptotically stable with $K' \times (\Theta - \Theta)$ contained in the region of attraction. □

*Remark* 5.4. Theorems 5.1 and 5.2 are intended to show that particular stability properties are guaranteed by choosing the gain $K_\phi$ sufficiently high; they are not intended as a practical guide to tuning the estimator gains. Attempting to find a numerical value for $k_\phi$, the lower bound on the eigenvalues of $K_\phi$, is likely to be complicated and of little practical use, owing to the conservative nature of Lyapunov-type analysis. In practical implementations, the gains are normally found through a tuning procedure involving simulations or tests with the actual system.

### 5.4.1 Vanishing Excitation at $x = 0$

So far we have only considered perturbations that are persistently excited in the sense that $\theta$ can always be estimated from $\phi$ with exponential convergence rate.

This strict requirement excludes a class of perturbations where we have persistent excitations as long as the controlled state $x$ is bounded away from the origin, but where the excitation is lost at the origin. Most importantly, this includes all perturbations that vanish for $x = 0$. As an example, consider the system $\dot{x} = -x + \arctan(\theta x) - \arctan(\hat{\theta} x)$. In the following theorem, we show that, under certain conditions, convergence of the controlled state to the origin is guaranteed even when excitation is lost at the origin.

**Theorem 5.3.** *Suppose that Assumptions* 5.1–5.3 *hold such that*

$$(L_1(x) + L_2(x))^2 \leq \rho a_3(x)$$

*for some number $\rho > 0$, locally around the origin. Then, for each compact neighborhood $K' \subset \mathbb{R}^{2n}$ of the origin, there exists $k_\phi > 0$ such that, if $K_\phi$ is chosen such that $\lambda_{\min}(K_\phi) > k_\phi$ and the trajectory of* (5.15), (5.11) *originates in $K' \times (\Theta - \Theta)$, then $\lim_{t\to\infty} x(t) = 0$ and $\xi(t)$ is bounded.*

*Proof.* As in the proof of Theorem 5.2, the UGB condition in Assumption 5.3 ensures that, for trajectories originating in $K' \times (\Theta - \Theta)$, the state $x(t)$ remains in a compact set $K$. To investigate what happens to the estimator, we follow the proof of Theorem 5.1, where we find that we have the requirement $a_3(x)\lambda_{\min}(K_\phi) > \frac{1}{4}(a_4 L_2(x) + L_1(x))^2$. Because $L_1(x)$ and $L_2(x)$ are bounded on any compact set, and due to the local condition around $x = 0$ in Theorem 5.3, the inequality can be satisfied outside the origin for $\lambda_{\min}(K_\phi) > k_\phi$, for some $k_\phi > 0$. This results in $\dot{V}_{\mathrm{p}}(t, \xi) \leq -\zeta^{\mathsf{T}} Q(x)\zeta$, where $\zeta = [\|\tilde{\phi}\|, \|\tilde{\theta}\|]^{\mathsf{T}}$, and where $Q(x)$ is positive definite for each $x \neq 0$, and positive semidefinite for $x = 0$. Define $U(x) = \lambda_{\min}(Q(x))/\max\{2a_2, 1\}$, which is a continuous positive-definite function (due to continuity of the eigenvalues and of $a_3(x)$, $L_1(x)$ and $L_2(x)$). Following the same argument as in the proof of Theorem 5.1, we can then write $\|\xi(t)\| \leq \beta(t) := k_{\mathrm{e}}\|\xi(t_0)\|\exp(-\int_{t_0}^{t} U(x(\tau))\,\mathrm{d}\tau)$. Hence, $\beta$ is a monotonically non-increasing function.

For the sake of establishing a contradiction, suppose that $x(t)$ does not converge to the origin. Then there exists a $\delta > 0$ such that, for all $t \geq t_0$, there exist $\tau \geq t$ such that $\|x(\tau)\| \geq 2\delta$. From Assumption 5.3, $\|B(t, x)(g(t, x, \theta) - g(t, x, \hat{\theta}))\|$ is uniformly bounded when $\|x(t)\| \in [\delta, 2\delta]$, and the same holds for $\|f(t, x)\|$, because $f(t, x)$ is locally Lipschitz continuous in $x$, uniformly in $t$, and $f(t, 0) = 0$. Hence, the right-hand side of (5.15) is uniformly bounded for $\|x(t)\| \in [\delta, 2\delta]$, and it follows that there exists $T > 0$ such that on each interval $[\tau - T, \tau + T]$, $\|x(t)\| \geq \delta$. On every such interval there is a decrease in the bounding function $\beta$; in particular, $\beta(\tau + T) \leq \beta(\tau - T)\exp(-2\bar{\lambda}T)$, where $\bar{\lambda} = \min_{x \in K \setminus B(\delta)} U(x)$ is a positive number. Moreover, for any integer $n > 0$,

there exists a $t_1 > t_0$ such that $[t_0, t_1]$ contains at least $n$ disjoint time intervals of length $2T$ with $\|x(t)\| \geq \delta$. The UGAS and UGB properties of the unperturbed system $\dot{x} = f(t,x)$ imply that if $\gamma(\|\tilde{\theta}(t)\|)$ is sufficiently small for all $t \geq t_1$, where $t_1 \geq t_0$ is arbitrary, then $\|x(t)\|$ is globally ultimately bounded by $\delta$. Let therefore $\varepsilon$ be chosen small enough that, if for all $t \geq t_1$, $\|\xi(t)\| \leq \varepsilon$, then $\|x(t)\|$ is globally ultimately bounded by $\delta$. Let $n \geq 0$ be an integer chosen large enough that $\beta(t_0)\exp(-2n\bar{\lambda}T) \leq \varepsilon$, and let $t_1$ be large enough that there are at least $n$ disjoint intervals of length $2T$ in $[t_0, t_1]$ with $\|x(t)\| \geq \delta$. This implies that, for all $t \geq t_1$, $\|\xi(t)\| \leq \varepsilon$. This, in turn, implies by the ultimate boundedness property that there exists a $t_2 \geq t_1$ such that, for all $t \geq t_2$, $\|x(t)\| \leq \delta$. But this contradicts our assumption that there exist arbitrarily large values $\tau$ such that $\|x(\tau)\| \geq 2\delta$. Hence, $x(t)$ does converge to the origin. □

The functions $L_1(x)$ and $L_2(x)$ represent Lipschitz-like bounds that are typically not derived explicitly in the design process. The condition in Theorem 5.3 concerns the growth rates of these functions as $x \to 0$, which can often be determined without developing explicit expressions for the functions.

## 5.5 Simulation Example

In the next example, we demonstrate the method on a first-order system with a nonlinear and time-varying perturbation.

**Example 5.6.** Consider the system

$$\dot{x} = -x + \mathrm{e}^{\sin(t)\theta} + u, \tag{5.20}$$

where $\theta \in [\theta_{\min}, \theta_{\max}] = [-5, 5]$. Here $f(t,x) = f(x) = -x$, $B(t,x) = 1$, and $g(t,x,\theta) = g(t,\theta) = \exp(\sin(t)\theta)$. We wish to use $u$ to cancel the perturbation, and we therefore let $u = -\exp(\sin(t)\hat{\theta})$. The first step is to design an update law to estimate $\theta$ from the full perturbation. We first note that $[\partial g/\partial\theta](t,\theta) = \sin(t)\exp(\sin(t)\theta)$, and hence (5.7) in Proposition 5.4 is satisfied by selecting $M(t,x,\hat{\theta}) = M(t) = \sin(t)$ with $S(t,x) = S(t) = \sin^2(t)\exp(-\theta')$, where $\theta' := \max_{\theta\in\Theta}|\theta|$. The remaining requirements in Proposition 5.4 can be confirmed in the same way as in Example 5.4. We now check that the conditions of Assumption 5.2 hold. We have that $d(t,x,\tilde{\theta}) = (\theta\exp(\sin(t)\theta) - \hat{\theta}\exp(\sin(t)\hat{\theta}))\cos(t)$. Using the mean value theorem, we find that $|d(t,x,\tilde{\theta})| \leq (1+\theta')\exp(\theta')|\tilde{\theta}|$. We also see that

$$|u_\theta(t,x,\phi,\hat{\theta}) - u_\theta(t,x,\hat{\phi},\hat{\theta})| = \Gamma|\sin(t)\tilde{\phi}| \leq \Gamma|\tilde{\phi}|.^3$$

[3] We recall from Remark 5.2 that we can disregard the projection when checking this condition.

Moving to Assumption 5.3, it is straightforward to see that the nominal, unperturbed system $\dot{x} = -x$ is UGAS and that the perturbed system is UGB when $\hat{\theta}$ is restricted to $\Theta$. Finally, we use $\gamma(s) = \exp(\theta')s$ to satisfy Assumption 5.3. We implement the full estimator from (5.8). After canceling terms, we obtain

$$\dot{z} = -K_\phi(K_\phi - 1)x - K_\phi z - \sin(t)\mathrm{e}^{\sin(t)\hat{\theta}}\mathrm{Proj}(\Gamma \sin(t)(z + K_\phi x)), \quad (5.21)$$

$$\dot{\hat{\theta}} = \mathrm{Proj}(\Gamma \sin(t)(z + K_\phi x)). \quad (5.22)$$

We simulate the system with $K_\phi = 10$ and $\Gamma = 3$, letting $\theta$ vary in steps between $-2$ and 4 to get an impression of the response. The results can be seen in Figure 5.1, where we have also plotted the response using a gradient-type algorithm $\dot{\hat{\theta}} = \Gamma \sin(t)\exp(\sin(t)\hat{\theta})x$ based on linearization around the estimate $\hat{\theta}$, with gain $\Gamma = 1$ and with the parameter estimate limited to $[-5, 5]$. Noise has been added with sample time 0.001 and variance 1 to the measurement of the state $x$ used in both algorithms. The parameter projection is not active at any point during the simulation.

## 5.6 Application: Downhole Pressure Estimation during Oil Well Drilling

When extracting hydrocarbons from underground geological formations it is usually necessary to create a well by drilling a wellbore. During drilling, a mud circulation system is used to transport cuttings from the drilling out of the wellbore. The mud is pumped downhole inside the drill string and through the drill bit, and returns to the top through the annulus containing the drill string. The downhole pressure needs to be controlled within its margins: above the reservoir pore pressure and wellbore collapse pressure, but below the wellbore fracture pressure. In many cases, this margin is quite wide and the pressure can be manually controlled, but as oil and gas reserves begin to be depleted, reservoirs with narrower margins are being drilled, demanding automated pressure control (see, e.g., Nygaard and Nævdal, 2006; Nygaard, Imsland, and Johannessen, 2007). The downhole pressure is usually measured, but with conventional equipment this measurement has low bandwidth and is unreliable. Good pressure control therefore demands pressure estimation based on topside measurements.

### 5.6.1 Modeling

Complex models of the drilling process exist, for example, in the simulator Wemod, provided by IRIS (Lage, Frøyen, Sævareid, and Fjelde, 2000). Here we shall

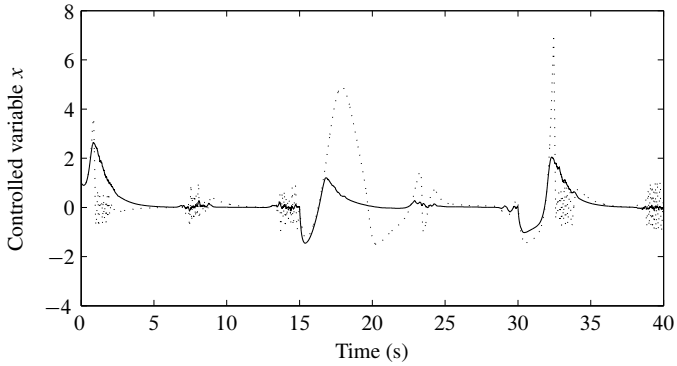


(a) Controlled variable, nonlinear method (solid), and gradient-type method (dotted)

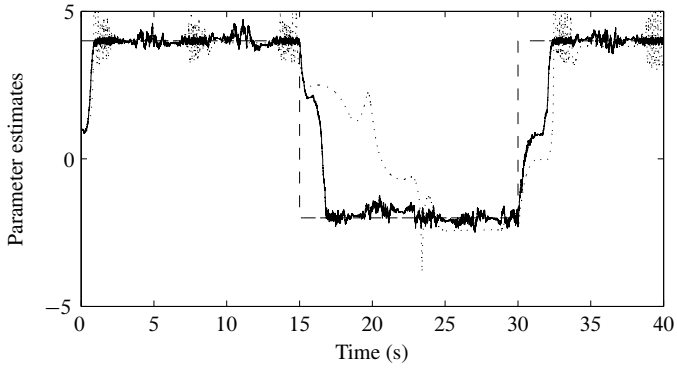


(b) Unknown parameter (dashed), estimate with nonlinear method (solid), and estimate with gradient-type method (dotted)

**Figure 5.1:** Simulation results for Example 5.6

use a low-complexity model for the development of the pressure estimation algorithm (see Stamnes, Zhou, Kaasa, and Aamo, 2008). In particular, we assume that the drilling process is described by the following dynamic model, derived from mass balances for the drill string and annulus:

$$\frac{V_d}{\beta_d}\dot{p}_p = q_p - q_b, \tag{5.23}$$

$$\frac{V_a}{\beta_a}\dot{p}_c = -\dot{V}_a + q_b + q_r + q_a - q_c, \tag{5.24}$$

where the states $p_p$ and $p_c$ are the pressures in the top of the drill string (standpipe pressure) and the annulus (choke pressure), both of which are measured. Furthermore, $V_d$ and $V_a$ denote the volumes of the drill string and the annulus; and $\beta_d$

and $\beta_a$ are the drill string and annulus bulk moduli, all known. The volume flows are the inflow to the drill string ($q_p$), flow from the back pressure (annulus) pump ($q_a$), and exit flow from the annulus through the choke ($q_c$), all measured, as well as the flow through the drill bit ($q_b$) and inflow from the reservoir ($q_r$). The flow $q_b$ is given by a steady-state momentum balance for the drill string and annulus (in a slight simplification of the model in Stamnes et al., 2008):

$$p_p - p_c = F_d q_b^2 + F_a(q_b + q_r)^2 - s(t). \tag{5.25}$$

The friction parameter $F_d$ in the drill string is assumed known, as is the function $s(t) = (\rho_d(t) - \rho_a(t))gh_b(t)$, which describes the difference in drill string and annulus downhole static head. We shall estimate the two remaining parameters, the friction coefficient $F_a$ and the reservoir inflow $q_r$, which will allow us to calculate the downhole pressure $p_b$ using a steady-state momentum balance for the annulus as $p_b = p_c + F_a(q_b + q_r)^2 + \rho_a(t)gh_b$. We assume that the parameters to be estimated are constant, and that $(q_b + q_r)^2 > \alpha$ for some $\alpha > 0$, which implies that we have flow into the annulus. In order to put the system in the form used in this paper, we write $x = [V_d/\beta_d\, p_p, V_a/\beta_a\, p_c]^\mathsf{T}$, $\theta = [q_r, F_a]^\mathsf{T}$, $f(t,x) = [q_p, (x_2/V_a - 1)\dot{V}_a + q_a - q_c]^\mathsf{T}$, $B(t,x) = \left[\begin{smallmatrix} -1 & 0 \\ 1 & 1 \end{smallmatrix}\right]$, and $g(t,x,\theta) = [q_b, q_r]^\mathsf{T}$.

### 5.6.2 Estimator Design

As before, we start by designing an update law for estimating $F_a$ and $q_r$ as if $\phi_1 = -q_b$ and $\phi_2 = q_b + q_r$ were known. We see that we can use a simple inversion according to Proposition 5.1 to create an update law for $q_r$:

$$\dot{\hat{q}}_r = \Gamma_1(\hat{\phi}_1 + \hat{\phi}_2 - \hat{q}_r), \tag{5.26}$$

where $\Gamma_1 > 0$ is a scalar gain. (For simplicity, we omit the projection in discussing this example.) For $F_a$, the approach is slightly more complicated. According to (5.25), we may define an estimated flow $\hat{q}_b$ through the bit, by the equation $p_p - p_c = F_d\hat{q}_b^2 + \hat{F}_a(\hat{q}_b + \hat{q}_r)^2 - s(t)$. Subtracting this from (5.25) and rearranging yields the relation $-F_d(q_b^2 - \hat{q}_b^2) - \hat{F}_a\left((q_b + q_r)^2 - (\hat{q}_b + \hat{q}_r)^2\right) = \tilde{F}_a(q_b + q_r)^2$. Define the update law

$$\dot{\hat{F}}_a = \Gamma_2[-F_d(\hat{\phi}_1^2 - \hat{q}_b^2) - \hat{F}_a(\hat{\phi}_2^2 - (\hat{q}_b + \hat{q}_r)^2)]. \tag{5.27}$$

For $\hat{\phi} = \phi$, we then have $\dot{\tilde{F}}_a = -\Gamma_2\tilde{F}_a(q_b + q_r)^2$. It is then straightforward to prove that Assumption 5.1 holds with $V_\mathrm{u}(\tilde{\theta}) = \frac{1}{2}\tilde{\theta}^\mathsf{T}\Gamma^{-1}\tilde{\theta}$, where $\Gamma$ is the gain matrix composed of $\Gamma_1$ and $\Gamma_2$. Implementation of the update law requires calculation of $\hat{q}_b$. We find $\hat{q}_b$ by taking the positive root of the second-order equation defining

the estimated flow through the bit, which we assume is always real. This solution is in turn used to find the partial derivative $[\partial g/\partial\theta](t, x, \hat{\theta})$, which is needed in the complete implementation of the system. Due to the quadratic terms in $\phi_1$ and $\phi_2$ in the update law for $F_a$, the Lipschitz condition on $u_\theta$ does not hold globally. This problem can easily be fixed by modifying the update law with a saturation, as described in Section 5.3.3.

### 5.6.3 Experimental Results

The estimator has been tested using the simulator Wemod (Lage et al., 2000), yielding very accurate results, and on real measurement data from drilling at the Grane field in the North Sea. The results for the real drilling data can be seen in Figure 5.2. The tuning used is $\Gamma_1 = 0.005$, $\Gamma_2 = 2$ and $K_\phi = 10I$. It should be noted that, although it is common to measure the flow $q_c$, no such measurement is available in the data set used, and $q_c$ is therefore estimated from a choke model and the available choke opening. Given the large uncertainties in this application, the downhole pressure estimate is considered good.

## 5.7 Concluding Remarks

We have introduced a modular design method for estimating unknown parameters in systems with nonlinearly parameterized perturbations, where the main design task is to construct an update law to asymptotically invert a nonlinear equation. As mentioned in the introduction, the modular structure allows for the perturbation estimator to be extended beyond what is presented in this paper. In Grip et al. (2009), it is extended to facilitate observer design for the case of partial state measurement, by using techniques from high-gain observer theory. We note that, for the results presented in this paper, we can write (5.8) in terms of a variable $\hat{x} = -K_\phi^{-1} z$ rather than $z$. It is then easy to see that $\hat{x}$ represents an estimate of the state $x$. It can furthermore be confirmed that, for linearly parameterized perturbations, the design closely resembles a standard linear observer with adaptation, if the update law is chosen as suggested in Remark 5.1.

## Acknowledgements

The authors thank Øyvind N. Stamnes for useful discussions and the use of data and figures for the oil drilling example; and Gerhard H. Nygaard and IRIS for providing the simulator Wemod.

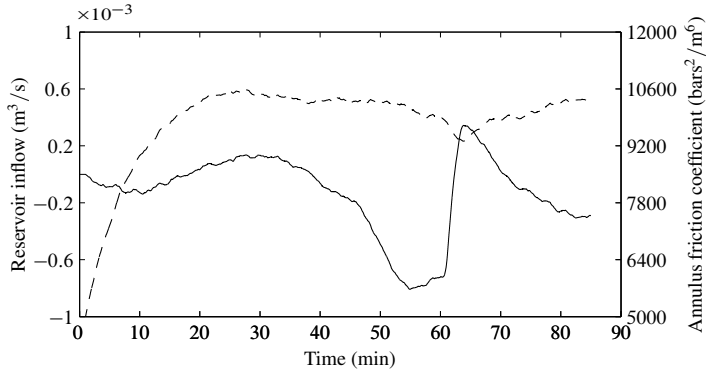


(a) Estimated reservoir inflow $q_r$ (solid, left axis) and estimated friction coefficient $F_a$ (dashed, right axis)

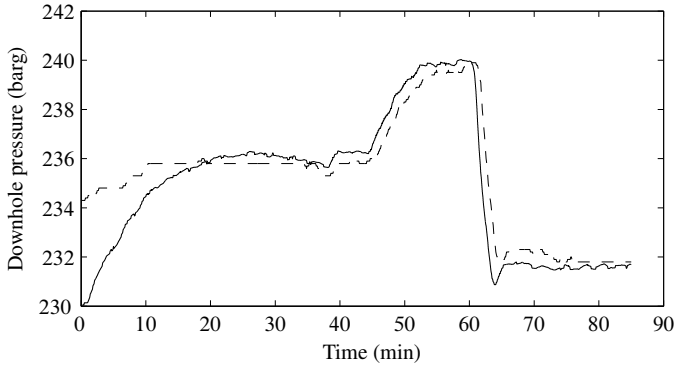


(b) Measured (dashed) and estimated (solid) downhole pressure $p_b$

**Figure 5.2:** Results for drilling application using real drilling data

# 5.A Parameter Projection

Let the set of possible parameters be defined by $\Pi := \{\hat{\theta} \in \mathbb{R}^p \mid \mathcal{P}(\hat{\theta}) \leq 0\}$, where $\mathcal{P}: \mathbb{R}^p \to \mathbb{R}$ is a smooth, convex function. Let $\Pi^0$ denote the interior of $\Pi$, and let $\Theta$ be defined by $\Theta = \{\hat{\theta} \in \mathbb{R}^p \mid \mathcal{P}(\hat{\theta}) \leq \varepsilon\}$, where $\varepsilon$ is a small positive number, making $\Theta$ a slightly larger superset of $\Pi$. Consider the update function $u_\theta(t, x, \hat{\phi}, \hat{\theta}) = \text{Proj}(\tau(t, x, \hat{\phi}, \hat{\theta}))$, where Proj$(\cdot)$ is the projection from Krstić et al. (1995, Appendix E). Proj is defined as $\text{Proj}(\tau(t, x, \hat{\phi}, \hat{\theta})) = p(t, x, \hat{\phi}, \hat{\theta})\tau(t, x, \hat{\phi}, \hat{\theta})$, with $p(t, x, \hat{\phi}, \hat{\theta})$ given by

- $p(t, x, \hat{\phi}, \hat{\theta}) = I$ if $\hat{\theta} \in \Pi^0$ or $\nabla_{\hat{\theta}} \mathcal{P}^\mathsf{T} \tau(t, x, \hat{\phi}, \hat{\theta}) \leq 0$,
- $p(t, x, \hat{\phi}, \hat{\theta}) = \left(I - c(\hat{\theta})\Gamma \nabla_{\hat{\theta}} \mathcal{P} \nabla_{\hat{\theta}} \mathcal{P}^\mathsf{T} / \|\nabla_{\hat{\theta}} \mathcal{P}\|_\Gamma^2\right)$ if $\hat{\theta} \in \Theta \setminus \Pi^0$ and $\nabla_{\hat{\theta}} \mathcal{P}^\mathsf{T} \tau(t, x, \hat{\phi}, \hat{\theta}) > 0$,

where $\Gamma$ is a symmetric positive-definite matrix corresponding to the gain matrix in the update law; $\nabla_{\hat{\theta}}\mathcal{P}^{\mathsf{T}}$ is the gradient of $\mathcal{P}(\hat{\theta})$ with respect to $\hat{\theta}$; and $c(\hat{\theta}) = \min\{1, \mathcal{P}(\hat{\theta})/\varepsilon\}$.

### 5.A.1 Lipschitz Continuity

We wish to show that, if, for each compact set $K \in \mathbb{R}^n$, $\tau$ has the property that, for all $(t, x, \phi, \hat{\phi}, \hat{\theta}) \in \mathbb{R}_{\geq 0} \times K \times \mathbb{R}^n \times \mathbb{R}^n \times \Theta$, $\|\tau(t, x, \phi, \hat{\theta}) - \tau(t, x, \hat{\phi}, \hat{\theta})\| \leq L_2(x)\|\tilde{\phi}\|$, then we also have $\|u_\theta(t, x, \phi, \hat{\theta}) - u_\theta(t, x, \hat{\phi}, \hat{\theta})\| \leq L_2'(x)\|\tilde{\phi}\|$, for some continuous function $L_2'(x) > 0$. In the following, we shall outline the proof of this assertion. To do this, we have to look at two distinct cases: when the parameter projection is either active or inactive for both $u_\theta(t, x, \phi, \hat{\theta})$ and $u_\theta(t, x, \hat{\phi}, \hat{\theta})$ (Case I); and when the parameter projection is active for one of $u_\theta(t, x, \phi, \hat{\theta})$ or $u_\theta(t, x, \hat{\phi}, \hat{\theta})$, but not the other (Case II). In the following, we shall write $u_\theta(\phi) = u_\theta(t, x, \phi, \hat{\theta})$, $u_\theta(\hat{\phi}) = u_\theta(t, x, \hat{\phi}, \hat{\theta})$, and similarly for $\tau$.

In Case I, $p(t, x, \phi, \hat{\theta}) = p(t, x, \hat{\phi}, \hat{\theta})$. The property therefore follows from uniform boundedness of $\|p(t, x, \phi, \hat{\theta})\|$. Case II occurs if $\hat{\theta} \in \Theta \setminus \Pi^0$, and $\nabla_{\hat{\theta}}\mathcal{P}^{\mathsf{T}}\tau(\phi)$ and $\nabla_{\hat{\theta}}\mathcal{P}^{\mathsf{T}}\tau(\hat{\phi})$ do not have the same sign. Without loss of generality, we assume that $\nabla_{\hat{\theta}}\mathcal{P}^{\mathsf{T}}\tau(\phi) \leq 0$ and $\nabla_{\hat{\theta}}\mathcal{P}^{\mathsf{T}}\tau(\hat{\phi}) > 0$. In this case, we have $u_\theta(\phi) - u_\theta(\hat{\phi}) = \tau(\phi) - (I - c(\hat{\theta})\Gamma\nabla_{\hat{\theta}}\mathcal{P}\nabla_{\hat{\theta}}\mathcal{P}^{\mathsf{T}}/\|\nabla_{\hat{\theta}}\mathcal{P}\|_\Gamma^2)\tau(\hat{\phi})$. Expanding this expression, we have, after some calculation, $\|u_\theta(\phi) - u_\theta(\hat{\phi})\|_{\Gamma^{-1}}^2 = \|\tau(\phi) - \tau(\hat{\phi})\|_{\Gamma^{-1}}^2 + c(\hat{\theta})/\|\nabla_{\hat{\theta}}\mathcal{P}\|_\Gamma^2\big[c(\hat{\theta})|\nabla_{\hat{\theta}}\mathcal{P}^{\mathsf{T}}\tau(\hat{\phi})|^2 + 2\tau(\hat{\phi})^{\mathsf{T}}\nabla_{\hat{\theta}}\mathcal{P}\nabla_{\hat{\theta}}\mathcal{P}^{\mathsf{T}}(\tau(\phi) - \tau(\hat{\phi}))\big]$. We now make the observation that, because $\nabla_{\hat{\theta}}\mathcal{P}^{\mathsf{T}}\tau(\phi)$ and $\nabla_{\hat{\theta}}\mathcal{P}^{\mathsf{T}}\tau(\hat{\phi})$ do not have the same sign, $|\nabla_{\hat{\theta}}\mathcal{P}^{\mathsf{T}}\tau(\hat{\phi})| \leq |\nabla_{\hat{\theta}}\mathcal{P}^{\mathsf{T}}(\tau(\phi) - \tau(\hat{\phi}))|$. Using this for substitution where $\nabla_{\hat{\theta}}\mathcal{P}^{\mathsf{T}}\tau(\hat{\phi})$ occurs alone, we obtain that $\|u_\theta(\phi) - u_\theta(\hat{\phi})\|_{\Gamma^{-1}}^2 \leq \|\tau(\phi) - \tau(\hat{\phi})\|_{\Gamma^{-1}}^2 + (c^2(\hat{\theta}) + 2c(\hat{\theta}))/\|\nabla_{\hat{\theta}}\mathcal{P}\|_\Gamma^2\|\nabla_{\hat{\theta}}\mathcal{P}\|^2\|\tau(\phi) - \tau(\hat{\phi})\|^2$. Using the property that for $P = P^{\mathsf{T}} > 0$, $\lambda_{\min}(P)\|\zeta\|^2 \leq \|\zeta\|_P^2 \leq \lambda_{\max}(P)\|\zeta\|^2$, we find that $\|u_\theta(\phi) - u_\theta(\hat{\phi})\| \leq \alpha\|\tau(\phi) - \tau(\hat{\phi})\| \leq \alpha L_2(x)\|\tilde{\phi}\|$, where

$$\alpha = \left(\frac{\lambda_{\max}(\Gamma^{-1})\lambda_{\min}(\Gamma) + 3}{\lambda_{\min}(\Gamma^{-1})\lambda_{\min}(\Gamma)}\right)^{\frac{1}{2}}.$$

## 5.B Proofs of Propositions 5.2–5.4

*Proof of Proposition* 5.2. Inspired by Loría, Panteley, Popović, and Teel (2005), we use the function $V_{\mathrm{u}}(t, \tilde{\theta}) = \frac{1}{2}\tilde{\theta}^{\mathsf{T}}\left(\Gamma^{-1} - \mu\int_t^\infty \exp(t - \tau) I l(\tau, x(\tau))\,\mathrm{d}\tau\right)\tilde{\theta}$,

where $\mu > 0$ is a constant yet to be specified.[4] We first note that

$$\frac{1}{2}\tilde{\theta}^{\mathsf{T}}\left(\Gamma^{-1} - \mu I\right)\tilde{\theta} \leq V_{\mathrm{u}}(t,\tilde{\theta}) \leq \frac{1}{2}\tilde{\theta}^{\mathsf{T}}\Gamma^{-1}\tilde{\theta}.$$

Hence, $V_{\mathrm{u}}$ is positive definite provided that $\mu < \lambda_{\min}(\Gamma^{-1})$. With $\hat{\phi} = \phi$, we get $\dot{\tilde{\theta}} = -\mathrm{Proj}(l(t,x)\Gamma\tilde{\theta})$. Using the property (Krstić et al., 1995, Lemma E.1) that $-\tilde{\theta}^{\mathsf{T}}\Gamma^{-1}\mathrm{Proj}(\tau) \leq -\tilde{\theta}^{\mathsf{T}}\Gamma^{-1}\tau$, we have

$$\begin{aligned}
\dot{V}_{\mathrm{u}}(t,\tilde{\theta}) = -\tilde{\theta}^{\mathsf{T}}&\left(\Gamma^{-1} - \mu\int_t^\infty \mathrm{e}^{t-\tau} I l(\tau,x(\tau))\mathrm{d}\tau\right)\\
&\cdot \mathrm{Proj}(l(t,x)\Gamma\tilde{\theta}) + \frac{1}{2}\mu\tilde{\theta}^{\mathsf{T}} I l(t,x)\tilde{\theta}\\
&- \frac{1}{2}\mu\tilde{\theta}^{\mathsf{T}}\int_t^\infty \mathrm{e}^{t-\tau} I l(\tau,x(\tau))\mathrm{d}\tau\,\tilde{\theta}\\
&\leq -(1-\frac{1}{2}\mu)l(t,x)\tilde{\theta}^{\mathsf{T}}\tilde{\theta} - \frac{1}{2}\mu\varepsilon\mathrm{e}^{-T}\tilde{\theta}^{\mathsf{T}}\tilde{\theta}\\
&+ \mu\|\tilde{\theta}\|\left\|\int_t^\infty \mathrm{e}^{t-\tau} I l(\tau,x(\tau))\mathrm{d}\tau\right\|\left\|\mathrm{Proj}(l(t,x)\Gamma\tilde{\theta})\right\|\\
&\leq -(1-\frac{1}{2}\mu - \mu\sqrt{\kappa}\|\Gamma\|)l(t,x)\|\tilde{\theta}\|^2 - \frac{1}{2}\mu\varepsilon\mathrm{e}^{-T}\|\tilde{\theta}\|^2, \quad (5.28)
\end{aligned}$$

where $\kappa$ is the ratio of the largest to the smallest eigenvalue of $\Gamma^{-1}$. Above, we have used the property (Krstić et al., 1995, Lemma E.1) that

$$\mathrm{Proj}(\tau)^{\mathsf{T}}\Gamma^{-1}\mathrm{Proj}(\tau) \leq \tau^{\mathsf{T}}\Gamma^{-1}\tau,$$

which implies that $\|\mathrm{Proj}(\tau)\| \leq \sqrt{\kappa}\|\tau\|$. We have also used that

$$\begin{aligned}
\int_t^\infty \mathrm{e}^{t-\tau} l(\tau,x(\tau))\,\mathrm{d}\tau &\geq \int_t^{t+T} \mathrm{e}^{t-\tau} l(\tau,x(\tau))\,\mathrm{d}\tau\\
&\geq \mathrm{e}^{-T}\int_t^{t+T} l(\tau,x(\tau))\,\mathrm{d}\tau\\
&\geq \mathrm{e}^{-T}\varepsilon.
\end{aligned}$$

[4] *Remark added after publiction:* The function $t \mapsto l(t,x(t))$ may be chosen to contain isolated discontinuities, in which case a minor technical modification of the integrand in $V_{\mathrm{u}}(t,\tilde{\theta})$ (namely, a continuous approximation of $l(\tau,x(\tau))$ from below) is needed to make $V_{\mathrm{u}}$ differentiable everywhere. This modification is easily constructed without interfering with the negative-definiteness property of $\dot{V}_{\mathrm{u}}(t,\tilde{\theta})$. Alternatively, differentiability with respect to $t$ may be interpreted as having a well-defined upper right-hand Dini derivative (see, e.g., Khalil, 2002, App. C.2), which is sufficient for use with the comparison lemma.

From the calculation above, we see that the time derivative is negative definite provided that $\mu < 1/(\frac{1}{2} + \sqrt{\kappa}\|\Gamma\|)$. □

*Proof of Proposition* 5.3. For the sake of brevity, we write $M = M(t, x, \hat{\theta})$ and $B = B(t, x)$. With $\hat{\phi} = \phi$, we get $\dot{\hat{\theta}} = -\text{Proj}(\Gamma M B(g(t, x, \theta) - g(t, x, \hat{\theta})))$. We use the function $V_u(t, \tilde{\theta}) = \frac{1}{2}\tilde{\theta}^T\Gamma^{-1}\tilde{\theta}$. Using the property (Krstić et al., 1995, Lemma E.1) that $-\tilde{\theta}^T\Gamma^{-1}\text{Proj}(\tau) \leq -\tilde{\theta}^T\Gamma^{-1}\tau$, we have

$$\dot{V}_u(t, \tilde{\theta}) \leq -\frac{1}{2}\tilde{\theta}^T MB(g(t, x, \theta) - g(t, x, \hat{\theta})) - \frac{1}{2}(g(t, x, \theta) - g(t, x, \hat{\theta}))^T B^T M^T \tilde{\theta}.$$

Since $g(t, x, \theta)$ is continuously differentiable with respect to $\theta$, we may write, according to Taylor's theorem (see, e.g., Nocedal and Wright, 1999, Theorem 11.1), $g(t, x, \theta) - g(t, x, \hat{\theta}) = \int_0^1 [\partial g/\partial\theta](t, x, \hat{\theta} + p\tilde{\theta})\tilde{\theta}\, \mathrm{d}p$. Hence, we have

$$\begin{aligned}
\dot{V}_u(t, \tilde{\theta}) &\leq -\frac{1}{2}\int_0^1 \tilde{\theta}^T \left(MB\frac{\partial g}{\partial\theta}(t, x, \hat{\theta} + p\tilde{\theta}) + \frac{\partial g}{\partial\theta}^T(t, x, \hat{\theta} + p\tilde{\theta})B^T M^T\right)\tilde{\theta}\, \mathrm{d}p \\
&\leq -\int_0^1 \tilde{\theta}^T P\tilde{\theta}\, \mathrm{d}p \\
&= -\tilde{\theta}^T P\tilde{\theta},
\end{aligned}$$

which proves that Assumption 5.1 holds. □

*Proof of Proposition* 5.4. We use the function

$$V_u(t, \tilde{\theta}) = \frac{1}{2}\tilde{\theta}^T\left(\Gamma^{-1} - \mu\int_t^\infty \exp(t - \tau)S(\tau, x(\tau))\mathrm{d}\tau\right)\tilde{\theta},$$

where $\mu > 0$ is a constant yet to be specified.[5] First, we confirm that the function $V_u$ is positive definite. We have $\frac{1}{2}(\lambda_{\min}(\Gamma^{-1}) - \mu\lambda'_S)\|\tilde{\theta}\|^2 \leq V_u(t, \tilde{\theta}) \leq \frac{1}{2}\lambda_{\min}(\Gamma^{-1})\|\tilde{\theta}\|^2$, where $\lambda'_S = \sup_{(t,x)\in\mathbb{R}_{\geq 0}\times K}\lambda_{\max}(S(t, x))$. It follows from this that $V_u$ is positive definite provided that $\lambda_{\min}(\Gamma^{-1}) - \mu\lambda'_S > 0$, which is guaranteed if $\mu < \lambda_{\min}(\Gamma^{-1})/\lambda'_S$. When we insert $\hat{\phi} = \phi$, we get the same error dynamics as in the proof of Proposition 5.3. Following a calculation similar to the proof of Proposition 5.2, we get

$$\begin{aligned}
\dot{V}_u(t, \tilde{\theta}) \leq &-\left(1 - \frac{1}{2}\mu\right)\tilde{\theta}^T S(t, x)\tilde{\theta} - \frac{1}{2}\mu\varepsilon\mathrm{e}^{-T}\|\tilde{\theta}\|^2 \\
&+ \mu\sqrt{\kappa}M_S\|\Gamma\|M_M L_g\|\tilde{\theta}\|(\tilde{\theta}^T S(t, x)\tilde{\theta})^{1/2},
\end{aligned}$$

[5] *Remark added after publication:* A remark similar to the footnote on page 143 also applies to this proof.

where $M_S$ and $M_M$ are bounds on $\|S(t,x)\|$ and $\|M(t,x,\hat{\theta})\|$ respectively, and $\kappa$ is the ratio of the largest to the smallest eigenvalue of $\Gamma^{-1}$. We may write this as a quadratic expression with respect to $[(\tilde{\theta}^\mathsf{T} S(t,x)\tilde{\theta})^{1/2}, \|\tilde{\theta}\|]^\mathsf{T}$. It is then easily confirmed that the expression is negative definite if

$$\mu < \frac{2}{1 + \kappa M_S^2 \|\Gamma\|^2 M_M^2 L_g^2 \varepsilon^{-1} \mathrm{e}^T}. \qquad \square$$

# Bibliography


A. M. Annaswamy, F. P. Skantze, and A.-P. Loh. Adaptive control of continuous time systems with convex/concave parametrization. *Automatica*, 34(1):33–49, 1998.

J. Bakkeheim, T. A. Johansen, Ø. N. Smogeli, and A. J. Sørensen. Lyapunov-based integrator resetting with application to marine thruster control. *IEEE Trans. Contr. Syst. Tech.*, 16(5):908–917, 2008.

J. D. Bošković. Stable adaptive control of a class of first-order nonlinearly parameterized plants. *IEEE Trans. Automat. Contr.*, 40(2):347–350, 1995.

J. D. Bošković. Adaptive control of a class of nonlinearly parameterized plants. *IEEE Trans. Automat. Contr.*, 43(7):930–934, 1998.

C. Cao, A. M. Annaswamy, and A. Kojić. Parameter convergence in nonlinearly parametrized systems. *IEEE Trans. Automat. Contr.*, 48(3):397–412, 2003.

A. Chakrabortty and M. Arcak. Time-scale separation redesigns for stabilization and performance recovery of uncertain nonlinear systems. *Automatica*, 45(1): 34–44, 2009.

V. Fomin, A. Fradkov, and V. Yakubovich, editors. *Adaptive Control of Dynamical Systems*. Nauka, Moskow, 1981.

H. F. Grip, A. Saberi, and T. A. Johansen. State and parameter estimation for linear systems with nonlinearly parameterized perturbations. In *Proc. IEEE Conf. Dec. Contr.*, pages 8218–8225, Shanghai, China, 2009.

P. A. Ioannou and J. Sun. *Robust Adaptive Control*. Prentice-Hall, Upper Saddle River, NJ, 1996.

H. K. Khalil. *Nonlinear Systems*. Prentice-Hall, Upper Saddle River, NJ, 3rd edition, 2002.

M. Krstić, I. Kanellakopoulos, and P. V. Kokotović. *Nonlinear and Adaptive Control Design*. Wiley, New York, 1995.

A. C. V. M. Lage, J. Frøyen, O. Sævareid, and K. K. Fjelde. Underbalanced drilling dynamics: Two-phase flow modelling, experiments and numerical solutions techniques. In *Proc. Rio Oil & Gas Conf.*, Rio de Janeiro, Brazil, 2000.

A.-P. Loh, A. M. Annaswamy, and F. P. Skantze. Adaptation in the presence of a general nonlinear parameterization: An error model approach. *IEEE Trans. Automat. Contr.*, 44(9):1634–1652, 1999.

A. Loría, E. Panteley, D. Popović, and A. R. Teel. A nested Matrosov theorem and persistency of excitation for uniform convergence in stable nonautonomous systems. *IEEE Trans. Automat. Contr.*, 50(2):183–198, 2005.

R. Marino and P. Tomei. *Nonlinear Control Design: Geometric, Adaptive and Robust*. Prentice-Hall, Upper Saddle River, NJ, 1995.

S. Nicosia, A. Tornambè, and P. Valigi. Nonlinear map inversion via state observers. *Circ. Syst. Signal Process.*, 13(5):571–589, 1994.

J. Nocedal and S. J. Wright. *Numerical Optimization*. Springer-Verlag, New York, 1999.

G. Nygaard and G. Nævdal. Non-linear model predictive control scheme for stabilizing annulus pressure during oil well drilling. *J. Process Contr.*, 16(7):719–732, 2006.

G. Nygaard, L. Imsland, and E. Johannessen. Using NMPC based on a low-order model for controlling pressure during oil well drilling. In *Proc. Int. Symp. Dyn. Contr. Process Syst.*, Cancun, Mexico, 2007.

R. Ortega. Some remarks on adaptive neuro-fuzzy systems. *Int. J. Adapt. Contr. Signal Process.*, 10(1):79–83, 1996.

E. Panteley and A. Loría. Growth rate conditions for uniform asymptotic stability of cascaded time-varying systems. *Automatica*, 37(3):453–460, 2001.

Z. Qu. Adaptive and robust controls of uncertain systems with nonlinear parameterization. *IEEE Trans. Automat. Contr.*, 48(10):1817–1823, 2003.

Z. Qu, R. A. Hull, and J. Wang. Globally stabilizing adaptive control design for nonlinearly-parametrized systems. *IEEE Trans. Automat. Contr.*, 51(6):1073–1079, 2006.

K. Reif, S. Günther, E. Yaz, and R. Unbehauen. Stochastic stability of the discrete-time extended Kalman filter. *IEEE Trans. Automat. Contr.*, 44(4):714–728, 1999.

Ø. N. Stamnes, J. Zhou, G.-O. Kaasa, and O. M. Aamo. Adaptive observer design for the bottomhole pressure of a managed pressure drilling system. In *Proc. IEEE Conf. Dec. Contr.*, pages 2961–2966, Cancun, Mexico, 2008.

I. Y. Tyukin. Adaptation algorithms in finite form for nonlinear dynamic objects. *Autom. Rem. Contr.*, 64(6):951–974, 2003.

I. Y. Tyukin, D. V. Prokhorov, and C. van Leeuwen. Adaptation and parameter estimation in systems with unstable target dynamics and nonlinear parametrization. *IEEE Trans. Automat. Contr.*, 52(9):1543–1559, 2007.

T. Zhang, S. S. Ge, C. C. Hang, and T. Y. Chai. Adaptive control of first-order systems with nonlinear parameterization. *IEEE Trans. Automat. Contr.*, 45(8): 1512–1516, 2000.

# Chapter 6

# Observer Design and Parameter Estimation for Linear Systems with Nonlinearly Parameterized Perturbations

***Abstract:*** *We consider systems that can be described by a linear part with a nonlinear perturbation, where the perturbation is parameterized by a vector of unknown, constant parameters. Under a set of technical assumptions about the perturbation and its relationship to the outputs, we present a modular observer design technique. The observers produced by this design technique consist of a modified high-gain observer that estimates the states of the system together with the full perturbation, and a parameter estimator. The parameter estimator is constructed by the designer to identify the unknown parameters by dynamically inverting a nonlinear equation. We illustrate the design technique by constructing an observer for a* DC *motor with friction modeled by the dynamic LuGre friction model.*

## 6.1 Introduction

A common problem in model-based estimation and control is the handling of unknown or partially unknown perturbations to system equations. Such perturbations can be the result of external disturbances or internal plant changes, such as a configuration change, system fault, or changes in physical plant characteristics. In this paper, we consider observer design for systems that can be described by a linear part with a nonlinear, time-varying perturbation that is parameterized by a vector of unknown, constant parameters. Our design extends the results of Grip,

Johansen, and Imsland (2008); Grip, Johansen, Imsland, and Kaasa (2010), where parameter identification for systems with full-state measurement was considered.

In the literature, many of the results that deal with the handling of unknown or partially unknown perturbations are based either on high-gain designs, where the perturbations are suppressed by using a sufficiently high gain, or adaptive designs, where online estimates of unknown parameters are used to cancel the perturbations. Many of the results on high-gain observer design for nonlinear systems, for example Khalil and Esfandiari (1993); Teel and Praly (1994), rely on placing the system in some variation of the normal form, where it is represented as a chain of integrators from the nonlinearities to the outputs, possibly with a separate subsystem representing the zero dynamics. An alternative to the normal form is the special coordinate basis (SCB) introduced in Sannuti and Saberi (1987), where the system is divided into subsystems that reflect its zero structure and invertibility properties. While high-gain designs based on the normal form are limited to systems that are square-invertible, minimum-phase, and of uniform relative degree with respect to the nonlinearities, Saberi and Sannuti (1990) shows that high-gain observers can be designed based on the SCB for more general multiple-input multiple-output (MIMO) systems that are left-invertible and minimum-phase with respect to the nonlinearities.

In the presence of an unknown perturbation, high-gain observer designs can be extended to estimate the perturbation as well, by considering the perturbation as an additional state. The perturbation estimate can be used for control, for example, to cancel the actual perturbation. This type of approach has been adopted recently in the context of performance recovery, in Chakrabortty and Arcak (2009), where the perturbation appears in the first derivatives, and in Freidovich and Khalil (2008), where it appears at the end of an integrator chain in a single-input single-output (SISO) system, and is estimated by an *extended high-gain observer*. When extending the state to include the perturbation, Lipschitz-like conditions must be imposed on the derivative of the perturbation. A strength of the high-gain designs mentioned above is that little structural information about the perturbation is needed for implementation. Conversely, however, these methods do not fully exploit structural information about uncertainties in the perturbation, even when such information is available.

Adaptive techniques are based on online estimation of unknown parameters that can be considered constant or slowly varying. Most of the adaptive literature deals with systems that are linear with respect to the unknown parameters (see, e.g., Krstić, Kanellakopoulos, and Kokotović, 1995). Ways of handling nonlinear parameterizations include the extended Kalman filter (see Brown and Hwang, 1997), various methods for handling nonlinearities with convex or concave parameterizations (e.g., Fomin, Fradkov, and Yakubovich, 1981; Annaswamy, Skantze, and

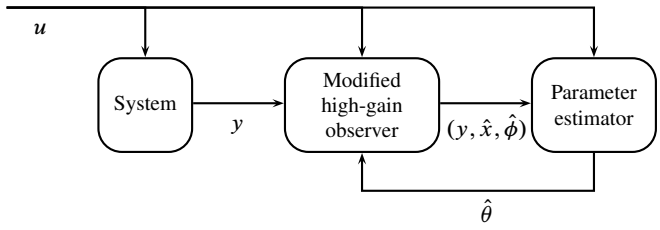


**Figure 6.1:** System structure

Loh, 1998), and methods for first-order systems with fractional parameterizations (e.g., Bošković, 1998; Zhang, Ge, Hang, and Chai, 2000). Adaptive techniques related to our work include Qu (2003); Tyukin, Prokhorov, and van Leeuwen (2007); Khalil (1996). In Qu (2003), perturbations with matrix fractional parameterizations are considered, by introducing an auxiliary estimate of the full perturbation that is used in estimation of the unknown parameters. In Tyukin et al. (2007), adaptive update laws for a class of nonlinearly parameterized perturbations in the first derivatives of the outputs are designed, by first creating virtual algorithms based on information from the derivatives, and then transforming these into implementable form without explicit differentiation. In Khalil (1996), adaptive control for linear parameterizations is designed for the case of full-state measurement, and then extended to the case of partial-state measurement by using high-gain estimates of output derivatives.

In this paper we introduce a modular design consisting of two separate but connected modules. The first module is a *modified high-gain observer* that estimates the states of the system and the unknown perturbation. The modified high-gain observer is closely related to the extended high-gain observer for SISO systems in Freidovich and Khalil (2008). The second module is a *parameter estimator* that uses the state and perturbation estimates to produce estimates of the unknown parameters, which are in turn fed back to the modified high-gain observer as illustrated in Figure 6.1. This approach allows us to exploit structural information about the perturbation instead of suppressing all uncertainties using high gain. The price we pay is that the method is restricted to a limited class of perturbations that satisfy persistency-of-excitation requirements allowing for exponentially stable estimation of the unknown parameters. We base our design on the SCB and the theory from Saberi and Sannuti (1990), enabling us to deal comfortably with a large class of MIMO systems.

### 6.1.1 Preliminaries

For a set of vectors $z_1, \ldots, z_n$, we denote by $\mathrm{col}(z_1, \ldots, z_n)$ the column vector obtained by stacking the elements of $z_1, \ldots, z_n$. The operator $\|\cdot\|$ denotes the Euclidean norm for vectors and the induced Euclidean norm for matrices. For a symmetric positive-semidefinite matrix $P$, the maximum and minimum eigenvalues are denoted $\lambda_{\max}(P)$ and $\lambda_{\min}(P)$. For a set $E \subset \mathbb{R}^n$, we write $(E - E) := \{z_1 - z_2 \in \mathbb{R}^n \mid z_1, z_2 \in E\}$. When considering systems of the form $\dot{z} = F(t, z)$, we assume that all functions involved are sufficiently smooth to guarantee that $F: \mathbb{R}_{\geq 0} \times \mathbb{R}^n \to \mathbb{R}^n$ is piecewise continuous in $t$ and locally Lipschitz continuous in $z$, uniformly in $t$, on $\mathbb{R}_{\geq 0} \times \mathbb{R}^n$. The solution of this system, initialized at time $t_0$ with initial condition $z(t_0)$ is denoted $z(t)$. We shall often simplify notation by omitting function arguments.

## 6.2 Problem Formulation

We consider systems of the following type:

$$\dot{x} = Ax + Bu + E\phi, \quad x \in \mathbb{R}^n, \quad u \in \mathbb{R}^m, \quad \phi \in \mathbb{R}^k, \tag{6.1a}$$

$$y = Cx, \quad y \in \mathbb{R}^r, \tag{6.1b}$$

where $x$ is the state; $y$ is the output; $\phi$ is a perturbation to the system equations; and $u$ is a time-varying input that is well-defined for all $t \in \mathbb{R}_{\geq 0}$ and may include control inputs, reference signals, measured disturbances, or other known influences. For ease of notation, we introduce the vector $\nu := \mathrm{col}(u, y)$ of known signals. The perturbation is given by the expression $\phi = g(\nu, x, \theta)$, where $g: \mathbb{R}^{m+r} \times \mathbb{R}^n \times \mathbb{R}^p \to \mathbb{R}^k$ is differentiable in $\nu$ and continuously differentiable in $(x, \theta)$, and $\theta \in \mathbb{R}^p$ is a vector of constant, unknown parameters. As we construct an estimator, additional smoothness requirements may be needed for $g$, as well as other functions, to guarantee that the piecewise continuity and local Lipschitz conditions in Section 6.1.1 hold for all systems involved. It is left to the designer to check these requirements.

We shall design an observer to estimate both the state $x$ and the unknown parameter vector $\theta$. The technicalities of this observer design are most easily overcome if the time derivative $\dot{u}$ is well-defined and piecewise continuous, and $x$, $u$, $\dot{u}$, and $\theta$ are known *a priori* to belong to compact sets. We shall therefore make this assumption throughout the paper. We note that this assumption also implies that $\nu$ and $\dot{\nu}$ belong to compact sets. In most estimation problems, the restriction of the variables to compact sets is reasonable, because the states and inputs are typically derived from physical quantities with natural bounds. When designing

update laws for parameter estimates, we also assume that a parameter projection can be implemented as described in Krstić et al. (1995), restricting the parameter estimates to a compact, convex set $\Theta \subset \mathbb{R}^p$, defined slightly larger than the set of possible parameter values. The parameter projection is denoted $\mathrm{Proj}(\cdot)$. We denote by $X \subset \mathbb{R}^n$, $V \subset \mathbb{R}^{m+r}$, and $V' \subset \mathbb{R}^{m+r}$ the compact sets to which $x$, $\nu$, and $\dot{\nu}$ belong, and by $\Phi$ the compact image of $V \times X \times \Theta$ under $g$.

For ease of notation, we define

$$d(\nu, \dot{\nu}, x, \theta, \phi) := \frac{\partial g}{\partial \nu}(\nu, x, \theta)\dot{\nu} + \frac{\partial g}{\partial x}(\nu, x, \theta)(Ax + Bu + E\phi),$$

representing the time derivative of the perturbation $\phi$.

**Assumption 6.1.** *The triple $(C, A, E)$ is left-invertible and minimum-phase.*

**Assumption 6.2.** *There exists a number $\beta > 0$ such that for all $(\nu, \dot{\nu}, x, \theta, \phi) \in V \times V' \times X \times \Theta \times \Phi$ and for all $(\hat{x}, \hat{\theta}, \hat{\phi}) \in \mathbb{R}^n \times \Theta \times \mathbb{R}^k$, $\|d(\nu, \dot{\nu}, x, \theta, \phi) - d(\nu, \dot{\nu}, \hat{x}, \hat{\theta}, \hat{\phi})\| \leq \beta \|\mathrm{col}(x - \hat{x}, \theta - \hat{\theta}, \phi - \hat{\phi})\|$.*

*Remark* 6.1. In Assumption 6.2, we specify a Lipschitz-like condition on $d$, which is global in the sense that there are no bounds on $\hat{x}$ and $\hat{\phi}$. Although this condition may appear restrictive, we are free to redefine $g(\nu, x, \theta)$ outside $V \times X \times \Theta$ without altering the accuracy of the system description (6.1). We may, for example, introduce a smooth saturation on $x$ outside $X$, in which case the condition can be satisfied by requiring that $g(\nu, x, \theta)$ is sufficiently smooth.

In the following sections, we shall first present the modified high-gain observer, and then the parameter estimator. While the modified high-gain observer has a fixed structure, the parameter estimator can be designed in a number of different ways to solve the equation $\phi = g(\nu, x, \theta)$ with respect to $\theta$. In Section 6.4 we discuss several ways to design the parameter estimator.

## 6.3 Modified High-Gain Observer

Our goal is to estimate both the state $x$ and the perturbation $\phi$. To accomplish this goal we extend the system by introducing $\phi$ as a state. The extended system then becomes

$$\begin{bmatrix} \dot{x} \\ \dot{\phi} \end{bmatrix} = \begin{bmatrix} A & E \\ 0 & 0 \end{bmatrix} \begin{bmatrix} x \\ \phi \end{bmatrix} + \begin{bmatrix} B \\ 0 \end{bmatrix} u + \begin{bmatrix} 0 \\ I_k \end{bmatrix} d(\nu, \dot{\nu}, x, \theta, \phi), \tag{6.2}$$

with $y = Cx$. We shall implement an observer for this system of the following form:

$$\dot{\hat{x}} = A\hat{x} + Bu + E\hat{\phi} + K_x(\varepsilon)(y - C\hat{x}), \tag{6.3a}$$

$$\dot{z} = -\frac{\partial g}{\partial \theta}(\nu, \hat{x}, \hat{\theta})\dot{\hat{\theta}} - \frac{\partial g}{\partial x}(\nu, \hat{x}, \hat{\theta})K_x(\varepsilon)(y - C\hat{x}) + K_\phi(\varepsilon)(y - C\hat{x}), \tag{6.3b}$$

$$\hat{\phi} = g(\nu, \hat{x}, \hat{\theta}) + z. \tag{6.3c}$$

where $K_x(\varepsilon) \in \mathbb{R}^{n\times r}$ and $K_\phi(\varepsilon) \in \mathbb{R}^{k\times r}$ are gain matrices parameterized by a number $0 < \varepsilon \leq 1$ to be specified later. In (6.3), we have made use of a parameter estimate $\hat{\theta}$ and its time derivative. These values are produced by the parameter estimation module, which we shall discuss in Section 6.4. The perturbation estimate $\hat{\phi}$ is seen to consist of $g(\nu, \hat{x}, \hat{\theta})$ plus an internal variable $z$. The variable $z$ can be viewed as an adjustment made to $g(\nu, \hat{x}, \hat{\theta})$ to produce a more accurate estimate of the perturbation. Taking the time derivative of $\hat{\phi}$ yields $\dot{\hat{\phi}} = d(\nu, \dot{\nu}, \hat{x}, \hat{\theta}, \hat{\phi}) + K_\phi(\varepsilon)(y - C\hat{x})$. Defining the errors $\tilde{x} = x - \hat{x}$, $\tilde{\phi} = \phi - \hat{\phi}$, and $\tilde{y} = y - C\hat{x}$, we may therefore write the error dynamics of the observer as

$$\begin{bmatrix} \dot{\tilde{x}} \\ \dot{\tilde{\phi}} \end{bmatrix} = \begin{bmatrix} A & E \\ 0 & 0 \end{bmatrix} \begin{bmatrix} \tilde{x} \\ \tilde{\phi} \end{bmatrix} + \begin{bmatrix} 0 \\ I_k \end{bmatrix} \tilde{d} - \begin{bmatrix} K_x(\varepsilon) \\ K_\phi(\varepsilon) \end{bmatrix} \tilde{y} \tag{6.4}$$

where $\tilde{d} := d(\nu, \dot{\nu}, x, \theta, \phi) - d(\nu, \dot{\nu}, \hat{x}, \hat{\theta}, \hat{\phi})$. In the error dynamics (6.4), the term $\tilde{d}$ acts as an unknown disturbance, and $\tilde{y}$ is an available output. Our goal is to design a family of gains $K(\varepsilon) := [K_x^\mathsf{T}(\varepsilon), K_\phi^\mathsf{T}(\varepsilon)]^\mathsf{T}$ such that, as the number $\varepsilon$ becomes small, the modified high-gain observer produces stable estimates with a diminishing effect from the parameter error $\tilde{\theta} := \theta - \hat{\theta}$.

**Lemma 6.1.** *The error dynamics* (6.4) *with input $\tilde{d}$ and output $\tilde{y}$, and gain $K(\varepsilon) = 0$, is left-invertible and minimum-phase.*

*Proof.* See Appendix 6.A. □

### 6.3.1 SISO Systems

Suppose first that $k = r = 1$, and consider the error dynamics (6.4) with $K(\varepsilon) = 0$. Let $n_a$ denote the number of invariant zeros in the system, and let $n_q = n - n_a$ denote the relative degree. Let $\Lambda_1$, $\Lambda_2$, and $\Lambda_3$ denote the nonsingular state, output, and input transformations that take the system (6.4) with input $\tilde{d}$ and output $\tilde{y}$, and with $K(\varepsilon) = 0$, to the SCB. We apply these transformations to the system (6.4) (without setting $K(\varepsilon) = 0$), by writing $\mathrm{col}(\tilde{x}, \tilde{\phi}) = \Lambda_1\chi$, $\tilde{y} = \Lambda_2\gamma$, and

$\tilde{d} = \Lambda_3 \delta$. From Saberi and Sannuti (1990, Theorem 2.2), the transformed state vector $\chi$ is partitioned as $\chi = \mathrm{col}(\chi_a, \chi_q)$, where $\chi_a$ has dimension $n_a$ and $\chi_q$ has dimension $n_q$, and the resulting system is written as

$$\dot{\chi}_a = A_a \chi_a + L_{aq} \gamma - K_a(\varepsilon)\gamma, \tag{6.5a}$$

$$\dot{\chi}_q = A_q \chi_q + B_q(\delta + D_a \chi_a + D_q \chi_q) - K_q(\varepsilon)\gamma, \quad \gamma = C_q \chi_q, \tag{6.5b}$$

where

$$A_q = \begin{bmatrix} 0 & 1 & \cdots & 0 \\ \vdots & \vdots & \ddots & \vdots \\ 0 & 0 & \cdots & 1 \\ 0 & 0 & \cdots & 0 \end{bmatrix}, \quad B_q = \begin{bmatrix} 0 \\ \vdots \\ 0 \\ 1 \end{bmatrix}, \quad C_q = \begin{bmatrix} 1 & 0 & \cdots & 0 \end{bmatrix}. \tag{6.6}$$

The matrices $K_a(\varepsilon)$ and $K_q(\varepsilon)$ in (6.5) are observer gains, related to the gain $K(\varepsilon)$ by $K(\varepsilon) = \Lambda_1 [K_a^{\mathsf{T}}(\varepsilon), K_q^{\mathsf{T}}(\varepsilon)]^{\mathsf{T}} \Lambda_2^{-1}$. Once we have chosen $K_a(\varepsilon)$ and $K_q(\varepsilon)$, we can therefore implement the modified high-gain observer (6.3).

#### SCB Structure

In (6.5), the $\chi_a$ subsystem represents the zero dynamics of (6.4). In particular, the eigenvalues of the matrix $A_a$ correspond to the invariant zeros of (6.4). Since the system is minimum-phase, this implies that $A_a$ is Hurwitz. The $\chi_q$ subsystem represents the infinite zero structure of (6.4), and consists of a single chain of integrators, from the input $\delta$ to the output $\gamma$, with an interconnection to the zero dynamics at the lowest level of the integrator chain.

#### Design of SISO Gains

To design the observer gains, let $\bar{K}_q := \mathrm{col}(\bar{K}_{q_1}, \ldots, \bar{K}_{q_{n_q}})$ be chosen such that the matrix $H := A_q - \bar{K}_q C_q$ is Hurwitz. Because of the special structure of $A_q$, this is always possible by using regular pole-placement techniques. Then, let $K_a(\varepsilon) = L_{aq}$ and $K_q(\varepsilon) = \mathrm{col}(\bar{K}_{q_1}/\varepsilon, \ldots, \bar{K}_{q_{n_q}}/\varepsilon^{n_q})$.

### 6.3.2 MIMO Systems

Consider again the error dynamics (6.4) with $K(\varepsilon) = 0$. Let $n_a$ and $n_q$ denote the number of invariant zeros and infinite zeros in the system, respectively, and define $n_b = n - n_a - n_q$. Let $\Lambda_1$, $\Lambda_2$, and $\Lambda_3$ denote the nonsingular state, output, and input transformations that take the system (6.4) with input $\tilde{d}$ and output $\tilde{y}$, and with $K(\varepsilon) = 0$, to the SCB. We apply these transformations to the system

(6.4) (without setting $K(\varepsilon) = 0$), by writing $\mathrm{col}(\tilde{x}, \tilde{\phi}) = \Lambda_1 \chi$, $\tilde{y} = \Lambda_2 \gamma$, and $\tilde{d} = \Lambda_3 \delta$. From Saberi and Sannuti (1990, Th. 2.6), the transformed state $\chi$ is partitioned as $\chi = \mathrm{col}(\chi_a, \chi_b, \chi_q)$, where $\chi_a$ has dimension $n_a$, $\chi_b$ has dimension $n_b$, and $\chi_q$ has dimension $n_q$. The subsystem $\chi_q$ can be further partitioned as $\chi_q = \mathrm{col}(\chi_{q_1}, \ldots, \chi_{q_k})$, where each $\chi_{q_j}$, $j = 1, \ldots, k$, has dimension $n_{q_j}$. The transformed output is partitioned as $\gamma = \mathrm{col}(\gamma_q, \gamma_b)$, where $\gamma_q$ has dimension $k$ and is further partitioned as $\gamma_q = \mathrm{col}(\gamma_{q_1}, \ldots, \gamma_{q_k})$, and $\gamma_b$ has dimension $r_b := r - k$. The transformed input has dimension $k$ and is further partitioned as $\delta = \mathrm{col}(\delta_1, \ldots, \delta_k)$. The resulting system is written as

$$\dot{\chi}_a = A_a \chi_a + L_{aq} \gamma_q + L_{ab} \gamma_b - K_{aq}(\varepsilon) \gamma_q - K_{ab}(\varepsilon) \gamma_b, \tag{6.7a}$$

$$\dot{\chi}_b = A_b \chi_b + L_{bq} \gamma_q - K_{bq}(\varepsilon) \gamma_q - K_{bb}(\varepsilon) \gamma_b, \tag{6.7b}$$

$$\begin{aligned} \dot{\chi}_{q_j} = {} & A_{q_j} \chi_{q_j} + L_{q_j q} \gamma_q - K_{q_j q}(\varepsilon) \gamma_q - K_{q_j b}(\varepsilon) \gamma_b \\ & + B_{q_j} (\delta_j + D_{a_j} \chi_a + D_{b_j} \chi_b + D_{q_j} \chi_q), \end{aligned} \tag{6.7c}$$

$$\gamma_b = C_b \chi_b, \quad \gamma_{q_j} = C_{q_j} \chi_{q_j}, \tag{6.7d}$$

where $A_{q_j}$, $B_{q_j}$, and $C_{q_j}$ have the same special structure as $A_q$, $B_q$, and $C_q$ in Section 6.3.1, and where $(C_b, A_b)$ is an observable pair. The gains $K_{aq}(\varepsilon)$, $K_{ab}(\varepsilon)$, $K_{bq}(\varepsilon)$, $K_{bb}(\varepsilon)$, $K_{q_j q}(\varepsilon)$, and $K_{q_j b}(\varepsilon)$, $j = 1, \ldots, k$, are related to $K(\varepsilon)$ by

$$K(\varepsilon) = \Lambda_1 \begin{bmatrix} K_{aq}(\varepsilon) & K_{ab}(\varepsilon) \\ K_{bq}(\varepsilon) & K_{bb}(\varepsilon) \\ K_{qq}(\varepsilon) & K_{qb}(\varepsilon) \end{bmatrix} \Lambda_2^{-1}, \tag{6.8}$$

where

$$K_{qq}(\varepsilon) = [K_{q_1 q}^{\mathsf{T}}(\varepsilon), \ldots, K_{q_k q}^{\mathsf{T}}(\varepsilon)]^{\mathsf{T}} \text{ and } K_{qb}(\varepsilon) = [K_{q_1 b}^{\mathsf{T}}(\varepsilon), \ldots, K_{q_k b}^{\mathsf{T}}(\varepsilon)]^{\mathsf{T}}.$$

Once we have chosen $K_{aq}(\varepsilon)$, $K_{ab}(\varepsilon)$, $K_{bq}(\varepsilon)$, $K_{bb}(\varepsilon)$, $K_{qq}(\varepsilon)$, and $K_{qb}(\varepsilon)$, we can therefore implement the modified high-gain observer (6.3) with the gains given by (6.8).

### SCB Structure

As in the SISO case, the $\chi_a$ subsystem in (6.7) represents the zero dynamics of (6.4), with the eigenvalues of $A_a$ corresponding to the invariant zeros of (6.4). The system (6.7) has a $\chi_b$ subsystem that is not present in the SISO case. This subsystem represents states that are observable from the output $\gamma_b$, but that are not directly affected by any inputs. As in the SISO case, the $\chi_q$ subsystem represents the infinite zero structure of (6.4). It is divided into $k$ integrator chains, from $\delta_j$ to $\gamma_{q_j}$, with interconnections to other subsystems at the lowest level of each integrator chain.

**Design of MIMO Gains**

Let $K_{bb}(\varepsilon) = K_{bb}$ be chosen independently from $\varepsilon$ such that the matrix $A_b - K_{bb}C_b$ is Hurwitz. This is always possible and can be carried out using standard pole-placement techniques, since the pair $(C_b, A_b)$ is observable. For each $j \in 1, \ldots, k$, select $\bar{K}_{q_j} := \mathrm{col}(\bar{K}_{q_j 1}, \ldots, \bar{K}_{q_j n_{q_j}})$ such that the matrix $H_j := A_{q_j} - \bar{K}_{q_j} C_{q_j}$ is Hurwitz. Then, let $K_{aq}(\varepsilon) = L_{aq}$, $K_{ab}(\varepsilon) = L_{ab}$, $K_{bq}(\varepsilon) = L_{bq}$, $K_{qb}(\varepsilon) = 0$, and let

$$K_{q_j q} = \left[ 0_{n_{q_j} \times (j-1)} \quad \mathrm{col}\left( \frac{\bar{K}_{q_j 1}}{\varepsilon^{\bar{n}_q - n_{q_j} + 1}}, \ldots, \frac{\bar{K}_{q_j n_{q_j}}}{\varepsilon^{\bar{n}_q}} \right) \quad 0_{n_{q_j} \times (k-j)} \right] + L_{q_j q},$$

where $\bar{n}_q := \max_{j=1,\ldots,k} n_{q_j}$.

**Lemma 6.2.** *If the gains are chosen according to Section* 6.3.1 (SISO) *or Section* 6.3.2 (MIMO)*, then there exists* $0 < \varepsilon^* \leq 1$ *such that for all* $0 < \varepsilon \leq \varepsilon^*$*, the error dynamics* (6.4) *is input-to-state stable (*ISS*) with respect to* $\tilde{\theta}$*.*

*Proof.* See Appendix 6.A. □

*Remark* 6.2. By selecting the gains as described above, we place $n_a$ poles of the linear part of the observer error dynamics at the locations of the invariant zeros of (6.4), and we place $n_b$ poles freely, as the poles of $A_b - K_{bb}C_b$. The last $n_q$ poles of the error dynamics are placed far into the left-half complex plane, asymptotically as $\varepsilon$ becomes small.

*Remark* 6.3. Software packages for numeric and symbolic transformations of linear systems to the SCB are presented in Liu, Chen, and Lin (2005) and Grip and Saberi (2010).

## 6.4 Parameter Estimator

As previously mentioned, the goal of the parameter estimation module is to produce an estimate of $\theta$ based on the perturbation estimate $\hat{\phi}$ and the state estimate $\hat{x}$. For this to work, we require an update law

$$\dot{\hat{\theta}} = u_\theta(\nu, \hat{x}, \hat{\phi}, \hat{\theta}), \tag{6.9}$$

which, in the hypothetical case of perfect state and perturbation estimates ($\hat{\phi} = \phi$ and $\hat{x} = x$), would provide an unbiased asymptotic estimate of $\theta$. This requirement is formally stated by the following assumption on the dynamics of the error variable $\tilde{\theta}$.

**Assumption 6.3.** *There exist a differentiable function* $V_u: \mathbb{R}_{\geq 0} \times (\Theta - \Theta) \to \mathbb{R}_{\geq 0}$ *and positive constants* $a_1, \ldots, a_4$ *such that for all* $(t, \tilde{\theta}) \in \mathbb{R}_{\geq 0} \times (\Theta - \Theta)$,

$$a_1 \|\tilde{\theta}\|^2 \leq V_u(t, \tilde{\theta}) \leq a_2 \|\tilde{\theta}\|^2, \tag{6.10}$$

$$\frac{\partial V_u}{\partial t}(t, \tilde{\theta}) - \frac{\partial V_u}{\partial \tilde{\theta}}(t, \tilde{\theta}) u_\theta(v(t), x(t), \phi(t), \hat{\theta}) \leq -a_3 \|\tilde{\theta}\|^2, \tag{6.11}$$

$$\left\| \frac{\partial V_u}{\partial \tilde{\theta}}(t, \tilde{\theta}) \right\| \leq a_4 \|\tilde{\theta}\|. \tag{6.12}$$

*Furthermore, the update law* (6.9) *ensures that if* $\hat{\theta}(t_0) \in \Theta$, *then for all* $t \geq t_0$, $\hat{\theta}(t) \in \Theta$.

Satisfying Assumption 6.3 constitutes the greatest challenge in applying the method presented in this paper, and this issue is therefore discussed in the next section.

### 6.4.1 Satisfying Assumption 6.3

Assumption 6.3 guarantees that the origin of the error dynamics

$$\dot{\tilde{\theta}} = -u_\theta(v, \hat{x}, \hat{\phi}, \theta - \tilde{\theta}), \tag{6.13}$$

is uniformly exponentially stable with $(\Theta - \Theta)$ contained in the region of attraction whenever $\hat{\phi} = \phi$ and $\hat{x} = x$. Essentially, this amounts to asymptotically solving the inversion problem of finding $\theta$ given $\phi = g(v, x, \theta)$. In the following, we shall discuss some possibilities for how to satisfy Assumption 6.3. As a useful reference, we point to Nicosia, Tornambè, and Valigi (1994), which deals with the use of state observers for inversion of nonlinear maps. The material in this section is a straightforward adaptation of Grip et al. (2010, Sec. 3.2), which also contains examples of each of the propositions below applied to particular perturbations.[1] The proofs of the propositions are therefore omitted.

The most obvious way to satisfy Assumption 6.3 is to invert the equality $\phi = g(v, x, \theta)$ algebraically, and to let $\hat{\theta}$ be attracted to the solution. This may be possible the whole time (Proposition 6.1), or just part of the time (Proposition 6.2).

**Proposition 6.1.** *Suppose that for all* $(v, x, \phi) \in V \times \mathbb{R}^n \times \mathbb{R}^k$, *we can find a unique solution* $\theta = \theta^*(v, x, \phi)$ *from the equation* $\phi = g(v, x, \theta)$. *Then Assumption* 6.3 *is satisfied with the update law* $u_\theta(v, \hat{x}, \hat{\phi}, \hat{\theta}) = \mathrm{Proj}(\Gamma(\theta^*(v, \hat{x}, \hat{\phi}) - \hat{\theta}))$, *where* $\Gamma$ *is a symmetric, positive-definite gain matrix.*

[1] *Remark added after submission:* See footnotes on pages 126 and 128 of Chapter 5 for a technical clarification regarding piecewise continuity.

**Proposition 6.2.** *Suppose that there exists a known, piecewise continuous function* $l: V \times \mathbb{R}^n \times \mathbb{R}^k \to [0, 1]$*, and that for all* $(\nu, x, \phi) \in V \times \mathbb{R}^n \times \mathbb{R}^k$*,* $l(\nu, x, \phi) > 0$ *implies that we can find a unique solution* $\theta = \theta^*(\nu, x, \phi)$ *from the equation* $\phi = g(\nu, x, \theta)$*. Suppose furthermore that there exist* $T > 0$ *and* $\sigma > 0$ *such that for all* $t \in \mathbb{R}_{\geq 0}$*,* $\int_t^{t+T} l(\nu(\tau), x(\tau), \phi(\tau))\,\mathrm{d}\tau \geq \sigma$*. Then Assumption* 6.3 *is satisfied with the update law* $u_\theta(\nu, \hat{x}, \hat{\phi}, \hat{\theta}) = \mathrm{Proj}(l(\nu, \hat{x}, \hat{\phi})\Gamma(\theta^*(\nu, \hat{x}, \hat{\phi}) - \hat{\theta}))$*, where* $\Gamma$ *is a symmetric, positive-definite gain matrix.*

When it is not possible or desirable to solve the inversion problem explicitly, it is often possible to implement the update function as a numerical search for the solution.

**Proposition 6.3.** *Suppose that there exist a positive-definite matrix* $P$ *and a function* $M: V \times \mathbb{R}^n \times \Theta \to \mathbb{R}^{p \times k}$ *such that for all* $(\nu, x) \in V \times \mathbb{R}^n$*, and for all pairs* $\theta_1, \theta_2 \in \Theta$*,*

$$M(\nu, x, \theta_1)\frac{\partial g}{\partial \theta}(\nu, x, \theta_2) + \frac{\partial g}{\partial \theta}^{\mathsf{T}}(\nu, x, \theta_2)M^{\mathsf{T}}(\nu, x, \theta_1) \geq 2P. \tag{6.14}$$

*Then Assumption* 6.3 *is satisfied with the update law*

$$u_\theta(\nu, \hat{x}, \hat{\phi}, \hat{\theta}) = \mathrm{Proj}(\Gamma M(\nu, \hat{x}, \hat{\theta})(\hat{\phi} - g(\nu, \hat{x}, \hat{\theta}))),$$

*where* $\Gamma$ *is a symmetric, positive-definite gain matrix.*

Proposition 6.3 applies to certain monotonic perturbations for which a solution can be found arbitrarily fast by increasing the gain $\Gamma$. In many cases this is not possible, because the inversion problem is singular the whole time or part of the time. The following proposition applies to cases where a solution is only available by using data over longer periods of time, by incorporating a persistency-of-excitation condition.

**Proposition 6.4.** *Suppose that there exist a piecewise continuous function* $S: V \times \mathbb{R}^n \to \mathbb{S}_{p+}$*, where* $\mathbb{S}_{p+}$ *is the cone of* $p \times p$ *positive-semidefinite matrices, and a function* $M: V \times \mathbb{R}^n \times \Theta \to \mathbb{R}^{p \times k}$*, both bounded for bounded* $x$*, such that for all* $(\nu, x) \in V \times \mathbb{R}^n$ *and for all pairs* $\theta_1, \theta_2 \in \Theta$*,*

$$M(\nu, x, \theta_1)\frac{\partial g}{\partial \theta}(\nu, x, \theta_2) + \frac{\partial g}{\partial \theta}^{\mathsf{T}}(\nu, x, \theta_2)M^{\mathsf{T}}(\nu, x, \theta_1) \geq 2S(\nu, x). \tag{6.15}$$

*Suppose furthermore that there exist numbers* $T > 0$ *and* $\sigma > 0$ *such that for all* $t \in \mathbb{R}_{\geq 0}$*,* $\int_t^{t+T} S(\nu(\tau), x(\tau))\,\mathrm{d}\tau \geq \sigma I_p$*, and a number* $L_g > 0$ *such that for all*

$(v, x, \hat{\theta}) \in V \times \mathbb{R}^n \times \Theta$, $\|g(v, x, \theta) - g(v, x, \hat{\theta})\| \leq L_g(\tilde{\theta}^\mathsf{T} S(v, x)\tilde{\theta})^{1/2}$. *Then Assumption* 6.3 *is satisfied with the update law*

$$u_\theta(v, \hat{x}, \hat{\phi}, \hat{\theta}) = \mathrm{Proj}(\Gamma M(v, \hat{x}, \hat{\theta})(\hat{\phi} - g(v, \hat{x}, \hat{\theta}))),$$

*where* $\Gamma$ *is a symmetric, positive-definite gain matrix.*

When looking for the function $M$, a good starting point is to select

$$M(v, \hat{x}, \hat{\theta}) = [\partial g/\partial\theta]^\mathsf{T}(v, \hat{x}, \hat{\theta}).$$

This choice makes the parameter update law into a gradient search in the direction of steepest descent for the function $\|g(v, x, \theta) - g(v, x, \hat{\theta})\|^2$, scaled by the gain $\Gamma$. This choice of $M$ often works even if it fails to satisfy either of Propositions 6.3 and 6.4. In the special case of a linear parameterization, this choice of $M$ always satisfies (6.15), and the remaining conditions in Proposition 6.4 coincide with standard persistency-of-excitation conditions for parameter identification in linear adaptive theory (see, e.g., Marino and Tomei, 1995, Ch. 5).

## 6.5 Stability of Interconnected System

When connecting the two modules, we need one additional assumption about the parameter update law.

**Assumption 6.4.** *The parameter update law* $u_\theta(v, \hat{x}, \hat{\phi}, \hat{\theta})$ *is Lipschitz continuous in* $(\hat{x}, \hat{\phi})$*, uniformly in* $(v, \hat{\theta})$*, on* $V \times \mathbb{R}^n \times \mathbb{R}^k \times \Theta$.

*Remark* 6.4. The Lipschitz condition in Assumption 6.4 is a global one, in the sense that $\hat{x}$ and $\hat{\phi}$ are not presumed to be bounded. Such a condition may fail to hold in many cases. However, if a local Lipschitz condition holds, then the update law is easily modified to satisfy Assumption 6.4 by introducing a saturation on $\hat{x}$ and $\hat{\phi}$ outside $X$ and $\Phi$. We also remark that when checking Assumption 6.4, the projection in the update law may be disregarded, since the Lipschitz property is retained under projection (Grip et al., 2010, App. A).

**Theorem 6.1.** *If the gains are chosen according to Section* 6.3.1 (SISO) *or Section* 6.3.2 (MIMO)*, then there exists* $0 < \varepsilon^* \leq 1$ *such that for all* $0 < \varepsilon \leq \varepsilon^*$*, the origin of the error dynamics* (6.4)*,* (6.13) *is exponentially stable with* $\mathbb{R}^{n+k} \times (\Theta - \Theta)$ *contained in the region of attraction.*

*Proof.* See Appendix 6.A. □

## 6.6 Redesign for Improved State Estimates

The modified high-gain observer is designed to estimate not only the state vector $x$, but also the perturbation $\phi$. This configuration may not result in optimal estimates of $x$. In many cases, less noisy estimates may be obtained by implementing a second observer that does not include a perturbation estimate. Instead, this observer has the form $\dot{\hat{x}} = A\hat{x} + Bu + Eg(\nu, \hat{x}, \hat{\theta}) + K_x(\varepsilon)(y - C\hat{x})$, with $\hat{\theta}$ obtained from the first observer. The second observer can be designed using the same high-gain methodology as the modified high-gain observer, by transforming the error dynamics $\dot{\tilde{x}} = A\tilde{x} + E\tilde{g} - K_x(\varepsilon)\tilde{y}$ to the form (6.7) and designing gains. In this case, $\tilde{g} := g(\nu, x, \theta) - g(\nu, \hat{x}, \hat{\theta})$, rather than $\tilde{d}$, is the input that is transformed to $\delta$, and we need to impose the same Lipschitz-like assumptions on $g$ as we previously did on $d$. The resulting ISS property of the second observer with respect to the parameter error $\tilde{\theta}$, and the boundedness of $\tilde{\theta}$, justifies this type of cascaded design.

## 6.7 Discussion

The purpose of the modified high-gain observer described in Section 6.3 is to estimate the states and the perturbation with sufficient accuracy to guarantee stability in closed loop with the parameter estimator. The design methodology in Section 6.3 ensures that this is possible by making the parameter $\varepsilon$ sufficiently small. As implied by the name, a high gain may sometimes be required to achieve stability. Such cases are of little practical interest, because a high gain usually results in unacceptable noise amplification. Often, however, only a moderate gain is required. Since the required gain depends on quantities that are difficult to determine analytically, such as Lipschitz constants, the observer is typically tuned by starting with $\varepsilon = 1$ and decreasing $\varepsilon$ in small decrements until satisfactory performance is achieved.

### 6.7.1 Zero Structure

The zero structure of the system is of vital importance in the design methodology presented in this paper, as it is for any design methodology that deals with a partial-state measurement. This fact is made explicitly clear by the decomposition of the system into subsystems representing the finite and infinite zero structure. It is well-known that small perturbations to system matrices can lead to dramatic changes in a system's zero structure. This phenomenon is investigated in Sastry, Hauser, and Kokotović (1989), where it is shown that an arbitrarily small perturba-

tion can reduce the relative degree of a SISO system, and thereby move some zeros from infinity to finite locations far into the left- or right-half plane. This leads to zero dynamics that are singularly perturbed. Such a perturbation reduces the dimension of the $\chi_q$ subsystem and increases the dimension of the $\chi_a$ subsystem, and it creates singularities in the elements of the SCB system matrices where the perturbation is zero. Not surprisingly, this can lead to poorly conditioned system descriptions, with very large elements in the system matrices. In these situations, it is often better to design the observer gains with respect to the unperturbed system matrices, by setting the perturbation to zero before performing the transformation to the SCB.[2] In Section 6.8, we discuss a problem for which this precise situation is encountered.

## 6.8 Simulation Example

We consider the example of a DC motor with friction modeled by the LuGre friction model, borrowed from Canudas de Wit and Lischinsky (1997). The model is described by $\dot{\Omega} = \omega$, $J\dot{\omega} = u - F$, where $\Omega$ is the measured angular position, $\omega$ is the angular velocity, $u$ is the motor torque, $F$ is the friction torque, and $J$ is the motor and load inertia. The friction torque is given by the dynamic LuGre friction model: $F = \sigma_0\eta + \sigma_1\dot{\eta} + \alpha_2\omega$, where the internal friction state $\eta$ is given by $\dot{\eta} = \omega - \sigma_0\eta|\omega|/\zeta(\omega)$, with $\zeta(\omega) = \alpha_0 + \alpha_1\exp(-(\omega/\omega_0)^2)$. The model parameters are listed in Table 6.1. We assume that these parameters are known, except for the uncertain parameter $\theta := \alpha_0$, which represents static Coloumb friction. To indicate that $\zeta$ depends on the unknown parameter, we shall henceforth write $\zeta(\omega, \theta)$. We assume that $\theta$ is known *a priori* to belong to the range $\Theta := [0.05\ \text{Nm}, 1\ \text{Nm}]$. Following the notation from previous sections, we write $x = \text{col}(\Omega, \omega, \eta)$, $y = \Omega$, and $\nu = \text{col}(u, y)$. Let us define the perturbation $\phi = g(\nu, x, \theta) := \sigma_0\eta|\omega|/\zeta(\omega, \theta)$. It is straightforward to confirm that the system with input $\phi$ and output $\Omega$ is left-invertible and minimum-phase, as required by Assumption 6.1. By extending the state space as described in Section 6.3, we obtain the system $\dot{\Omega} = \omega$, $J\dot{\omega} = u - (\alpha_2 + \sigma_1)\omega - \sigma_0\eta + \sigma_1\phi$, $\dot{\eta} = \omega - \phi$, $\dot{\phi} = d(\nu, x, \theta, \phi)$.

A technical problem arises due to the presence of $|\omega|$ in the perturbation, which causes the Lipschitz-like condition on $d$ in Assumption 6.2 to fail. In the observer we therefore approximate the absolute value function by $|\omega| \approx a(\omega) := \omega^2/(2\kappa) + \kappa/2$ on the interval $[-\kappa, \kappa]$, where $\kappa$ is a small number that we choose as 0.1. This approximation is continuously differentiable.

[2] Note that in this context, we are referring to a perturbation of the system matrices, not to $\phi$.

### 6.8.1 Observer Design

We start the observer design by creating a modified high-gain observer according to Section 6.3. We then obtain error dynamics of the form (6.4):

$$\begin{bmatrix} \dot{\tilde{\Omega}} \\ \dot{\tilde{\omega}} \\ \dot{\tilde{\eta}} \\ \dot{\tilde{\phi}} \end{bmatrix} = \begin{bmatrix} 0 & 1 & 0 & 0 \\ 0 & -\frac{1}{J}(\alpha_2+\sigma_1) & -\frac{1}{J}\sigma_0 & \frac{1}{J}\sigma_1 \\ 0 & 1 & 0 & -1 \\ 0 & 0 & 0 & 0 \end{bmatrix} \begin{bmatrix} \tilde{\Omega} \\ \tilde{\omega} \\ \tilde{\eta} \\ \tilde{\phi} \end{bmatrix} + \begin{bmatrix} 0 \\ 0 \\ 0 \\ 1 \end{bmatrix} \tilde{d} - \begin{bmatrix} K_x(\varepsilon) \\ K_\phi(\varepsilon) \end{bmatrix} \tilde{\Omega}, \tag{6.16}$$

where $K_x(\varepsilon)$ and $K_\phi(\varepsilon)$ are to be designed. Using the software from Grip and Saberi (2010) to transform the error dynamics to the SCB, we obtain

$$\begin{aligned} \dot{\chi}_a &= -\frac{\sigma_0}{\sigma_1}\chi_a - \frac{\sigma_0^2(-\sigma_1\alpha_2 + J\sigma_0)}{\sigma_1^4}\gamma - K_a(\varepsilon)\gamma, \\ \dot{\chi}_{q_1} &= \chi_{q_2} - K_{q_1}(\varepsilon)\gamma, \quad \dot{\chi}_{q_2} = \chi_{q_2} - K_{q_2}(\varepsilon)\gamma, \\ \dot{\chi}_{q_3} &= \frac{\sigma_0^2(-\sigma_1\alpha_2 + J\sigma_0)}{J\sigma_1^3}\chi_{q_1} + \frac{\sigma_0(\sigma_1\alpha_2 - J\sigma_0)}{J\sigma_1^2}\chi_{q_2} \\ &\quad + \frac{J\sigma_0 - \sigma_1\alpha_2 - \sigma_1^2}{\sigma_1 J}\chi_{q_3} + \frac{\sigma_0}{J}\chi_a + \delta - K_{q_3}(\varepsilon)\gamma, \quad \gamma = \chi_{q_1}. \end{aligned}$$

We may now proceed to design the gains according to Section 6.3.1. However, we quickly discover that the problem is poorly conditioned, and that, consequently, we require an unacceptably large gain. Some elements of the SCB system matrices are very large, due to powers of the small constant $\sigma_1$ in the denominators and powers of the large constant $\sigma_0$ in the numerators. The constant $\sigma_1$ can be viewed as a small perturbation to the system matrices in (6.16), which fundamentally alters the

| Parameter | Value | Parameter | Value |
|---|---|---|---|
| $J$ | 0.0023 kg m$^2$ | $\alpha_0$ | 0.28 Nm |
| $\sigma_0$ | 260.0 Nm/rad | $\alpha_1$ | 0.05 Nm |
| $\sigma_1$ | 0.6 Nm s/rad | $\alpha_2$ | 0.176 Nm s/rad |
| $\omega_0$ | 0.01 rad/s | | |

**Table 6.1:** Numerical values for simulation example

zero structure of the system by reducing the relative degree. This is indicated by the zero dynamics subsystem, which is singularly perturbed with respect to $\sigma_1$. As discussed in Section 6.7.1, it is better to design the gains with respect to the system obtained by setting $\sigma_1 = 0$. We then obtain the simplified design system

$$\begin{bmatrix} \dot{\tilde{\Omega}} \\ \dot{\tilde{\omega}} \\ \dot{\tilde{\eta}} \\ \dot{\tilde{\phi}} \end{bmatrix} = \begin{bmatrix} 0 & 1 & 0 & 0 \\ 0 & -\frac{1}{J}\alpha_2 & -\frac{1}{J}\sigma_0 & 0 \\ 0 & 1 & 0 & -1 \\ 0 & 0 & 0 & 0 \end{bmatrix} + \begin{bmatrix} 0 \\ 0 \\ 0 \\ 1 \end{bmatrix} \tilde{d} - \begin{bmatrix} K_x(\varepsilon) \\ K_\phi(\varepsilon) \end{bmatrix} \tilde{\Omega},$$

which is transformed to

$$\dot{\chi}_{q_1} = \chi_{q_2} - K_{q_1}(\varepsilon)\gamma, \quad \dot{\chi}_{q_2} = \chi_{q_3} - K_{q_2}(\varepsilon)\gamma,$$
$$\dot{\chi}_{q_3} = \chi_{q_4} - K_{q_3}(\varepsilon)\gamma, \quad \dot{\chi}_{q_4} = -\frac{\sigma_0}{J}\chi_{q_3} - \frac{\alpha_2}{J}\chi_{q_4} + \delta - K_{q_4}(\varepsilon)\gamma, \quad \gamma = \chi_{q_1}.$$

We now design the gains according to Section 6.3.1, placing the poles of $H = A_q - \bar{K}_q C_q$ at $-1 \pm 0.2j$ and $-2 \pm 0.2j$.

To design the parameter estimator, we note that whenever $\phi \neq 0$, we have $\theta = \sigma_0 \eta |\omega| / \phi - \alpha_1 \exp(-(\omega/\omega_0)^2)$. We may therefore apply Proposition 6.2, by defining $\dot{\hat{\theta}} = \text{Proj}(l(\nu, \hat{x}, \hat{\phi})\Gamma(\theta^*(\nu, \hat{x}, \hat{\theta}) - \hat{\theta}))$, where $\theta^*$ represents the algebraic solution $\theta^*(\nu, \hat{x}, \hat{\phi}) := \sigma_0 \hat{\eta} a(\hat{\omega})/\hat{\phi} - \alpha_1 \exp(-(\hat{\omega}/\omega_0)^2)$, found whenever $l(\nu, \hat{x}, \hat{\phi}) > 0$. We define $l(\nu, \hat{x}, \hat{\phi})$ as $l(\nu, \hat{x}, \hat{\phi}) = 1$ when $|\hat{\phi}| \geq 1$, and $l(\nu, \hat{x}, \hat{\phi}) = 0$ otherwise, and choose the gain $\Gamma = 1$. According to Proposition 6.2, this approach works, assuming that $|\phi| > 1$ is guaranteed to occur some portion of the time.

*Remark* 6.5. For simplicity, we have ignored a couple of technicalities in the example: we have not used any projections or saturations; and we have defined $l(\nu, \hat{x}, \hat{\phi})$ to be discontinuous in $\hat{\phi}$, thereby breaking the Lipschitz condition in Assumption 6.4. It is easy to redefine $l(\nu, \hat{x}, \hat{\phi})$ to fix this problem.

### 6.8.2 Simulation Results

We simulate with the output $y$ corrupted by noise. The noisy output can be seen together with the actual angular position $\Omega$ in Figure 6.2. Using $\varepsilon = 1$ gives stable estimates, which results in the gains $K(\varepsilon) \approx [6, 13, 0, 13]^\mathsf{T}$. To improve the state estimates, we use the redesign discussed in Section 6.6, by creating a second observer that uses the parameter estimate $\hat{\theta}$ from the first observer. Since in this case, Lipschitz-like conditions must only be placed on $g$, and not on the derivative $d$, we can implement $g(\nu, \hat{x}, \hat{\theta})$ in the second observer without using

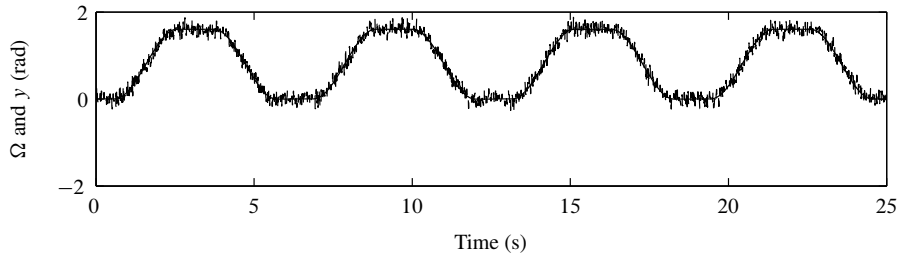


**Figure 6.2:** Angular position Ω (solid) and noisy measurement $y$ (dashed)

the continuously differentiable approximation of the absolute value. We follow the same high-gain methodology to construct the second observer, placing the poles of the matrix $H$ at $-1 \pm 0.2j$ and $-2$ and selecting $\varepsilon = 1$, which gives the gains $K(\varepsilon) \approx [4, 5, 0]^{\mathsf{T}}$. The resulting state estimates can be seen in Figure 6.3, together with the parameter estimate.

## 6.9 Concluding Remarks

We have presented an observer design methodology for linear systems with nonlinearly parameterized perturbations. As illustrated by the simulation example from Section 6.8, this design methodology can yield good results when applied to a system with noise-corrupted measurements. By estimating unknown parameters in the nonlinear perturbation, we avoid having to suppress the effect of these unknowns using high gain alone, and we thereby reduce noise sensitivity of the observer estimates compared to a pure high-gain design. By decomposing the linear part of the error dynamics to the SCB, which explicitly reveals the system's zero structure and invertibility properties, we are able to treat a large class of MIMO systems.

## Acknowledgments

The work of Håvard Fjær Grip is supported by the Research Council of Norway. The work of Ali Saberi is partially supported by National Science Foundation grant NSF-0901137 and NAVY grants ONR KKK777SB001 and ONR KKK760SB0012.

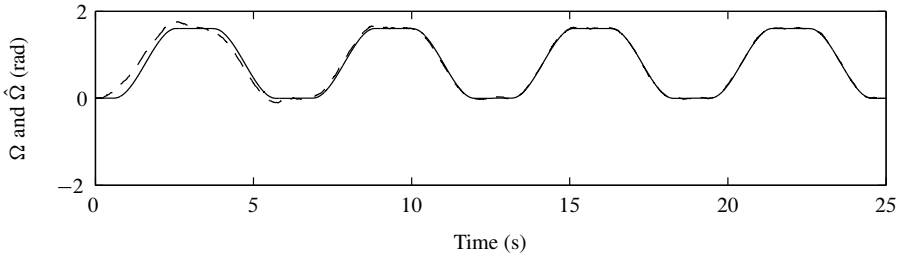


(a) Angular position $\Omega$ (solid) and estimate $\hat{\Omega}$ (dashed)

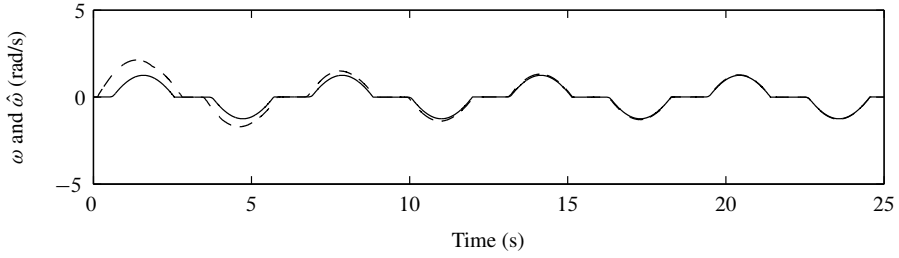


(b) Angular velocity $\omega$ (solid) and estimate $\hat{\omega}$ (dashed)

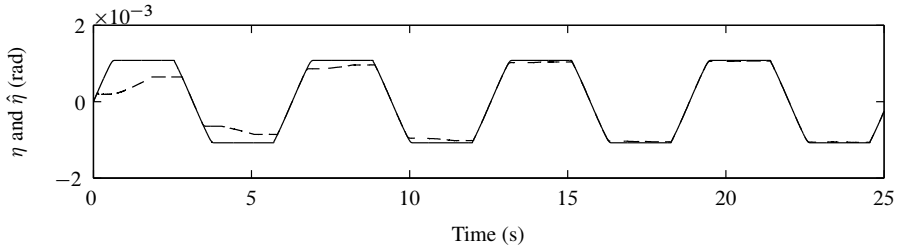


(c) Internal friction state $\eta$ (solid) and estimate $\hat{\eta}$ (dashed)

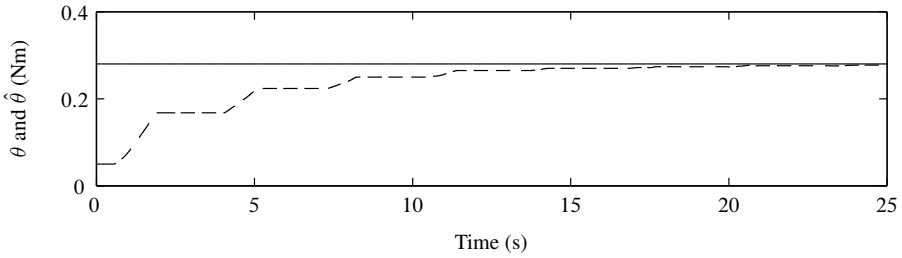


(d) Unknown parameter $\theta$ (solid) and parameter estimate $\hat{\theta}$ (dashed)

**Figure 6.3:** Simulation results

## 6.A Proofs

*Proof of Lemma* 6.1. The error dynamics (6.4) with $K(\varepsilon) = 0$ consists of a system described by the left-invertible, minimum-phase triple $(C, A, E)$, augmented by adding an integrator at each input point. Because integrators are left-invertible, it follows from the definition of left-invertibility that the augmented system is also left-invertible. The invariant zeros of a left-invertible triple $(C, A, E)$ are the values of $z$ for which the Rosenbrock system matrix $\left[\begin{smallmatrix} zI-A & -E \\ -C & 0 \end{smallmatrix}\right]$ loses rank. It is easy to confirm that when the triple $(C, A, E)$ is augmented with an integrator at each input point, the resulting Rosenbrock system matrix loses rank for precisely the same values of $z$ as before, and hence the invariant zeros (and the minimum-phase property) remain the same. □

*Proof of Lemma* 6.2. This proof is based on the theory of Saberi and Sannuti (1990). The proof is stated for the MIMO case, but is valid for SISO systems as a special case. Define $\xi_a = \chi_a$, $\xi_b = \chi_b$, and $\xi_q = \mathrm{col}(\xi_{q_1}, \ldots, \xi_{q_k})$, where for each $j \in 1, \ldots, k$, $\xi_{q_j} := S_j \chi_{q_j}$, where $S_j = \varepsilon^{\bar{n}_q - n_{q_j}} \mathrm{diag}(1, \ldots, \varepsilon^{n_{q_j}-1})$. We then obtain the following equations:

$$\dot{\xi}_a = A_a \xi_a, \quad \dot{\xi}_b = (A_b - K_{bb} C_b)\xi_b, \tag{6.17a}$$

$$\varepsilon \dot{\xi}_{q_j} = H_j \xi_{q_j} + B_{q_j} \varepsilon^{\bar{n}_q} (D_{a_j} \xi_a + D_{b_j} \xi_b + \delta_j + D^{\varepsilon}_{q_j} \xi_q), \tag{6.17b}$$

where $D^{\varepsilon}_{q_j} = D_{q_j} \mathrm{diag}(S_1^{-1}, \ldots, S_k^{-1})$. Let $P_a$, $P_b$, and $P_{q_j}$, $j = 1, \ldots, k$, be the symmetric, positive-definite solutions of the Lyapunov equations $P_a A_a + A_a^{\mathsf{T}} P_a = -I_{n_a}$, $P_b(A_b - K_{bb}C_b) + (A_b - K_{bb}C_b)^{\mathsf{T}} P_b = -I_{n_b}$, and $P_{q_j} H_j + H_j^{\mathsf{T}} P_{q_j} = -I_{n_{q_j}}$, respectively. Define

$$W = \xi_a^{\mathsf{T}} P_a \xi_a + \xi_b^{\mathsf{T}} P_b \xi_b + \varepsilon \sum_{j=1}^{k} \xi_{q_j}^{\mathsf{T}} P_{q_j} \xi_{q_j}.$$

We then have

$$\dot{W} \leq -\|\xi_a\|^2 - \|\xi_b\|^2 - \sum_{j=1}^{k} \|\xi_{q_j}\|^2 + \varepsilon^{\bar{n}_q} \sum_{j=1}^{k} 2\|P_{q_j}\| \times (\|D_{a_j}\|\|\xi_a\| + \|D_{b_j}\|\|\xi_b\| + \|\delta_j\| + \|D^{\varepsilon}_{q_j}\|\|\xi_q\|)\|\xi_{q_j}\|.$$

From the Lipschitz-like condition on $d$ from Assumption 6.2, we know that for each $j \in 1, \ldots, k$, there exist constants $\beta_{a_j}$, $\beta_{b_j}$, $\beta_{\theta_j}$, and $\beta_{q_j}$ such that

$$\|\delta_j\| \leq \beta_{a_j}\|\chi_a\| + \beta_{b_j}\|\chi_b\| + \beta_{\theta_j}\|\tilde{\theta}\| + \beta_{q_j}\|\chi_q\|,$$

which means that $\|\delta_j\| \le \beta_{a_j}\|\xi_a\| + \beta_{b_j}\|\xi_b\| + \beta_{\theta_j}\|\tilde{\theta}\| + \varepsilon^{-(\bar{n}_q-1)}\beta_{q_j}\|\xi_q\|$. We furthermore have $\|D^{\varepsilon}_{q_j}\| \le \varepsilon^{-(\bar{n}_q-1)}\|D_{q_j}\|$.

Let $\rho_a = \sum_{j=1}^{k} 2\|P_{q_j}\|(\|D_{a_j}\| + \beta_{a_j})$, $\rho_b = \sum_{j=1}^{k} 2\|P_{q_j}\|(\|D_{b_j}\| + \beta_{b_j})$, $\rho_q = \sum_{j=1}^{k} 2\|P_{q_j}\|(\|D_{q_j}\| + \beta_{q_j})$, and $\rho_\theta = \sum_{j=1}^{k} 2\|P_{q_j}\|\beta_{\theta_j}$. Then we may write

$$\begin{aligned}\dot{W} \le &-\|\xi_a\|^2 - \|\xi_b\|^2 - (1-\varepsilon\rho_q)\|\xi_q\|^2 \\ &+ \varepsilon^{\bar{n}_q}\rho_a\|\xi_a\|\|\xi_q\| + \varepsilon^{\bar{n}_q}\rho_b\|\xi_b\|\|\xi_q\| + \varepsilon^{\bar{n}_q}\rho_\theta\|\tilde{\theta}\|\|\xi_q\|.\end{aligned}$$

Note that $\rho_q$ is multiplied by $\varepsilon$. Furthermore, note that the cross terms between $\|\xi_a\|$ and $\|\xi_q\|$, and between $\|\xi_b\|$ and $\|\xi_q\|$, are multiplied by $\varepsilon^{\bar{n}_q}$ relative to the stabilizing quadratic terms in $\|\xi_a\|^2$, $\|\xi_b\|^2$, and $\|\xi_q\|^2$. It is therefore straightforward to show that, by decreasing $\varepsilon$, the cross terms are dominated, and there exist positive constants $c_a$, $c_b$, and $c_q$ such that $\dot{W} \le -c_a\|\xi_a\|^2 - c_b\|\xi_b\|^2 - c_q\|\xi_q\|^2 + \varepsilon^{\bar{n}_q}\rho_\theta\|\tilde{\theta}\|\|\xi_q\|$. This expression shows that $\dot{W}$ is negative outside a ball around the origin, the size of which is proportional to $\tilde{\theta}$. From Khalil (2002, Th. 4.19), we conclude that (6.17) is ISS with respect to $\tilde{\theta}$. Since (6.17) is obtained through a nonsingular transformation of (6.4), the same holds for (6.4). □

*Proof of Theorem* 6.1. We first note that Assumption 6.3 ensures that if $\hat{\theta}(t_0) \in \Theta$, then for all $t \in \mathbb{R}_{\ge 0}$, $\hat{\theta}(t) \in \Theta$. From Lemma 6.2, the error dynamics (6.4) is ISS with respect to $\tilde{\theta}$. Hence, any trajectory of (6.4), (6.13) originating in $\mathbb{R}^{n+k} \times (\Theta - \Theta)$ remains in a compact subset of $\mathbb{R}^{n+k} \times (\Theta - \Theta)$ for all future time. In the remainder of this proof, we shall deal with the transformed system (6.17) from the proof of Lemma 6.2, and prove that this system, together with (6.13), is exponentially stable with $\mathbb{R}^{n+k} \times (\Theta - \Theta)$ contained in the region of attraction. This will imply that the theorem holds with respect to the error dynamics (6.4), (6.13). Based on Assumption 6.4, we know, by following the same argument as for $\|\delta_j\|$ in the proof of Lemma 6.2, that there exist positive constants $\bar{\beta}_a$, $\bar{\beta}_b$, $\bar{\beta}_q$ such that $\|u_\theta(\nu, x, \phi, \hat{\theta}) - u_\theta(\nu, \hat{x}, \hat{\phi}, \hat{\theta})\| \le \bar{\beta}_a\|\xi_a\| + \bar{\beta}_b\|\xi_b\| + \varepsilon^{-(\bar{n}_q-1)}\bar{\beta}_q\|\xi_q\|$. Define $V := W + \varepsilon^{2\bar{n}_q-1}V_u$, where $W$ is from the proof of Lemma 6.2. We then obtain

$$\begin{aligned}\dot{V} \le &-c_a\|\xi_a\|^2 - c_b\|\xi_b\|^2 - c_q\|\xi_q\|^2 - a_3\varepsilon^{2\bar{n}_q-1}\|\tilde{\theta}\|^2 \\ &+ \varepsilon^{\bar{n}_q}[(\rho_\theta + a_4\bar{\beta}_q)\|\xi_q\| + a_4\bar{\beta}_a\|\xi_a\| + a_4\bar{\beta}_b\|\xi_b\|]\|\tilde{\theta}\|.\end{aligned}$$

To show that we may dominate all the cross terms in the expression above by decreasing $\varepsilon$, note that for arbitrary positive constants $\alpha_1$, $\alpha_2$, and $\alpha_3$, the expression $-\alpha_1\zeta_1^2 - \alpha_2\varepsilon^{2\bar{n}_q-1}\zeta_2^2 + \alpha_3\varepsilon^{\bar{n}_q}\zeta_1\zeta_2$ can be made negative definite by selecting $\varepsilon < 4\alpha_1\alpha_2/\alpha_3^2$. Since we may split out expressions like the one above for each of

the cross terms (by letting $\alpha_1$ and $\alpha_2$ be small fractions of the negative quadratic terms, and $\alpha_3$ the constant in the cross term) and make them negative definite by decreasing $\varepsilon$, it is clear that there exists $\varepsilon^*$ and a constant $c > 0$ such that for all $0 < \varepsilon < \varepsilon^*$, $\dot{V} \leq -c(\|\xi_a\|^2 + \|\xi_b\|^2 + \|\xi_q\|^2 + \|\tilde{\theta}\|^2)$. This expression holds on the set $\mathbb{R}^{n+k} \times (\Theta - \Theta)$. By invoking the comparison lemma (Khalil, 2002, Lemma 3.4), we may therefore conclude that the origin of (6.17), (6.13) is exponentially stable with $\mathbb{R}^{n+k} \times (\Theta - \Theta)$ contained in the region of attraction, and the same holds for (6.4), (6.13). □

# Bibliography

A. M. Annaswamy, F. P. Skantze, and A.-P. Loh. Adaptive control of continuous time systems with convex/concave parametrization. *Automatica*, 34(1):33–49, 1998.

J. D. Bošković. Adaptive control of a class of nonlinearly parameterized plants. *IEEE Trans. Automat. Contr.*, 43(7):930–934, 1998.

R. G. Brown and P. Y. C. Hwang. *Introduction to Random Signals and Applied Kalman Filtering*. Wiley, New York, 3rd edition, 1997.

C. Canudas de Wit and P. Lischinsky. Adaptive friction compensation with partially known dynamic friction model. *Int. J. Adapt. Contr. Signal Process.*, 11 (1):65–80, 1997.

A. Chakrabortty and M. Arcak. Time-scale separation redesigns for stabilization and performance recovery of uncertain nonlinear systems. *Automatica*, 45(1): 34–44, 2009.

V. Fomin, A. Fradkov, and V. Yakubovich, editors. *Adaptive Control of Dynamical Systems*. Nauka, Moskow, 1981.

L. B. Freidovich and H. K. Khalil. Performance recovery of feedback-linearization-based designs. *IEEE Trans. Automat. Contr.*, 53(10):2324–2334, 2008.

H. F. Grip and A. Saberi. Structural decomposition of linear multivariable systems using symbolic computations. *Int. J. Contr.*, 2010. Accepted.

H. F. Grip, T. A. Johansen, and L. Imsland. Estimation and control for systems with nonlinearly parameterized perturbations. In *Proc. IFAC World Congr.*, pages 11178–11183, Seoul, South Korea, 2008.

H. F. Grip, T. A. Johansen, L. Imsland, and G.-O. Kaasa. Parameter estimation and compensation in systems with nonlinearly parameterized perturbations. *Automatica*, 46(1):19–28, 2010.

H. Khalil and F. Esfandiari. Semiglobal stabilization of a class of nonlinear systems using output feedback. *IEEE Trans. Automat. Contr.*, 38(9):1412–1415, 1993.

H. K. Khalil. Adaptive output feedback control of nonlinear systems represented by input-output models. *IEEE Trans. Automat. Contr.*, 41(2):177–188, 1996.

H. K. Khalil. *Nonlinear Systems*. Prentice-Hall, Upper Saddle River, NJ, 3rd edition, 2002.

M. Krstić, I. Kanellakopoulos, and P. V. Kokotović. *Nonlinear and Adaptive Control Design*. Wiley, New York, 1995.

X. Liu, B. M. Chen, and Z. Lin. Linear systems toolkit in Matlab: Structural decompositions and their applications. *J. Contr. Theor. Appl.*, 3(3):287–294, 2005.

R. Marino and P. Tomei. *Nonlinear Control Design: Geometric, Adaptive and Robust*. Prentice-Hall, Upper Saddle River, NJ, 1995.

S. Nicosia, A. Tornambè, and P. Valigi. Nonlinear map inversion via state observers. *Circ. Syst. Signal Process.*, 13(5):571–589, 1994.

Z. Qu. Adaptive and robust controls of uncertain systems with nonlinear parameterization. *IEEE Trans. Automat. Contr.*, 48(10):1817–1823, 2003.

A. Saberi and P. Sannuti. Observer design for loop transfer recovery and for uncertain dynamical systems. *IEEE Trans. Automat. Contr.*, 35(8):878–897, 1990.

P. Sannuti and A. Saberi. Special coordinate basis for multivariable linear systems—Finite and infinite zero structure, squaring down and decoupling. *Int. J. Contr.*, 45(5):1655–1704, 1987.

S. Sastry, J. Hauser, and P. V. Kokotović. Zero dynamics of regularly perturbed systems may be singularly perturbed. *Syst. Contr. Lett.*, 13(4):299–314, 1989.

A. Teel and L. Praly. Global stabilizability and observability imply semi-global stabilizability by output feedback. *Syst. Contr. Lett.*, 22(5):313–325, 1994.

I. Y. Tyukin, D. V. Prokhorov, and C. van Leeuwen. Adaptation and parameter estimation in systems with unstable target dynamics and nonlinear parametrization. *IEEE Trans. Automat. Contr.*, 52(9):1543–1559, 2007.

T. Zhang, S. S. Ge, C. C. Hang, and T. Y. Chai. Adaptive control of first-order systems with nonlinear parameterization. *IEEE Trans. Automat. Contr.*, 45(8): 1512–1516, 2000.

# Chapter 7

# Structural Decomposition of Linear Multivariable Systems Using Symbolic Computations

***Abstract:*** *We introduce a procedure written in the mathematics software suite Maple, which transforms linear time-invariant systems to a special coordinate basis that reveals the internal structure of the system. The procedure creates exact decompositions, based on matrices that contain elements represented by symbolic variables or exact fractions. Throughout the procedure, transformations are constructed with the goal of avoiding unnecessary changes to the original states. The procedure is intended to complement numerical software algorithms developed by others for the same purpose. We discuss various system-theoretic aspects of the special coordinate basis as well as numerical issues related to the decomposition procedure, and illustrate use of the procedure by examples.*

## 7.1 Introduction

In 1987 Sannuti and Saberi introduced a structural transformation of multivariable linear time-invariant (LTI) systems to a special coordinate basis (SCB) (Sannuti and Saberi, 1987). The transformation partitions a system into separate but interconnected subsystems that reflect the inner workings of the system. In particular, the SCB representation explicitly reveals the system's finite and infinite zero structure, and invertibility properties. Since its introduction, the SCB has been used in a large body of research, on topics including loop transfer recovery, time scale assignment, disturbance rejection, $H_2$ control, and $H_\infty$ control. It has also been used as a fundamental tool in the study of linear systems theory. For details on these

topics, we refer to the books Saberi, Chen, and Sannuti (1993); Saberi, Sannuti, and Chen (1995); Chen (2000); Chen, Lin, and Shamash (2004); Saberi, Stoorvogel, and Sannuti (2006), all of which are based on the SCB, and references therein. Other topics include decoupling theory (Sannuti and Saberi, 1987), factorization of linear systems (Chen, Saberi, and Sannuti, 1992), squaring down of non-square systems (Sannuti and Saberi, 1987; Saberi and Sannuti, 1990b), and model reduction (Ozcetin, Saberi, and Sannuti, 1990).

While the SCB provides a fine-grained decomposition of multivariable LTI systems, transforming an arbitrary system to the SCB is a complex operation. A constructive algorithm for strictly proper systems is provided in Sannuti and Saberi (1987), based on a modified Silverman algorithm (Silverman, 1969). This algorithm is lengthy and involved, and includes repeated rank operations and construction of non-unique transformations to divide the state space. Thus, the algorithm can realistically be executed by hand only for very simple systems.

To automate the process of finding transformations to the SCB, numerical algorithms have been developed (see Chu, Liu, and Tan, 2002; Chen et al., 2004) and implemented as part of the *Linear Systems Toolkit* for *Matlab* (Liu, Chen, and Lin, 2005). Although these numerical algorithms are invaluable in practical applications, engineers often operate on systems where some or all of the elements of the system matrices have a symbolic representation. There are obvious advantages in being able to transform these systems to the SCB symbolically, without having to insert numerical values in place of symbolic variables. Furthermore, the numerical algorithms are based on inherently inaccurate floating-point operations that make them prone to numerical errors. Ideally, if the elements of the system matrices are represented by symbols and exact fractions, one would be able to obtain an exact SCB representation of that system, also represented by symbols and exact fractions. To address these issues, we have developed a procedure for symbolic transformation of multivariable LTI systems to the SCB, using the commercial mathematics software suite *Maple*. The procedure is based on the modified Silverman algorithm from Sannuti and Saberi (1987), with a modification to achieve a later version of the SCB that includes an additional structural property (see, e.g., Saberi, Chen, and Sannuti, 1991), and an extension to SCB for non-strictly proper systems (Saberi and Sannuti, 1990b). The purpose of this paper is to introduce this procedure, and to explain how it is implemented using Maple and the *LinearAlgebra* package. The paper is also intended to serve as an introduction to the SCB, in particular for readers that might benefit from the possibility of working with symbolically represented systems in SCB form.

We believe that our procedure serves as a useful complement to available numerical tools. Symbolic transformation to the SCB makes it possible to work di-

rectly on the SCB representation of a system without first inserting numerical values, thereby removing an obstacle to more widespread use. The work presented in this paper also constitutes the first step in a wider effort to apply symbolic SCB representations to topics where the SCB has previously been applied, such as squaring down of non-square systems and asymptotic time scale assignment.

### 7.1.1 Notation

We denote by $\mathrm{col}(z_1, \ldots, z_n)$ the column vector obtained by stacking the column vectors $z_1, \ldots, z_n$. We denote by $\mathrm{diag}(M_1, \ldots, M_n)$ the matrix with submatrices $M_1, \ldots, M_n$ (not necessarily of the same dimensions) along the diagonal. We denote by $I_n$ the $n \times n$ identity matrix. The symbol 0 may refer to the scalar number zero, or a zero matrix of appropriate dimensions.

## 7.2 The Special Coordinate Basis

In this section we give a review of the SCB. For readers unfamiliar with the topic, the complexities of the SCB may initially appear overwhelming. This is only a reflection, however, of the inherent complexities that exist in general multivariable LTI systems. For a less technical introduction to the SCB, we recommend Berg (1998). In the following exposition, significant complexity is added to accommodate non-strictly proper systems. To get an initial overview of the SCB, we recommend ignoring the non-strictly proper case and the complexities that follow from it.

Consider the LTI system

$$\dot{\hat{x}} = \hat{A}\hat{x} + \hat{B}\hat{u}, \tag{7.1a}$$

$$\hat{y} = \hat{C}\hat{x} + \hat{D}\hat{u}. \tag{7.1b}$$

where $\hat{x} \in \mathbb{R}^n$ is the state, $\hat{u} \in \mathbb{R}^m$ is the input, and $\hat{y} \in \mathbb{R}^p$ is the output. We assume without loss of generality that the matrices $[\hat{B}^\mathsf{T}, \hat{D}^\mathsf{T}]^\mathsf{T}$ and $[\hat{C}, \hat{D}]$ are of full rank.

For simplicity in the non-strictly proper case (i.e., $\hat{D} \neq 0$), we assume in this section that the input and output are partitioned as

$$\hat{u} = \begin{bmatrix} u_0 \\ \hat{u}_1 \end{bmatrix} \text{ and } \hat{y} = \begin{bmatrix} y_0 \\ \hat{y}_1 \end{bmatrix},$$

where $u_0$ and $y_0$ are of dimension $m_0$, and furthermore that $\hat{D}$ has the form $\hat{D} = \text{diag}(I_{m_0}, 0)$. Then we may write

$$\hat{y} = \begin{bmatrix} y_0 \\ \hat{y}_1 \end{bmatrix} = \begin{bmatrix} \hat{C}_0\hat{x} + u_0 \\ \hat{C}_1\hat{x} \end{bmatrix}, \tag{7.2}$$

where $\hat{C}_0$ consists of the upper $m_0$ rows of $\hat{C}$, and $\hat{C}_1$ consists of the remaining rows of $\hat{C}$. The special form in (7.2) means that the input-output map is partitioned to separate the direct-feedthrough part from the rest: the output $y_0$ is directly affected by $u_0$, and the remainder of the output $\hat{y}_1$ is not directly affected by any input. Note that by substituting $u_0 = y_0 - \hat{C}_0\hat{x}$, we can write the system (7.1) in the alternative form

$$\dot{\hat{x}} = (\hat{A} - \hat{B}_0\hat{C}_0)\hat{x} + \hat{B}\begin{bmatrix} y_0 \\ \hat{u}_1 \end{bmatrix}, \tag{7.3a}$$

$$\hat{y} = \hat{C}\hat{x} + \hat{D}\hat{u}. \tag{7.3b}$$

where $\hat{B}_0$ consists of the left $m_0$ columns of $\hat{B}$. In the strictly proper case, $\hat{B}_0$ and $\hat{C}_0$ are nonexistent.

By nonsingular transformation of the state, output, and input, the system (7.1) can be transformed to the SCB. We use the symbols $x$, $y$, and $u$ to denote the state, output, and input of the system transformed to SCB form. The transformations between the original system (7.1) and the SCB are called $\Gamma_1$, $\Gamma_2$, and $\Gamma_3$, and we write $\hat{x} = \Gamma_1 x$, $\hat{y} = \Gamma_2 y$, and $\hat{u} = \Gamma_3 u$.

The state $x$ is partitioned as $x = \text{col}(x_a, x_b, x_c, x_d)$, where each component represents a particular subsystem described in the next section. The output is partitioned as $y = \text{col}(y_0, y_d, y_b)$, where $y_0$ is the original output $y_0$ from (7.1), $y_d$ is the output from the $x_d$ subsystem, and $y_b$ is the output from the $x_b$ subsystem. The input is partitioned as $u = \text{col}(u_0, u_d, u_c)$, where $u_0$ is the original input $u_0$ from (7.1), $u_d$ is the input to the $x_d$ subsystem, and $u_c$ is the input to the $x_c$ subsystem. The transformation $\Gamma_3$ is on the form $\text{diag}(I_{m_0}, \bar{\Gamma}_3)$, where $\bar{\Gamma}_3$ is nonsingular.

### 7.2.1 Structure of the SCB

Consider first the case when (7.1) is strictly proper. The meaning of the four subsystems can be explained as follows:

- The $x_a$ subsystem represents the zero dynamics. This part of the system is not directly affected by any inputs, nor does it affect any outputs directly. It may be affected, however, by the outputs $y_b$ and $y_d$ from the $x_b$ and $x_d$ subsystems.

- The $x_b$ subsystem has a direct effect on the output $y_b$, but it is not directly affected by any inputs. It may be affected, however, by the output $y_d$ from the $x_d$ subsystem. The $x_b$ subsystem is observable from $y_b$.

- The $x_c$ subsystem is directly affected by the input $u_c$, but it does not have a direct effect on any outputs. It may also be affected by the outputs $y_b$ and $y_d$ from the $x_b$ and $x_d$ subsystems, as well as the state $x_a$. However, the influence from $x_a$ is matched with the input $u_c$. The $x_c$ subsystem is controllable from $u_c$.

- The $x_d$ subsystem represents the infinite zero structure. This part of the system is directly affected by the input $u_d$, and it also affects the output $y_d$ directly. The $x_d$ subsystem can be further partitioned into $m_d$ single-input single-output (SISO) subsystems $x_i$ for $i = 1, \ldots, m_d$. Each of these subsystems consists of a chain of integrators of length $q_i$, from the $i$'th element of $u_d$ to the $i$'th element of $y_d$. Each integrator chain may be affected at each stage by the output $y_d$ from the $x_d$ subsystem, and at the lowest level of the integrator chain (where the input appears), it may be affected by all the states of the system. The $x_d$ subsystem is observable from $y_d$, and controllable from $u_d$.

The structure of strictly proper SCB systems is summarized in Table 7.1. For non-strictly proper systems the structure is the same, except for the existence of the direct-feedthrough output $y_0$, which is directly affected by the input $u_0$, and can be affected by any of the states of the system. It can also affect all the states of the system.

| Subsystem | Input | Output | Interconnections | Remarks |
|---|---|---|---|---|
| $x_a$ | — | — | $y_b$, $y_d$ | Zero dynamics |
| $x_b$ | — | $y_b$ | $y_d$ | Observable |
| $x_c$ | $u_c$ | — | $y_b$, $y_d$, $x_a{}^\star$ | Controllable |
| $x_d$ | $u_d$ | $y_d$ | $x_a{}^\star$, $x_b{}^\star$, $x_c{}^\star$ | Observable and controllable |

$^\star$Matched with input

**Table 7.1:** Summary of strictly proper SCB structure. The *Interconnections* column indicates influences from other subsystems.

### 7.2.2 SCB Equations

The SCB representation of the system (7.1) is given by

$$\dot{x}_a = A_{aa}x_a + B_{a0}y_0 + L_{ad}y_d + L_{ab}y_b, \tag{7.4a}$$
$$\dot{x}_b = A_{bb}x_b + B_{b0}y_0 + L_{bd}y_d, \tag{7.4b}$$
$$\dot{x}_c = A_{cc}x_c + B_{c0}y_0 + L_{cd}y_d + L_{cb}y_b + B_c(u_c + E_{ca}x_a), \tag{7.4c}$$
$$\dot{x}_i = A_{q_i}x_i + B_{d0}y_0 + L_{id}y_d + B_{q_i}(u_i + E_{ia}x_a + E_{ib}x_b + E_{ic}x_c + E_{id}x_d), \tag{7.4d}$$

for $i = 1, \ldots, m_d$. The outputs are given by

$$y_0 = C_{0a}x_a + C_{0b}x_b + C_{0c}x_c + C_{0d}x_d + u_0, \tag{7.5a}$$
$$y_i = C_{q_i}x_i, \quad i = 1, \ldots, m_d, \tag{7.5b}$$
$$y_b = C_b x_b. \tag{7.5c}$$

The $q_i$-dimensional states $x_i$ make up the state $x_d = \mathrm{col}(x_1, \ldots, x_{m_d})$; the scalar outputs $y_i$ make up the output $y_d = \mathrm{col}(y_1, \ldots, y_{m_d})$; and the scalar inputs $u_i$ make up the input $u_d = \mathrm{col}(u_1, \ldots, u_{m_d})$. The matrices $A_{q_i}$, $B_{q_i}$, and $C_{q_i}$ have the special structure

$$A_{q_i} = \begin{bmatrix} 0 & 1 & \cdots & 0 \\ \vdots & \vdots & \ddots & \vdots \\ 0 & 0 & \cdots & 1 \\ 0 & 0 & \cdots & 0 \end{bmatrix}, \quad B_{q_i} = \begin{bmatrix} 0 \\ \vdots \\ 0 \\ 1 \end{bmatrix}, \quad C_{q_i} = \begin{bmatrix} 1 & 0 & \cdots & 0 \end{bmatrix}.$$

The pair $(C_b, A_{bb})$ is observable, and the pair $(A_{cc}, B_c)$ is controllable. In the strictly proper case, the input $u_0$ and output $y_0$ are nonexistent, as are the matrices $B_{a0}$, $B_{b0}$, $B_{c0}$, $B_{d0}$, $C_{0a}$, $C_{0b}$, $C_{0c}$, and $C_{0d}$.

### 7.2.3 Compact Form

We may write (7.4) as

$$\dot{x} = Ax + B \begin{bmatrix} y_0 \\ u_d \\ u_c \end{bmatrix}, \tag{7.6a}$$
$$y = Cx + Du, \tag{7.6b}$$

with the SCB system matrices $A$, $B$, $C$, and $D$ defined as

$$A = \begin{bmatrix} A_{aa} & L_{ab}C_b & 0 & L_{ad}C_d \\ 0 & A_{bb} & 0 & L_{bd}C_d \\ B_c E_{ca} & L_{cb}C_b & A_{cc} & L_{cd}C_d \\ B_d E_{da} & B_d E_{db} & B_d E_{dc} & A_{dd} \end{bmatrix}, \quad B = \begin{bmatrix} B_{a0} & 0 & 0 \\ B_{b0} & 0 & 0 \\ B_{c0} & 0 & B_c \\ B_{d0} & B_d & 0 \end{bmatrix},$$

$$C = \begin{bmatrix} C_{0a} & C_{0b} & C_{0c} & C_{0d} \\ 0 & 0 & 0 & C_d \\ 0 & C_b & 0 & 0 \end{bmatrix}, \quad D = \begin{bmatrix} I_{m_0} & 0 & 0 \\ 0 & 0 & 0 \\ 0 & 0 & 0 \end{bmatrix},$$

where

$$\begin{aligned} A_{dd} &= \operatorname{diag}(A_{q_1}, \ldots, A_{q_{m_d}}) + L_{dd}C_d + B_d E_{dd}, \\ B_d &= \operatorname{diag}(B_{q_1}, \ldots, B_{q_{m_d}}), \\ C_d &= \operatorname{diag}(C_{q_1}, \ldots, C_{q_{m_d}}), \\ L_{dd} &= [L_{1d}^\mathsf{T}, \ldots, L_{m_d d}^\mathsf{T}]^\mathsf{T}, \\ E_{da} &= [E_{1a}^\mathsf{T}, \ldots, E_{m_d a}^\mathsf{T}]^\mathsf{T}, \end{aligned}$$

and similar for $E_{db}$, $E_{dc}$, and $E_{dd}$.

To see the relationship between the system matrices $\hat{A}$, $\hat{B}$, $\hat{C}$, and $\hat{D}$ and the SCB matrices $A$, $B$, $C$, and $D$ from (7.6), substitute $\hat{x} = \Gamma_1 x$, $\hat{y} = \Gamma_2 y$, and $\hat{u} = \Gamma_3 u$ in equation (7.3). Also, note that since $\Gamma_3$ is of the form $\operatorname{diag}(I_{m_0}, \bar{\Gamma}_3)$, we can make the substitution $\operatorname{col}(y_0, \hat{u}_1) = \Gamma_3 \operatorname{col}(y_0, u_d, u_c)$. We then obtain the equations

$$\begin{aligned} \dot{x} &= \Gamma_1^{-1}(\hat{A} - \hat{B}_0\hat{C}_0)\Gamma_1 x + \Gamma_1^{-1}\hat{B}\Gamma_3 \begin{bmatrix} y_0 \\ u_d \\ u_c \end{bmatrix}, \\ y &= \Gamma_2^{-1}\hat{C}\Gamma_1 x + \Gamma_2^{-1}\hat{D}\Gamma_3 u. \end{aligned}$$

Comparison with (7.6) then shows that $A = \Gamma_1^{-1}(\hat{A} - \hat{B}_0\hat{C}_0)\Gamma_1$, $B = \Gamma_1^{-1}\hat{B}\Gamma_3$, $C = \Gamma_2^{-1}\hat{C}\Gamma_1$, and $D = \Gamma_2^{-1}\hat{D}\Gamma_3$. In the strictly proper case, the expression for $A$ reduces to $A = \Gamma_1^{-1}\hat{A}\Gamma_1$.

### 7.2.4 Pre-Transformation of Non-Strictly Proper Systems

We assumed initially that the input and output vectors $\hat{u}$ and $\hat{y}$ have a special partitioning that separates the direct-feedthrough part from the rest, as shown in (7.2). A strictly proper system already has this form, but given a general non-strictly

proper system, a pre-transformation may have to be applied to put the system in the required form. Suppose that the we initially have a system with input $\tilde{u}$, output $\tilde{y}$, input matrix $\tilde{B}$, and output matrices $\tilde{C}$ and $\tilde{D}$. Then there are nonsingular transformations $U$ and $Y$ such that $\tilde{u} = U\hat{u}$ and $\tilde{y} = Y\hat{y}$, where $\hat{u}$ and $\hat{y}$ have the structure required in (7.2). The dimension $m_0$ of $u_0$ and $y_0$ is the rank of $\tilde{D}$. The matrices $\hat{B}$, $\hat{C}$, and $\hat{D}$ are obtained from $\tilde{B}$, $\tilde{C}$, and $\tilde{D}$ by $\hat{B} = \tilde{B}U$, $\hat{C} = Y^{-1}\tilde{C}$, and $\hat{D} = Y^{-1}\tilde{D}U$. Our Maple procedure, in addition to returning the matrices $A$, $B$, $C$, and $D$ of the SCB system, the transformations $\Gamma_1$, $\Gamma_2$, and $\Gamma_3$ to transform (7.1) to SCB form, and the dimension of each subsystem, returns the transformations $U$ and $Y$, to take a general non-strictly proper system to the form required in (7.1), (7.2).

## 7.3 Properties of the SCB

The SCB is closely related to the canonical form of Morse (Morse, 1973), which is obtained through transformations of the state, input, and output spaces, and the application of state feedback and output injection. A system in the canonical form of Morse consists of four decoupled subsystems that reflect essential geometric properties of the original system. The SCB form of a system largely reflects the same properties; however, the SCB is obtained through transformations of the state, input, and output spaces alone, without the application of state feedback and output injection. Thus, the SCB is merely a representation of the original system in a different coordinate basis, and it can therefore be used directly for design purposes.

Some properties of the SCB, which correspond directly to properties of the canonical form of Morse, are the following:

- The invariant zeros of the system (7.1) are the eigenvalues of the matrix $A_{aa}$. Hence, the system is minimum-phase if, and only if, the eigenvalues of $A_{aa}$ are located in the open left-half complex plane.
- The system (7.1) is right-invertible if, and only if, the subsystem $x_b$ is nonexistent.
- The system (7.1) is left-invertible if, and only if, the subsystem $x_c$ is nonexistent.
- The system (7.1) is invertible if, and only if, both the subsystem $x_b$ and the subsystem $x_c$ are nonexistent.
- The system (7.1) has $m_0$ infinite zeros of order 0 and $i\bar{q}_i$ infinite zeros of order $i$, where $\bar{q}_i$ is the number of integrator chains of length $i$ in the $x_d$ subsystem.

By studying the dynamics of the $x_a$ subsystem and its connections to the rest of the system, one obtains a precise description of the invariant zero dynamics of the system and the classes of input signals that may be blocked by these zeros. The information thus obtained goes beyond what can be obtained through the notions of state and input *pseudo zero directions* (see MacFarlane and Karcanias, 1976; Saberi et al., 1991).

The representation of the infinite zero structure through integrator chains in the $x_d$ subsystem allows for the explicit construction of high-gain controllers and observers in a general multiple-input multiple-output setting (see, e.g., Saberi and Sannuti, 1990a). This removes unnecessary restrictions of square-invertibility and uniform relative degree that are found in much of the high-gain literature.

### 7.3.1 Connection to Geometry Theory

Geometry theory is concerned with the study of subspaces of the state space with certain invariance properties, for example, $A$-invariant subspaces (which remain invariant under the unforced motion of the system), $(A, B)$-invariant subspaces (which can be made invariant by the proper application of state feedback), and $(C, A)$ invariant subspaces (which can be made invariant by the proper application of output injection) (see, e.g., Wonham, 1979; Trentelman, Stoorvogel, and Hautus, 2001). Prominent examples of $A$-invariant subspaces are the controllable subspace (i.e., the image of the controllability matrix) and the unobservable subspace (the kernel of the observability matrix).

The development of geometry theory has in large part been motivated by the challenge of decoupling disturbance inputs from the outputs of a system, either exactly or approximately. Toward this end, a number of subspaces have been identified, which can be related to the partitioning in the SCB. Of particular importance in the context of control design for exact disturbance decoupling are the *weakly unobservable subspace*, which, by the proper selection of state feedback, can be made not to affect the outputs; and the *controllable weakly unobservable subspace*, which has the additional property that the dynamics restricted to this subspace is controllable. Of particular importance in the context of observer design for exact disturbance decoupling are the *strongly controllable subspace*, which, by the proper selection of output injection, is such that its quotient space can be rendered unaffected by the system inputs; and the *distributionally weakly unobservable subspace*, which has the additional property that the dynamics restricted to its quotient space is observable.

We denote by $\mathcal{X}_a$, $\mathcal{X}_b$, $\mathcal{X}_c$, and $\mathcal{X}_d$ the subspaces spanned by the states $x_a$, $x_b$, $x_c$, and $x_d$, and by $\oplus$ the direct sum of two subspaces that intersect only at the origin. The subspaces mentioned above can then be related to the SCB as follows:

- The weakly unobservable subspace is given by $\mathcal{X}_a \oplus \mathcal{X}_c$.
- The controllable weakly unobservable subspace is given by $\mathcal{X}_c$.
- The strongly controllable subspace is given by $\mathcal{X}_c \oplus \mathcal{X}_d$.
- The distributionally weakly unobservable subspace is given by $\mathcal{X}_a \oplus \mathcal{X}_c \oplus \mathcal{X}_d$.

A list of further subspaces identified in geometry theory and their relationship to the SCB can be found in Saberi et al. (1991).

The SCB provides a more direct and tangible path to disturbance decoupling design than the somewhat abstract notions of geometry theory. For example, geometry theory tells us that a disturbance entering into the weakly unobservable subspace can be decoupled from the outputs by the proper selection of state feedback. In the SCB the weakly unobservable subspace is represented by the state variables $x_a$ and $x_c$; thus, a disturbance affecting only $x_a$ and $x_c$ can be decoupled from the outputs. This decoupling is achieved by selecting the state feedback $u_0 = -C_{0a}x_a - C_{0c}x_c + v_0$, $u_i = -E_{ia}x_a - E_{ic}x_c + v_i$, $i = 1, \ldots, m_d$, where $v_0$ and $v_i$, as well as $u_c$, can be chosen freely. It can be verified by direction inspection of (7.4) that this state feedback cancels the influence of $x_a$ and $x_c$ on the rest of the system, and therefore on the outputs. With the help of symbolic transformations, such decoupling design can be carried out directly on systems with a symbolic representation.

### 7.3.2 Further Properties

Some useful connections can be made between the SCB representation of a system and the properties of controllability, stabilizability, observability, and detectability:

- The system (7.1) is controllable (stabilizable) if, and only if, the pair

$$\left( \begin{bmatrix} A_{aa} & L_{ab}C_b \\ 0 & A_{bb} \end{bmatrix}, \begin{bmatrix} B_{a0} & L_{ad} \\ B_{b0} & L_{bd} \end{bmatrix} \right)$$

  is controllable (stabilizable).

- The system (7.1) is observable (detectable) if, and only if, the pair

$$\left( \begin{bmatrix} C_{0a} & C_{0c} \\ E_{da} & E_{dc} \end{bmatrix}, \begin{bmatrix} A_{aa} & 0 \\ B_c E_{ca} & A_{cc} \end{bmatrix} \right)$$

  is observable (detectable).

- The system (7.1) is stabilizable if it is right-invertible and minimum-phase (i.e., the $x_b$ subsystem is nonexistent and the eigenvalues of $A_{aa}$ are in the open left-half plane).

- The system (7.1) is detectable if it is left-invertible and minimum-phase (i.e., the $x_c$ subsystem is nonexistent and the eigenvalues of $A_{aa}$ are in the open left-half plane).

The subsystem partitioning of the SCB remains the same when state feedback and output injection is applied to the system. This is in contrast to the system obtained by a Kalman decomposition, which is partitioned according to the properties of controllability and observability.

## 7.4 Maple Procedure

Our Maple procedure is invoked as follows:

```
A, B, C, D, G1, G2, G3, U, Y, dim := scb(Ai, Bi, Ci, Di);
```

The inputs Ai, Bi, Ci, and Di are system matrices describing a general multivariable LTI system. The outputs A, B, C, and D are the system matrices describing a corresponding SCB system. The outputs G1, G2, and G3 are the transformation matrices $\Gamma_1$, $\Gamma_2$, and $\Gamma_3$ between the system (7.1) and the SCB. The outputs U and Y are the pre-transformations that must be applied to the system to put it in the form required of (7.1), (7.2), as described in Section 7.2.4. Finally, the output dim is a list of four integers representing the dimensions of the $x_a$, $x_b$, $x_c$, and $x_d$ subsystems, in that order. The Maple source code is available from Grip and Saberi (2010).

The modified Silverman algorithm for transformation to the SCB is much too long to be presented in this article. For the details of the algorithm, we refer to Sannuti and Saberi (1987). In the following we shall present a broad outline of the steps of the algorithm and discuss issues that require particular attention in a symbolic implementation. Much of the algorithm consists of tedious but straightforward manipulation of matrices, which is not discussed in this article.

Throughout the algorithm, we identify a large number of variables that are linear transformations of the original state. We keep track of these by storing the matrices that transform the original state to the new variables. For example, the temporary variable $y_{i0}$, given by the expression $y_{i0} = C_i\hat{x}$, is represented internally by a **Matrix** data structure containing $C_i$. The procedure is not written to perform well on floating-point data. For this reason, all floating-point elements of the matrices passed to the procedure are converted to exact fractions before any other operations are performed, using Maple's **convert** function. In many cases, we need

to store a whole list of matrices, representing variables obtained during successive iterations of a particular part of the algorithm. To do this, we use the Maple data structures **Vector** and **Matrix**, which can be used to store vectors or matrices whose elements are **Matrix** data structures.

### 7.4.1 Strictly Proper Case

The algorithm for strictly proper systems is implemented as **scbSP**. The first part of this algorithm identifies the two subsystems that directly influence the outputs, namely the $x_b$ and $x_d$ subsystems, through a series of steps that are repeated until the outputs are exhausted. The algorithm works by identifying transformed input and output spaces such that each input channel is directly connected to one output channel by a specific number of inherent integrations.

Let the strictly proper system passed to the **scbSP** procedure be represented by the state equations $\dot{\hat{x}} = \hat{A}\hat{x} + \hat{B}\hat{u}$, $\hat{y} = \hat{C}\hat{x}$. In the first iteration we start with the output $y_{10} = \hat{C}\hat{x}$, and determine whether its derivative $\dot{y}_{10} = \hat{C}\hat{A}\hat{x} + \hat{C}\hat{B}\hat{u}$ depends on any part of the input $\hat{u}$. If so, we use a transformation $\bar{S}_1$ to separate out a linear combination of outputs and inputs that are separated by one integration in a linearly independent manner. This will create an integrator chain of length one, as part of the $x_d$ subsystem. A transformed part of the output derivative that is not directly influenced by the input is denoted $\tilde{C}_1\hat{x}$, and is processed further. We use a transformation $\bar{\phi}_1$ to separate out any part of $\tilde{C}_1\hat{x}$ that is linearly dependent on $y_{10}$. This will create states that are part of the $x_b$ subsystem. After the linearly dependent components are separated out, the remaining part of the output derivative is given the name $y_{20}$. In the next iteration we process $y_{20}$ in the same fashion as $y_{10}$, to identify integrator chains of length two, and possibly further additions to the $x_b$ subsystem. The algorithm continues in this fashion until the outputs are exhausted.

#### Constructing Transformation Matrices

When implementing these steps in Maple, the main part of each iteration consists of constructing transformation matrices $\bar{S}_i$ and $\bar{\phi}_i$. In particular, we are faced with the following problem at step $i$: given a matrix $C_i$ of dimension $p_i \times n$ and a matrix $\bar{D}_{i-1}$ of dimension $\bar{\mathfrak{q}}_{i-1} \times m$ of maximal rank $\bar{\mathfrak{q}}_{i-1}$, let $\bar{\mathfrak{q}}_i$ be the rank of $[\bar{D}_{i-1}^{\mathsf{T}}, (C_i\hat{B})^{\mathsf{T}}]^{\mathsf{T}}$, and let $\mathfrak{q}_i = \bar{\mathfrak{q}}_i - \bar{\mathfrak{q}}_{i-1}$. Find a nonsingular matrix $\bar{S}_i$ such that

$$\bar{S}_i \begin{bmatrix} \bar{D}_{i-1} \\ C_i\hat{B} \end{bmatrix} = \begin{bmatrix} \bar{D}_{i-1} \\ \hat{D}_i \\ 0 \end{bmatrix}, \quad \bar{S}_i = \begin{bmatrix} I_{\bar{\mathfrak{q}}_i - 1} & 0 \\ S_{ia} & S_i \end{bmatrix}, \quad S_{ia} = \begin{bmatrix} 0 \\ S_{ib} \end{bmatrix}, \quad S_i = \begin{bmatrix} S_{i1} \\ S_{i2} \end{bmatrix},$$

where $\hat{D}_i$ is a $\mathfrak{q}_i \times m$ matrix of maximal rank, and where $S_{i1}$, $S_{i2}$, and $S_{ib}$ are of dimensions $\mathfrak{q}_i \times p_i$, $(p_i - \mathfrak{q}_i) \times p_i$, and $(p_i - \mathfrak{q}_i) \times \bar{\mathfrak{q}}_{i-1}$. The meaning of the various dimensions is not important in this context. In general, $\bar{S}_i$ is not unique.

The rank of the matrix $[\bar{D}_{i-1}^{\mathsf{T}}, (C_i \hat{B})^{\mathsf{T}}]^{\mathsf{T}}$ can be obtained with the **Rank** function in the LinearAlgebra package. To construct the matrix $\bar{S}_i$, the first observation we make is that, since $S_{ib}\bar{D}_{i-1} + S_{i2}C_i\hat{B} = 0$, the rows of the matrix $[S_{ib}, S_{i2}]$ must belong to the left null space of $[\bar{D}_{i-1}^{\mathsf{T}}, (C_i \hat{B})^{\mathsf{T}}]^{\mathsf{T}}$. If $[\bar{D}_{i-1}^{\mathsf{T}}, (C_i \hat{B})^{\mathsf{T}}]^{\mathsf{T}}$ has full rank $\bar{\mathfrak{q}}_{i-1} + p_i$, then $S_{ib}$ and $S_{i2}$ are empty matrices, and we may select $S_{ia} = 0$ and $S_{i1} = I_{p_i}$. Otherwise, we can obtain a set of linearly independent basis vectors for the left null space of $[\bar{D}_{i-1}^{\mathsf{T}}, (C_i \hat{B})^{\mathsf{T}}]^{\mathsf{T}}$, or equivalently, for the right null space of its transpose, using the **NullSpace** function of the LinearAlgebra package. The transpose of the basis vectors can then be stacked to form the matrix $[S_{ib}, S_{i2}]$, which can be split up to form $S_{ib}$ and $S_{i2}$. However, the null space basis is not unique and, moreover, the order in which the basis vectors are returned by Maple is not consistent. This may cause our procedure to produce different results on different executions with the same matrices, which is undesirable. To avoid this, we first stack the transpose of the basis vectors, and then transform the resulting matrix to the unique reduced-row echelon form, by using the **ReducedRowEchelonForm** function of the LinearAlgebra package. Since the transformation involves a finite number of row operations, the rows of the matrix in reduced-row echelon form remain in the left null space.

Since $\bar{S}_i$ should be a nonsingular matrix, the submatrix $S_i$ must be nonsingular. This requires that $S_{i2}$ has maximal rank, which is confirmed as follows: if any of the rows of $S_{i2}$ are linearly dependent, a linear combination of rows in $[S_{ib}, S_{i2}]$ can be constructed to create a row vector $v$ such that $v[\bar{D}_{i-1}^{\mathsf{T}}, (C_i \hat{B})^{\mathsf{T}}]^{\mathsf{T}} = 0$, where the rightmost $p_i$ columns of $v$ are zero. However, since the rows of $\bar{D}_{i-1}$ are linearly independent, this implies that $v = 0$, which in turn implies that $[S_{ib}, S_{i2}]$ must have linearly dependent rows. Since this is not the case, $S_{i2}$ must have maximal rank.

We continue by constructing the matrix $S_{i1}$. Nonsingularity of $S_i$ requires that the rows of $S_{i1}$ must be linearly independent of the rows of $S_{i2}$. One way to produce $S_{i1}$ is to choose its rows to be orthogonal to the rows of $S_{i2}$, which can be achieved by using a basis for the right null space of $S_{i2}$. However, since the matrix $\bar{S}_i$ will be used to transform the state of the original system, it is generally desirable for this matrix to have the simplest possible structure. This helps avoids unnecessary changes to the original states, and thus it generally produces more appealing solutions. We therefore construct $S_{i1}$ by the following procedure: we start by initializing $S_{i1}$ as the identity matrix of dimension $p_i \times p_i$. We then create a reduced-row echelon form of $S_{i2}$, and iterate backwards over the rows of this

matrix. For each row, we search along the columns from the left until we reach the leading 1 on that row. We then delete the row in $S_{i1}$ corresponding to the column with the leading 1. This ensures that $S_i = [S_{i1}^{\mathsf{T}}, S_{i2}^{\mathsf{T}}]^{\mathsf{T}}$ is nonsingular, with $S_{i1}$ consisting of zeros except for a single element equal to 1 on each row. The construction of $\bar{S}_i$ is now easily completed.

At each step, we must also construct a nonsingular matrix $\bar{\phi}_i$. The problem of finding this matrix is analogous to the problem of finding $\bar{S}_i$, and we therefore use the same procedure. Finding the transformations $\bar{S}_i$ and $\bar{\phi}_i$ constitute the most important part of finding the states $x_b$ and $x_d$. After $x_b$ and $x_d$ are identified, finding the output transformation $\Gamma_2$ is straightforward, based on Sannuti and Saberi (1987). We also find an input transformation $\Gamma_3'$ based on Sannuti and Saberi (1987) and write $\hat{u} = \Gamma_3'[u_d{}^{\mathsf{T}}, u_c'{}^{\mathsf{T}}]^{\mathsf{T}}$, where $u_c'$ is a temporary input. Unlike Sannuti and Saberi (1987), we shall apply a further transformation to $u_c'$ to achieve an input $u_c$ that is matched with the influence from $x_a$ on the right-hand side of the $x_c$ equation.

### 7.4.2 Constructing the $x_a$ and $x_c$ States

After finding the transformations from the original states to the $x_b$ and $x_d$ states, the next step is to find a transformation to a temporary state vector $x_s$ that will be further decomposed into the states $x_a$ and $x_c$. The requirements on $x_s$ is that it must be linearly independent of the already identified states $x_b$ and $x_d$, so that $x_s$, $x_b$, and $x_d$ together span the entire state space; and that its derivative $\dot{x}_s$ must only depend on $x_s$ itself, plus $y_b$, $y_d$, and $u_c'$, because those are the only quantities allowed in the derivatives of $x_a$ and $x_c$ in the strictly proper case.

Suppose that $\mathrm{col}(x_b, x_d) = \Gamma_{bd}\hat{x}$. The procedure for finding $x_s$ is to start with a temporary state vector $x_s^0 = \Gamma_s^0\hat{x}$ that is linearly independent of $x_b$ and $x_d$. Hence, we select $\Gamma_s^0$ such that $[\Gamma_s^{0\mathsf{T}}, \Gamma_{bd}^{\mathsf{T}}]^{\mathsf{T}}$ is nonsingular. To do so in our Maple procedure, we use the same technique as for finding $S_{i1}$ based on $S_{i2}$ in Section 7.4.1.

The derivative of $x_s^0$, written in terms of the states $x_s^0$, $x_b$, and $x_d$, and the inputs $u_c'$ and $u_d$, can be written as

$$\dot{x}_s^0 = A^0 \begin{bmatrix} x_s^0 \\ x_b \\ x_d \end{bmatrix} + B^0 \begin{bmatrix} u_d \\ u_c' \end{bmatrix} = A_s^0 x_s^0 + A_b^0 x_b + A_d^0 x_d + B_d^0 u_d + B_c^0 u_c',$$

for some matrices $A^0 = [A_s^0, A_b^0, A_d^0]$ and $B^0 = [B_d^0, B_c^0]$. In our Maple procedure, we can easily calculate $A^0 = \Gamma_s^0\hat{A}([\Gamma_s^{0\mathsf{T}}, \Gamma_{bd}^{\mathsf{T}}]^{\mathsf{T}})^{-1}$ and $B^0 = \Gamma_s^0\hat{B}\Gamma_3'$, and then extract the matrices $A_s^0$, $A_b^0$, $A_c^0$, $B_d^0$, and $B_c^0$. To do so, we use the **MatrixInverse** function of the LinearAlgebra package.

To conform with the SCB, we need to modify $x_s^0$ to eliminate the input $u_d$ in $\dot{x}_s^0$. To eliminate $u_d$, we create a temporary state vector $x_{d0} = \Gamma_{d0}\hat{x}$, consisting of the lowermost level of each integrator chain in the $x_d$ subsystem (that is, the point where the input enters the integrator chain). According to (7.4), we then have $\dot{x}_{d0} = u_d + A_{d0}[x_s^{0\mathsf{T}}, x_b{}^{\mathsf{T}}, x_d{}^{\mathsf{T}}]^{\mathsf{T}}$, for some matrix $A_{d0}$. Therefore, by defining a new temporary state $x_s^1 = x_s^0 - B_d^0 x_{d0}$, we have $\dot{x}_s^1 = (A^0 - B_d^0 A_{d0})[x_s^{0\mathsf{T}}, x_b{}^{\mathsf{T}}, x_d{}^{\mathsf{T}}]^{\mathsf{T}} + B_c^0 u_c'$. Hence, the derivative of the new temporary state vector $x_s^1$ is independent of $u_d$, bringing us one step closer to obtaining $x_s$. The elimination procedure is continued in a similar fashion, as described in Sannuti and Saberi (1987), until we obtain a state $x_s$ such that $\dot{x}_s$ depends only on $x_s$, $y_b$, $y_d$, and $u_c'$.

The final step is to decompose $x_s$ into two subsystems, $x_a$ and $x_c$, and to transform the input $u_c'$ into $u_c$, in such a way that $x_a$ is unaffected by $u_c$ and $x_c$ is controllable from $u_c$. Furthermore, the influence of $x_a$ on $x_c$ should be matched with $u_c$, as seen in (7.4). If $u_c'$ is nonexistent, then we simply set $x_a = x_s$. If $u_c'$ does exist, we proceed by first finding the derivative $\dot{x}_s = A_{ss}x_s + L_{sb}y_b + L_{sd}y_d + B_{sc}u_c'$, for some matrices $A_{ss}$, $L_{sb}$, $L_{sd}$, and $B_{sc}$. We then obtain the proper transformations by calling **scbSP** recursively on the transposed system with system matrix $A_{ss}^{\mathsf{T}}$, output matrix $B_{sc}^{\mathsf{T}}$, and an empty input matrix. This recursive call returns a system consisting only of an $x_a$ and an $x_b$ subsystem. It is easily confirmed that, when transposed back again, this system has the desired structure. We therefore let $[x_a{}^{\mathsf{T}}, x_c{}^{\mathsf{T}}]^{\mathsf{T}} = \Gamma_1^{\star\mathsf{T}} x_s$ and $u_c = \Gamma_2^{\star\mathsf{T}} u_c'$, where $\Gamma_1^\star$ and $\Gamma_2^\star$ are the state and output transformations returned by the recursive call.

### 7.4.3 Non-Strictly Proper Case

To handle the non-strictly proper case, the first step is to find the pre-transformation matrices $U$ and $Y$, described in Section 7.2.4. Suppose that the matrices passed to the procedure **scb** are $\hat{A}$, $\tilde{B}$, $\tilde{C}$, and $\tilde{D}$. We need to find nonsingular $U$ and $Y$ such that, according to Section 7.2.4, $\hat{B} = \tilde{B}U$, $\hat{C} = Y^{-1}\tilde{C}$, and $\hat{D} = Y^{-1}\tilde{D}U$, where $\hat{D}$ is of the form $\mathrm{diag}(I_{m_0}, 0)$. The rank $m_0$ of $\tilde{D}$ is found using the **Rank** function. Let $Y^{-1} = [Y_1^{\mathsf{T}}, Y_2^{\mathsf{T}}]^{\mathsf{T}}$, where $Y_1$ has $m_0$ rows. Then we have the equations

$$Y^{-1}\tilde{D}U = \begin{bmatrix} Y_1\tilde{D}U \\ Y_2\tilde{D}U \end{bmatrix} = \begin{bmatrix} I_{m_0} & 0 \\ 0 & 0 \end{bmatrix}.$$

To solve these equations, we choose the rows of $Y_2$ from the left null space of $\tilde{D}$, using the functions **NullSpace** and **ReducedRowEchelonForm** as before; and we select $Y_1$ such that $[Y_1^{\mathsf{T}}, Y_2^{\mathsf{T}}]^{\mathsf{T}}$ is nonsingular, using the same procedure as for finding $S_{i1}$ given $S_{i2}$ in Section 7.4.1. This leaves us to solve the equation $Y_1\tilde{D}U =$

$[I_{m_0}, 0]$ with respect to some nonsingular $U$. Let $U^{-1} = [U_1^\mathsf{T}, U_2^\mathsf{T}]^\mathsf{T}$ such that $U_1$ has $m_0$ rows. We select $U_1 = Y_1\tilde{D}$, and we select $U_2$ such that $[U_1^\mathsf{T}, U_2^\mathsf{T}]^\mathsf{T}$ is nonsingular, by the same procedure as before. It is then straightforward to confirm that $Y_1\tilde{D}U = [I_{m_0}, 0]$. We can now calculate the matrices $\hat{B}$, $\hat{C}$, and $\hat{D}$ that conform with the required structure of (7.1), (7.2).

Let $\hat{B}_0$ consist of the left $m_0$ columns of $\hat{B}$, and let $\hat{B}_1$ consist of the remaining columns of $\hat{B}$. Similar to (7.3), we can write the system equations (7.1) as

$$\dot{\hat{x}} = (\hat{A} - \hat{B}_0\hat{C}_0)\hat{x} + \hat{B}_0 y_0 + \hat{B}_1\hat{u}_1, \tag{7.7a}$$

$$y_0 = \hat{C}_0\hat{x} + u_0, \tag{7.7b}$$

$$\hat{y}_1 = \hat{C}_1\hat{x}. \tag{7.7c}$$

Suppose we obtain the SCB form of the strictly proper system described by the matrices $(\hat{A} - \hat{B}_0\hat{C}_0)$, $\hat{B}_1$, and $\hat{C}_1$, by invoking the procedure **scbSP**, and suppose the transformation matrices returned for this system are $\bar{\Gamma}_1$, $\bar{\Gamma}_2$, and $\bar{\Gamma}_3$. Substituting $\hat{x} = \bar{\Gamma}_1 x$, $\hat{y}_1 = \bar{\Gamma}_2[y_d{}^\mathsf{T}, y_b{}^\mathsf{T}]^\mathsf{T}$, and $\hat{u}_1 = \bar{\Gamma}_3[u_d{}^\mathsf{T}, u_c{}^\mathsf{T}]^\mathsf{T}$ in (7.7) yields

$$\begin{aligned}
\dot{x} &= \bar{\Gamma}_1^{-1}(\hat{A} - \hat{B}_0\hat{C}_0)\bar{\Gamma}_1 x + \bar{\Gamma}_1^{-1}\hat{B}_0 y_0 + \bar{\Gamma}_1^{-1}\hat{B}_1\bar{\Gamma}_3\begin{bmatrix} u_d \\ u_c \end{bmatrix}, \\
y_0 &= \hat{C}_0\bar{\Gamma}_1 x + u_0, \\
\begin{bmatrix} y_d \\ y_b \end{bmatrix} &= \bar{\Gamma}_2^{-1}\hat{C}_1\bar{\Gamma}_1 x.
\end{aligned}$$

It is easily confirmed that this system conforms to the SCB, by defining $A = \bar{\Gamma}_1^{-1}(\hat{A} - \hat{B}_0\hat{C}_0)\bar{\Gamma}_1$, $B = \bar{\Gamma}_1^{-1}[\hat{B}_0, \hat{B}_1\bar{\Gamma}_3]$, $C = [\hat{C}_0^\mathsf{T}, (\bar{\Gamma}_2^{-1}\hat{C}_1)^\mathsf{T}]^\mathsf{T}\bar{\Gamma}_1$, and $D = \mathrm{diag}(I_{m_0}, 0)$. Defining the transformations for the non-strictly proper system as $\Gamma_1 = \bar{\Gamma}_1$, $\Gamma_2 = \mathrm{diag}(I_{m_0}, \bar{\Gamma}_2)$, and $\Gamma_3 = \mathrm{diag}(I_{m_0}, \bar{\Gamma}_3)$, we obtain $A = \Gamma_1^{-1}(\hat{A} - \hat{B}_0\hat{C}_0)\Gamma_1$, $B = \Gamma_1^{-1}\hat{B}\Gamma_3$, $C = \Gamma_2^{-1}\hat{C}\Gamma_1$, and $D = \Gamma_2^{-1}\hat{D}\Gamma_3$, which are the proper expressions relating the matrices $\hat{A}$, $\hat{B}$, $\hat{C}$, and $\hat{D}$ to the SCB matrices (see Section 7.2.3).

## 7.5 Examples

In this section, we apply the decomposition procedure to several example systems.

### 7.5.1 Linear Single-Track Model

A widely used model for the lateral dynamics of a car is the linear single-track model (see, e.g., Kiencke and Nielsen, 2000). For a car on a horizontal surface,

this model is described by the equations

$$\dot{v}_y = \frac{1}{m}(F_\mathrm{f} + F_\mathrm{r}) - r v_x,$$
$$\dot{r} = \frac{1}{J}(l_\mathrm{f} F_\mathrm{f} - l_\mathrm{r} F_\mathrm{r}),$$

where $v_y$ is the lateral velocity at the center of gravity; $r$ is the yaw rate (angular rate around the vertical axis); $m$ is the mass; $J$ is the moment of inertia around the vertical axis through the car's center of gravity; $l_\mathrm{f}$ and $l_\mathrm{r}$ are the longitudinal distances from the center of gravity to the front and rear axles; and $F_\mathrm{f}$ and $F_\mathrm{r}$ are the lateral road-tire friction forces on the front and rear axles. The longitudinal velocity $v_x$ is assumed to be positive and to vary slowly enough compared to the lateral dynamics that it can be considered a constant. The friction forces can be modeled by the equations

$$\dot{F}_\mathrm{f} = \frac{c_\mathrm{f}}{T_\mathrm{r}}\left(\delta_\mathrm{f} - \frac{v_y}{v_x} - l_\mathrm{f}\frac{r}{v_x}\right) - \frac{1}{T_\mathrm{r}}F_\mathrm{f},$$
$$\dot{F}_\mathrm{r} = \frac{c_\mathrm{r}}{T_\mathrm{r}}\left(-\frac{v_y}{v_x} + l_\mathrm{r}\frac{r}{v_x}\right) - \frac{1}{T_\mathrm{r}}F_\mathrm{r},$$

where $\delta_\mathrm{f}$ is the front-axle steering angle; $c_\mathrm{f}$ and $c_\mathrm{r}$ are the front- and rear-axle cornering stiffnesses; and $T_\mathrm{r}$ is a speed-dependent tire relaxation constant (see, e.g., Pacejka, 2006). In modern cars with electronic stability control, the main measurements that describe the lateral dynamics are the yaw rate $r$ and the lateral acceleration $a_y = \frac{1}{m}(F_\mathrm{f} + F_\mathrm{r})$. Considering $\delta_\mathrm{f}$ as the input, the system is described by

$$\hat{A} = \begin{bmatrix} 0 & -v_x & \frac{1}{m} & \frac{1}{m} \\ 0 & 0 & \frac{l_\mathrm{f}}{J} & -\frac{l_\mathrm{r}}{J} \\ -\frac{c_\mathrm{f}}{T_\mathrm{r} v_x} & -\frac{l_\mathrm{f} c_\mathrm{f}}{T_\mathrm{r} v_x} & -\frac{1}{T_\mathrm{r}} & 0 \\ -\frac{c_\mathrm{r}}{T_\mathrm{r} v_x} & \frac{l_\mathrm{r} c_\mathrm{r}}{T_\mathrm{r} v_x} & 0 & -\frac{1}{T_\mathrm{r}} \end{bmatrix}, \qquad \hat{B} = \begin{bmatrix} 0 \\ 0 \\ \frac{c_\mathrm{f}}{T_\mathrm{r}} \\ 0 \end{bmatrix},$$
$$\hat{C} = \begin{bmatrix} 0 & 1 & 0 & 0 \\ 0 & 0 & \frac{1}{m} & \frac{1}{m} \end{bmatrix}, \qquad \hat{D} = \begin{bmatrix} 0 \\ 0 \end{bmatrix}.$$

If we pass these matrices to our Maple procedure, we obtain SCB system matrices

$$A = \begin{bmatrix} -\frac{1}{T_\mathrm{r}} & 1 & 0 & \frac{T_\mathrm{r} l_\mathrm{f} m}{c_\mathrm{r}(l_\mathrm{f}+l_\mathrm{r})} \\ -\frac{l_\mathrm{r} c_\mathrm{r}(l_\mathrm{f}+l_\mathrm{r})}{v_x T_\mathrm{r} J} & 0 & 1 & \frac{l_\mathrm{f} m}{c_\mathrm{r}(l_\mathrm{f}+l_\mathrm{r})} \\ -\frac{c_\mathrm{r}(l_\mathrm{f}+l_\mathrm{r})}{T_\mathrm{r} J} & 0 & 0 & \frac{1}{v_x} \\ \frac{c_\mathrm{r}(l_\mathrm{r} c_\mathrm{r} - l_\mathrm{f} c_\mathrm{f})(l_\mathrm{f}+l_\mathrm{r})}{m T_\mathrm{r}^2 v_x J} & 0 & -\frac{c_\mathrm{f}+c_\mathrm{r}}{m T_\mathrm{r}} & -\frac{1}{T_\mathrm{r}} \end{bmatrix}, \qquad B = \begin{bmatrix} 0 \\ 0 \\ 0 \\ 1 \end{bmatrix},$$

$$C = \begin{bmatrix} 0 & 0 & 0 & 1 \\ 1 & 0 & 0 & 0 \end{bmatrix}, \quad D = \begin{bmatrix} 0 \\ 0 \end{bmatrix},$$

and the transformations

$$\Gamma_1 = \begin{bmatrix} 0 & 0 & v_x & 0 \\ \frac{c_r(l_f+l_r)}{T_r J} & 0 & 0 & 0 \\ -\frac{c_r}{T_r^2} & \frac{c_r}{T_r} & 0 & m \\ \frac{c_r}{T_r^2} & -\frac{c_r}{T_r} & 0 & 0 \end{bmatrix}, \quad \Gamma_2 = \begin{bmatrix} 0 & \frac{c_r(l_f+c_r)}{T_r J} \\ 1 & 0 \end{bmatrix}, \quad \Gamma_3 = \frac{m T_r}{c_f}.$$

The dimension list dim returned by the procedure is $0, 3, 0, 1$, meaning that the first three states belong to the $x_b$ subsystem, and the last state is an integrator chain of length 1, belonging to the $x_d$ subsystem. Inspection of the SCB system immediately reveals that the system is observable, since both the $x_b$ and $x_d$ subsystems are always observable. The system is left-invertible, since the state $x_c$ is non-existent, meaning that the steering angle can be identified from the outputs if the initial conditions are known. The system is not right-invertible, since it has an $x_b$ subsystem, reflecting the obvious fact that the yaw rate and lateral acceleration cannot be independently controlled from a single steering angle. The system has no invariant zero dynamics, since the state $x_a$ is non-existent.

If we add rear-axle steering by augmenting the $\hat{B}$ matrix with a column

$$\begin{bmatrix} 0 \\ 0 \\ 0 \\ \frac{c_r}{T_r} \end{bmatrix},$$

the Maple procedure returns the SCB system matrices

$$A = \begin{bmatrix} 0 & 1 & -v_x & 0 \\ -\frac{c_f+c_r}{m T_r v_x} & -\frac{1}{T_r} & \frac{l_r c_r - l_f c_f}{m T_r v_x} & 0 \\ 0 & 0 & 0 & 1 \\ \frac{l_r c_r - l_f c_f}{J T_r v_x} & 0 & -\frac{l_f^2 c_f + l_r^2 c_r}{J T_r v_x} & -\frac{1}{T_r} \end{bmatrix}, \qquad B = \begin{bmatrix} 0 & 0 \\ 1 & 0 \\ 0 & 0 \\ 0 & 1 \end{bmatrix},$$

$$C = \begin{bmatrix} 0 & 1 & 0 & 0 \\ 0 & 0 & 1 & 0 \end{bmatrix}, \qquad D = \begin{bmatrix} 0 & 0 \\ 0 & 0 \end{bmatrix},$$

and the transformations

$$\Gamma_1 = \begin{bmatrix} 1 & 0 & 0 & 0 \\ 0 & 0 & 1 & 0 \\ 0 & \frac{l_r m}{l_f+l_r} & 0 & \frac{J}{l_f+l_r} \\ 0 & \frac{l_f m}{l_f+l_r} & 0 & -\frac{J}{l_f+l_r} \end{bmatrix}, \quad \Gamma_2 = \begin{bmatrix} 0 & 1 \\ 1 & 0 \end{bmatrix}, \quad \Gamma_3 = \begin{bmatrix} \frac{l_r T_r m}{c_f(l_f+l_r)} & \frac{T_r J}{c_f(l_f+l_r)} \\ \frac{l_f T_r m}{c_r(l_f+l_r)} & -\frac{T_r J}{c_r(l_f+l_r)} \end{bmatrix},$$

with dimensions $1, 0, 0, 3$. This means that the first state of the system belongs to the zero dynamics subsystem $x_a$, and the remaining three states belong to the $x_d$ subsystem. The $x_d$ subsystem consists of two integrator chains; one of dimension one, and one of dimension two. We conclude that the system is invertible, due to the lack of $x_b$ and $x_c$ subsystems. The $A_{aa}$ matrix is identically 0, meaning that the system has a zero at the origin. Hence, the relationship between the steering angle inputs and the yaw rate and lateral acceleration outputs is non-minimum phase.

Referring back to our discussion of geometry theory, we see that the weakly unobservable subspace is spanned by the vector $[1, 0, 0, 0]^\mathsf{T}$. Transformed back to the original coordinate basis, this corresponds to the state $v_y$. We therefore know that a hypothetical disturbance occurring in $\dot{v}_y$ can be decoupled from the outputs $a_y$ and $r$ by state feedback (and the SCB representation tells us exactly how to do it). However, we also know that the resulting subsystem would not be asymptotically stable, since the non-minimum phase zero would become a pole of the closed-loop system.

### 7.5.2 DC Motor with Friction

According to Canudas de Wit and Lischinsky (1997), a DC motor process can be described by the equations

$$\begin{aligned} \dot{\Omega} &= \omega, \\ J\dot{\omega} &= u - F, \end{aligned}$$

where $\Omega$ is the shaft angular position, $\omega$ is the angular rate, $u$ is the DC motor torque, $F$ is a friction torque, and $J = 0.0023\ \mathrm{kg\,m^2}$ is the motor and load inertia. The friction torque can be modeled by the dynamic LuGre friction model

$$\begin{aligned} F &= \sigma_0 z + \sigma_1 \dot{z} + \alpha_2 \omega, \\ \dot{z} &= \omega - \frac{\sigma_0 z|\omega|}{\zeta(\omega)}, \end{aligned}$$

where $\zeta(\omega) = \alpha_0 + \alpha_1 \exp(-(\omega/\omega_0)^2)$. Numerical values for the friction parameters are $\sigma_0 = 260.0$ Nm/rad, $\sigma_1 = 0.6$ Nm s/rad, $\alpha_0 = 0.28$ Nm, $\alpha_1 = 0.05$ Nm, $\alpha_2 = 0.176$ Nm s/rad, and $\omega_0 = 0.01$ rad/s. The system can be viewed as consisting of a linear part with a nonlinear perturbation $\sigma_0 z|\omega|/\zeta(\omega)$. Assuming that only the shaft position $\Omega$ is measured, a nonlinear observer can be designed for this system by using the time scale assignment techniques from Saberi and Sannuti (1990a). To do so, it is necessary to find the SCB form of the system, with the nonlinear perturbation $\sigma_0 z|\omega|/\zeta(\omega)$ considered as the sole input. The original

system with the nonlinear perturbation as the input is described by the matrices

$$\hat{A} = \begin{bmatrix} 0 & 1 & 0 \\ 0 & -\frac{1}{J}(\alpha_2 + \sigma_1) & -\frac{1}{J}\sigma_0 \\ 0 & 1 & 0 \end{bmatrix}, \qquad \hat{B} = \begin{bmatrix} 0 \\ \frac{1}{J}\sigma_1 \\ -1 \end{bmatrix}, \tag{7.8a}$$

$$\hat{C} = \begin{bmatrix} 1 & 0 & 0 \end{bmatrix}, \qquad \hat{D} = 0. \tag{7.8b}$$

Inserting numerical values and using the Linear Systems Toolkit (Liu et al., 2005) yields the SCB matrices

$$A \approx \begin{bmatrix} -433.3 & -592.7 & 0 \\ 0 & 0 & 1 \\ -1.1 \cdot 10^5 & -1.5 \cdot 10^5 & 95.9 \end{bmatrix}, \qquad B = \begin{bmatrix} 0 \\ 0 \\ 1 \end{bmatrix},$$

$$C = \begin{bmatrix} 0 & 1 & 0 \end{bmatrix}, \qquad D = 0,$$

where the first state belongs to the zero dynamics subsystem $x_a$, and the remaining two states consist of an integrator chain of length two, in the $x_d$ subsystem. As suggested by the large elements in the system matrices, the problem is poorly conditioned, and we find that we require very large gains to stabilize the system. Using our Maple procedure, we obtain the SCB matrices

$$A = \begin{bmatrix} -\frac{\sigma_0}{\sigma_1} & -\frac{\sigma_0(\sigma_0 J - \sigma_1\alpha_2)}{\sigma_1^3} & 0 \\ 0 & 0 & 1 \\ -\frac{\sigma_0}{J} & -\frac{\sigma_0(\sigma_0 J - \sigma_1\alpha_2)}{J\sigma_1^2} & \frac{\sigma_0 J - \sigma_1\alpha_2 - \sigma_1^2}{J\sigma_1} \end{bmatrix}, \qquad B = \begin{bmatrix} 0 \\ 0 \\ 1 \end{bmatrix},$$

$$C = \begin{bmatrix} 0 & 1 & 0 \end{bmatrix}, \qquad D = 0.$$

This reveals that the small parameter $\sigma_1$ generates a singularity for several elements of $A$, even though the original matrices in (7.8) did not have any singularities with respect to this parameter. In particular, we see that $\sigma_1$ acts as a small regular perturbation that results in singularly perturbed zero dynamics, which happens when a regular perturbation reduces a system's relative degree (Sastry, Hauser, and Kokotović, 1989). Using the approximation $\sigma_1 = 0$ results in a dramatically different structure, with the SCB consisting of a single integrator chain of length three, represented by the SCB matrices

$$A = \begin{bmatrix} 0 & 1 & 0 \\ 0 & 0 & 1 \\ 0 & -\frac{\sigma_0}{J} & -\frac{\alpha_2}{J} \end{bmatrix}, \qquad B = \begin{bmatrix} 0 \\ 0 \\ 1 \end{bmatrix}$$

$$C = \begin{bmatrix} 1 & 0 & 0 \end{bmatrix}, \qquad D = 0.$$

Proceeding with the observer gain selection based on this system, we obtain good results without using high gains.

### 7.5.3 Tenth-Order System

Our last example is a strictly proper, tenth-order system from Sannuti and Saberi (1987):

$$\hat{A} = \begin{bmatrix} 0 & 0 & 0 & 0 & 1 & 1 & 0 & 0 & 0 & 0 \\ -1 & 0 & 0 & 0 & 1 & 0 & 1 & 0 & 0 & 0 \\ 1 & 1 & -1 & -1 & 0 & 0 & -1 & 0 & 0 & 0 \\ 0 & 1 & 1 & 1 & 0 & 0 & 0 & 0 & 0 & 0 \\ -1 & 2 & 0 & -1 & 2 & 0 & 1 & 0 & 0 & 0 \\ 0 & 0 & 0 & 0 & 1 & 0 & 0 & 0 & 0 & 0 \\ 0 & 0 & 0 & 0 & 0 & 1 & 0 & 0 & 0 & 0 \\ -1 & -1 & 0 & 0 & 1 & 0 & 1 & 0 & 0 & 1 \\ 0 & 0 & 0 & 0 & 0 & 0 & 0 & 0 & 0 & 0 \\ 0 & 0 & 0 & 0 & 0 & 0 & 0 & 0 & 1 & 0 \end{bmatrix},$$

$$\hat{B} = \begin{bmatrix} 0 & 1 & 0 & 1 \\ 0 & 0 & 0 & 0 \\ 0 & 0 & 0 & 0 \\ 0 & 1 & 0 & 1 \\ 0 & 2 & 0 & 1 \\ 0 & 0 & 1 & 0 \\ 0 & 0 & 0 & 0 \\ 0 & 0 & 0 & 0 \\ 1 & 0 & 1 & 0 \\ 0 & 0 & 0 & 0 \end{bmatrix}, \quad \hat{C}^{\mathsf{T}} = \begin{bmatrix} -1 & 0 & 0 & 0 \\ -1 & 0 & 0 & 0 \\ 0 & 0 & 1 & 0 \\ 0 & 0 & 0 & 0 \\ 1 & 0 & 0 & 0 \\ 0 & 0 & 0 & 0 \\ 2 & 1 & 0 & 0 \\ 0 & 1 & 0 & 1 \\ 0 & 0 & 0 & 0 \\ 0 & 0 & 0 & 0 \end{bmatrix}.$$

The Maple procedure gives the SCB system matrices

$$A = \begin{bmatrix} 1 & 0 & 0 & 0 & 1 & -1 & 0 & -1 & 0 & 0 \\ 0 & 0 & 1 & 0 & 0 & 0 & 0 & 0 & 0 & 0 \\ 0 & 0 & 0 & 0 & -1 & 1 & 0 & 1 & 0 & 0 \\ 2 & -12 & 0 & 2 & -8 & 8 & 0 & 8 & 0 & 0 \\ 2 & -4 & -2 & \frac{1}{2} & -2 & 1 & 1 & 1 & 1 & 0 \\ 0 & 0 & 0 & 0 & 0 & 0 & 1 & 0 & 0 & 0 \\ 2 & -2 & -2 & 0 & 0 & -1 & 1 & -1 & 1 & -1 \\ 0 & 0 & 0 & 0 & -1 & 0 & 0 & 0 & 1 & 0 \\ 0 & 0 & 0 & 0 & 0 & 0 & 0 & 0 & 0 & 1 \\ 0 & 2 & 0 & -\frac{1}{2} & 2 & -2 & 0 & -2 & 0 & 0 \end{bmatrix},$$

$$B = \begin{bmatrix} 0 & 0 & 0 & 0 \\ 0 & 0 & 0 & 0 \\ 0 & 0 & 0 & 0 \\ 0 & 0 & 0 & 1 \\ 1 & 0 & 0 & 0 \\ 0 & 0 & 0 & 0 \\ 0 & 1 & 0 & 0 \\ 0 & 0 & 0 & 0 \\ 0 & 0 & 0 & 0 \\ 0 & 0 & 1 & 0 \end{bmatrix}, \quad C^{\mathsf{T}} = \begin{bmatrix} 0 & 0 & 0 & 0 \\ 0 & 0 & 0 & 1 \\ 0 & 0 & 0 & 0 \\ 0 & 0 & 0 & 0 \\ 1 & 0 & 0 & 0 \\ 0 & 1 & 0 & 0 \\ 0 & 0 & 0 & 0 \\ 0 & 0 & 1 & 0 \\ 0 & 0 & 0 & 0 \\ 0 & 0 & 0 & 0 \end{bmatrix},$$

and the dimensions $1, 2, 1, 6$. Hence, the first state belongs to the $x_a$ subsystem, and we can therefore easily see that the system has a non-minimum phase invariant zero at 1. The next two states belong to the $x_b$ subsystem; thus, the system is not right-invertible. The fourth state belongs to the $x_c$ subsystem; thus, the system is not left-invertible. Finally, the last six states consists of three integrator chains of length 1, 2, and 3, respectively, belonging to the $x_d$ subsystem.

## 7.6 Numerical Issues

The procedure described in this paper uses exact operations only; thus, there is no uncertainty in the results produced by the decomposition algorithm. The algorithm is primarily based on rank operations and the construction of bases for various subspaces. Rank operations are discontinuous, in the sense that arbitrarily small perturbations to a matrix may alter its rank. This implies that, when a decomposition is carried out using exact operations, arbitrarily small perturbations to system matrices may fundamentally alter the identified structure of a system. This is in contrast to decompositions based on floating-point operations, which may be insensitive to small perturbations to the system matrices.

Whether exactness is desirable or not depends on the application. When the input data is exact or the system model is based on first principles, an exact decomposition may help to reveal fundamental structural properties of the system and how these properties are affected by various quantities in the system matrices. If, on the other hand, the system matrices have been derived based on experimental system identification, an exact decomposition may not be desirable, and it may even provide misleading information about the system structure. Thus, the exact procedure presented here is not a replacement for numerical tools developed for the same purpose.

Throughout the decomposition algorithm, a number of non-unique transformation matrices must be constructed. In the Maple procedure, these matrices are

constructed with the goal of having a simple structure, based on the assumption that fewer changes to the original states will result in less complicated symbolic expressions in the computed SCB system. Depending on the structure and dimensions of the system, however, the procedure may still result in complicated expressions, and if the original system matrices contain complicated expressions, these will in general not be simplified.

A precise analysis of the computational complexity of the procedure is difficult, due to the complex nature of the decomposition algorithm and the underlying Maple functions. However, it is possible to make some practical observations regarding this issue. Executed in Maple 12 on an Intel Pentium processor with two 2-MHz cores, the total CPU time needed for decomposition of the single-track model was approximately 0.30 s for the single-input case and 0.21 s for the double-input case. For the DC motor example, the total CPU time was approximately 0.19 s for the original matrices in (7.8) and 0.25 s with the modification $\sigma_1 = 0$. For the tenth-order example, the total CPU time was approximately 0.48 s. These execution times illustrate that an increase in the order of the system does not automatically result in a large increase in execution time; the structure of the system and the complexity of the expressions in the system matrices has a greater impact on execution time. For example, randomly generated, strictly proper systems with 20 states, 4 inputs and 4 outputs, with the system matrices made up of integers between $-10$ and 10 with 25% density, are generally decomposed in less than 0.4 s. If, on the other hand, the number of inputs is reduced to 3, the decomposition generally takes around 50 s. The reason for this large difference is that, in the former case, the computed SCB systems generally consist of an $x_a$ subsystem with 16 states and an $x_d$ subsystem with four states, which requires only a single iteration of the algorithm for identifying $x_b$ and $x_d$ (described at the beginning of Section 7.4.1). In the latter case, the computed SCB systems generally consist of an $x_b$ subsystem with 17 states, and an $x_d$ subsystem with three states, which requires 17 increasingly complex iterations of the algorithm for identifying $x_b$ and $x_d$.

## 7.7 Concluding Remarks

We have presented a procedure written in the mathematics software suite Maple, which is capable of transforming any linear time-invariant system described by exact symbols and fractions to the SCB, and we have illustrated the use of this algorithm on several examples.

The DC motor example shows that the symbolic form of the SCB can be used to reveal structural bifurcations in linear systems due to parameter changes. Systematic ways of using symbolic representations of the SCB for this purpose is a topic

of future research. Future research will also investigate application of symbolic SCB representations to topics such as squaring down of non-square systems and asymptotic time scale assignment.

## Acknowledgments

The work of Håvard Fjær Grip is supported by the Research Council of Norway. The work of Ali Saberi is partially supported by National Science Foundation grant NSF-0901137 and NAVY grants ONR KKK777SB001 and ONR KKK760SB0012.

## Bibliography

M. C. Berg. Introduction to a special coordinate basis for multivariable linear systems. *IEE Proc. Contr. Theor. Appl.*, 145(2):204–210, 1998.

C. Canudas de Wit and P. Lischinsky. Adaptive friction compensation with partially known dynamic friction model. *Int. J. Adapt. Contr. Signal Process.*, 11 (1):65–80, 1997.

B. M. Chen. *Robust and $H_\infty$ Control*. Springer, London, 2000.

B. M. Chen, A. Saberi, and P. Sannuti. Explicit expressions for cascade factorization of general nonminimum phase systems. *IEEE Trans. Automat. Contr.*, 37 (3):358–363, 1992.

B. M. Chen, Z. Lin, and Y. Shamash. *Linear Systems Theory: A Structural Decomposition Approach*. Birkhäuser, Boston, 2004.

D. Chu, X. Liu, and R. C. E. Tan. On the numerical computation of a structural decomposition in systems and control. *IEEE Trans. Automat. Contr.*, 47(11): 1786–1799, 2002.

H. F. Grip and A. Saberi. Maple source code for structural decomposition of linear multivariable systems, version 0.2, 2010. Available from: http://www.itk.ntnu.no/ansatte/Grip_Havard.Fjar/sw/scb.mpl.

U. Kiencke and L. Nielsen. *Automotive Control Systems: For Engine, Driveline, and Vehicle*. Springer, Berlin, 2000.

X. Liu, B. M. Chen, and Z. Lin. Linear systems toolkit in Matlab: Structural decompositions and their applications. *J. Contr. Theor. Appl.*, 3(3):287–294, 2005.

A. G. J. MacFarlane and N. Karcanias. Poles and zeros of linear multivariable systems: A survey of the algebraic, geometric and complex-variable theory. *Int. J. Contr.*, 24(1):33–74, 1976.

A. S. Morse. Structural invariants of linear multivariable systems. *SIAM J. Contr.*, 11(3), 1973.

H. K. Ozcetin, A. Saberi, and P. Sannuti. Special coordinate basis for order reduction of linear multivariable systems. *Int. J. Contr.*, 52(1):191–226, 1990.

H. B. Pacejka. *Tire and Vehicle Dynamics*. SAE, Warrendale, PA, 2nd edition, 2006.

A. Saberi and P. Sannuti. Observer design for loop transfer recovery and for uncertain dynamical systems. *IEEE Trans. Automat. Contr.*, 35(8):878–897, 1990a.

A. Saberi and P. Sannuti. Squaring down of non-strictly proper systems. *Int. J. Contr.*, 51(3):621–629, 1990b.

A. Saberi, B. M. Chen, and P. Sannuti. Theory of LTR for non-minimum phase systems, recoverable target loops, and recovery in a subspace Part 1. Analysis. *Int. J. Contr.*, 53(5):1067–1115, 1991.

A. Saberi, B. M. Chen, and P. Sannuti. *Loop Transfer Recovery: Analysis and Design*. Springer, London, 1993.

A. Saberi, P. Sannuti, and B. M. Chen. *$H_2$ Optimal Control*. Prentice-Hall, London, 1995.

A. Saberi, A. A. Stoorvogel, and P. Sannuti. *Filtering Theory*. Birkhäuser, Boston, 2006.

P. Sannuti and A. Saberi. Special coordinate basis for multivariable linear systems—Finite and infinite zero structure, squaring down and decoupling. *Int. J. Contr.*, 45(5):1655–1704, 1987.

S. Sastry, J. Hauser, and P. V. Kokotović. Zero dynamics of regularly perturbed systems may be singularly perturbed. *Syst. Contr. Lett.*, 13(4):299–314, 1989.

L. M. Silverman. Inversion of multivariable linear systems. *IEEE Trans. Automat. Contr.*, 14(3):270–276, 1969.

H. L. Trentelman, A. A. Stoorvogel, and M. L. J. Hautus. *Control Theory for Linear Systems*. Springer, London, 2001.

W. M. Wonham. *Linear Multivariable Control: A Geometric Approach*. Springer, New York, 2nd edition, 1979.

# Part III

# Estimation and Control for Systems with Saturations

# Chapter 8

# Stabilization of Multiple-Input Multiple-Output Linear Systems with Saturated Outputs

***Abstract:*** *We consider linear time-invariant multiple-input multiple-output systems that are controllable and observable, where each output component is saturated. We demonstrate by constructive design that such systems can be globally asymptotically stabilized by output feedback without further restrictions. This result is an extension of a previous result by Kreisselmeier for single-input single-output systems. The control strategy consists of driving the components of the output vector out of saturation one by one, to identify the state of the system. Deadbeat control is then applied to drive the state to the origin.*

## 8.1 Introduction

Saturations are ubiquitous in physical control systems, and occur both in actuators, states, and outputs. In this note we focus on linear time-invariant multiple-input multiple-output (MIMO) systems with saturated outputs. An output saturation typically occurs when a measured quantity exceeds the range of the sensor used to measure it. It can also occur as a result of a nonlinear measurement equation. An example of the latter can be found in the automotive industry, where the measured lateral acceleration of a car can be used to estimate its sideslip angle (Grip, Imsland, Johansen, Kalkkuhl, and Suissa, 2009). The response of the lateral acceleration to changes in the sideslip angle is approximately linear for small sideslip angles, but a saturation occurs for large sideslip angles.

Several results in the literature deal with the issue of output saturations. Kreisselmeier demonstrated in Kreisselmeier (1996) that it is possible to design a control law for any linear time-invariant single-input single-output (SISO) system with a saturated output to make it globally asymptotically stable, provided the linear system is controllable and observable. It is not obvious that this should be possible, because globally stabilizable and observable systems may not be globally stabilizable by output feedback, as demonstrated in Mazenc and Praly (1994). Observability of systems with saturated outputs was studied in detail in Koplon, Sontag, and Hautus (1994).

Lin and Hu (2001) presented a design that applies to stabilizable and detectable SISO systems with all the invariant zeros located in the closed left-half plane. The design in Lin and Hu (2001) is semiglobal, but it is based on a linear control law, unlike the discontinuous control law from Kreisselmeier (1996). As pointed out by the authors, the approach in Lin and Hu (2001) cannot easily be extended to MIMO systems. In Marconi (2003), the result in Lin and Hu (2001) was extended to handle tracking of signals produced by marginally stable exosystems.

Kaliora and Astolfi (2004) presented an approach for global stabilization of linear systems with output saturations, under the conditions that the linear system is controllable and observable, and that the open-loop system is stable. The design in Kaliora and Astolfi (2004) is formulated for SISO systems, but it is also applicable to MIMO systems, as remarked by the authors. Recent results on anti-windup strategies for systems with output saturations (see, e.g., Turner and Tarbouriech, 2009), as well as an $H_\infty$-based approach (Cao, Lin, and Chen, 2003) for systems with output nonlinearities, also deal with MIMO systems. However, these methods can in general provide neither global nor semiglobal stabilization, unless the open-loop system is already asymptotically stable.

To the best of our knowledge, no previous results address stabilization of general controllable and observable linear MIMO systems with output saturations, either globally or semiglobally. The purpose of this note is to demonstrate by constructive design that such stabilization is possible without further restrictions, by extending the result of Kreisselmeier for SISO systems. In Kreisselmeier's design, the output is first brought out of saturation using a control strategy that relies only on the sign of the output. When the output comes out of saturation, the state of the system is identified exactly by using a deadbeat observer. This is possible, even if the output is out of saturation only for a brief interval, because the system behaves like a linear observable system during that time. Once the state of the system has been identified, it is brought to the origin in finite time by using a deadbeat control strategy. At first glance, the MIMO case looks considerably more complicated. The analogous strategy would be to drive the output of the linear system into the hyperrectangle where every output component is unsaturated. It is exceedingly difficult

to do so, however, because one needs to coordinate several output components to make them simultaneously unsaturated, based only on their signs.

The central point in this note is that it is unnecessary to make the output components simultaneously unsaturated. Instead it is sufficient to bring each component out of saturation at least once, even if some or all of the other components are saturated when this happens. Our control strategy is therefore to drive the components out of saturation one by one. The data gathered from each component when it was unsaturated is then pieced together to identify the state of the system. Finally, the state is brought to the origin by deadbeat control.

We emphasize that the focus of this note is not on issues of performance; rather, the goal is to prove that global asymptotic stabilization by output feedback is possible for the class of systems under considerations, and to illustrate the principle that information from multiple output components that come out of saturation at different points in time can be combined to identify the state of the system. Nevertheless, we present a numerical simulation example that illustrates the workings of the control law, and we discuss various numerical issues related to implementation of the control law.

## 8.2 Problem Formulation

We consider a linear time-invariant system with saturated outputs:

$$\dot{x}(t) = Ax(t) + Bu(t), \quad x(t) \in \mathbb{R}^n, u(t) \in \mathbb{R}^m, \tag{8.1a}$$

$$y(t) = \text{sat}(Cx(t)), \quad y(t) \in \mathbb{R}^p, \tag{8.1b}$$

where $\text{sat}(\cdot)$ represents a standard component-wise saturation. That is,

$$y(t) = \begin{bmatrix} \text{sat}(C_1 x(t)) \\ \vdots \\ \text{sat}(C_p x(t)) \end{bmatrix},$$

where $\text{sat}(C_i x(t)) = \text{sign}(C_i x(t)) \min\{1, |C_i x(t)|\}$ and $C_i$, $i = 1, \ldots, p$, are the rows of $C$.

**Assumption 8.1.** *The pair $(A, B)$ is controllable, and the pair $(C, A)$ is observable.*

We assume that the system is initialized at time $t = 0$. We seek to render to the origin of the system (8.1) globally asymptotically stable by output feedback.

## 8.3 Control

For the purpose of control, we divide the time $t > 0$ into intervals $(kT, kT + T]$, where $k = 0, 1, 2, \ldots$, and $T > 0$ is a constant chosen by the designer. On each interval, the control is given as in Kreisselmeier (1996) by

$$u(kT + \tau) = -B^{\mathsf{T}} \mathrm{e}^{-A^{\mathsf{T}}\tau} U_k, \quad \tau \in (0, T], \tag{8.2}$$

where $U_k$ is constant on the interval $(kT, kT + T]$. We define $U_k$ as follows:

$$U_k = \begin{cases} \bar{B}^{-1}\alpha^k(\alpha h_{j_k} - \mathrm{e}^{AT} h_{j_k}) y_{j_k}(kT), & \prod_{i=1}^{p} \sigma_i(kT) = 0, \\ \bar{B}^{-1}\mathrm{e}^{AT}(\mathrm{e}^{AkT} D^{-1}(kT)\xi(kT) + \mu(kT)), & \prod_{i=1}^{p} \sigma_i(kT) > 0, \end{cases} \tag{8.3}$$

where $j_k$ is defined as the smallest $i \in 1, \ldots, p$ such that $\sigma_i(kT) = 0$. The vectors $h_i \in \mathbb{R}^n$, $i = 1, \ldots, p$, are chosen by the designer in such a way that $C_i h_i > 0$. The scalar $\alpha$ is defined as $\alpha = \rho \|\exp(AT)\|$, where $\rho > 1$ is a number chosen by the designer. The constant matrix $\bar{B} \in \mathbb{R}^{n \times n}$ is defined as

$$\bar{B} = \int_0^T \mathrm{e}^{A(T-\tau)} B B^{\mathsf{T}} \mathrm{e}^{-A^{\mathsf{T}}\tau} \, \mathrm{d}\tau. \tag{8.4}$$

We note that $\bar{B}$ is invertible, due to controllability of the pair $(A, B)$. The quantities $\sigma_i(t) \in \mathbb{R}$, $i = 1, \ldots, p$, $\xi(t) \in \mathbb{R}^n$, $\mu(t) \in \mathbb{R}^n$, and $D(t) \in \mathbb{R}^{n \times n}$ are given by the following expressions:

$$\sigma_i(t) = \int_0^t (1 - |y_i(\tau)|) \, \mathrm{d}\tau, \quad i = 1, \ldots, p, \tag{8.5a}$$

$$\xi(t) = \sum_{i=1}^{p} \int_0^t (1 - |y_i(\tau)|) \mathrm{e}^{A^{\mathsf{T}}\tau} C_i^{\mathsf{T}} \left(y_i(\tau) - C_i \mu(\tau)\right) \, \mathrm{d}\tau, \tag{8.5b}$$

$$\mu(t) = \int_0^t \mathrm{e}^{A(t-\tau)} B u(\tau) \, \mathrm{d}\tau, \tag{8.5c}$$

$$D(t) = \sum_{i=1}^{p} \int_0^t (1 - |y_i(\tau)|) \mathrm{e}^{A^{\mathsf{T}}\tau} C_i^{\mathsf{T}} C_i \mathrm{e}^{A\tau} \, \mathrm{d}\tau. \tag{8.5d}$$

In the following section, we provide a simple explanation of how the control algorithm works. The details of this explanation will become clear from the proof of Theorem 8.1 in Section 8.3.2.

### 8.3.1 Explanation of the Control Law

The control strategy is based on dividing the time $t > 0$ into intervals $(kT, kT+T]$. At the beginning of each interval, the control to be applied over the interval is determined by calculating the vector $U_k$ according to (8.3). The scalar functions $\sigma_i(t)$, $i = 1, \ldots, p$, play a crucial role in this process. Each signal $\sigma_i(t)$ is an indicator of whether the corresponding output component $y_i(t)$ has been out of saturation at any time since initialization at time $t = 0$. If $y_i(t)$ has been saturated the whole time, then $\sigma_i(t) = 0$; if $y_i(t)$ has been out of saturation at any point since initialization, then $\sigma_i(t) > 0$.

#### Driving the Outputs Out of Saturation

The initial task of the controller is to ensure that each output component $y_i(t)$ comes out of saturation at least once. This task is accomplished sequentially, by first ensuring that $y_1(t)$ comes out of saturation, then ensuring that $y_2(t)$ comes out of saturation, and so on. At the start of an interval $(kT, kT + T]$, the value $j_k$ is set to the smallest $i$ such that $\sigma_i(kT) = 0$, meaning that $y_i(t)$ has not yet been out of saturation. Assuming such an $i$ exists, $U_k$ is set to $U_k = \bar{B}^{-1}\alpha^k(\alpha h_{j_k} - \mathrm{e}^{AT}h_{j_k})y_{j_k}(kT)$, according to (8.3). This choice of $U_k$ is the same as the one used in Kreisselmeier (1996) to drive the output of a SISO system out of saturation. The strategy behind this choice is to drive the output in the direction of the origin, based only on the sign of the output. For each interval that passes, the control amplitude grows larger, due to the factor $\alpha^k$. The increasing control amplitude is needed in order to catch up with any instabilities in the system that may be driving the output away from the origin.

#### Deadbeat Control

Eventually, every output component will have been out of saturation at least once, and thus there will be an integer $\hat{k}$ such that at time $\hat{k}T$, we have $\sigma_i(\hat{k}T) > 0$ for all $i \in 1, \ldots, p$. This can also be expressed as $\prod_{i=1}^{p}\sigma_i(\hat{k}T) > 0$. At this point, $U_{\hat{k}}$ is chosen as $U_{\hat{k}} = \bar{B}^{-1}\mathrm{e}^{AT}(\mathrm{e}^{A\hat{k}T}D^{-1}(\hat{k}T)\xi(\hat{k}T) + \mu(\hat{k}T))$, according to (8.3). To justify this choice, we first note that the initial condition of the system can be related to the quantities in (8.5) by the expression $\xi(\hat{k}T) = D(\hat{k}T)x(0)$ (this relationship will become clear from the proof of Theorem 8.1 below). Since every component of the output has been out of saturation at least once, $D(\hat{k}T)$ is a nonsingular matrix, and hence $x(0)$ can be calculated as $x(0) = D^{-1}(\hat{k}T)\xi(\hat{k}T)$. Once $x(0)$ is known, $x(\hat{k}T)$ can also be calculated from the standard variation-of-constants formula (DeCarlo, 1989) as $x(\hat{k}T) = \mathrm{e}^{A\hat{k}T}x(0) +$

$\int_0^{\hat{k}T} \mathrm{e}^{A(\hat{k}T-\tau)} Bu(\tau)\,\mathrm{d}\tau = \mathrm{e}^{A\hat{k}T} D^{-1}(\hat{k}T)\xi(\hat{k}T) + \mu(\hat{k}T)$. We have therefore identified the state of the system at time $\hat{k}T$ precisely. We can now rewrite $U_{\hat{k}}$ as $U_{\hat{k}} = \bar{B}^{-1}\mathrm{e}^{AT}x(\hat{k}T)$, which yields the same deadbeat control as in Kreisselmeier (1996) and ensures that $x(\hat{k}T + T) = 0$. The difference between this note and Kreisselmeier (1996) lies in how the information from different output components, which become unsaturated at different times, is pieced together to allow deadbeat observation of the state of the system.

*Remark* 8.1. We remark that $\alpha$ in this note is chosen somewhat differently from Kreisselmeier (1996), where $\alpha$ was defined as $\alpha = \exp(2\|A\|T)$. The point of redefining $\alpha$ is to ensure that the factor $\alpha^k$ does not grow much faster than what is necessary to drive the output components out of saturation. The definition used here also ensures that $\alpha > \|\exp(AT)\|$, even when $A = 0$. Technically, an additional condition of this kind is also needed in Kreisselmeier (1996), to handle the particular case where the system consists of a single integrator.

### 8.3.2 Stability

We now state the stability results of the closed-loop system in a formal manner.

**Theorem 8.1.** *The origin of* (8.1) *with the control* (8.2)–(8.5) *is globally asymptotically stable.*

*Proof.* Given $t_1$ and $t_2$ such that $t_2 \geq t_1 \geq 0$, we know from the standard variation-of-constants formula (DeCarlo, 1989) that

$$x(t_2) = \mathrm{e}^{A(t_2-t_1)}x(t_1) + \int_0^{t_2-t_1} \mathrm{e}^{A(t_2-t_1-\tau)} Bu(t_1+\tau)\,\mathrm{d}\tau. \tag{8.6}$$

Applying this formula over an interval by setting $t_1 = kT$ and $t_2 = kT + T$, and inserting the expression (8.2) for the control law, it is easily confirmed that we obtain, as in Kreisselmeier (1996),

$$x(kT + T) = \mathrm{e}^{AT}x(kT) - \bar{B}U_k. \tag{8.7}$$

We shall use the expression (8.7) in the remainder of the proof, which is divided into two parts, similar to Kreisselmeier (1996). First, we show that the origin is globally attractive, and then we show that it is a Lyapunov stable equilibrium point.

**The origin is globally attractive** We start by showing that there is an integer $\hat{k}$ such that each output component has been out of saturation on $[0, \hat{k}T]$. For the sake of establishing a contradiction, suppose that this is not the case. Then there

is a set of output components that remain in saturation for all time. Let $l$ denote the smallest integer such that $y_l(t)$ remains in saturation for all time. Then there is an integer $\bar{k}$ such that for all $k \geq \bar{k}$, $\sigma_i(kT) > 0$ for all $i = 1, \ldots, l-1$. It follows that $j_k = l$ for all $k \geq \bar{k}$. We now establish the contradiction by showing that $y_l(t)$ will eventually become unsaturated. This is established in the same way as in the proof from Kreisselmeier (1996).

Since $j_k = l$ for all $k \geq \bar{k}$, we have from (8.3) that for all $k \geq \bar{k}$, $U_k = \bar{B}^{-1}\alpha^k(\alpha h_l - \mathrm{e}^{AT}h_l)y_l(kT)$. Inserting this expression for $U_k$ into (8.7), we see that for all $k \geq \bar{k}$, $x(kT+T) = \mathrm{e}^{AT}x(kT) - \alpha^k(\alpha h_l - \mathrm{e}^{AT}h_l)y_l(kT)$, which can be reformulated as

$$x(kT+T) = \mathrm{e}^{AT}(x(kT) + \alpha^k h_l y_l(kT)) - \alpha^{k+1}h_l y_l(kT). \tag{8.8}$$

Since $y_l(t)$ is assumed to be saturated for all time, we can replace $y_l(kT)$ in (8.8) by $y_l(\bar{k}T)$. We can furthermore calculate the solution recursively as

$$x(kT+T) = \mathrm{e}^{A\tilde{k}T}(x(\bar{k}T) + \alpha^{\bar{k}}h_l y_l(\bar{k}T)) - \alpha^{k+1}h_l y_l(\bar{k}T),$$

where $\tilde{k} = k - \bar{k} + 1$. Premultiplying this expression by $y_l(\bar{k}T)C_l$ and making the substitution $k+1 = \tilde{k} + \bar{k}$ gives

$$y_l(\bar{k}T)y_l(kT+T) = C_l\mathrm{e}^{A\tilde{k}T}(x(\bar{k}T)y_l(\bar{k}T) + \alpha^{\bar{k}}h_l) - \alpha^{\tilde{k}+\bar{k}}C_l h_l.$$

We now upper-bound the first term on the right-hand side, using the expression $\alpha^{\tilde{k}} = \rho^{\tilde{k}}\|\exp(AT)\|^{\tilde{k}}$, which yields

$$y_l(\bar{k}T)y_l(kT+T) \leq \|\mathrm{e}^{AT}\|^{\tilde{k}}\left(\|C_l\|(\|x(\bar{k}T)\| + \alpha^{\bar{k}}\|h_l\|) - \rho^{\tilde{k}}\alpha^{\bar{k}}C_l h_l\right).$$

Considering the expression inside the parenthesis, we see that the first term remains constant as $k$, and therefore $\tilde{k}$, grows larger, whereas the second term becomes more and more negative (recall that $C_l h_l > 0$). Thus, we eventually have $y_l(\bar{k}T)y_l(kT+T) < 0$, which implies that the sign of $y_l(kT+T)$ is different from the sign of $y_l(\bar{k}T)$. This contradicts the assumption that $y_l(t)$ remains saturated for all time, and we have therefore proven that there exists an integer $\hat{k}$ such that all the output components have been out of saturation at least once on $[0, \hat{k}T]$.

It follows from the above discussion that $\prod_{i=1}^{p}\sigma_i(\hat{k}T) > 0$. Thus, we have from (8.3) that

$$U_{\hat{k}} = \bar{B}^{-1}\mathrm{e}^{AT}(\mathrm{e}^{A\hat{k}T}D^{-1}(\hat{k}T)\xi(\hat{k}T) + \mu(\hat{k}T)).$$

As discussed in Section 8.3.1, the idea behind this choice is to make $U_{\hat{k}}$ satisfy the expression $U_{\hat{k}} = \bar{B}^{-1}\mathrm{e}^{AT}x(\hat{k}T)$. This would result in deadbeat control as

in Kreisselmeier (1996), which is easily seen by inserting the expression $U_{\hat{k}} = \bar{B}^{-1}\mathrm{e}^{AT}x(\hat{k}T)$ into (8.7), to obtain $x(\hat{k}T+T) = \mathrm{e}^{AT}x(\hat{k}T) - \mathrm{e}^{AT}x(\hat{k}T) = 0$. We now need to show that $\mathrm{e}^{A\hat{k}T}D^{-1}(\hat{k}T)\xi(\hat{k}T) + \mu(\hat{k}T) = x(\hat{k}T)$.

Using (8.6) with $t_1 = 0$ and $t_2 = t$, it is easily confirmed that we have $x(t) = \mathrm{e}^{At}x(0) + \mu(t)$. Premultiplying this expression by $(1-|y_i(t)|)\mathrm{e}^{A^{\mathsf{T}}t}C_i^{\mathsf{T}}C_i$ for any $i \in 1,\ldots,p$ and rearranging yields

$$(1-|y_i(t)|)\mathrm{e}^{A^{\mathsf{T}}t}C_i^{\mathsf{T}}\left(y_i(t) - C_i\mu(t)\right) = (1-|y_i(t)|)\mathrm{e}^{A^{\mathsf{T}}t}C_i^{\mathsf{T}}C_i\mathrm{e}^{At}x(0),$$

where we have used the fact that $C_i x_i(t) = y_i(t)$ whenever $(1-|y_i(t)|) \neq 0$. If we now integrate this expression from 0 to $\hat{k}T$ and take the sum over $i$ from 1 to $p$, we obtain the expression $\xi(\hat{k}T) = D(\hat{k}T)x(0)$. Assuming for the moment that $D(\hat{k}T)$ is nonsingular, we can calculate the initial condition as $x(0) = D^{-1}(\hat{k}T)\xi(\hat{k}T)$. Again using (8.6) with $t_1 = 0$ and $t_2 = \hat{k}T$, we obtain the desired expression $\mathrm{e}^{A\hat{k}T}D^{-1}(\hat{k}T)\xi(\hat{k}T) + \mu(\hat{k}T) = x(\hat{k}T)$.

We still have to show that $D(\hat{k}T)$ is nonsingular. We can write $D(\hat{k}T) = \sum_{i=1}^{p} D_i(\hat{k}T)$, where

$$D_i(\hat{k}T) = \int_0^{\hat{k}T} (1-|y_i(\tau)|)\mathrm{e}^{A^{\mathsf{T}}\tau}C_i^{\mathsf{T}}C_i\mathrm{e}^{A\tau}\,\mathrm{d}\tau. \tag{8.9}$$

Each matrix $D_i(\hat{k}T)$ is positive semidefinite, because the integrand in (8.9) is positive semidefinite. It follows that $D(\hat{k}T)$ is also positive semidefinite. We shall prove that $D(\hat{k}T)$ is in fact positive *definite*, by showing that $z^{\mathsf{T}}D(\hat{k}T)z > 0$ for each $z \neq 0$.

Since each component of the output has been out of saturation on the interval $[0,\hat{k}T]$ and the solutions are continuous, there exists a number $m > 0$ and a set of intervals $(t_i, t_i+\varepsilon) \subset (0,\hat{k}T)$, $i = 1,\ldots,p$, of length $\varepsilon > 0$ such that for all $t \in (t_i, t_i+\varepsilon)$, $1-|y_i(t)| > m$. It therefore follows that

$$z^{\mathsf{T}}D(\hat{k}T)z = \sum_{i=1}^{p} z^{\mathsf{T}}D_i(\hat{k}T)z > m\sum_{i=1}^{p}\int_{t_i}^{t_i+\varepsilon} z^{\mathsf{T}}\mathrm{e}^{A^{\mathsf{T}}\tau}C_i^{\mathsf{T}}C_i\mathrm{e}^{A\tau}z\,\mathrm{d}\tau. \tag{8.10}$$

Suppose for the sake of establishing a contradiction that there exists a $z \neq 0$ such that the right-hand side of (8.10) is zero. This implies that for each $i \in 1,\ldots,p$ and for all $t \in (t_i, t_i+\varepsilon)$, $z^{\mathsf{T}}\mathrm{e}^{A^{\mathsf{T}}t}C_i^{\mathsf{T}}C_i\mathrm{e}^{At}z = 0$. This furthermore implies that for each $i = 1,\ldots,p$ and for all $t \in (t_i, t_i+\varepsilon)$, $C_i\mathrm{e}^{At}z = 0$, which means that for all $t \in (t_i, t_i+\varepsilon)$, $\mathrm{e}^{At}z$ must belong to the unobservable subspace of the pair $(C_i, A)$. Since the unobservable subspace is $A$-invariant (see DeCarlo, 1989, Ch. 21), the vector $z$ must also belong to the unobservable subspace with respect to the pair

$(C_i, A)$. However, if the vector $z$ belongs to unobservable subspace of $(C_i, A)$ for each $i \in 1, \ldots, p$, then it belongs to the unobservable subspace of $(C, A)$, which consists only of the origin. This shows that the right-hand side of (8.10) cannot be zero unless $z = 0$, and it follows that $D(\hat{k}T)$ is positive definite (and therefore nonsingular).

The above argument proves that $U_{\hat{k}}$ satisfies $U_{\hat{k}} = \bar{B}^{-1}\mathrm{e}^{AT}x(\hat{k}T)$, so that deadbeat control is applied over the interval $(\hat{k}T, \hat{k}T + T]$. This yields $x(\hat{k}T + T) = 0$. The same argument can be used to show that $U_{\hat{k}+1} = \bar{B}^{-1}\mathrm{e}^{AT}x(\hat{k}T + T) = 0$, and thus the control $u(t) = 0$ is applied over the interval $(\hat{k}T + T, \hat{k}T + 2T]$. It follows that $x(t)$ remains at the origin on this interval, and by induction, on every subsequent interval.

**The origin is a Lyapunov stable equilibrium point** Lyapunov stability is established by the same approach as in Kreisselmeier (1996). Suppose that $\|x(0)\|$ is sufficiently small such that all the output components are unsaturated at $t = 0$ (i.e., $|y_i(0)| < 1, i = 1, \ldots, p$). Clearly $\sigma_i(0) = 0$ for all $i \in 1, \ldots, p$. Hence, $j_0 = 1$, and $U_0$ is given by $U_0 = \bar{B}^{-1}(\alpha h_1 - \mathrm{e}^{AT}h_1)y_1(0)$, according to (8.3). It follows that $\|U_0\|$ is bounded by an expression proportional to $\|y_1(0)\|$, and therefore also by an expression proportional to $\|x(0)\|$. Using (8.6), it is now straightforward to show that there is a $\gamma_1 > 1$ such that for all $t \in (0, T]$, $\|x(t)\| \leq \gamma_1\|x(0)\|$. Since every output component is out of saturation for at least part of the first interval, we have $\sigma_i(T) > 0$ for all $i \in 1, \ldots, p$. By the above discussion of global attractivity, we therefore have $U_1 = \bar{B}^{-1}\mathrm{e}^{AT}x(T)$, and it follows that $\|U_1\|$ is bounded by an expression proportional to $\|x(T)\|$. Using (8.6), it is now straightforward to show that there is a $\gamma_2 > 1$ such that for all $t \in (T, 2T]$, $\|x(t)\| \leq \gamma_2\|x(T)\|$. For all $t > 2T$, we have $x(t) = 0$. Combining the above inequalities, we therefore find that for sufficiently small $\|x(0)\|$, $\|x(t)\| \leq \gamma_1\gamma_2\|x(0)\|$ for all $t \geq 0$. This shows that the origin is a Lyapunov stable equilibrium point. □

## 8.4 Numerical Issues and Tuning

As mentioned above, the input applied to the system to drive the outputs out of saturation grows larger with each time interval, in order to catch up with any instabilities in the system. As a consequence of this, the state of the system may grow large, and an output component may come out of saturation only briefly before again becoming saturated. The calculation of the state of the system may therefore be poorly conditioned and sensitive to measurement noise, disturbances, and model inaccuracies.

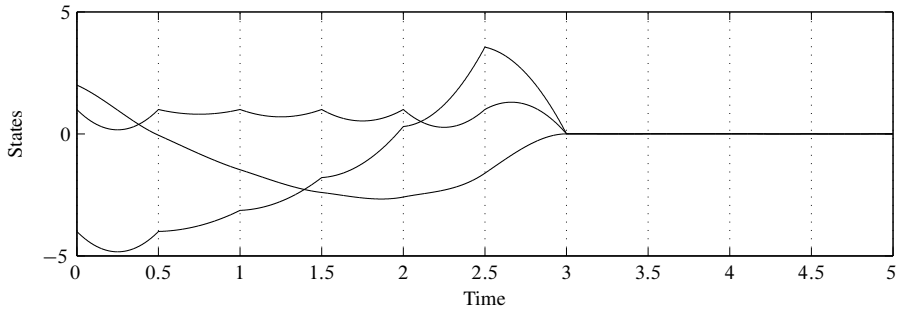


(a) State

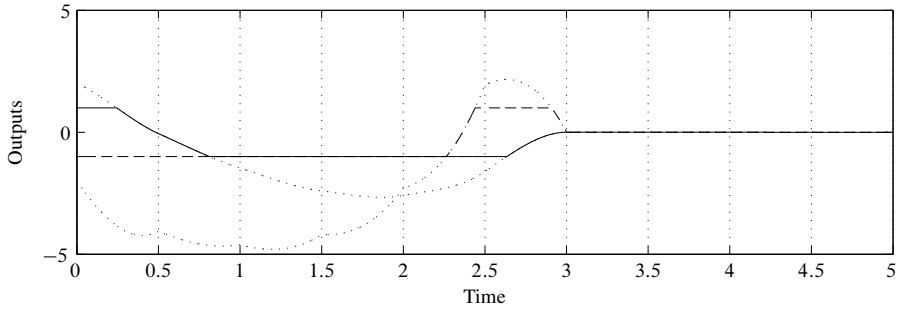


(b) Outputs (solid: $y_1$, dashed: $y_2$). Unsaturated versions of the outputs are shown with dotted lines.

**Figure 8.1:** Simulation results

Applying a growing input is not necessary for systems that are open-loop stable (as, for example, in Kaliora and Astolfi, 2004). In this case, there is no danger of the state escaping, and so a small input may be applied over a long period of time to bring all the outputs out of saturation. An alternative to applying a growing input is to adjust the controller parameters according to the size of an admissible set of initial conditions, leading to semiglobal results, as in Lin and Hu (2001).

We follow the approach of Kreisselmeier (1996) in applying deadbeat control to bring the state to the origin. However, deadbeat control is rarely used in practical implementations, in particular, due to robustness problems. There is no theoretical requirement that deadbeat control be used in the present case; once the state of the system has been identified, it is in principle known for all future time, and thus any state-feedback controller may be applied instead of the deadbeat controller.

Several of the quantities used in the controller can be adjusted by the designer, in particular, $T$, $\rho$, and $h_i$, $i = 1, \ldots, p$. These quantities can be viewed as tuning parameters with associated tradeoffs. Choosing $T$ small ensures that, once an

output has been driven out of saturation, the controller quickly jumps to the next task, which may be to drive another output out of saturation or to apply deadbeat control. On the other hand, using a small $T$ may cause the identification of the system state to be based on a smaller amount of data, thereby increasing sensitivity to uncertainties such as measurement noise. Choosing $\rho$ low limits the growth rate of the input, but may increase the time spent on bringing the outputs out of saturation. The direction of the vector $h_i$ affects the direction of the input applied to bring the output $y_i(t)$ out of saturation. Without further knowledge about the state, however, it is difficult to interpret how different choices affect the outcome. One option is therefore to use $h_i = C_i^\mathsf{T}$, possibly with a scaling to adjust the magnitude of the applied input.

We end this section by remarking that, although the integrals in (8.5) are always well-defined, some of them may grow unbounded as $t \to \infty$. The reason for this is that the controller needs to piece together data from different output components that become unsaturated at different times. The integrals in (8.5) are used to gather the necessary data from the time of initialization, without any form of forgetting. Unbounded internal signals are obviously undesirable; however, the integrals in (8.5) are only needed up until the point when deadbeat control is applied. After deadbeat control has been applied, the state is at the origin and the outputs are all out of saturation. Thus, the issue of unbounded internal signals can easily be resolved by switching to a different controller (e.g., a linear control law) after deadbeat control has been applied. Alternatively, the controller algorithm in (8.2)–(8.5) may be reset with regular intervals from this point on.

## 8.5 Simulation Example

Consider the system

$$\begin{aligned} &\dot{x}_1(t) = x_2(t) + x_3(t), \qquad \dot{x}_2(t) = u_1(t), \qquad \dot{x}_3(t) = u_2(t), \\ &y_1(t) = x_1(t), \qquad y_2(t) = x_1(t) + x_2(t). \end{aligned}$$

This system has an eigenvalue with multiplicity one and an eigenvalue with multiplicity two, both at the origin; thus the system is open-loop unstable. We implement the controller algorithm using $T = 0.5$, $\rho = 1.1$, $h_1 = C_1^\mathsf{T}$, and $h_2 = C_2^\mathsf{T}$ and simulate with initial conditions $x_1(0) = 2$, $x_2(0) = -4$, and $x_3(0) = 1$. The results can be seen in Figure 8.1, where the intervals are marked by vertical dashed lines.

The controller begins by driving $y_1(t)$ out of saturation, and achieves this in the first time interval. The controller then proceeds with driving $y_2(t)$ out of saturation, which is achieved in the fifth time interval. At this point $y_1(t)$ is again

saturated. In the sixth time interval deadbeat control is applied, so that for $t \geq 6T$, the state is at rest at the origin.

## 8.6 Concluding Remarks

We have demonstrated that the origin of a linear time-invariant MIMO system with saturated outputs can be globally asymptotically stabilized, provided the linear system is controllable and observable. We have done so by extending the design presented in Kreisselmeier (1996) for SISO systems. We note, however, that if the controller presented in this note is applied to a SISO system, it does not coincide precisely with the controller in Kreisselmeier (1996). This is because deadbeat identification of the state in Kreisselmeier (1996) is done using data only from the previous interval.

The focus of this note is not on performance; indeed, it is unlikely that an unmodified version of the controller presented here would be suitable for practical implementation. Nevertheless, the results illustrate a general principle, namely, that one may drive each component of the output out of saturation separately to identify the state of the system, and thereafter control the state to the origin. Within this framework, both the approach used to drive the outputs out of saturation and the controller used to drive the state to the origin can be modified to improve performance.

## Bibliography

Y.-Y. Cao, Z. Lin, and B. M. Chen. An output feedback $\mathcal{H}_\infty$ controller design for linear systems subject to sensor nonlinearities. *IEEE Trans. Circ. Syst. Fund. Theor. Appl.*, 50(7):914–921, 2003.

R. A. DeCarlo. *Linear Systems: A State Variable Approach with Numerical Implementation*. Prentice-Hall, Upper Saddle River, NJ, 1989.

H. F. Grip, L. Imsland, T. A. Johansen, J. C. Kalkkuhl, and A. Suissa. Vehicle sideslip estimation: Design, implementation, and experimental validation. *IEEE Contr. Syst. Mag.*, 29(5):36–52, 2009.

G. Kaliora and A. Astolfi. Nonlinear control of feedforward systems with bounded signals. *IEEE Trans. Automat. Contr.*, 49(11):1975–1990, 2004.

R. Koplon, E. D. Sontag, and M. L. J. Hautus. Observability of linear systems with saturated outputs. *Lin. Algebra Appl.*, 205–206:909–936, 1994.

G. Kreisselmeier. Stabilization of linear systems in the presence of output measurement saturation. *Syst. Contr. Lett.*, 29(1):27–30, 1996.

Z. Lin and T. Hu. Semi-global stabilization of linear systems subject to output saturation. *Syst. Contr. Lett.*, 43(3):211–217, 2001.

L. Marconi. Semiglobal regulation of linear systems in presence of measurement constraint. *IEEE Trans. Automat. Contr.*, 48(8):1417–1421, 2003.

F. Mazenc and L. Praly. Global stabilization by output feedback: Examples and counterexamples. *Syst. Contr. Lett.*, 23(2):119–125, 1994.

M. C. Turner and S. Tarbouriech. Anti-windup compensation for systems with sensor saturation: A study of architecture and structure. *Int. J. Contr.*, 82(7): 1253–1266, 2009.

# Chapter 9

# Semiglobal Stabilization of Sandwich Systems by Dynamic Output Feedback

***Abstract:*** *We consider the problem of stabilizing a class of sandwich systems, consisting of two linear subsystems connected in cascade by a saturated scalar signal, with partial-state measurement available from the second subsystem only. We present conditions for semiglobal stabilization and demonstrate their sufficiency by explicit construction of a stabilizing controller. This controller is a mathematical construction that is not intended for practical implementation in its current form. Central to the stabilization strategy is a detection scheme that determines whether the saturation is active or inactive within intervals of a freely chosen length.*

## 9.1 Introduction

Many physical systems can be modeled as interconnections of several distinct subsystems, some of which are linear and some of which are nonlinear. One common type of structure consists of a static nonlinear element *sandwiched* between two linear systems, as illustrated in Figure 9.1. This type of structure can occur, for example, when an actuator with linear dynamics and an output nonlinearity is connected to a linear system. We refer to the system in Figure 9.1 as a *sandwich system*.

In this paper we focus on sandwich systems where the sandwiched nonlinearity is a saturation. Saturations can occur due to the limited capacity of an actuator, limited range of a sensor, or physical limitations within a system. Physical quantities such as speed, acceleration, pressure, flow, current, voltage, and so on, are

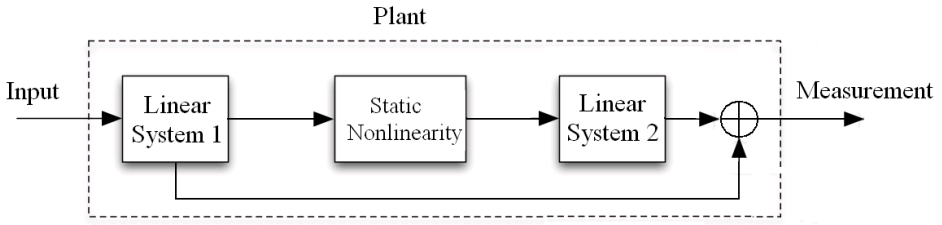


**Figure 9.1:** Sandwich system

always limited to a finite range, and saturations are therefore a ubiquitous feature of physical systems. Our primary goal is to investigate conditions for semiglobal stabilization by output feedback. Due to space constraints we limit ourselves to the case when the available output is a linear combination of the states of the second subsystem only, as illustrated in Figure 9.2. This formulation captures the main challenge of the output-feedback stabilization problem, namely, that the states of the first subsystem can only be observed when the saturation is inactive. We refer to the two linear subsystems as the $L_1$ and $L_2$ subsystems.

Stabilization of sandwich systems has been studied previously, for example, in Taware and Tao (2002, 2003a,b); Taware, Tao, and Teolis (2002). The main technique used in Taware and Tao (2002, 2003a,b); Taware et al. (2002) is based on approximate inversion of the sandwiched nonlinearity. Inversion is a viable approach for some types of nonlinearities, a prominent example being the dead-zone nonlinearity, which is right-invertible. Saturations, however, have a limited range and are therefore not amenable to inversion except in a small region; thus, a different approach is required. In Wang, Stoorvogel, Saberi, Grip, Roy, and Sannuti (2009), the authors considered full-state feedback stabilization of sandwich systems with saturation nonlinearities. The technique introduced in Wang et al. (2009) is a generalization of the *low-gain* design methodologies developed in Lin and Saberi (1993, 1995); Lin (1999) for stabilization of linear systems subject to actuator saturation. Roughly, a pre-feedback is designed to make the $L_1$ subsystem exponentially stable, so that saturation is avoided after an initial transient. The pre-feedback is then augmented by a control law designed for the overall system with a sufficiently low gain to guarantee that saturation is avoided as the whole state is brought to the origin.

When full-state measurement is not available, it is natural to construct an observer to estimate the states. For the system in question, observer design is complicated by the saturation, which separates the $L_1$ subsystem from the output. In general, the saturation must therefore be deactivated before all the states of the system can be identified.

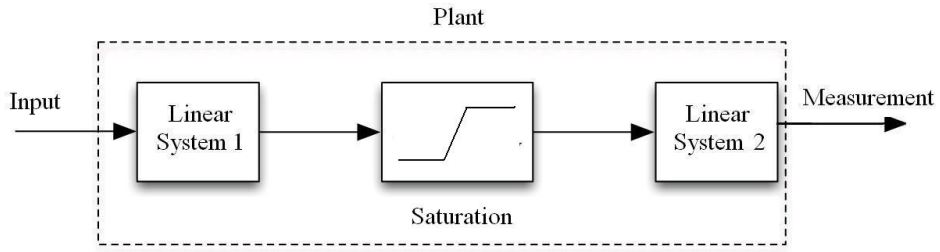


**Figure 9.2:** Sandwich system with saturation nonlinearity and partial-state measurement from second subsystem only

The problem considered in this paper is related to the problem of stabilizing a linear system with a saturated output. This problem has been considered for single-input single-output (SISO) systems in Kreisselmeier (1996); Lin and Hu (2001), and the results in Kreisselmeier (1996) have been extended to multiple-input multiple-output (MIMO) systems in Grip, Saberi, and Wang (2010). In the approach from Kreisselmeier (1996), the output is brought out of saturation by applying an input that grows sufficiently fast to catch up with any internal instabilities, based only on the sign of the output. When the output comes out of saturation, the state is identified and controlled to the origin in a deadbeat manner.

### 9.1.1 Stabilization Strategy

In this paper we combine the method from Wang et al. (2009) for state-feedback stabilization of sandwich systems with the method from Kreisselmeier (1996) for stabilization of systems with an output saturation. As in Kreisselmeier (1996), our strategy is to deactivate the saturation without knowing the full state of the system. Once the saturation is deactivated, the states are identified and controlled to the origin using the method from Wang et al. (2009). A difficulty with this approach is the lack of direct knowledge of whether the saturation is active or inactive at any given time. Consequently, an integral part of the strategy is to detect whether the saturation is active or not based only on the available output.

Because the saturation is separated from the output by a dynamical system, we generally cannot expect to detect activation or deactivation of the saturation instantly. Instead, we shall consider arbitrarily small time intervals and create a detection scheme to determine whether, on any such interval, the saturation is active or not. We shall furthermore determine the sign of the saturation if it is indeed active. When the saturation is detected as inactive for an entire interval, the state of the full system can be determined. This strategy requires that the output

of the $L_1$ subsystem is driven out of saturation for at least one entire interval. To guarantee that this happens, we make the time intervals sufficiently small relative to the size of a bounded set of admissible initial conditions. Our result is therefore semiglobal rather than global; that is, the region of attraction is bounded but can be made arbitrarily large by decreasing the length of the time intervals.

We emphasize that the main purpose of this paper is to investigate solvability conditions for semiglobal stabilization of the sandwich system in Figure 9.2. Although we do so by explicit construction of a stabilizing controller, we do not claim that this controller achieves good performance in most cases. Nevertheless, we introduce design ideas that will be used in future work with attention to performance.

## 9.2 System Description

The class of sandwich systems considered in this paper is described by the following equations:

$$L_1 : \begin{cases} \dot{x}(t) = Ax(t) + Bu(t), \\ z(t) = Cx(t), \end{cases} \tag{9.1a}$$

$$L_2 : \begin{cases} \dot{\omega}(t) = M\omega(t) + N\sigma(z(t)), \\ y(t) = G\omega(t), \end{cases} \tag{9.1b}$$

where $x(t) \in \mathbb{R}^n$, $\omega(t) \in \mathbb{R}^m$, $u(t) \in \mathbb{R}$, $y(t) \in \mathbb{R}^p$, and $z(t) \in \mathbb{R}$. The function $\sigma(\cdot)$ is a standard saturation described by $\sigma(z(t)) = \operatorname{sign}(z(t)) \min\{1, |z(t)|\}$. The input $u(t)$ is assumed to be piecewise continuous. We assume without loss of generality that $G$ has full row rank. For ease of notation, we define $\chi(t) := \operatorname{col}(x(t), \omega(t))$.

In the region where the saturation is inactive (that is, when $|z(t)| \leq 1$), the system equations can be merged in a single linear system:

$$\dot{\chi}(t) = \mathcal{A}\chi(t) + \mathcal{B}u(t) \tag{9.2a}$$

$$y(t) = \mathcal{C}\chi(t). \tag{9.2b}$$

where

$$\mathcal{A} := \begin{bmatrix} A & 0 \\ NC & M \end{bmatrix}, \quad \mathcal{B} := \begin{bmatrix} B \\ 0 \end{bmatrix}, \quad \mathcal{C} := \begin{bmatrix} 0 & G \end{bmatrix}.$$

The system is initialized at time $t = 0$.

**Assumption 9.1.** *The pair $(\mathcal{A}, \mathcal{B})$ is controllable, and the pair $(\mathcal{C}, \mathcal{A})$ is observable.*

It follows from Assumption 9.1 that the pairs $(A, B)$ and $(M, N)$ are controllable, and that the pairs $(C, A)$ and $(G, M)$ are observable.

**Assumption 9.2.** *The eigenvalues of $M$ are located in the closed left-half plane, and the triple $(G, M, N)$ has no invariant zeros at the origin.*

The assumption that the eigenvalues of $M$ are located in the closed left-half plane is necessary to ensure stabilizability of the system, even in the case of full-state feedback, as explained in Wang et al. (2009). We use the assumption that the triple $(G, M, N)$ has no zeros at the origin to facilitate detection of an active or inactive saturation. This can be intuitively understood by noting that a zero at the origin would block constant inputs to the $L_2$ subsystem from being visible at the output $y(t)$. It would therefore be impossible to use the output $y(t)$ to separate between different constant inputs to the $L_2$ subsystem, including a positive saturation ($\sigma(z(t)) = 1$), a negative saturation ($\sigma(z(t)) = -1$), and a zero signal ($\sigma(z(t)) = 0$).

## 9.3 Saturation Detection

We wish to design a detection scheme to determine whether the saturation in (9.1) is active or inactive, based only on knowledge of the output $y(t)$ and the input $u(t)$. To this end, we divide the time $t > 0$ into intervals $(kT - T, kT]$, $k = 1, 2, \ldots$, where the interval length $T > 0$ is a design parameter that can be made arbitrarily small. The detection scheme will determine at time $kT$ whether on the preceding interval $(kT - T, kT]$, the saturation was active for the entire interval, inactive for the entire interval, or both active and inactive within the interval.

To illustrate the approach, suppose that the saturation is active in the positive direction for an entire interval; that is, for some arbitrary $k \in 1, 2, \ldots$, $z(t) \geq 1$ for all $t \in (kT - T, kT]$. On this interval the $L_2$ subsystem behaves like a linear system with $\sigma(z(t)) = 1$ as a constant input. Hence the output satisfies the following equation for all $\tau \in (0, T]$:

$$y(kT - T + \tau) = G\mathrm{e}^{M\tau}\omega(kT - T) + Gu_s^*(\tau), \tag{9.3}$$

where

$$u_s^*(\tau) := \int_0^\tau \mathrm{e}^{M(\tau-\gamma)}N \, \mathrm{d}\gamma. \tag{9.4}$$

If we premultiply (9.3) by $\mathrm{e}^{M^\top\tau}G^\top$ and integrate from 0 to $\tau$, we obtain

$$\xi_s(kT - T; \tau) = D_s(\tau)\omega(kT - T) + S_s(\tau), \tag{9.5}$$

where

$$\xi_s(kT-T;\tau) = \int_0^\tau \mathrm{e}^{M^\top \gamma} G^\top y(kT-T+\gamma)\,\mathrm{d}\gamma, \tag{9.6a}$$

$$D_s(\tau) = \int_0^\tau \mathrm{e}^{M^\top \gamma} G^\top G \mathrm{e}^{M\gamma}\,\mathrm{d}\gamma, \tag{9.6b}$$

$$S_s(\tau) = \int_0^\tau \mathrm{e}^{M^\top \gamma} G^\top G u_s^*(\gamma)\,\mathrm{d}\gamma. \tag{9.6c}$$

Each of the quantities in (9.6) can be computed based on the available output data. Furthermore, we can use (9.5) to calculate $\omega(kT-T)$ as

$$\omega(kT-T) = D_s^{-1}(\tau)(\xi_s(kT-T;\tau) - S_s(\tau)). \tag{9.7}$$

Thus (9.7) represents a deadbeat observer for the $L_2$ subsystem when the saturation is active in the positive direction. Note that $D_s(\tau)$ is the observability Gramian of the observable pair $(G, M)$, and thus it is invertible for all $\tau \in (0, T]$.

We wish to use (9.7) to detect whether the saturation really is active in the positive direction on the entire interval $(kT-T, kT]$. To do so we premultiply (9.7) by $G\mathrm{e}^{M\tau}$. Since $D_s(\tau)$ becomes singular as $\tau \to 0$, we also multiply the expression by $\det(D_s(\tau))$ to obtain $\det(D_s(\tau))D_s^{-1}(\tau) = \mathrm{adj}(D_s(\tau))$, where $\mathrm{adj}(D_s(\tau))$ is the adjugate of $D_s(\tau)$, which is bounded on $(0, T]$. Rearranging the resulting expression and using (9.3), we obtain

$$\begin{aligned}\det(D_s(\tau))(y(kT-T+\tau) - Gu_s^*(\tau)) \\ - G\mathrm{e}^{M\tau}\mathrm{adj}(D_s(\tau))(\xi_s(kT-T;\tau) - S_s(\tau)) = 0.\end{aligned} \tag{9.8}$$

Equation (9.8) can be checked using available output data, and it holds for each $\tau \in (0, T]$ if the saturation is active in the positive direction on the entire interval. If the saturation is not active in the positive direction on the entire interval, one might expect (9.8) not to hold, at least for some $\tau \in (0, T]$. Indeed, this expectation turns out to be true under the assumptions made in this paper. Our detection scheme is therefore based on checking the validity of (9.8). We create a similar test to check whether the saturation is active in the negative direction on the entire interval. Finally, we do the same based on the model (9.2) and input $u(t)$ to check whether the saturation is inactive on the entire interval.

### 9.3.1 Detectors

We define the following quantities:

$$e_{k+} = \int_0^T \|\det(D_s(\tau))(y(kT - T + \tau) - Gu_s^*(\tau)) - G\mathrm{e}^{M\tau}\mathrm{adj}(D_s(\tau))(\xi_s(kT - T;\tau) - S_s(\tau))\|\,\mathrm{d}\tau,$$

$$e_{k-} = \int_0^T \|\det(D_s(\tau))(y(kT - T + \tau) + Gu_s^*(\tau)) - G\mathrm{e}^{M\tau}\mathrm{adj}(D_s(\tau))(\xi_s(kT - T;\tau) + S_s(\tau))\|\,\mathrm{d}\tau,$$

$$e_{k0} = \int_0^T \|\det(D_0(\tau))(y(kT - T + \tau) - Gu_0^*(kT - T;\tau)) - \mathcal{C}\mathrm{e}^{\mathcal{A}\tau}\mathrm{adj}(D_0(\tau))(\xi_0(kT - T;\tau) - S_0(kT - T;\tau))\|\,\mathrm{d}\tau,$$

where

$$\begin{aligned} u_0^*(kT - T;\tau) &= \int_0^\tau \mathrm{e}^{\mathcal{A}(\tau-\gamma)}\mathcal{B}u(kT - T + \gamma)\,\mathrm{d}\gamma, \\ \xi_0(kT - T;\tau) &= \int_0^\tau \mathrm{e}^{\mathcal{A}^\mathsf{T}\gamma}\mathcal{C}^\mathsf{T}y(kT - T + \gamma)\,\mathrm{d}\gamma, \\ D_0(\tau) &= \int_0^\tau \mathrm{e}^{\mathcal{A}^\mathsf{T}\gamma}\mathcal{C}^\mathsf{T}\mathcal{C}\mathrm{e}^{\mathcal{A}\gamma}\,\mathrm{d}\gamma, \\ S_0(kT - T;\tau) &= \int_0^\tau \mathrm{e}^{\mathcal{A}^\mathsf{T}\gamma}\mathcal{C}^\mathsf{T}\mathcal{C}u_0^*(kT - T;\gamma)\,\mathrm{d}\gamma. \end{aligned}$$

The functions $u_0^*$, $\xi_0$, $D_0$, and $S_0$ correspond to the functions defined in (9.4), (9.6) but are based on the system matrices of the system (9.2) and the input $u(t)$, rather than the system matrices of the $L_2$ subsystem and the input 1.

To facilitate detection, we also need an assumption regarding the control input $u(t)$.

**Assumption 9.3.** *If for any $k \in 1, 2, \ldots$, the function $\tau \mapsto u(kT - T + \tau)$ is a Bohl function on $(0, T)$,*[1] *then its spectrum does not contain any invariant zeros of the triple $(G, M, N)$.*[2]

[1] *Remark added after publication:* Technically, this statement should read "If for any $k \in 1, 2, \ldots$, the function $\tau \mapsto u(kT - T + \tau)$ is a Bohl function *almost everywhere* on $(0, T), \ldots$"

[2] A function $f(t)$ is a Bohl function if it is a linear combination of signals of the form $t^\alpha \mathrm{e}^{\lambda t}$, where the $\alpha$'s are nonnegative integers and the $\lambda$'s are complex numbers. The set of $\lambda$'s is called the spectrum of $f(t)$ (Trentelman, Stoorvogel, and Hautus, 2001).

*Remark* 9.1. Assumption 9.3 specifies a mild restriction on the allowable input signals $u(t)$ on any interval. The reason for this restriction is that some signals may create an output from the $L_1$ subsystem that is blocked by the zeros of the $L_2$ subsystem.

We can now state our result on saturation detection.

**Theorem 9.1.** *For each* $k \in 1, 2, \ldots$

1. $e_{k+} = 0$ *if and only if for all* $t \in (kT - T, kT]$, $z(t) \geq 1$
2. $e_{k-} = 0$ *if and only if for all* $t \in (kT - T, kT]$, $z(t) \leq -1$
3. $e_{k0} = 0$ *and* $e_{k+}, e_{k-} > 0$ *if and only if for all* $t \in (kT - T, kT]$, $-1 \leq z(t) \leq 1$ *and for some* $t \in (kT - T, kT]$, $|z(t)| < 1$

*Proof.* See Appendix 9.A. □

## 9.4 Semiglobal Stabilization

In this section we use the detection scheme from the previous section to create a stabilizing control law for the system (9.1). Because the approach is semiglobal, we make the following assumption:

**Assumption 9.4.** *The state* $\chi(t)$ *is initialized from some* a priori *known compact set* $K_0$.

The control strategy can be divided into three consecutive stages, described in the following sections. In Stage 2, we apply a control on the form $-B^{\mathsf{T}}\mathrm{e}^{-A^{\mathsf{T}}\tau}\kappa$ on intervals $(0, \bar{T}]$, where $\kappa$ is a constant. This approach is borrowed from Kreisselmeier (1996) and is used to deactivate the saturation. To ensure that the control law satisfies the assumption about $u(t)$ in Theorem 9.1, we therefore replace it with the following assumption:

**Assumption 9.3′.** *No eigenvalues of* $-A$ *coincide with any invariant zeros of the triple* $(G, M, N)$.

We remark that this is not a necessary condition, as the control law in Stage 2 can easily be modified to ensure that Assumption 9.3 holds, even when Assumption 9.3′ does not hold.

### Stage 1

In Stage 1 we do not apply any control, but wait until the saturation is either active or inactive for an entire interval $(k_1T - T, k_1T]$, as indicated by the condition $e_{k_1+}e_{k_1-}e_{k_10} = 0$. This is guaranteed to occur for some finite $k_1 \geq 1$ if $T$ is chosen sufficiently small, because the unforced system cannot oscillate arbitrarily fast. In Stage 1, the control is therefore specified by

$$u(t) = 0, \quad t \in [0, k_1T]. \tag{9.9}$$

At time $t = k_1T$ we move to Stage 2.

### Stage 2

In Stage 2 we apply a control to ensure that $z(t)$ is brought out of saturation for an entire interval $(k_2T - T, k_2T]$, as indicated by the condition $e_{k_20} = 0$ and $e_{k_2+}e_{k_2-} > 0$. Define

$$\delta = \begin{cases} 1, & e_{k_1+} = 0, \\ -1, & e_{k_1-} = 0, \\ 0, & \text{otherwise.} \end{cases}$$

Let $\bar{T} > 0$ be some arbitrary fixed constant. We divide the time $t \geq k_1T$ into intervals $(k_1T + j\bar{T} - \bar{T}, k_1T + j\bar{T}]$, $j = 0, 1, \ldots$ The control in Stage 2 is defined based on Kreisselmeier (1996) by

$$u(k_1T + j\bar{T} + \tau) = -B^{\mathsf{T}}\mathrm{e}^{-A^{\mathsf{T}}\tau}U_j, \ \forall t \in (k_1T, k_2T], \tag{9.10}$$

where $j = 0, 1, \ldots$ and $\tau \in (0, \bar{T}]$. The quantities $U_j$ and $\beta(\bar{T})$ are defined by

$$U_j = \alpha^j\beta^{-1}(\bar{T})(\alpha h - \mathrm{e}^{A\bar{T}}h)\delta,$$

$$\beta(\bar{T}) = \int_0^{\bar{T}} \mathrm{e}^{A(\bar{T}-\gamma)}BB^{\mathsf{T}}\mathrm{e}^{-A^{\mathsf{T}}\gamma}\mathrm{d}\gamma,$$

Finally, $\alpha$ is defined such that $\alpha > \mathrm{e}^{2\bar{T}\|A\|}$ and $h$ is any vector such that $Ch > 0$. At time $k_2T$, we move to Stage 3.

The following lemma shows that we will indeed move to Stage 3 within finite time.

**Lemma 9.1.** *If $T > 0$ is chosen sufficiently small, then there exists a $k_2 \geq k_1$ such that $e_{k_20} = 0$ and $e_{k_2+}e_{k_2-} > 0$.*

*Proof.* See Appendix 9.A. □

### Stage 3

In Stage 3 we bring the states to the origin by using the state-feedback approach from Wang et al. (2009). To do so, we need access to the full state $\chi(t)$. Since the saturation is inactive on the interval $(k_2T - T, k_2T]$, the full state $\chi(t)$ at time $k_2T - T$ can be calculated precisely by using a deadbeat approach, as indicated by the discussion in Section 9.3. After this point $\chi(t)$ can be calculated by integrating (9.1). Thus, we define a state estimate $\hat{\chi}(t)$ for $t \geq k_2T$ by

$$\dot{\hat{\chi}}(t) = f(\hat{\chi}(t), u(t)), \tag{9.11a}$$

$$\begin{aligned}\hat{\chi}(k_2T) = {} & \mathrm{e}^{\mathcal{A}T} D_0^{-1}(T)(\xi_0(k_2T - T; T) \\ & - S_0(k_2T - T; T)) + u_0^*(k_2T - T; T),\end{aligned} \tag{9.11b}$$

where $f(\hat{\chi}(t), u(t))$ represents the right-hand side of (9.1).

**Lemma 9.2.** *For all $t \geq k_2T$, $\hat{\chi}(t) = \chi(t)$.*

*Proof.* See Appendix 9.A. □

We use the precise knowledge of $\chi(t)$ for all $t \geq k_2T$ to implement a linear state-feedback control law according to Wang et al. (2009). We start by selecting $F$ such that $A + BF$ is Hurwitz. We then find the unique solution $P_\varepsilon = P_\varepsilon^\mathsf{T} > 0$ of the algebraic Riccati equation

$$\begin{bmatrix} A + BF & 0 \\ NC & M \end{bmatrix}^\mathsf{T} P_\varepsilon + P_\varepsilon \begin{bmatrix} A + BF & 0 \\ NC & M \end{bmatrix} - P_\varepsilon \begin{bmatrix} BB^\mathsf{T} & 0 \\ 0 & 0 \end{bmatrix} P_\varepsilon + \varepsilon I = 0,$$

where $\varepsilon > 0$ is a low-gain parameter that must be chosen sufficiently small. The control in Stage 3 is now defined by

$$u(t) = \left(\begin{bmatrix} F & 0 \end{bmatrix} - \mathcal{B}^\mathsf{T} P_\varepsilon\right) \hat{\chi}(t), \quad \forall t > k_2T. \tag{9.12}$$

Since $\hat{\chi}(t) = \chi(t)$, we may use the state-feedback theory from Wang et al. (2009). From the proof of Lemma 9.1, we know that $\chi(k_2T)$ belongs to a compact set $K_2 \subset \mathbb{R}^{n+m}$, the size of which is bounded as a function of the set $K_0$ of admissible initial conditions. By Wang et al. (2009, Theorem 3), the control law therefore ensures that $\chi(t) \to 0$ as $t \to \infty$, provided the low-gain parameter $\varepsilon > 0$ is chosen sufficiently small depending on $K_0$.

### 9.4.1 Asymptotic Stability

Based on the discussion in the previous section, we can now state the main result on semiglobal stabilization of the sandwich system.

**Theorem 9.2.** *For any compact set $K_0 \subset \mathbb{R}^{n+m}$, there exist $T^* > 0$ and $\varepsilon^* > 0$ such that for all $0 < \varepsilon \leq \varepsilon^*$ and $0 < T \leq T^*$, the control law described in Stages* 1–3 *asymptotically stabilizes the system* (9.1) *with $K_0$ contained in the region of attraction.*

*Proof.* See Appendix 9.A. □

## 9.5 Discussion

As emphasized in the introduction, the primary purpose of this paper is to investigate solvability conditions for the semiglobal stabilization problem, not to construct a control law to ensure good performance. Although the control law presented in Section 9.4 is theoretically stabilizing, there are several obvious drawbacks that must be addressed in a practical implementation.

First, the input applied to the system to deactivate the saturation grows exponentially larger for each interval $(k_1 T + j\bar{T} - \bar{T}, k_1 T + j\bar{T}]$, even when this is not necessary. If, for example, $L_1$ is asymptotically stable with $u(t) = 0$, then no input needs to be applied to deactivate the saturation, and if $L_1$ is marginally stable, only a small input needs to be applied. The exponentially growing input may cause $z(t)$ to pass quickly through the saturation, thus requiring $T$ to be chosen small. As a consequence, the deadbeat observation of $\chi(t)$ may become poorly conditioned.

Second, the state estimation of $\chi(t)$ is based on deadbeat observation at $t = k_2 T$ and integration of the system equations from that point on. Clearly this is not a robust approach; any disturbance or modeling inaccuracy may cause the state estimate to diverge as $t \to \infty$. An obvious improvement would be to update $\hat{\chi}(t)$ using the deadbeat approach every time the saturation is inactive for an entire interval. Indeed, after some finite amount of time the saturation becomes inactive in every time interval.

Third, the algorithm passes through the three stages in a linear manner. A more robust approach would include a path back to Stage 2 from Stage 3, in case the control in Stage 3 fails to make the state converge and the saturation remains active. This can occur, for example, if an unknown disturbance to (9.2) causes $\hat{\chi}(t)$ to become inaccurate.

Design of a controller that includes the above improvements, as well as others, is the subject of current research.

## 9.6 Concluding Remarks

We have presented conditions for semiglobal stabilization of systems consisting of two linear systems connected in a saturated cascade connection. Sufficiency of the conditions is demonstrated through constructive design of a semiglobally stabilizing controller. Current research is focused on further development of a controller with emphasis on performance.

## 9.A Proofs

*Proof of Theorem* 9.1. We first prove that if for all $\tau \in (0, T]$, $\sigma(z(kT-T+\tau)) = 1$, then $e_{k+} = 0$. Taking the norm on both sides of (9.8), we obtain

$$\|\det(D_s(\tau))(y(kT - T + \tau) - Gu_s^*(\tau)) - G\mathrm{e}^{M\tau}\mathrm{adj}(D_s(\tau))(\xi_s(kT - T; \tau) - S_s(\tau))\| = 0, \quad (9.13)$$

for all $\tau \in (0, T]$. To form $e_{k+}$ we integrate the left-hand side of (9.13) from 0 to $T$, and it follows that $e_{k+} = 0$. The same argument can be applied for $e_{k-}$ and $e_{k0}$. This proves the *if* part of statements 1 and 2 of the theorem.

We now prove that if $e_{k+} = 0$, then for all $\tau \in (0, T]$, $z(kT - T + \tau) \geq 1$. We shall need the following lemma, which specifies that the output must correspond to a solution of $L_2$ with input 1, for some set of initial conditions.

**Lemma 9.3.** *For each $k \in 1, 2, \ldots$, if $e_{k+} = 0$, then there exists a vector $\omega_0 \in \mathbb{R}^m$ such that for all $\tau \in (0, T]$, $y(kT - T + \tau)$ corresponds to the output of $L_2$ with input* 1*, initialized at time $t = kT - T$ with initial condition $\omega_0$.*

*Proof.* Suppose that $e_{k+} = 0$. Then from (9.8), we have

$$y(kT - T + \tau) - Gu_s^*(\tau) - G\mathrm{e}^{M\tau}D_s^{-1}(\tau)(\xi_s(kT - T; \tau) - S_s(\tau)) = 0.$$

Premultiplying by $D_s^{-1}(\tau)\mathrm{e}^{M^\top\tau}G^\top$, it is easily verified that we obtain

$$D_s^{-1}(\tau)\frac{\mathrm{d}}{\mathrm{d}\tau}(\xi(kT - T; \tau) - S_s(\tau)) + \frac{\mathrm{d}}{\mathrm{d}\tau}(D_s^{-1}(\tau))(\xi_s(kT - T; \tau) - S_s(\tau)) = 0.$$

Using integration by parts from 0 to $\tau$ therefore yields

$$D_s^{-1}(\tau)(\xi_s(kT - T; \tau) - S_s(\tau)) = \kappa,$$

where $\kappa$ is a constant vector. Premultiplying by $D_s(\tau)$ and differentiating on $(0, T)$ yields

$$\mathrm{e}^{M^\top\tau}G^\top y(kT - T + \tau) - \mathrm{e}^{M^\top\tau}G^\top Gu_s^*(\tau) = \mathrm{e}^{M^\top\tau}G^\top G\mathrm{e}^{M\tau}\kappa.$$

Because $G^\top$ has full column rank and $e^{M^\top \tau}$ is nonsingular, the above expression implies that

$$y(kT - T + \tau) - Gu_s^*(\tau) = Ge^{M\tau}\kappa.$$

Comparison with (9.3) shows that $y(kT - T + \tau)$ corresponds to the output of $L_2$ with input 1, initialized at time $t = kT - T$ with initial condition $\kappa$ on $(0, T)$, which by continuity extends to $(0, T]$. □

Based on Lemma 9.3, suppose that for all $\tau \in (0, T]$, the output $y(kT-T+\tau)$ corresponds to the response of the $L_2$ subsystem with input 1, initialized at time $t = kT - T$ with initial condition $\omega_0$. Then we may write $y(kT - T + \tau) = G\hat{\omega}(kT-T+\tau)$, where $\dot{\hat{\omega}}(kT-T+\tau) = M\omega(kT-T+\tau)+N$ and $\hat{\omega}(kT-T) = \omega_0$. Defining $\tilde{\omega}(kT - T + \tau) = \hat{\omega}(kT - T + \tau) - \omega(kT - T + \tau)$, we obtain the system

$$\dot{\tilde{\omega}}(kT - T + \tau) = M\tilde{\omega}(kT - T + \tau) + N\mu(kT - T + \tau),$$

where $\mu(kT-T+\tau) := 1-\sigma(z(kT-T+\tau))$. From Sannuti and Saberi (1987) it is easy to show that the $\tilde{\omega}$ system with output $\tilde{y}(kT-T+\tau) := G\tilde{\omega}(kT-T+\tau)$ is left-invertible with respect to the input $\mu(kT-T+\tau)$, because it is observable and the input is scalar. Since $\tilde{y}(kT - T + \tau) = 0$, it follows that $\mu(kT - T + \tau)$ must either be zero, or it must be blocked by the invariant zeros of the triple $(G, M, N)$. If $\mu(kT - T + \tau) = 0$, then we have $\sigma(z(kT - T + \tau)) = 1$, as desired. If $\mu(kT - T + \tau)$ is a nonzero signal blocked by the invariant zeros of the triple $(G, M, N)$, then it must be a Bohl function on the interval $(0, T)$ with a spectrum that contains only invariant zeros of $(G, M, N)$. Furthermore, this signal must be non-constant, since $(G, M, N)$ has no invariant zeros at the origin. This implies that $z(kT - T + \tau)$ must be a nonzero Bohl function with a spectrum containing an invariant zero of $(G, M, N)$. Since the $L_1$ subsystem is a controllable and observable SISO system, this can only occur if either $A$ has an eigenvalue that coincides with an invariant zero of $(G, M, N)$ or if the input $u(kT - T + \tau)$ is a Bohl function on $(0, T)$ with a spectrum containing an invariant zero of $(G, M, N)$. By Assumption 9.3, $u(kT - T + \tau)$ cannot be a Bohl function with a spectrum containing an invariant zero of $(G, M, N)$, and thus $A$ must have an eigenvalue that coincides with an invariant zero of $(G, M, N)$. However, since the $L_1$ and $L_2$ subsystems are connected in cascade by a scalar signal, it is easy to show that this would lead to a pole-zero cancellation in the linear system (9.2), with a resulting loss of observability. This contradicts Assumption 9.1, and hence we must have $z(kT - T + \tau) \geq 1$.

The same argument holds for $e_{k-}$ as for $e_{k+}$. We have therefore proven the *only if* part of statements 1 and 2 of the theorem, as well as the *if* part of statement

3. For statement 3, we still have to prove that $e_{k0} = 0$ and $e_{k+}, e_{k-} > 0$ cannot occur unless for all $\tau \in (0, T]$, $-1 \leq z(kT - T + \tau) \leq 1$ and for some $\tau \in (0, T]$, $|z(kT - T + \tau)| < 1$. We can use the same argument as in Lemma 9.3 to prove that $e_{k0} = 0$ implies that for all $\tau \in (0, T]$, $y(kT - T + \tau)$ corresponds exactly to the response of the $\chi$ system with input $u(kT - T + \tau)$, initialized at time $t = kT - T$ with some initial condition $\chi_0$. Let $\hat{x}(kT - T + \tau)$ and $\hat{\omega}(kT - T + \tau)$ represent the corresponding trajectories. Following the same argument as above, we define $\tilde{\omega}(kT - T + \tau) = \hat{\omega}(kT - T + \tau) - \omega(kT - T + \tau)$ and obtain the system

$$\dot{\tilde{\omega}}(kT - T + \tau) = M\tilde{\omega}(kT - T + \tau) + N\mu(kT - T + \tau),$$

where $\mu(kT - T + \tau) := C\hat{x}(kT - T + \tau) - \sigma(z(kT - T + \tau))$. This can be rewritten as $\mu(kT - T + \tau) = z(kT - T + \tau) - \sigma(z(kT - T + \tau)) + C\tilde{x}(\tau)$, where $\dot{\tilde{x}}(\tau) = A\tilde{x}(\tau)$. As before, $\mu(kT - T + \tau)$ must be a Bohl function to ensure $\tilde{y}(kT - T + \tau) = 0$. Since $\tilde{x}(\tau)$ is a Bohl function, $z(kT - T + \tau) - \sigma(z(kT - T + \tau))$ must also be a Bohl function, which shows that either $|z(kT - T + \tau)| \geq 1$ or $|z(kT - T + \tau)| \leq 1$ holds for all $\tau \in (0, T]$ (otherwise $z(kT - T + \tau) - \sigma(z(kT - T + \tau))$ would be zero on a subinterval in $(0, T]$ and nonzero on another subinterval).

If $|z(kT - T + \tau)| \geq 1$, then $e_{k+}$ or $e_{k-} = 0$. Hence, $e_{k0} = 0$ and $e_{k+}, e_{k-} > 0$ can only occur if for all $\tau \in (0, T]$, $-1 \leq z(kT - T + \tau) \leq 1$ and for some $\tau \in (0, T]$, $|z(kT - T + \tau)| < 1$. □

*Proof of Lemma* 9.1. We start by noting that from the dynamics of the system, there is an upper bound on the maximum time before the saturation is active or inactive for an entire interval when $u(t) = 0$, provided $T$ is sufficiently small. Using the fact that $\chi(t)$ is initialized from a compact set $K_0$, we therefore know that for small $T$ there is a $T$-independent bound on $\|x(k_1 T)\|$.

We now prove that there is a finite $k_2 \geq k_1$ so that $e_{k_2 0} = 0$ and $e_{k_2+} e_{k_2-} > 0$. If $\delta = 0$, then $e_{k_1 0} = 0$ and $e_{k_1+} e_{k_1-} > 0$, and hence $k_2 = k_1$. Suppose instead that $\delta = 1$ and, for the purpose of establishing a contradiction, that $e_{k0} = 0$ and $e_{k+} e_{k-} > 0$ does not take place for any $k \geq k_1$, no matter how small $T > 0$ is chosen. Noting that $\delta = \text{sign}(z(k_1 T))$, it follows directly from Kreisselmeier (1996) that the sign of $z(t)$ switches before time $k_1 T + j' \bar{T}$, where $j'$ is the smallest integer $j$ that satisfies

$$\alpha^{j/2} > \frac{\|C\|(\|x(k_1 T)\| + \|h\|)}{Ch}.$$

Since there is a $T$-independent bound on $\|x(k_1 T)\|$, it follows that $j'$ is independent of $T$. From (9.10), we therefore see that there is a $T$-independent bound on

$u(t)$ for all $t \in (k_1T, k_1T + j'\bar{T}]$. It follows that there is a $T$-independent bound on $x(t)$ for all $t \leq k_1T + j'\bar{T}$. Based on this we know that there is a lower bound on the time that $z(t)$ is out of saturation before switching sign. However, if $T$ is chosen smaller than half the length of that minimum interval, it is guaranteed that there is an entire interval $(k_2T - T, k_2T]$ in which $z(t)$ is out of saturation before switching sign, and hence $e_{k_20} = 0$ and $e_{k_2+}e_{k_2-} > 0$. The same argument holds if $\delta = -1$. □

*Proof of Lemma* 9.2. Since the saturation is inactive on the interval $(k_2 - T, k_2T]$, (9.2) is valid on this interval. Just as we may use (9.7) for the saturated system, we may therefore calculate $\chi(k_2T - T)$ by

$$\chi(k_2T - T) = D_0^{-1}(T)(\xi_0(k_2T - T; T) - S_0(k_2T - T; T)).$$

It therefore follows from the solution of the linear system (9.2) on $(k_2T - T, k_2T]$ that $\hat{\chi}(k_2T)$ as defined in (9.11) satisfies $\hat{\chi}(k_2T) = \chi(k_2T)$. For $t \geq k_2T$, $\hat{\chi}(t)$ evolves according to the same differential equation as $\chi(t)$, with the same initial condition and the same input. Hence for all $t \geq k_2T$, $\hat{\chi}(t) = \chi(t)$. □

*Proof of Theorem* 9.2. Through our discussion of the various stages, we have already proven that $\chi(t) \to 0$ as $t \to \infty$, provided $\varepsilon > 0$ and $T > 0$ are chosen sufficiently small. It remains to be shown that the origin of (9.1) is a stable equilibrium point.

On the interval $[0, T]$, we have $u(t) = 0$. Hence, if $\|\chi(0)\| \leq c$ for some sufficiently small constant $c > 0$, then the state evolves according to $\chi(t) = \mathrm{e}^{\mathcal{A}t}\chi(0)$ and the saturation remains strictly inactive for all $t \in [0, T]$. This implies that $e_{10} = 0$ and $e_{1+}, e_{1-} > 0$, and hence we move directly past Stage 2 to Stage 3. For sufficiently small $\chi(T) = \mathrm{e}^{\mathcal{A}t}\chi(0)$, the controller in Stage 3 ensures that for all $t \geq T$, $\|\chi(t)\| \leq \gamma\|\chi(T)\|$ for some $\gamma \geq 1$. It follows that for all sufficiently small $\|\chi(0)\|$, $\|\chi(t)\| \leq \gamma\|\mathrm{e}^{\mathcal{A}T}\|\|\chi(0)\|$, which shows that the origin is a stable equilibrium point. □

# Bibliography

H. F. Grip, A. Saberi, and X. Wang. Stabilization of multiple-input multiple-output linear systems with saturated outputs. *IEEE Trans. Automat. Contr.*, 2010. Accepted.

G. Kreisselmeier. Stabilization of linear systems in the presence of output measurement saturation. *Syst. Contr. Lett.*, 29(1):27–30, 1996.

Z. Lin. *Low gain feedback*, volume 240 of *Lecture Notes in Contr. Inform. Sci.* Springer, Berlin, 1999.

Z. Lin and T. Hu. Semi-global stabilization of linear systems subject to output saturation. *Syst. Contr. Lett.*, 43(3):211–217, 2001.

Z. Lin and A. Saberi. Semi-global exponential stabilization of linear systems subject to "input saturation" via linear feedbacks. *Syst. Contr. Lett.*, 21(3):225–239, 1993.

Z. Lin and A. Saberi. Semi-global exponential stabilization of linear discrete-time systems subject to input saturation via linear feedbacks. *Syst. Contr. Lett.*, 24 (2):125–132, 1995.

P. Sannuti and A. Saberi. Special coordinate basis for multivariable linear systems—Finite and infinite zero structure, squaring down and decoupling. *Int. J. Contr.*, 45(5):1655–1704, 1987.

A. Taware and G. Tao. Neural-hybrid control of systems with sandwiched dead-zones. *Int. J. Adapt. Contr. Signal Process.*, 16(7):473–496, 2002.

A. Taware and G. Tao. *Control of sandwich nonlinear systems*, volume 288 of *Lecture Notes in Contr. Inform. Sci.* Springer, Berlin, 2003a.

A. Taware and G. Tao. An adaptive dead-zone inverse controller for systems with sandwiched dead-zones. *Int. J. Contr.*, 76(8):755–769, 2003b.

A. Taware, G. Tao, and C. Teolis. Design and analysis of a hybrid control scheme for sandwich nonsmooth nonlinear systems. *IEEE Trans. Automat. Contr.*, 47 (1):145–150, 2002.

H. L. Trentelman, A. A. Stoorvogel, and M. L. J. Hautus. *Control Theory for Linear Systems*. Springer, London, 2001.

X. Wang, A. A. Stoorvogel, A. Saberi, H. F. Grip, S. Roy, and P. Sannuti. Stabilization of a class of sandwich nonlinear systems via state feedback. In *Proc. IEEE Conf. Dec. Contr.*, pages 1417–1421, Shanghai, China, 2009.

# Thesis Conclusion

This thesis covers three different topics within state and parameter estimation for nonlinear and uncertain systems.

Part I presents a nonlinear observer for estimating the vehicle sideslip angle and compares its performance to an EKF developed for the same purpose. It is found that the nonlinear observer performs as well as the EKF while achieving a significant reduction in computational complexity. However, there is still room for improvement of the vehicle sideslip observer; in particular, there are still problems related to the difficulty of separating a nonzero bank angle from the effect of driving on a low-friction road surface. The nonlinear analysis fails to prove stability of the observer when friction estimation and bank-angle estimation are combined, and the ad hoc solution of adjusting the bank-angle gain according to heuristic rules is unsatisfactory, both in terms of theoretical justification and performance in some situations. This aspect of the design must be improved before the observer can reach production quality. Nevertheless, improvements made in this regard are unlikely to have a significant effect on the performance in the majority of situations, and improvements in the sensor configuration are therefore needed to achieve a goal of consistently estimating the vehicle sideslip angle with $1^\circ$ accuracy. The most promising avenue for increasing accuracy seems to be the addition of sensors for measuring the roll and pitch rate and the vertical acceleration. Preliminary tests with this type of sensor configuration suggest that significant improvements in performance can be achieved. In terms of sensor inaccuracy, bias and drift are the most limiting factors, and a reduction in these types of low-frequency errors would have a large impact on performance.

Part II presents a framework for state and parameter estimation for linear systems that are perturbed by a nonlinear function of the system state, external time-varying signals, and a set of unknown, constant parameters. The focus of the theory in Part II is on proving asymptotically exact estimation of both of the parameters and the state of the system through Lyapunov-type analysis. This strategy is advantageous when parameter estimation is a goal in itself, but it may be a drawback in control problems where parameter estimation is of secondary importance, as in

traditional adaptive control formulations. An improvement to the results may be possible by investigating convergence of the parameter-estimation error to some larger subset than the origin, in cases where persistency-of-excitation conditions are not fulfilled. Further development of techniques for constructing the parameter estimator is another topic for future research. One possibility is to use time delays to create a set of equations that are uniquely solvable, even when the perturbation is not invertible with respect to the unknown parameters at any single point in time.

Part III presents designs for output-feedback stabilization of two classes of systems containing saturations. The first class of systems is multivariable linear systems with saturated outputs, and the second class of systems is sandwich systems consisting of two linear subsystems with a saturation sandwiched between them. Although output-feedback controllers are explicitly constructed for both classes of systems, the results presented in Part III should primarily be viewed as proofs of existence of stabilizing controllers, rather than practical design methods. The presented controllers have some obvious drawbacks, and addressing these is a topic of current research. Forthcoming publications will also deal with sandwich systems where the outputs are linear combinations of the states of both subsystems.

# Corrigendum to "Topics in State and Parameter Estimation for Nonlinear and Uncertain Systems"

Håvard Fjær Grip

In Chapter 6, Section 6.3.2, there is a scaling error in the expression for $K_{q_j q}$. The correct expression is

$$K_{q_j q}(\varepsilon) = \left[ 0_{n_{q_j} \times (j-1)} \quad \operatorname{col}\left( \frac{\bar{K}_{q_j 1}}{\varepsilon}, \ldots, \frac{\bar{K}_{q_j n q_j}}{\varepsilon^{n q_j}} \right) \quad 0_{n_{q_j} \times (k-j)} \right] + L_{q_j q}.$$

Left uncorrected, the error affects MIMO systems of non-uniform rank, but not SISO systems or MIMO systems of uniform rank.